Title
Relationship between the pore water pressure buildup and the change of stiffness in sands subjected to uniform and variable small to moderate cyclic shear strains

Author
Thangavel, Harish

Publication Date
2019

Peer reviewed|Thesis/dissertation

UNIVERSITY OF CALIFORNIA

Los Angeles

Relationship between the pore water pressure buildup and the change of stiffness in sands subjected to uniform and variable small to moderate cyclic shear strains

A thesis submitted in partial satisfaction

of the requirements for the degree Master of Science

in Civil Engineering

by

Harish Thangavel

2019

ABSTRACT OF THE THESIS

Relationship between the pore water pressure buildup

and the change of stiffness in sands subjected to

uniform and variable small to moderate cyclic shear strains

by

Harish Thangavel

Master of Science in Civil Engineering

University of California, Los Angeles, 2019

Professor Mladen Vucetic, Chair

This thesis was undertaken in order to expand upon the study conducted at UCLA by Mortezaie (2012) and Mortezaie and Vucetic (2012) to show that the phenomenon of stiffness increase in saturated sands with the buildup of cyclic pore water pressure, Δu_N, at small cyclic shear strain amplitude, γ_c, as discovered by them is universal. Results of six new single-stage and multi-stage cyclic strain-controlled tests conducted in the NGI type simple shear device and four cyclic strain-controlled and two stress-controlled tests from a previous investigation are analyzed. These tests were conducted at conditions that have not been scrutinized yet, such as different vertical consolidation stresses, σ'_{vc}, and different sequences of γ_c. Amplitude γ_c varied between 0.005% and 0.08% except at the end of two tests when it reached 0.16%.

The study confirmed that below Υ_c=0.1% the stiffness index, $\delta=G_{SN}/G_{S1}$, where G_{SN} is the secant shear modulus at cycle N, increases with N in spite of the continuous buildup of Δu_N and then decreases, and that before G_{SN} drops back to G_{S1} pressure Δu_N may reach 40% of σ'_{vc}. Current liquefaction models assume that δ must go down if Δu_N goes up so the corresponding software can be improved if the above phenomenon is incorporated. The variation of damping ratio, λ, with N was also analyzed and was found consistent with previous findings that λ always decreases with N.

The thesis of Harish Thangavel is approved.

Ertugrul Taciroglu

Jian Zhang

Mladen Vucetic, Committee Chair

University of California, Los Angeles

2019

Table of Contents

List of Figures

Page No.

List of Tables

Page No.

1. Introduction

During earthquakes, traffic vibrations, machine foundation vibrations, ocean wave storms and other dynamic events, waves propagate through soil deposits and the soils are subjected to cyclic loading and deformations. Due to the cyclic deformations, soil structure changes and with it the soil stiffness and strength and some other properties. Such changes affect the wave propagation through soil deposits, bearing capacity and stability of soil deposits and the cyclic movements of the ground surface. Consequently, all of these changes due to the cyclic deformations of soil affect the shaking and stability of supported structures and their study is therefore very important.

If the soils are fully saturated with water (e.g., below the ground water table) and without a possibility or a limited possibility of drainage, the pore water pressure, u, will change during cyclic loading. The pore water pressure will fluctuate in every cycle and increase or decrease with the number of cycles, N, from its initial value. In research and practice, this increase or decrease is typically recorded and/or considered at the end of a given deformation or loading cycle, N, and is called the cyclic pore water pressure change, Δu_N. In fully saturated sands and silts and normally consolidated clays Δu_N will just increase cycle after cycle (e.g., see books by O'Reilly and Brown, 1991; Towhata, 2008). In overconsolidated clays, with a relatively significant overconsolidation ratio, OCR, Δu_N may first decrease and then increase (Andersen et al., 1980; Dobry and Vucetic, 1987, Vucetic, 1988).

In soil mechanics and its subfield soil dynamics, one of the main principles for evaluating soil behavior under loads and deformations that is intimately associated with the pore water pressure change is the effective stress principle. The effective stress principle stipulates that soil behavior under load is fundamentally dependent on the confining normal stresses which are responsible for the forces at soil particle contacts. Higher confining stresses result in larger

forces at particle contacts and therefore larger resistance to restructuring of particles and associated soil distortion, i.e., larger stiffness and resistance to shear deformation and ultimate shear strength. The effective stress principle further stipulates that the confining stress that is effectively affecting the forces transmitted through the particle contacts increases by the value equal to the decrease of the pore water pressure and conversely, decreases by the value equal to the increase of pore water pressure. Figure 1.1 shows the calculation of the initial vertical effective stress at level ground, σ'_{vo}, as the difference between the initial total vertical stress, σ_{vo}, and the initial (hydrostatic) pore water pressure, u_o. If in this situation, due to certain cyclic loading the pore water pressure increases in N cycles by Δu_N, the effective stress at the end of cycle N, $\sigma'_{vN} = \sigma'_{vo} - \Delta u_N$. In other words, according to the effective stress principle the effective stress is reduced by Δu_N.

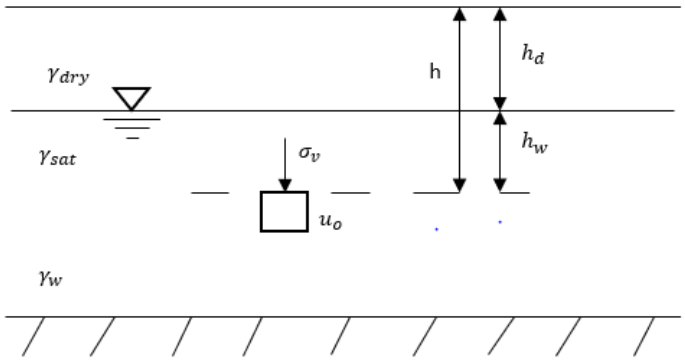

γ_{dry}= dry unit weight (solids only)
γ_{sat} = saturated unit weight (solids + water)
γ_w = unit weight of water
Effective stress = Total stress - Pore water pressure
$\sigma'_{vo} = \sigma_{vo} - u_o$
$\sigma'_{vo} = \gamma_{dry}.h_d + \gamma_{sat}.h_w - \gamma_w.h_w$

Figure 1.1 Effective stress principle applied to vertical stresses at horizontally layered deposit

Consequently, the development of the cyclic pore water pressures has been one of the major subjects and considerations in soil dynamics investigations and practice. This is

particularly true for fully saturated sandy and silty deposits because in sands and nonplastic silts the cyclic pore water pressure changes much faster than in clays. In sandy and such silty soils subjected to cyclic loading and deformations significant pore water pressure can develop in just a few cycles, leading to substantial soil softening. The most extreme practical case is liquefaction of sandy and silty deposits during earthquakes when, due to the cyclic pore water pressure buildup, the consistency of soil transforms from solid to liquid. In fact, the softening of sandy and silty deposits due to the cyclic shearing leading to liquefaction has been so far evaluated by using the cyclic pore water pressure change, Δu_N, as the degradation parameter. That is, as explained below, the cyclic pore water pressure buildup has been used directly as the parameter to calculate the sand's degradation of stiffness and strength.

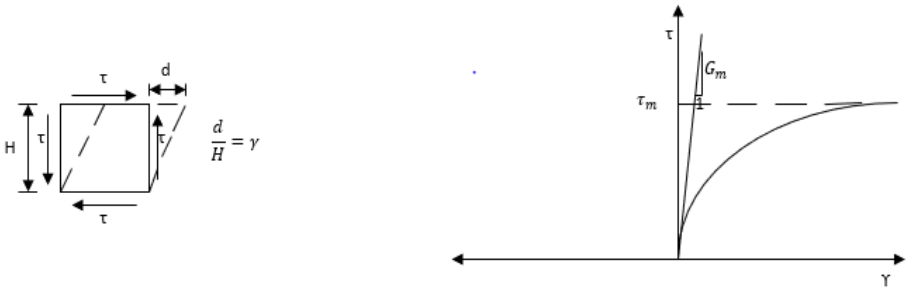

(a) Behavior of soil element due to monotonic shear straining

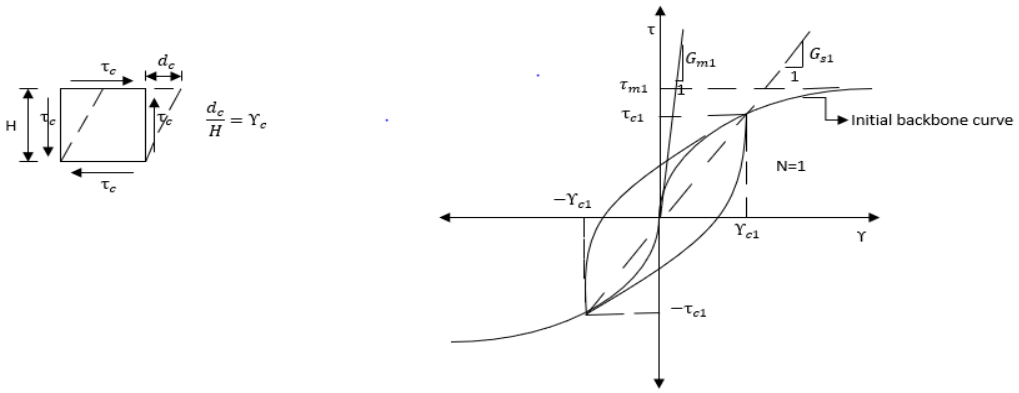

(b) Behavior of soil element due to uniform cyclic shear straining

Figure 1.2 Behavior of soil due to monotonic and uniform cyclic shear straining

In figure 1.2, the behavior of soil element under monotonic and uniform cyclic shear straining is presented. During the monotonic shear straining presented in figure 1.2(a), where Υ is shear strain and τ is shear stress, the initial stiffness is characterized by the initial maximum tangent shear modulus, G_m, while the ultimate maximum shear stiffness is τ_m. The corresponding cyclic shearing of the same soil is presented in figure 1.2(b), where is the cyclic shear strain amplitude in the first cycle, N=1, τ_{c1} is associated cyclic shear stress amplitude at N=1, G_{m1} is the initial (maximum) tangent shear modulus of the initial first cycle curve, while G_{s1} is the secant shear modulus in the first cycle obtained by connecting the tips of the uniform cyclic loop that is therefore equivalent to the slope of the cyclic loop. In general, in this thesis, Υ_c is the cyclic shear strain amplitude, Υ_{cN} is the cyclic shear strain amplitude at cycle N, τ_c is the cyclic shear stress amplitude, τ_{cN} is the cyclic shear stress amplitude at cycle N, while G_{sN} is the secant shear modulus at cycle N. Figure 1.2(b) shows also the, so called, initial backbone curve that is constructed by connecting the tips of uniform cyclic loops obtained for different first cycle amplitudes Υ_{c1} from a series of cyclic tests conducted on the same soil under the same conditions. The positive part of the initial backbone curve corresponding to the first cycle loops is for sand practically identical to the monotonic loading curve in Figure 1.2(a). In practice, the initial backbone curve is therefore very often defined by assuming that the values of τ_m and G_m are the same as τ_{m1} and G_{m1} in Figure 1.2(a). In any case, since the backbone curve is the locus of the tips of the first cycle loops, when known, it can be used to construct the first cyclic loop for any given Υ_{c1}. The construction of the branches of cyclic loop from the initial backbone curve can be done according to the Masing rules (Masing, 1926; Vucetic, 1990; Matasovic and Vucetic, 1993). However, explaining Masing rules and elaborating on how to use them to construct cyclic loops from the backbone curve is beyond the scope of this thesis.

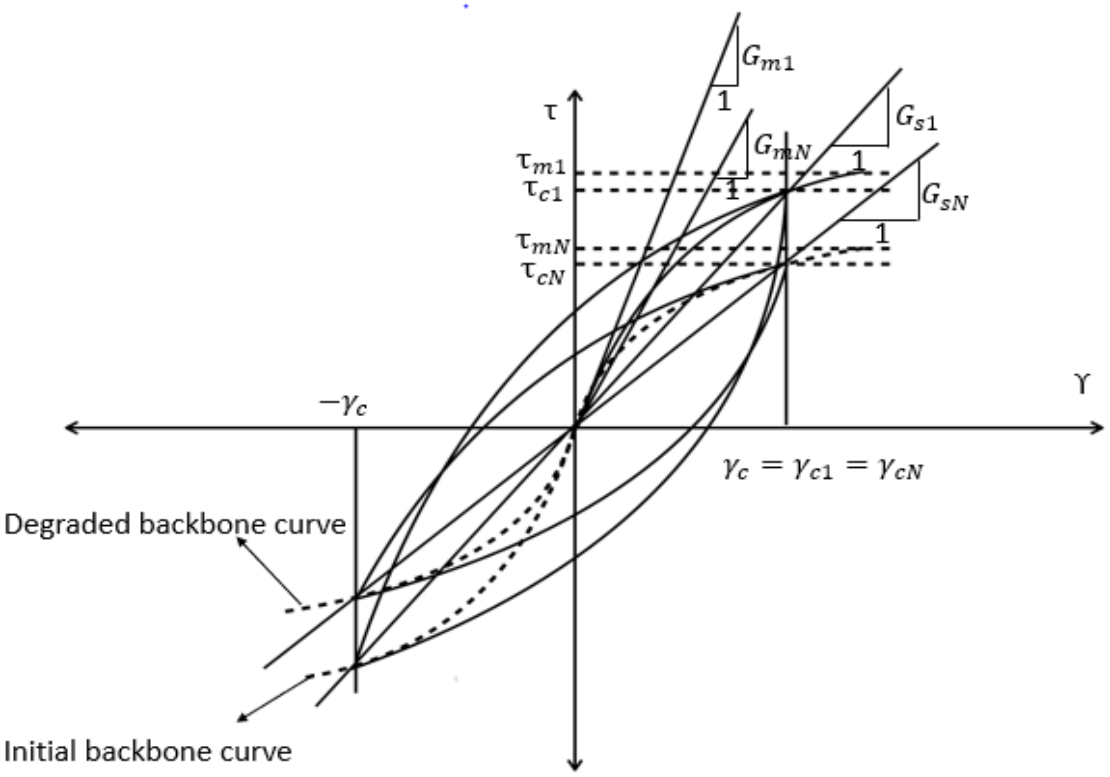

Figure 1.3 Characterization of the behavior in the first cycle (N=1) and subsequent cycle, N

Figure 1.3 shows a typical sketch of two loops from the same uniform cyclic test with constant $\Upsilon_c = \Upsilon_{cN}$ on fully saturated sand, i.e., from a cyclic strain-controlled test, the loop obtained in the first cycle and the loop in cycle N. Prior to cyclic shearing the sand was consolidated to the effective isotropic confining stress σ'_o. The loop in cycle N has smaller secant shear modulus, G_{sN}, because in N cycles the pore water pressure increased by Δu_N and the initial effective isotropic confining stress, σ'_o, decreased accordingly by Δu_N. In other words, at cycle N the effective confining stress is ($\sigma'_o - \Delta u_N$). If at this reduced confining stress, a series of tests at different cyclic shear strain amplitudes is conducted and a corresponding backbone curve is constructed, the degraded backbone curve presented in Figure 1.3 would be obtained, i.e., the backbone curve corresponding to a soil degraded in stiffness and strength due to Δu_N. The popular methods for predicting the degraded backbone curve defined at cycle N by τ_{mN} and G_{mN} from given Δu_N and initial backbone curve having τ_{m1} and G_{m1} employ the

following relationships between the shear strength, initial tangent shear modulus and effective confining stress (see discussion in Matasovic and Vucetic, 1993):

$$\tau_{m_1} = \sigma'_o \cdot tan\emptyset \quad (1)$$

$$\tau_{m_N} = (\sigma'_0 - \Delta u_N)\,.\,tan\emptyset \quad (2)$$

$$\frac{\tau_{m_N}}{\tau_{m_1}} = \frac{(\sigma'_0 - \Delta u_N)\,tan\,\emptyset}{\sigma'_0\,tan\,\emptyset} = 1 - \frac{\Delta u_N}{\sigma'_0} = 1 - \Delta u^*_N \quad (3)$$

$$\tau_{m_N} = \tau_{m_1}(1 - \Delta u^*_N) \quad (4)$$

$$G_{m_1} = f(e)\sqrt{\sigma'_0} \quad (5)$$

$$G_{m_N} = f(e)\sqrt{\sigma'_0 - \Delta u_N} \quad (6)$$

$$\frac{G_{m_N}}{G_{m_1}} = \frac{f(e)\sqrt{\sigma'_0 - \Delta u_N}}{f(e)\sqrt{\sigma'_0}} = \sqrt{1 - \Delta u^*_N} \quad (7)$$

$$G_{m_N} = G_{m_1}\sqrt{1 - \Delta U^*_N} \quad (8)$$

Here, ϕ is the friction angle of the sand, f(e) is a function of void ratio which is essentially constant for the same sandy soil at the same void ratio, e, regardless of the confining stress, and $\Delta u_N^* = \Delta u_N/\sigma'_o$ = normalized cyclic pore water pressure.

Equations 4 and 8 above stipulate that the degrading backbone curve defined by τ_{mN} and G_{mN} can be obtained just from the initial backbone curve and pore water pressure buildup Δu_N, meaning that for practical purposes the soil degrades proportional to the cyclic pore water pressure buildup and subsequent loops can be constructed by knowing just τ_{m1}, G_{m1} and Δu_N. Such considerations and degradation models in equations 4 and 8 are incorporated in popular computer programs for nonlinear analyses of the response of soils to vertically propagating seismic waves, i.e., to the most damaging earthquake motions. They include DESRA-2 (Lee

and Finn, 1978) and its modifications DESRAMOD (Vucetic and Dobry, 1986) and D-MOD (Matasovic and Vucetic, 1993, 1995) and DEEPSOIL (Hashash et al., 2016). In fact, a literature review revealed that publications on liquefaction and pore water pressure buildup leading to liquefaction consider without any restriction the same mechanism of softening, i.e., when pore water pressure buildup occurs, effective confining stress goes down and consequently soil degrades and softens (see books by Ishihara, 1996; Kramer, 1996 and Towhata, 2008; and reports by National Research Council, 1985 and National Academies of Sciences, Engineering and Medicine, 2016).

All of the models and mechanisms mentioned above assume that when the pore water pressure builds up during cyclic loading in saturated sandy soils, the soil necessarily degrades in stiffness and strength. However, recent research by Mortezaie and Vucetic (Mortezaie, 2012; Vucetic and Mortezaie, 2015) revealed that that may not be the case at smaller cyclic shear strain amplitudes. They investigated cyclic behavior of sands in undrained conditions by conducting constant-volume equivalent–undrained cyclic simple shear strain-controlled tests at small cyclic shear strain amplitudes, Υ_c, around the threshold shear strain for cyclic pore water pressure buildup, $\Upsilon_{tp}\approx 0.01\%$. Furthermore, they analyzed cyclic triaxial and simple shear test results obtained in the past in different experimental investigations. Their tests and literature review reveal the following:

"(i) at very small γ_c below γ_{tp} where there is no buildup of cyclic pore water pressure, Δu_N, with the number of cycles, N, the cyclic secant shear modulus, G_{SN}, initially increases with N for 10 to 20% of its initial value G_{S1} and then levels off or just slightly decreases,

(ii) at small γ_c between $\gamma_{tp}\approx 0.01\%$ and 0.10 to 0.15%, Δu_N continuously increases with N while modulus G_{SN} first increases for up to 10% of G_{S1} and then gradually decreases, and

(iii) at γ_c approximately larger than 0.15% relatively large Δu_N develops with N while modulus G_{SN} constantly and significantly decreases.

This means that at γ_c between γ_{tp} and 0.10 to 0.15% the sand stiffness initially increases with N in spite of the reduction of effective stresses caused by the cyclic pore water pressures buildup. In this range of γ_c the pore water pressure Δu_N can reach up to 40% of the initial effective confining stress before G_{SN} drops below G_{S1}."

This is illustrated in Figures 1.4 and 1.5 on an example of cyclic strain-controlled test conducted at Υ_c=0.08%, where the stiffness index, δ_N, that measures the change of the average soil stiffness in a cyclic strain-controlled test is defined as:

$$\delta_N = \frac{G_{SN}}{G_{S1}} = \frac{\tau_{CN} / \gamma_C}{\tau_{C1} / \gamma_C} = \frac{\tau_{CN}}{\tau_{C1}} \tag{9}$$

In these figures and throughout the text σ'_{vc}= effective vertical consolidation stress. This stress is also sometimes denoted throughout the text as σ'_{vo}. That is, σ'_{vc} and σ'_{vo} often have the same meaning.

It should also be noted that, strictly speaking, the Equation 9 is valid only if the cyclic loop is uniform such that the cyclic shear strain amplitudes, Υ_c, in negative and positive domains are the same and the origin of the Υ-τ coordinate system is in the center of the loop. If this is not the case, and very often it is not, the secant shear moduli, G_{SN}, should be calculated by measuring the height of the loop (from τ_c in the negative domain to τ_c in the positive domain) and the width of the loop (from Υ_c in the negative domain to Υ_c in the positive domain) and divide them. In fact, in the present study G_{SN} is determined that way.

Vucetic and Mortezaie (2015) also discussed and concluded the following:

"Such a complex cyclic behavior was obtained for clean sands and silty sands under simple shear and triaxial loading conditions. Same behavior was also obtained on naturally structured intact sand specimens and the specimens reconstituted from fully disturbed sand. It also occurred in the cyclic strain-controlled and cyclic stress-controlled mode of shearing. And furthermore, this behavior was obtained independently in several geotechnical laboratories by different research teams at different times. Such overwhelming evidence shows that this kind of behavior is neither a consequence of laboratory procedure nor the specimen boundary conditions, nor the errors by experimentalists. In conclusion, the above undrained cyclic behavior is intrinsic to fully saturated sands, i.e., such a behavior is a common property of fully saturated sands cyclically sheared under different undrained loading conditions."

The findings by Mortezaie (2012) and Mortezaie and Vucetic (2015) are perhaps summarized the best in Figure 1.6 that presents the results obtained on two sands tested in two different types of tests (cyclic triaxial and cyclic simple shear) at two different laboratories and over a wide range of Υ_c.

However, Mortezaie and Vucetic have not investigated various combinations of consecutive cyclic straining with different levels of Υ_c and tested directly the effect of the confining stress to confirm beyond any doubt that sandy soils also behave as described above under such various conditions. They only discussed and presented the results of the following types of cyclic tests:

- Single stage cyclic strain-controlled simple shear constant-volume equivalent-undrained tests with Υ_c ranging between 0.0045% and 0.47%.
- Just a few single stage cyclic stress-controlled simple shear constant-volume equivalent-undrained tests, some of them not fully processed.

- Multi-stage cyclic strain-controlled simple shear constant-volume equivalent-undrained tests with Υ_c increasing in each subsequent stage.
- Multi-stage cyclic strain-controlled undrained triaxial tests with Υ_c increasing in each subsequent stage.

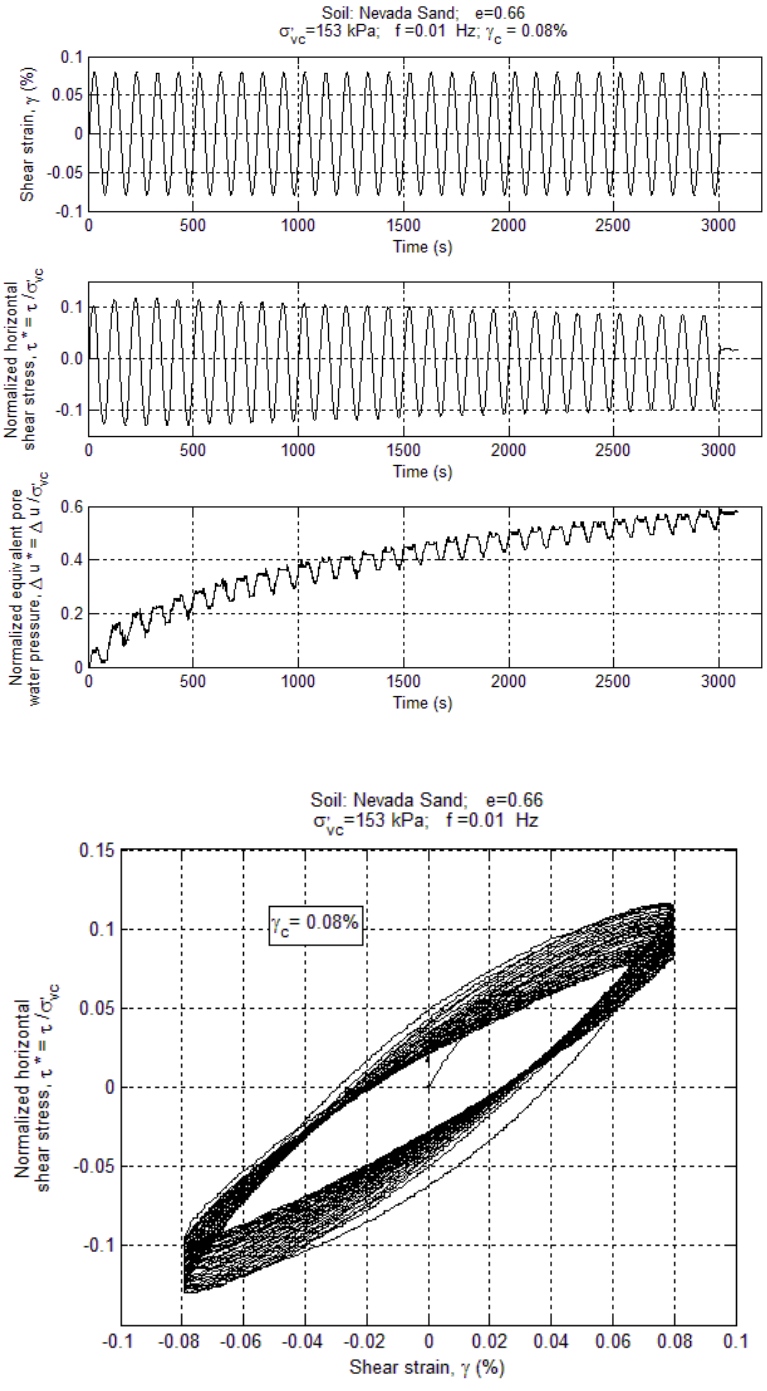

Figure 1.4 Cyclic strain-controlled behavior of sand in undrained conditions in the simple shear test at relatively small cyclic strain Υ_c=0.08% (Vucetic and Mortezaie, 2015)

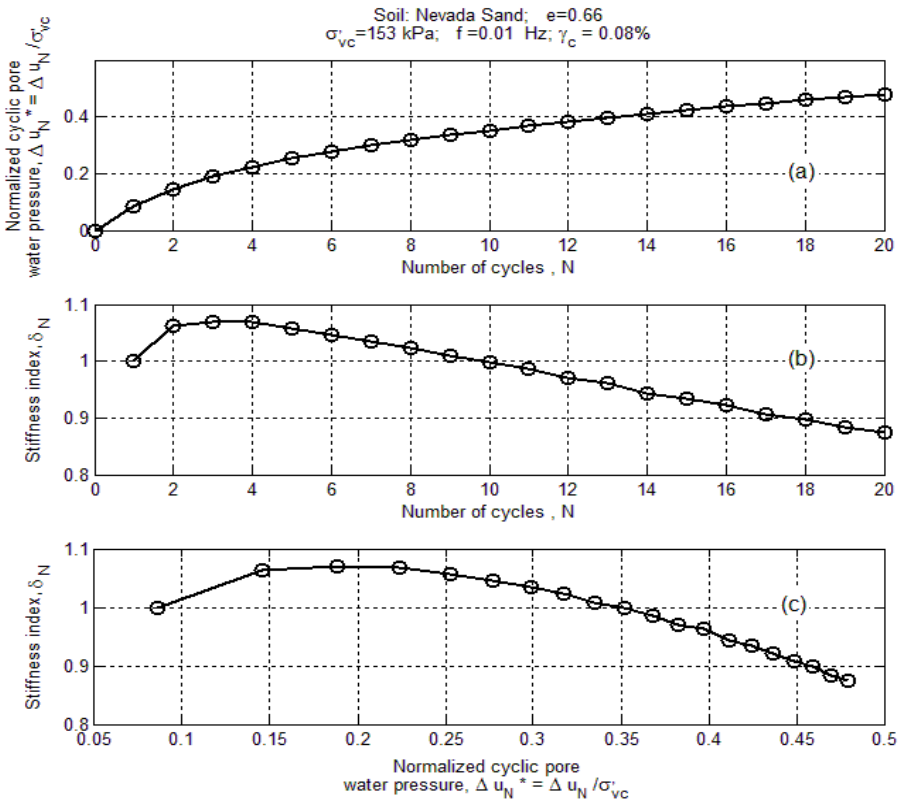

Figure 1.5 Change of the cyclic pore water pressure, Δu_N*, and cyclic stiffness index, δ_N, with the number of cycles, N, at relatively small cyclic strain Υ_c=0.08% in simple shear test and their relationship – derived from results presented in Figure 1.4 (Vucetic and Mortezaie, 2015).

In the present investigation described below the work by Mortezaie and Vucetic is continued and expanded upon by:

(i) testing various additional combinations of consecutive cyclic strains,

(ii) testing behavior during a large number of cycles,

(iii) analyzing test results on several soils conducted by Mortezaie and Vucetic but not fully processed,

(iv) testing the same soil at different consolidation stresses, and

(v) testing same soil in constant-volume equivalent–undrained cyclic NGI DSS tests in dry and saturated states.

Such an investigation is deemed necessary because of the fundamental nature of the above newly discovered behavior of saturated sands. As shown in this thesis, the results of the present investigation confirm that the same behavior occurs at various combinations of small cyclic strains and stresses, at different consolidation stresses, and in dry and saturated sands. Accordingly, the results in this thesis and those by Mortezaie and Vucetic should be used to improve the cyclic behavior models in Equations 4 and 8. Such improvements can make the analyses of the seismic response of liquefaction sites more accurate.

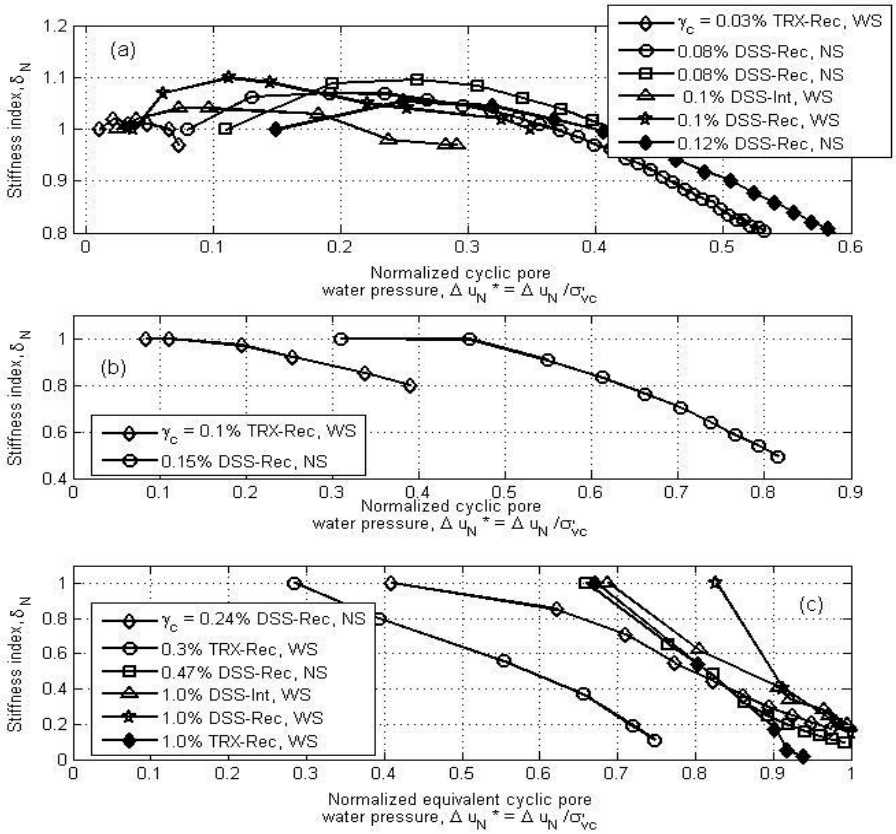

Fig. 1.6 Relationships between the stiffness index, δ_N, and the normalized cyclic pore water pressure, Δu_N*, for the Wildlife Site silty sand and Nevada clean sand – the results are obtained from the cyclic strain-controlled undrained triaxial tests and the cyclic strain-controlled constant-volume equivalent–undrained NGI-DSS cyclic tests (Vucetic and Mortezaie, 2015)

2. Scope of the present testing and analyses of a previous investigation

The work done for this thesis looks to expand upon the work done by Mortezaie and Vucetic and looks to prove that the phenomenon where fully saturated soil stiffens while the pore water pressure increases at smaller cyclic shear strains is universal. Mortezaie and Vucetic mainly studied single-stage cyclic strain-controlled tests and the multi-stage cyclic strain-controlled tests with combinations of cyclic strains that increased in each stage. In their cyclic strain-controlled multi-stage tests they started with cyclic strain amplitudes that were below the cyclic threshold shear strain and then just increased the amplitudes in subsequent stages. They also analyzed just one cyclic stress-controlled test. Furthermore, they did not analyze tests with a large number of cycles. Also, analyses of their testing focused almost exclusively on just one sand, Nevada Sand, although they conducted tests on two more sands, Red Course Sand and Toyoura Sand. However, they analyzed and presented results on several different sands published by others.

In the present research the results of the constant-volume equivalent–undrained cyclic NGI DSS tests obtained for the following situations that were not considered before are analyzed:

(i) one single-stage and two two–stage cyclic strain-controlled tests with a large number of cycles,

(ii) several multi-stage cyclic strain-controlled tests with different combinations of subsequent cyclic strain amplitudes, notably the combination where amplitudes decrease stage after stage,

(iii) a couple of test on the same soil at the same cyclic shear strain but at very different consolidation stresses,

(iv) a couple of identical tests on the same dry and saturated soil, and

(v) the analyses of the previously obtained results on Red Course Sand and Toyoura Sand.

The work presented in this thesis is divided into two parts. The first part includes the analyses of new cyclic simple shear tests and the second part includes the analyses of the tests conducted by Mortezaie and Vucetic that have not been fully analyzed. Table 2.1 shows the new tests that were conducted as a part of this thesis. Table 2.2 shows the tests that were conducted by Mortezaie and Vucetic and now analyzed in this thesis. The tables below describe the test conditions which include the cyclic shear strain amplitude, Υ_c, vertical stress at the beginning of each cyclic stage, σ'_{vo}, also denoted by σ'_{vc}, void ratio of the specimen, e, and the number of cycles run in each stage, N.

As shown in Table 2.1, six different tests were conducted in the present investigation. They were one single-stage test (Test 1) with a large number of cycles (N=200) and five multi-stage cyclic strain-controlled tests (Test 2 through 6). All of these tests were conducted on Nevada Sand. The cyclic shear strain amplitude was decreased in subsequent stages of the multi stage tests except for Tests 2 and 3. In Tests 2 and 3 the subsequent, second stage had the same cyclic shear strain amplitude as the previous stage but the vertical stress was significantly increased and the number of cycles in both stages was rather large. These two tests were conducted to study the effects of the vertical stress and large number of cycles on the phenomenon. Furthermore, Tests 1, 4 and 6 were conducted in the constant-volume equivalent-undrained mode on dry sand, while Tests 2, 3 and 5 were conducted on saturated sand. In this way the difference in the behavior in constant-volume tests due to the presence of water and saturation could be examined.

As shown in Table 2.2, six different tests were taken from the investigation by Mortezaie and Vucetic and are here fully analyzed or processed. These tests include two single-stage

cyclic stress-controlled tests (Tests 11 and 12) and four multi-stage cyclic strain-controlled tests (Tests 7 through 10). Tests 7 and 8 are conducted on Nevada sand, while Tests 9 and 10 on Toyoura Sand and Red Coarse Sand respectively. It should be noted that all of the tests in Table 2.2 were conducted on dry sand specimens. Also, it should be noted that all of the multi-stage tests of the previous investigation were conducted without any reconsolidation between subsequent stages, i.e., there was a continuous pore water pressure buildup from stage to stage. In contrast to that, in the tests conducted in this thesis there was reconsolidation between the cyclic stages.

In conclusion, the combination of the results already presented by Mortezaie and Vucetic and the new results analyzed in this thesis provides ample evidence of the cyclic behavior of sands in true undrained conditions and the constant-volume equivalent–undrained conditions at smaller cyclic strains. If all of these small-strain cyclic tests show that there is an increase in soil stiffness during the cyclic straining while the cyclic pore water pressure increases and the corresponding effective stress decreases, this phenomenon may be considered universal and applicable to all sands under various small-strain cyclic loading undrained conditions.

Table 2.1 Present single-stage and multi-stage constant-volume equivalent-undrained simple shear cyclic strain-controlled tests conducted

Test	Soil	Dry or saturated	Strain or Stress Controlled	Stage 1	Stage 2	Stage 3	Stage 4	Stage 5	Stage 6	Comments
				Amplitude, γ_c	Amplitude, γ_c	Amplitude, γ_c	Amplitude, γ_c	Amplitude, γ_c	Amplitude, γ_c	
				Vertical stress, σ'_{vo} (kPa)	Vertical stress, σ'_{vo} (kPa)	Vertical stress, σ'_{vo} (kPa)	Vertical stress, σ'_{vo} (kPa)	Vertical stress, σ'_{vo} (kPa)	Vertical stress, σ'_{vo} (kPa)	
				e	e	e	e	e	e	
				N	N	N	N	N	N	
1	Nevada Sand	Dry	Strain-controlled	0.06%						
				150 kPa						
				0.43						
				200						
2	Nevada Sand	Saturated	Strain-controlled	0.04%	0.04%					The specimen was reconsolidated after every stage. In that respect, each stage can be considered a separate test.
				150 kPa	300 kPa					
				0.47	0.48					
				255	395					
3	Nevada Sand	Saturated	Strain-controlled	0.06%	0.06%					The specimen was reconsolidated after every stage. In that respect, each stage can be considered a separate test.
				150 kPa	300 kPa					
				0.48	0.46					
				200	330					
4	Nevada Sand	Dry	Strain-controlled	0.08%	0.08%	0.04%	0.02%	0.01%	0.005%	(a) The specimen was reconsolidated after every stage. In that respect, each stage was a separate cyclic test.

				145 kPa	145 kPa	145 kPa	145 kPa	145 kPa	145 kPa	However, the reconsolidation was at locked-in zero shear strain and residual shear stress from the previous stage (the residual stress that apparently has not relaxed between the stages). (b) The top cap was not secured by clamps. There was possibility of slippage between top cap and the plate above, but most likely it did not happen. This was confirmed in the first stage of Test 6 that was conducted under the same conditions with secured cap.
				0.806	0.803	0.802	0.801	0.801	0.801	
				10	10	10	10	10	10	
5	Nevada Sand	Saturated	Strain-controlled	0.08%	0.08%	0.04%	0.02%	0.01%	0.005%	Same as Test 4 but saturated. The specimen was reconsolidated after every stage. In that respect, each stage can be considered a separate test.
				145 kPa	145 kPa	145 kPa	145 kPa	145 kPa	145 kPa	
				0.774	0.771	0.771	0.771	0.771	0.771	
				10	10	10	10	10	10	
6	Nevada Sand	Dry	Strain-controlled	0.08% (Same conditions as in Stage 1 of Test 4)	0.04%	0.02%	0.01%	0.005%		After Stage 1, specimen was reconsolidated. Stages 2 to 5 were conducted without reconsolidation between the Stages. In that respect, Stage 1 can be considered one separate cyclic test and Stages 2 to 5 another separate cyclic test. However, the reconsolidation was at locked-in zero shear strain and residual stress from the previous stage (the residual stress that apparently has not relaxed between the stages).
				150 kPa	150 kPa	117 kPa	115 kPa	114 kPa		
				0.641	0.64	0.64	0.64	0.64		
				10	10	10	10	10		

Table 2.2 Previous single-stage and multi-stage constant-volume equivalent-undrained simple shear cyclic strain-controlled and stress-controlled tests conducted by Mortezaie and Vucetic

Test	Soil	Dry or saturated	Strain or Stress Controlled	Stage 1	Stage 2	Stage 3	Stage 4	Stage 5	Stage 6	Stage 7	Comments
				Amplitude, γ_c	Amplitude, γ_c	Amplitude, γ_c	Amplitude, γ_c	Amplitude, γ_c	Amplitude, γ_c	Amplitude, γ_c	
				Vertical stress, σ'_{vo} (kPa)	Vertical stress, σ'_{vo} (kPa)	Vertical stress, σ'_{vo} (kPa)	Vertical stress, σ'_{vo} (kPa)	Vertical stress, σ'_{vo} (kPa)	Vertical stress, σ'_{vo} (kPa)	Vertical stress, σ'_{vo} (kPa)	
				e	e	e	e	e	e	e	
				N	N	N	N	N	N	N	
7	Nevada Sand	Dry	Strain-controlled	0.0031%	0.0065%	0.0103%	0.021%	0.041%	0.082%	0.16%	There was no reconsolidation between the stages.
				220 kPa	220 kPa	220 kPa	217 kPa	207 kPa	178 kPa	126 kPa	
				0.63	0.63	0.63	0.63	0.63	0.63	0.63	
				10	10	10	10	10	10	10	
8	Nevada Sand	Dry	Strain-controlled	0.080%	0.02%	0.03%					There was no reconsolidation between the stages.
				145 kPa	75 kPa	73.5 kPa					
				0.63	0.63	0.63					
				10	10	14					
9	Toyoura sand	Dry	Strain-controlled	0.004%	0.008%	0.015%	0.031%	0.077%			There was no reconsolidation between the stages.
				146 kPa	139 kPa	135.5 kPa	127.5 kPa	101.5 kPa			
				0.71	0.71	0.71	0.71	0.71			
				10	10	10	20	20			
10	Red coarse sand	Dry	Strain-controlled	0.0041%	0.008%	0.016%	0.032%	0.080%			There was no reconsolidation between the stages.
				152 kPa	149 kPa	145 kPa	134 kPa	89 kPa			
				0.63	0.63	0.63	0.63	0.63			
				10	10	10	20	20			

11	Nevada Sand	Dry	Stress-controlled	τ_c=0.08 σ'_{vc}	Uniform cyclic stress amplitude						
				156.5 kPa							
				0.6							
				30							
12	Nevada Sand	Dry	Stress-controlled	τ_c=0.1 σ'_{vc}	Uniform cyclic stress amplitude						
				162 kPa							
				0.63							
				27							

3. Materials tested and analyzed

Three different sands were tested and analyzed in the present investigation. They are:

- Nevada sand
- Toyoura sand
- Red coarse sand

Their grain size distributions are shown in Figure 3.1 and their classifications according to the Unified Soil Classification System (USCS) in Table 3.1.

Nevada sand has been used widely in various investigations (e.g., Arulanandan et al., 1994; Hsu and Vucetic, 2002). Toyoura sand is found in Japan and Japanese researchers have used it extensively for their research (e.g., Ishihara 1996). Red coarse sand was used for this research because the other two sands, Nevada sand and Toyoura sand, are fine grained sands whereas Red coarse sand contains larger particles and is much coarser.

The coefficient of uniformity $Cu=D_{60}/D_{10}$ and the coefficient of curvature $Cc=D_{30}^2/(D_{10}*D_{60})$ are calculated for each sand from the grain size distributions shown in Figure 3.1. All three sands are classified as poorly graded sands, with classification symbol SP.

Table 3.1 Classification of the three sands tested in this investigation

Sand	**D_{10}**	**D_{30}**	**D_{60}**	**Cu**	**Cc**	**Classification**
Nevada sand	0.11	0.17	0.21	1.91	1.25	SP
Toyoura sand	0.13	0.18	0.23	1.77	1.08	SP
Red coarse sand	0.43	0.85	1.1	2.56	1.53	SP

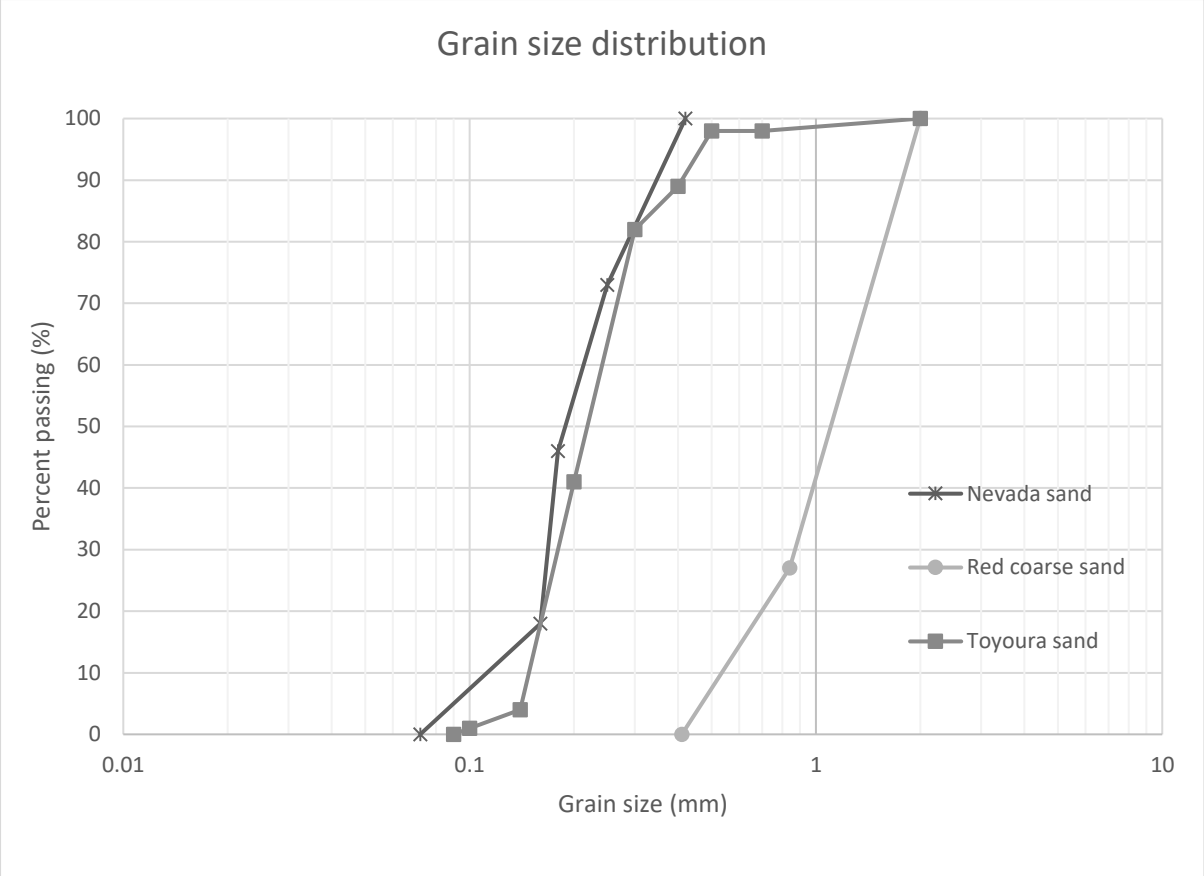

Figure 3.1 Grain size distribution curve for the three sands tested

4. Description of testing device

The Norwegian Geotechnical Institute direct simple shear (NGI-DSS) device was used to conduct the tests for this thesis. The device is shown in Figure 4.1. The NGI-DSS device was originally introduced by Bjerrum and Landva (1966) for monotonic loading testing and was later modified in a number of laboratories for cyclic testing. The NGI-DSS specimen is a short cylinder of soil placed between the top and bottom porous stones embedded in metal caps and surrounded by the wire-reinforced rubber membrane. During consolidation and shearing the reinforced membrane almost completely prevents radial strains so that the specimen is consolidated at essentially K_o condition and cyclically sheared under practically no-lateral-strains condition. The specimens were prepared by the method of air-pluviation of

air dry sand. The bottom cap with porous stone was first fastened to a pedestal and the bottom part of the membrane was pulled on it with the help of a vacuum membrane stretcher. Appropriate amount of sand was then rained through a custom-made sieve into the membrane. After the completion of the air-pluviation the top cap with porous stone was placed on the sand surface, membrane was flipped around it, vacuum was released and the membrane edges tightly surrounded both caps with porous stones. The whole setup was then mounted in the NGI DSS device frame where the specimen was first consolidated, then saturated with water if that is required and then cyclically sheared.

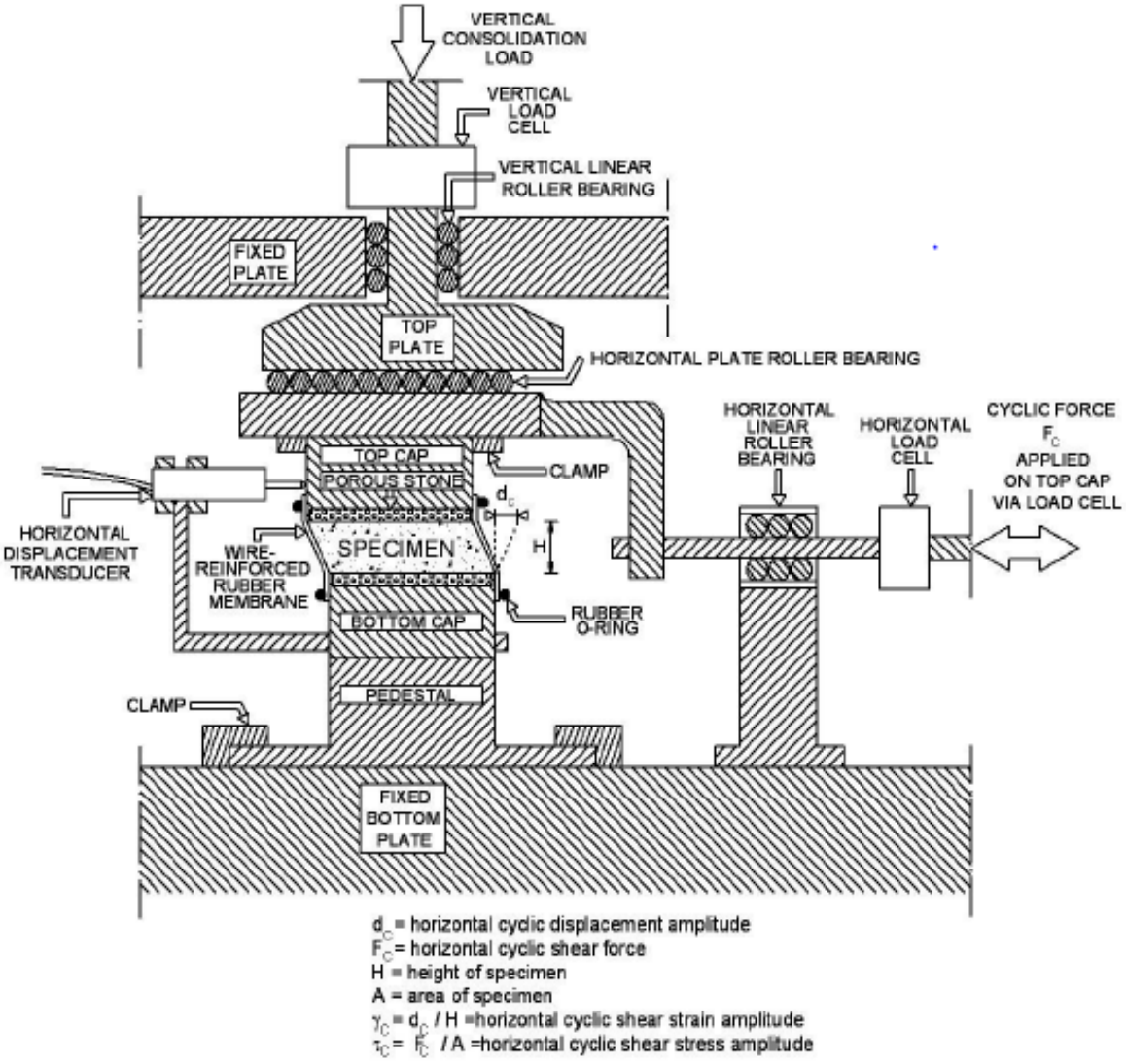

Figure 4.1 Specimen setup in the NGI-DSS device

Typical tests in the NGI DSS device are constant-volume equivalent-undrained tests. The undrained conditions are simulated by maintaining the volume of the specimen constant during the shearing, just like it is in a truly undrained test, while the actual pore water pressure is zero. Assuming that the radial strains of the specimen are practically zero due to the membrane confinement, the volume can be maintained constant by just keeping the height of the specimen constant. To maintain the constant height during the shearing the vertical stress must be changed and this change of the vertical stress is equivalent to the pore water pressure that would have developed in a truly undrained test. That is why the pore water pressure change in such a test is also called the equivalent pore water pressure.

The NGI-DSS device used in this study is equipped with the computer-controlled closed-loop servo-hydraulic loading system and a modern data acquisition system. In all tests the constant cyclic shear strain amplitude, Υ_c, was applied in sinusoidal mode, while the variations of the shear stress, τ, and the equivalent pore water pressures, Δu, were recorded with time.

In most of the tests the frequency of cyclic straining was f=0.01 Hz but in some tests, it was f=0.1 and f=0.2. Such a relatively low frequency was applied to better facilitate the application and recording of the test parameters during sensitive small-strain cyclic testing, with understanding that in many practical problems the effects of frequency on sand cyclic behavior are relatively small.

Since the NGI-DSS device was originally designed for the classical soil mechanics problems involving medium and large strains, it is not suitable for the small-strain cyclic testing due to the false loads recorded along with the loads applied to soil specimen. In other words, it is not suitable because of the inherent false displacements and forces which are picked up by the displacement transducers and load cells but are not experienced by the soil specimen. That is, it is not suitable unless the false displacements and forces are extracted from the recorded

raw data. Such correction of the cyclic strain-controlled raw data was performed earlier by Mortezaie and Vucetic (2012) and it is repeated in this investigation.

Horizontal displacements between the bottom and top faces of the specimen required to obtain shear strain can be measured accurately with the horizontal displacement transducer bridged directly between the bottom and top specimen caps, which was done in this investigation. In this case, the horizontal false deformations consist only of the shear deformations of the porous stones and the bottom and top caps which are made of brass. Since these deformations are truly negligible in comparison to those of the soil, they do not have to be taken into account.

As opposed to that, the false loads recorded by the horizontal load cell are relatively large in comparison to loads applied to soil and the appropriate corrections must be made. According to Figure 4.1, besides the shear resistance of the soil specimen the horizontal load cell detects the following:

- Shear resistance of the wire-reinforced rubber membrane.
- Force applied by the probe of the displacement transducer on the top cap (force of the spring in the transducer).
- Friction of the horizontal linear roller bearing.
- Friction of the horizontal plate roller bearing.

The method used to correct the data for the above false loads is described in the following chapter.

5. Procedures for the correction of cyclic test results

The test results obtained in two direct simple shear devices (DSS devices) on similar soils, one that has no false loads and the other that has them, are presented in Figures 5.1 and 5.2 respectively. By comparing these results, it can be observed what the effects of the false loads on the stress-strain behavior are. In Figure 5.1 are the results of a small-strain cyclic test on low-plasticity clay having the plasticity index, PI=26, that was conducted in the DSS device designed by Doroudian and Vucetic (1995) that has practically no false loads. This device is called the dual-specimen direct simple shear device (DS-DSS device) because it employs two specimens in a single test instead of just one. The shape of cyclic straining obtained in this device, and consequently that of cyclic stresses, was close to triangular with rather sharp peaks of the cyclic strain-time and stress-time histories. The tips of the loops are also sharp. In Figure 5.2 are the results of a DSS test on kaolinite clay having PI=28 conducted in the standard NGI-DSS device that has false loads already described above. The test includes triangular and sinusoidal cyclic straining phases and regardless of the shape of straining the results exhibit large rounded tips of the loops. Both tests, DS-DSS and NGI-DSS, had rather small cyclic shear strain amplitude, Υ_c, around 0.035%.

In Figure 5.1, the stress continually increases and after reversal instantly decreases with strain which results in perfectly pointed tips of the stress-strain loops. In Figure 5.2, after the strain reversal in the case of triangular straining there is a sudden drop in stress denoted by $\Delta\tau_f$, while the tips of the loops are rather square. The same stress drop occurs in the case of the sinusoidal straining and the tips of the loops are again rather square. Evidently, due to the false loads the tips of the loops that are supposed to be pointed are now quite large and square shaped. The drop $\Delta\tau_f$ is the false stress caused by the reversal of the friction forces of the horizontal plate bearing and linear bearing that are activated during the shearing. When the specimen top cap changes the direction at the strain-reversal, the direction of these friction forces changes

too. Consequently, the magnitude of $\Delta\tau_f$ is twice the stress corresponding to the sum of these two friction forces. During the shear loading phase when the movement of the top cap is to the left, both roller bearings are resisting the motion which is recorded by the horizontal load cell as compression. This compression corresponds to approximately half of $\Delta\tau_f$. During the shearing unloading phase when the movement of the top cap is to the right, both roller bearings are again resisting the motion which is now recorded by the load cell as extension. This extension load corresponds approximately to the other half of $\Delta\tau_f$.

The procedure for correcting such data from the strain-controlled tests has been explained before by Mortezaie and Vucetic (2012) and will be just summarized here, whereas the procedure for correcting the stress-controlled tests will be explained in detail for the first time.

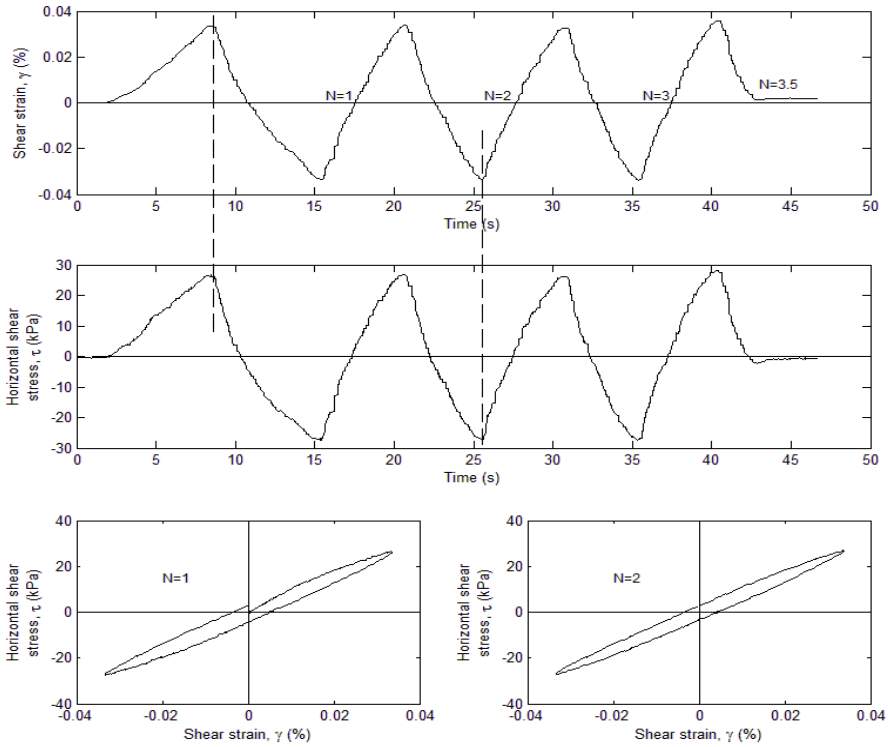

Figure 5.1 Records from a test conducted in the DS-DSS device on low-plasticity clay having PI=26 and consolidated to σ'_{vc}=390 kPa (from Vucetic et. al., 1999)

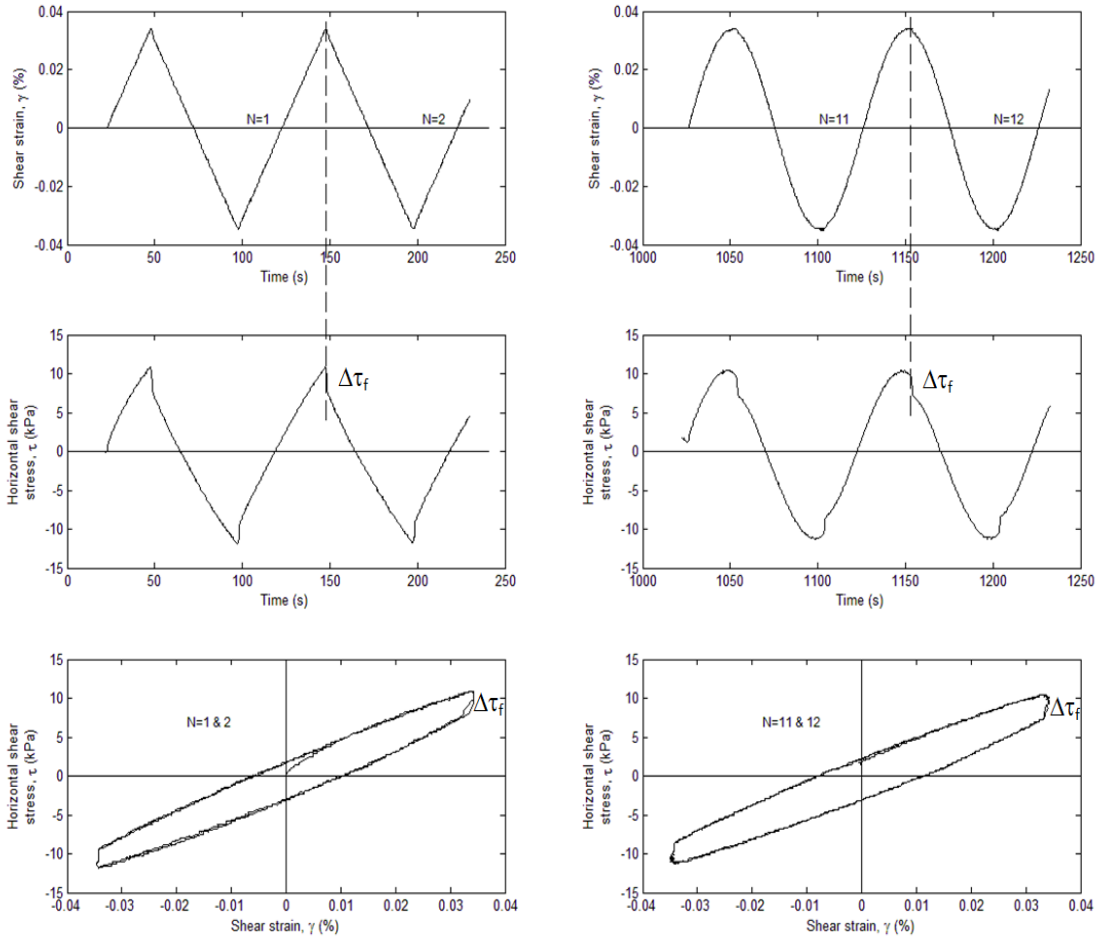

Figure 5.2 Records from a test conducted in the NGI-DSS device on clay having PI=28 and consolidated to σ'_{vc}=148kPa (Mortezaie and Vucetic, 2012)

5.1 Procedure for correcting strain-controlled test records

The procedure for correcting the strain-controlled test records such as those presented in Figure 5.2 and the strain-controlled test records obtained in this investigation developed by Mortezaie and Vucetic (2012) neglects the false load from the shear resistance of the wire-reinforced rubber membrane and the force applied by the probe of the displacement transducer on the top cap. These two forces are negligible small in comparison to the soil shear resistance. Accordingly, the procedure takes into consideration only the false loads from the friction of the horizontal linear roller bearing and horizontal plate roller bearing. The procedure is illustrated in Figures 5.3 through 5.6.

The figures show cyclic test results obtained on kaolinite clay having PI=28 and classified as MH. The clay was consolidated under σ'_{vc}=148 kPa and cycled in sinusoidal mode at Υ_c=0.035% at the frequency of f=0.01 Hz. Figure 5.3 shows the stress drops in the stress-time history curve for one cycle. Two consecutive stress drops, $\Delta\tau_f$, are shown in Figure 5.4 in much larger scale so that their magnitude can be measured manually. In this particular case the stress drops are $(\Delta\tau_f)_b$=2.1 kPa and $(\Delta\tau_f)_c$=1.9 kPa. Knowing these values, the stress record can now be corrected for $(\Delta\tau_f/2)$ between each two consecutive strain reversals. Between the reversal points *a* and *b*, the false stress $[(\Delta\tau_f)_b/2]$ must be added, and between the points *b* and *c* the stress $[(\Delta\tau_f)_c/2]$ must be subtracted. The result of such correction is displayed in Figure 5.5, showing that such a procedure yields almost perfectly smooth stress-time history. Figure 5.6 shows the difference in the stress-strain loops between the corrected and uncorrected data, where the corrected loop has a regular and proper shape. It should be noted that this procedure contains a slight error because $(\Delta\tau_f)_b$ and $(\Delta\tau_f)_c$ are not exactly the same. However, two consecutive drops are always very similar, similar enough that the resulting error can be neglected.

The procedure looks simple and easy and can be implemented manually when it is applied to a few cycles. However, for tests with many cycles manual procedure is not feasible because it is extremely time-consuming. Consequently, the procedure has been automated by coding it with the Matlab software. The resulting code, which is rather elaborate, is described in the PhD thesis by Mortezaie (2012). The code includes automatic and precise identification of the points on the stress-time history where the stress drop starts and ends, yielding a precise measure of $\Delta\tau_f$. It should be noted that in Figures 5.3 and 5.4 $\Delta\tau_f$ drop does not occur instantaneously at the strain reversal but gradually over a short period of time, because reversal of the friction of

real roller bearings is rather complex. The Matlab code automatically and correctly captures this process. The code also includes calculation of damping and some other features.

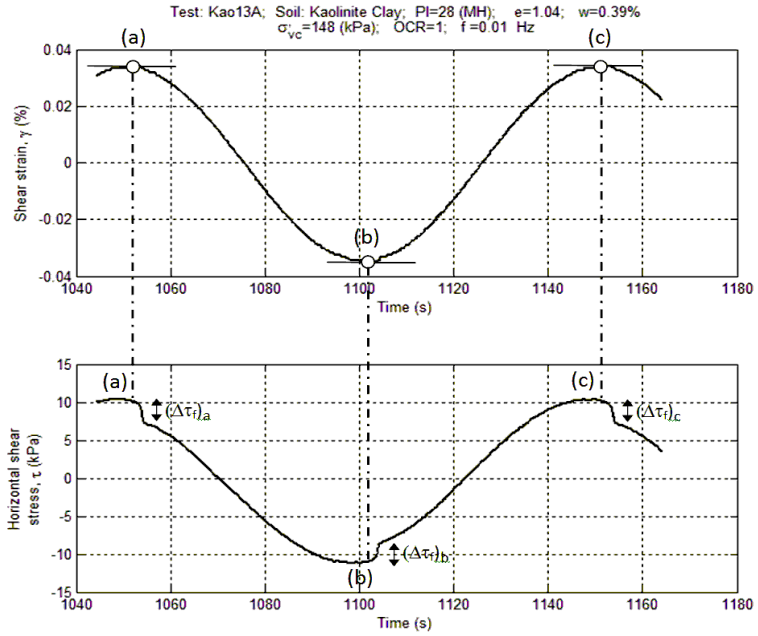

Figure 5.3. Uncorrected strain-time and stress-time histories during one cycle of sinusoidal straining on kaolinite clay taken from Mortezaie and Vucetic (2012)

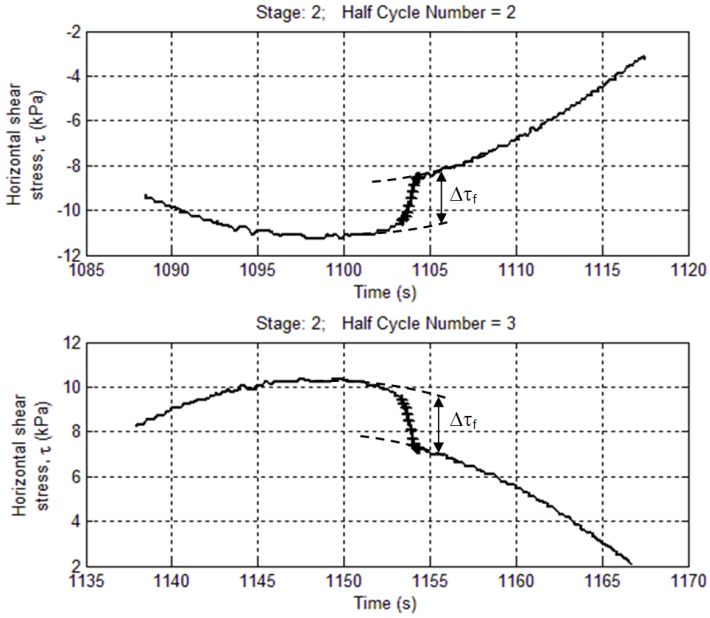

Figure 5.4 Identification and quantification of the false stresses, $\Delta\tau_f$, at two consecutive strain reversals taken from Mortezaie and Vucetic (2012)

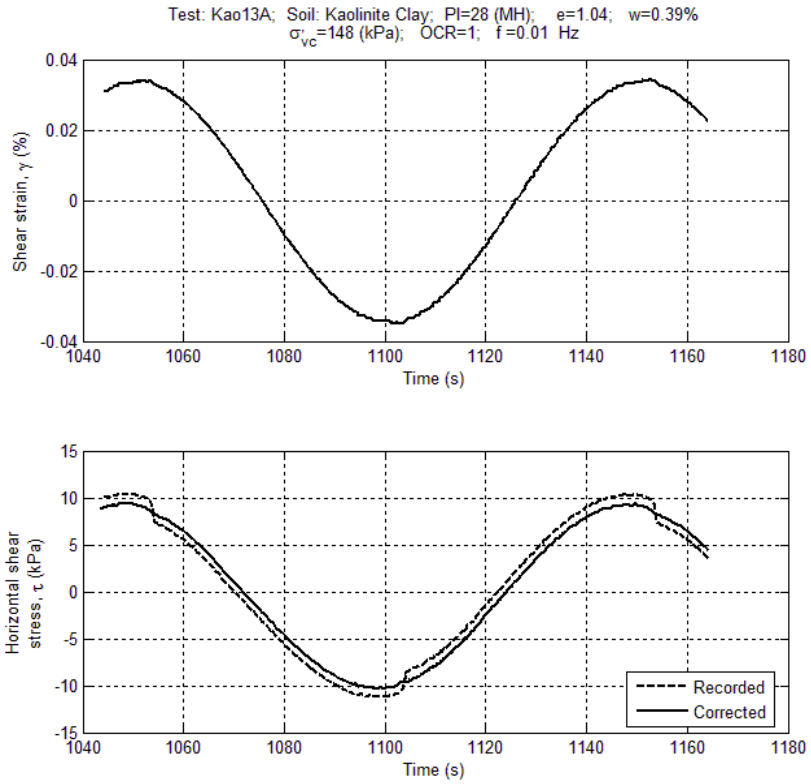

Figure 5.5 Strain-time history and the uncorrected (dashed line) and corrected (solid line) stress-time histories taken from Mortezaie and Vucetic (2012)

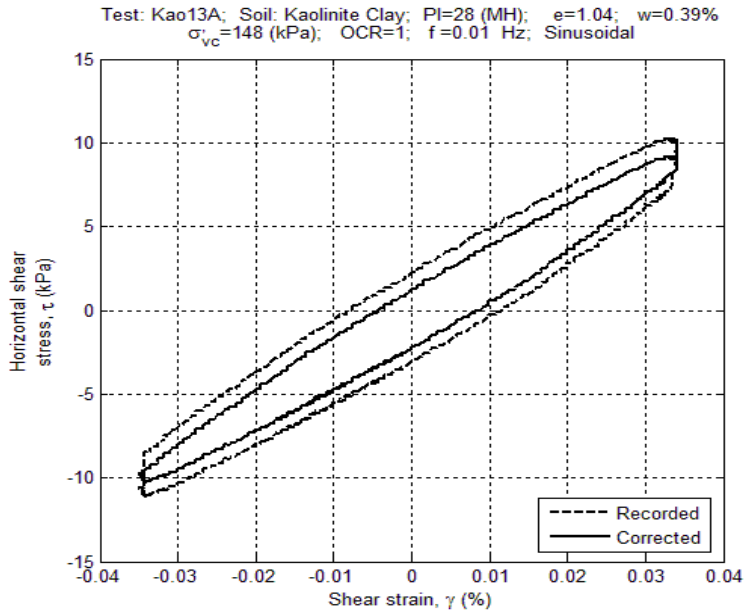

Figure 5.6 Corrected (solid line) and uncorrected (dashed line) stress-strain loops for sinusoidal straining of kaolinite clay taken from Mortezaie and Vucetic (2012)

5.2 Procedure for correcting stress-controlled test records

The procedure for correcting the data from the stress-controlled tests is somewhat different than the procedure used to correct the strain-controlled test data. Figure 5.7 shows strain-time and stress-time histories from a record of just one cycle from a stress-controlled test conducted on Nevada sand in the NGI-DSS device. From the figure it is evident that the stress-time curve is perfectly sinusoidal just as applied by the computer-controlled loading system. On the other hand, the strain-time history curve becomes flat at the maximum and minimum strain levels, starting at the peaks of the shear stress curve, i.e., from points a to b and points c to d. The strain is apparently constant during these time periods because during these periods the false loads are changing direction. The stress between a and b and c and d is due to the friction in the testing system and is thus denoted as $\Delta\tau_f$. This stress increment is equivalent to $\Delta\tau_f$ at the strain reversal in the strain-controlled test presented in Figure 5.4, except that now it happens gradually over a period of time. The soil does not actually experience that stress. This is stress from false loads that needs to be corrected.

The procedure to correct the data corresponding to this false stress is as follows:

- The stress curves from point a to b and point c to d should be completely removed.
- The half of the false stress, $(\Delta\tau_f/2)$ should be added to the stress after point b till point c.
- The other half of the false stress $(\Delta\tau_f/2)$ should be subtracted from the stress after point d till the next strain reversal point.
- The empty sections between points a and b and points c and d should then be horizontally connected.

The above steps should be repeated for each cycle in order to correct the entire test record for false loads. Figure 5.8 shows one cycle of the corrected and uncorrected stress for a test

shown in Figure 5.7. Figure 5.9 shows the difference in the stress-strain loops between the corrected and uncorrected data. Now the corrected loop has sharp tips as should be expected for sand tested and the area of the loop and corresponding damping ratio have the values expected for achieved Υ_c. As the soil stiffness and confining stress change during cyclic loading the stress drop, $\Delta\tau_f$, differs slightly from strain reversal to strain reversal.

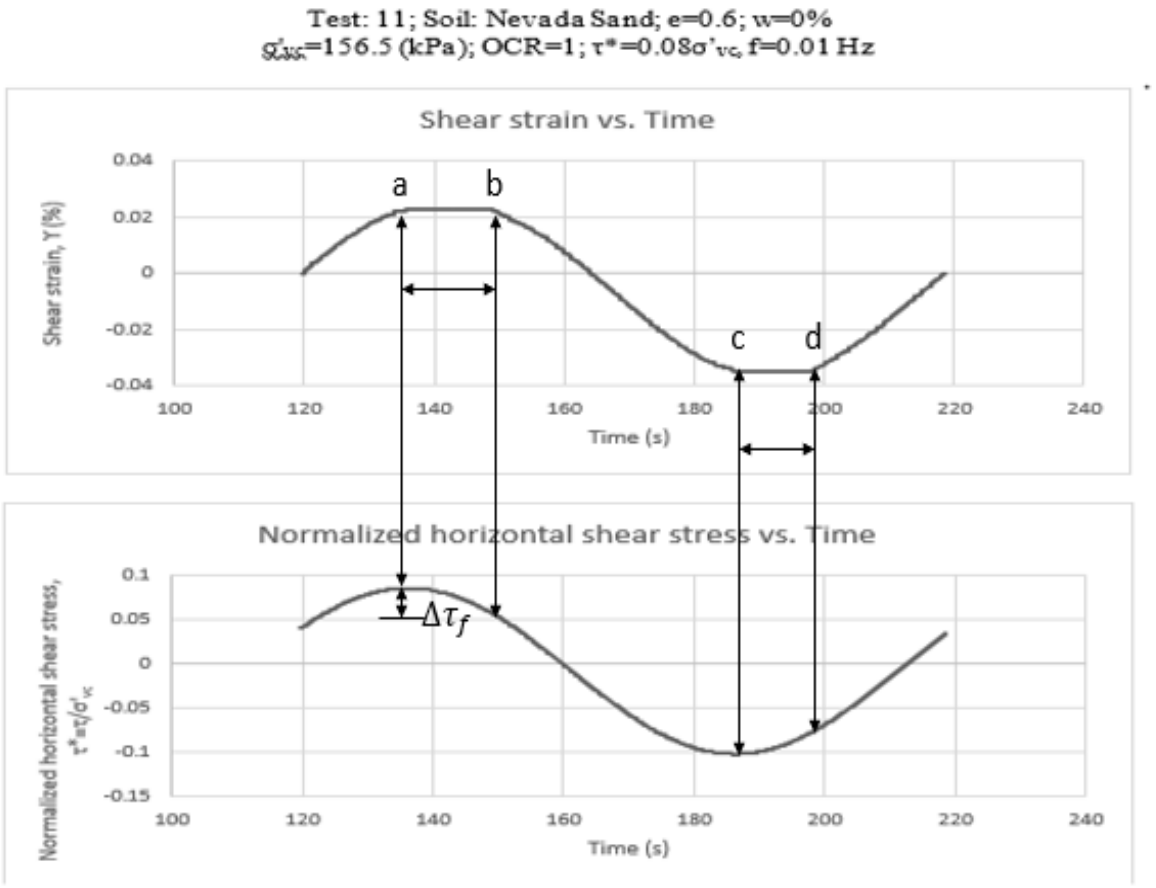

Figure 5.7 Uncorrected record of one cycle of strain and stress-time history of a stress-controlled test

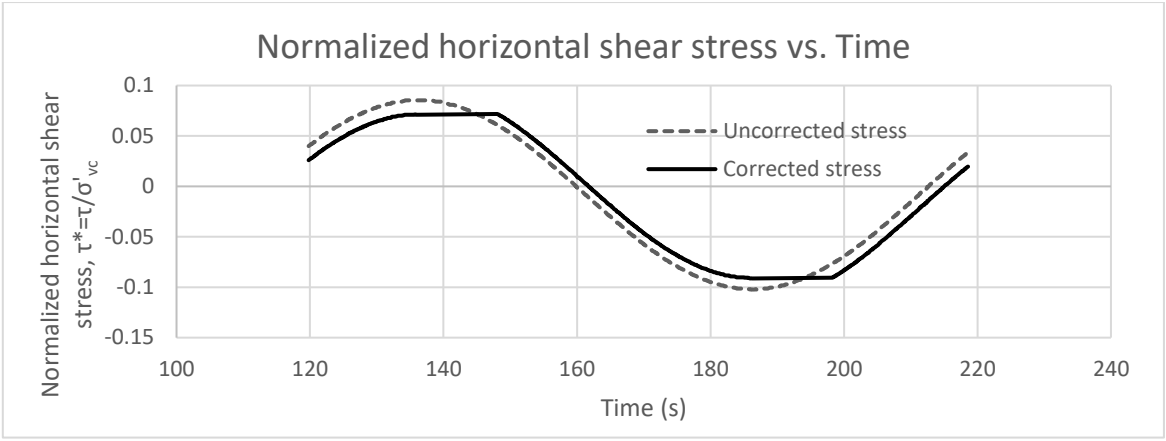

Figure 5.8 Corrected and uncorrected stress-time history of one cycle of stress-controlled test

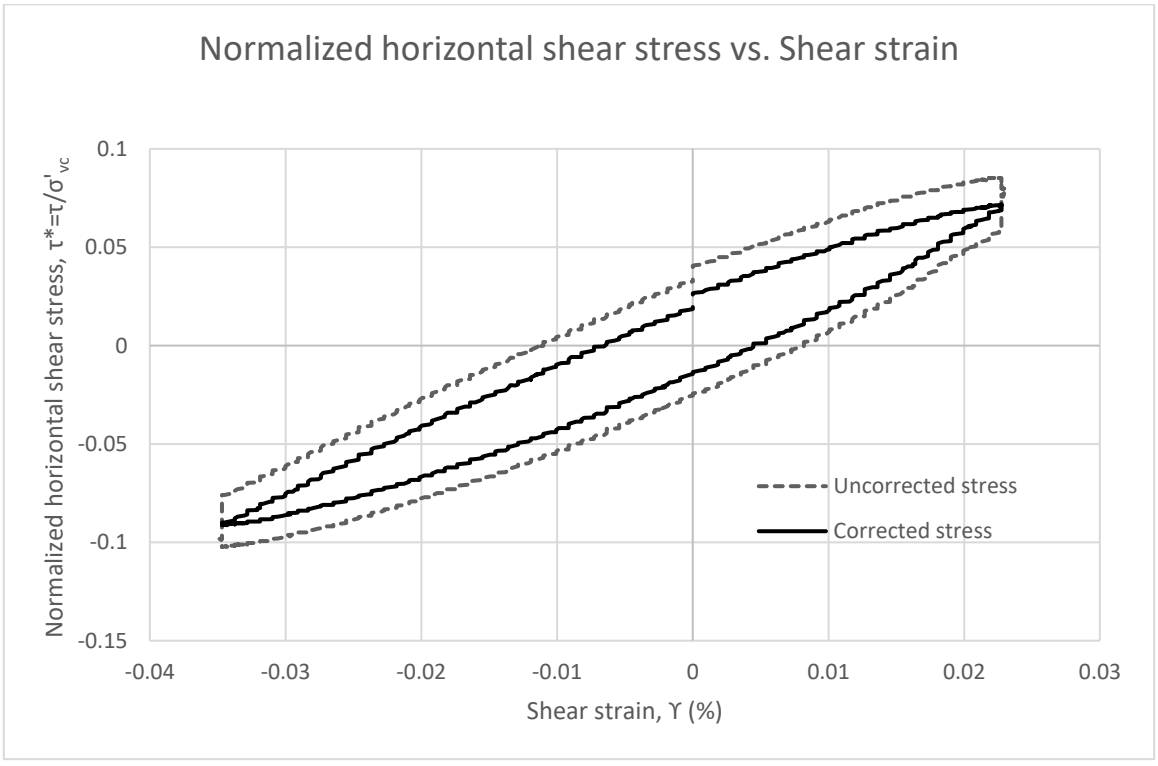

Figure 5.9 Corrected and uncorrected stress-strain loop of stress-controlled test

6. Procedures for calculation of the equivalent viscous damping ratio

In Chapter 10 the equivalent viscous damping ratios and associated areas of the loops obtained in several tests are analyzed and related to changes in soil stiffness. The procedures employed for calculating the equivalent viscous damping ratio are discussed below.

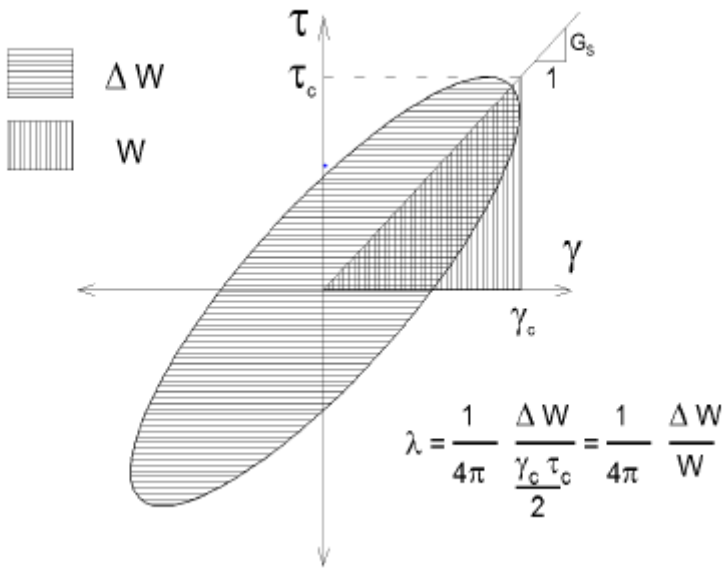

Figure 6.1 Stress-strain loop with the definition of the equivalent viscous damping ratio, λ

In Figure 6.1, the stress-strain loop with the definition of the equivalent viscous damping ratio, λ, is presented. The definition and corresponding formula are derived for the case of perfectly uniform elliptical force=displacement loop obtained during the forced harmonic vibration of the one-degree-of freedom oscillator with mass, linear spring and viscous dashpot. The loop presented above is therefore an ideal uniform loop, unlike loops typically obtained for soils in different cyclic tests. Using the formula shown in Figure 6.1 for calculating λ from loops that are nonuniform may therefore lead to considerable error, depending on the loop nonuniformity and the position of the origin of the coordinate system inside the loop. Therefore, a method that takes into account the nonuniform nature of the recorded stress-strain loops should be used to calculate the equivalent viscous damping ratio, λ.

Figure 6.2 shows a stress-strain loop that is nonuniform, i.e., magnitudes of Υ_c and τ_c are not the same in the positive and negative domains. To calculate more accurately the equivalent viscous damping ratio for the stress-strain loop in Figure 6.2, the formula shown in the figure can be used, where ΔOAB and ΔOCD represent the areas under the respective triangles. In this thesis, both methods for calculating the equivalent viscous damping ratio, λ, are used and the results were compared. That is, for each test considered λ is calculated using standard equation in Figure 6.1 and the equation in Figure 6.2 and the two variations of λ with the number of cycles, N, are presented together.

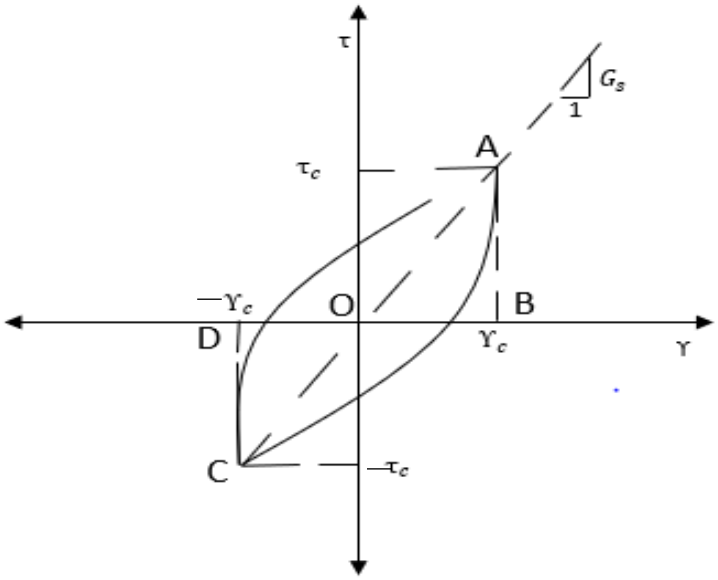

Area of the loop above the x-axis = W1
Area of the loop below the x-axis = W2

$$\lambda = 1/4\pi \left(W1/\Delta OAB + W2/\Delta OCD \right)$$

Figure 6.2 Nonuniform stress-strain loop and alternative equation to calculate more accurately the equivalent viscous damping ratio

It should be noted at the end that to calculate λ from a nonuniform loop the area of the triangle can be also determined in the following manner. The height of the loop from τ_c in the

negative domain to τ_c in the positive domain must be first multiplied by the width of the loop from Υ_c in the negative domain to Υ_c in the positive domain. This product than needs to be divided by 8. To obtain λ the area of the loop then needs to be divided with triangle determined in such a manner and further divided by 4π. In this study, this method to calculate λ was not used, but just the two methods described above.

7. Test results

As shown in Tables 2.1 and 2.2, in some multi-stage tests the specimen was reconsolidated between the stages and in some it was not. If the specimen was reconsolidated the stages can be treated as separate tests and, for convenience, in the text below such stages are referred to as tests. For example, stage 2 of Test 5 is called Test 5.2. For each test/stage defined in the above manner the following curves are constructed from the corrected data: shear strain versus time, normalized shear stress versus time, normalized pore water pressure versus time, shear strain versus normalized shear stress (cyclic loops), and the shear strain versus normalized pore water pressure. Based on these elementary cyclic soil behavior curves, the following relationships are derived: stiffness index versus number of cycles, normalized cyclic pore water pressure versus number of cycles, and stiffness index versus normalized cyclic pore water pressure. In addition to that, for some tests the equivalent viscous damping ratio versus the number of cycles is also constructed.

For the tests with the reconsolidation between the stages, to construct the relationship between the cyclic pore water pressure and stiffness index in a given stage, in the definition of the normalized equivalent cyclic pore water pressure $\Delta u_N^* = \Delta u_N / \sigma'_{vc}$ stress σ'_{vc} is σ'_{vo} at the beginning of the stage. The values of σ'_{vo} are specified in Table 2.1 for such tests or parts of

tests. Stress σ'_{vo} is also specified in both tables for every stage without reconsolidation, in which case it is calculated by subtracting Δu_N at the end of previous stage from the initial σ'_{vc}.

For the tests without the reconsolidation between the stages the variation of $\Delta u_N^* = \Delta u_N / \sigma'_{vc}$ with time is presented for the entire test only. In such cases σ'_{v0} in the first stage is equal to σ'_{vc}. However, the variation of the stiffness index, δ, with the number of cycles, N, is still constructed for each individual stage.

TEST 1

Test: 1; Soil: Nevada Sand; e=0.43; w=0%
σ'_{vc}=150 (kPa); OCR=1; Υ_c=0.06%, f=0.02 Hz

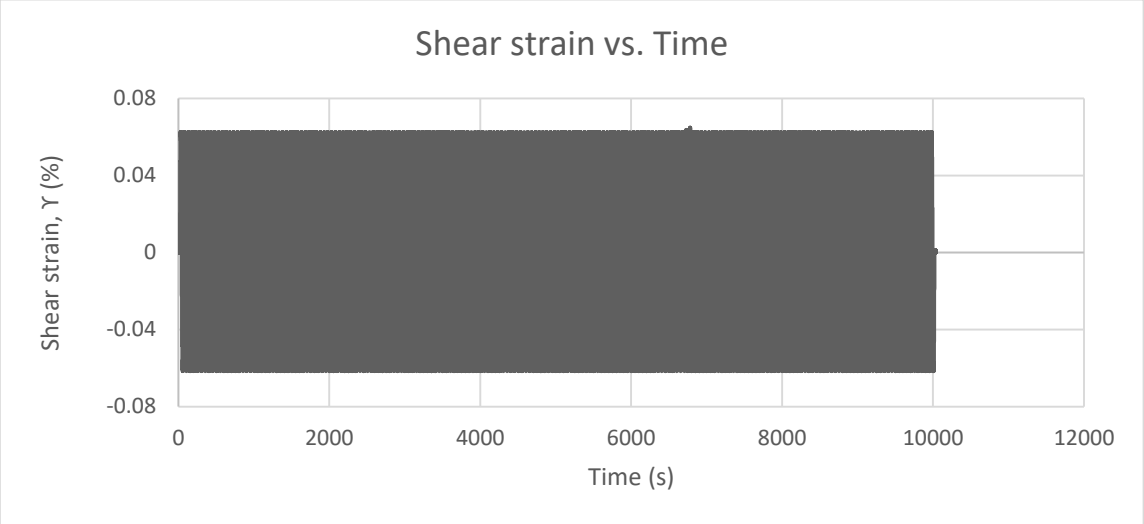

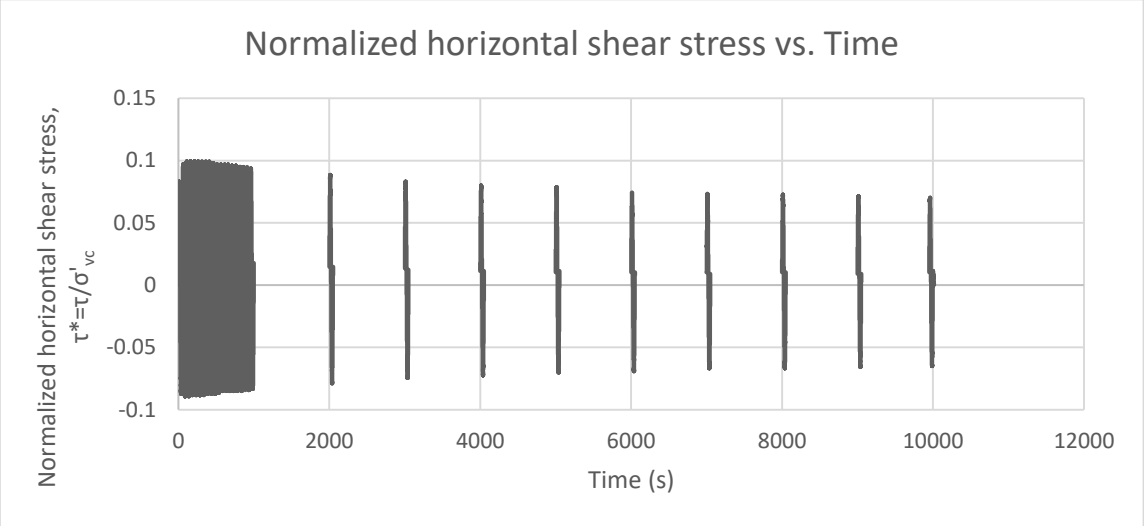

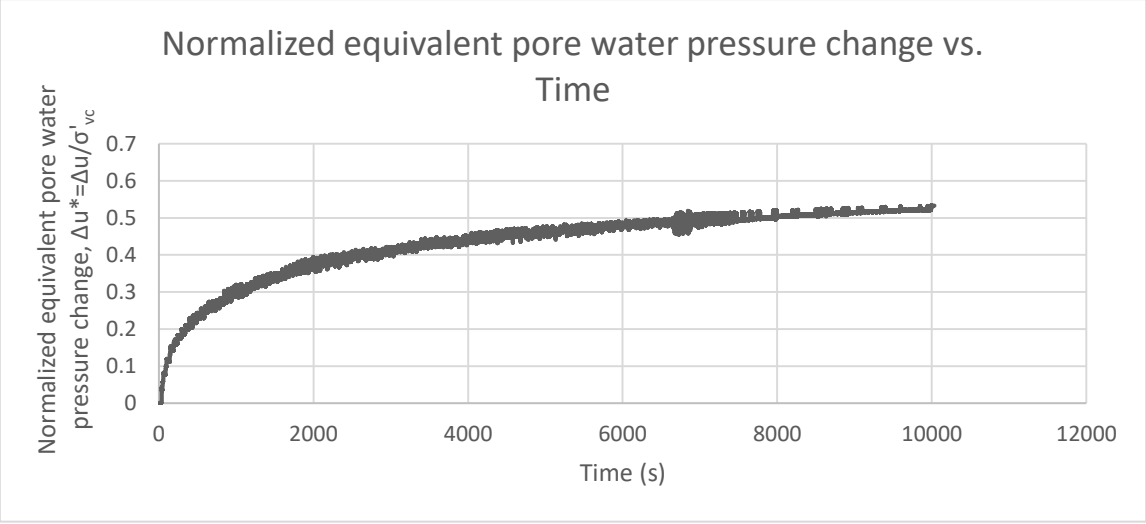

Test: 1; Soil: Nevada Sand; e=0.43; w=0%
σ'_{vc}=150 (kPa); OCR=1; Υ_c=0.06%, f=0.02 Hz

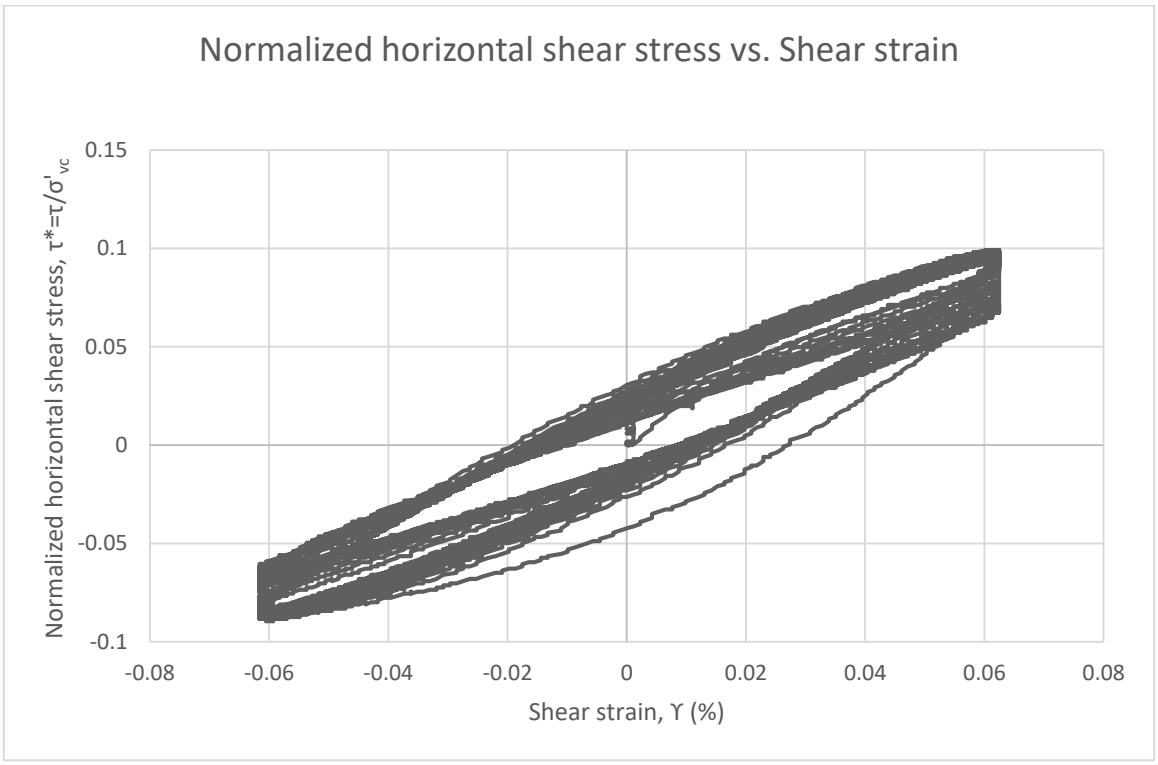

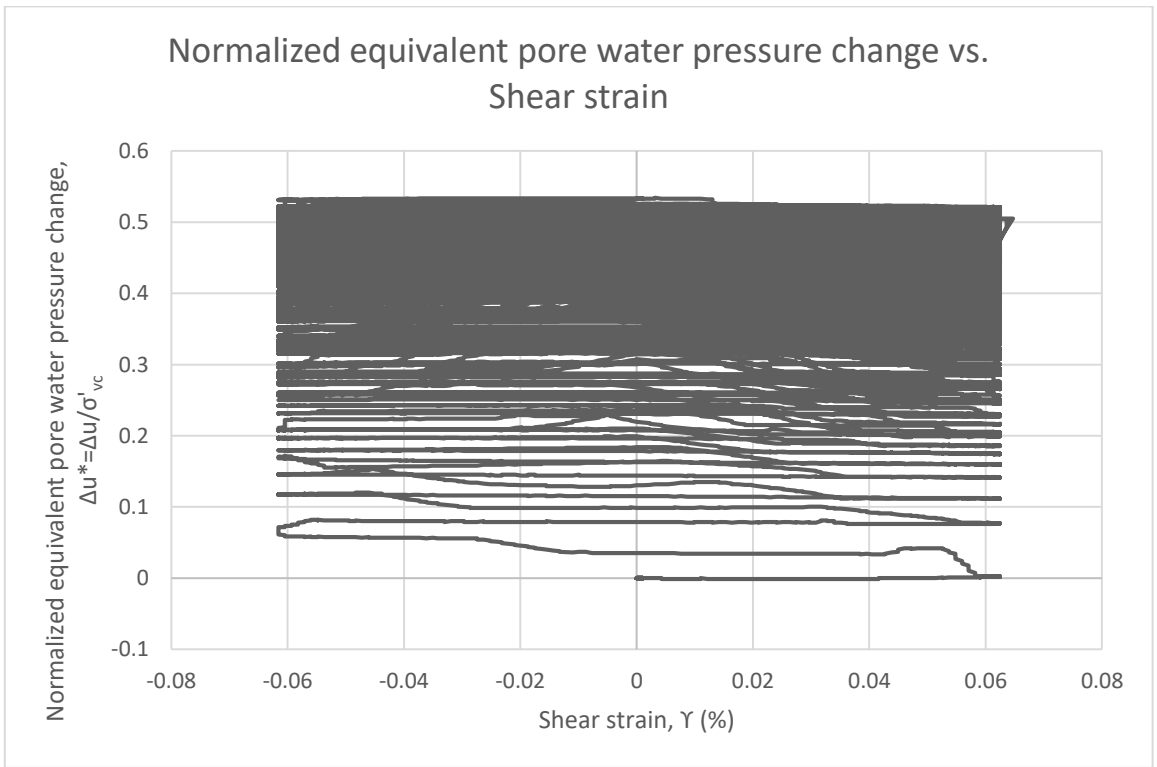

Test: 1; Soil: Nevada Sand; e=0.43; w=0%
σ'_{vc}=150 (kPa); OCR=1; Υ_c=0.06%, f=0.02 Hz

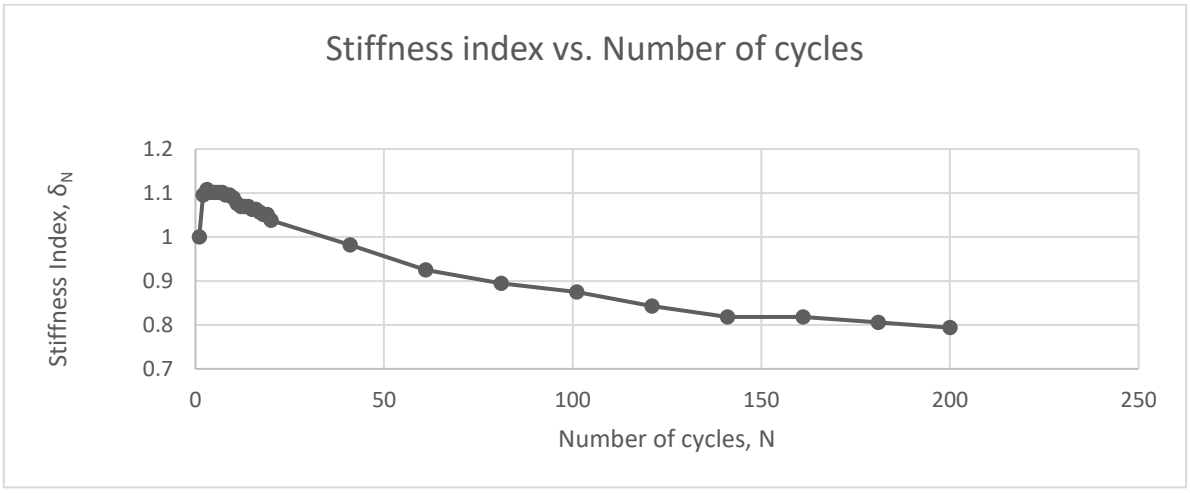

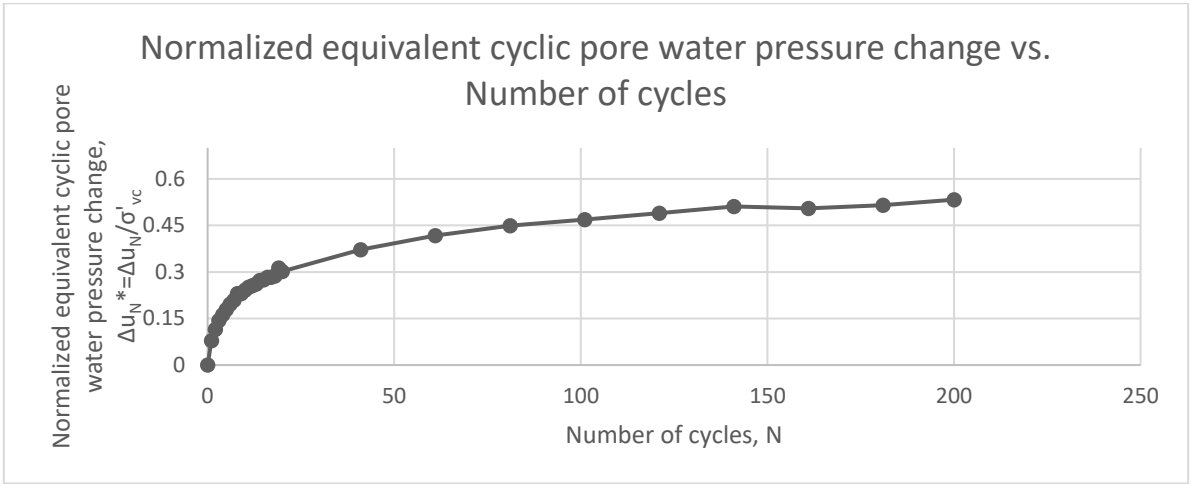

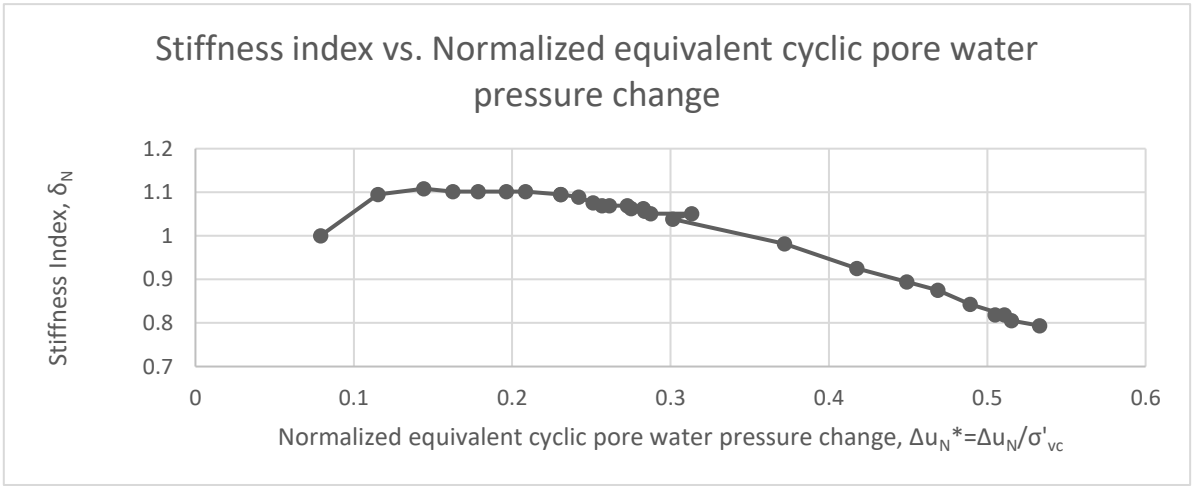

TEST 2

Test: 2.1; Soil: Nevada Sand; e=0.47; w=15.25%, S=87.6%
σ'_{vc}=150 (kPa); OCR=1; Υ_c=0.04%, f=0.02 Hz

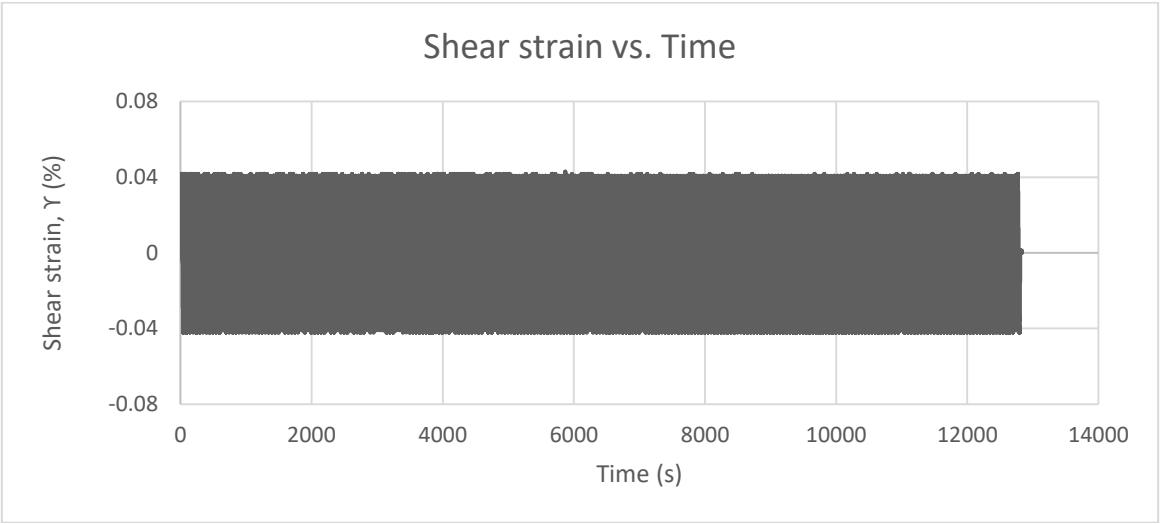

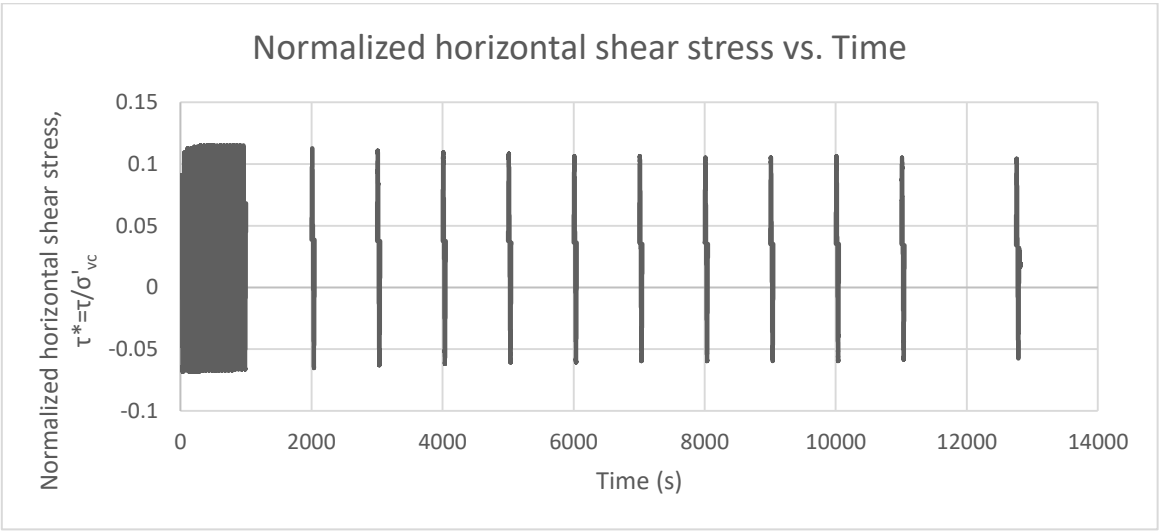

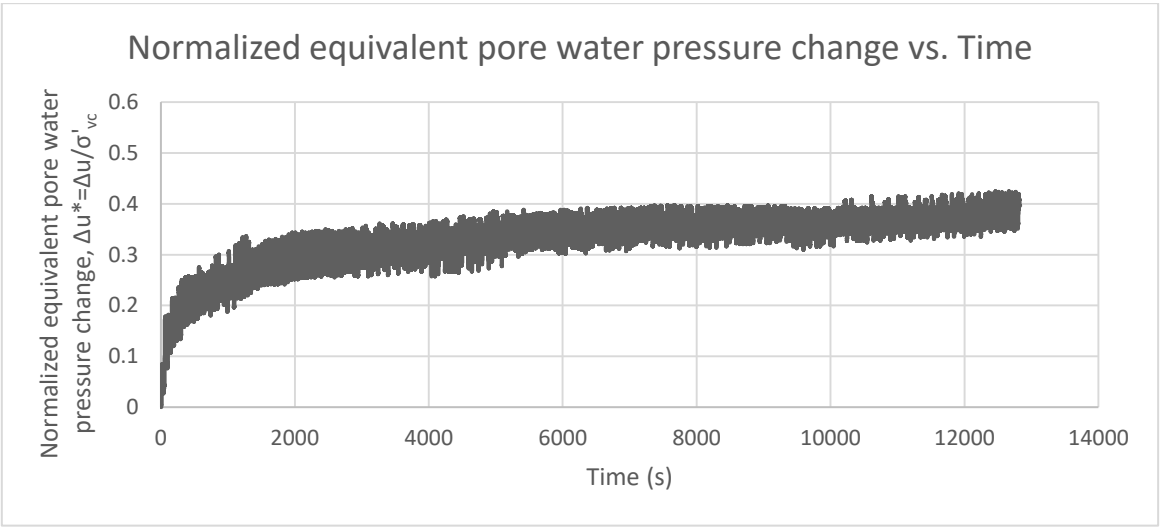

Test: 2.1; Soil: Nevada Sand; e=0.47; w=15.25%, S=87.6%
σ'_{vc}=150 (kPa); OCR=1; Υ_c=0.04%, f=0.02 Hz

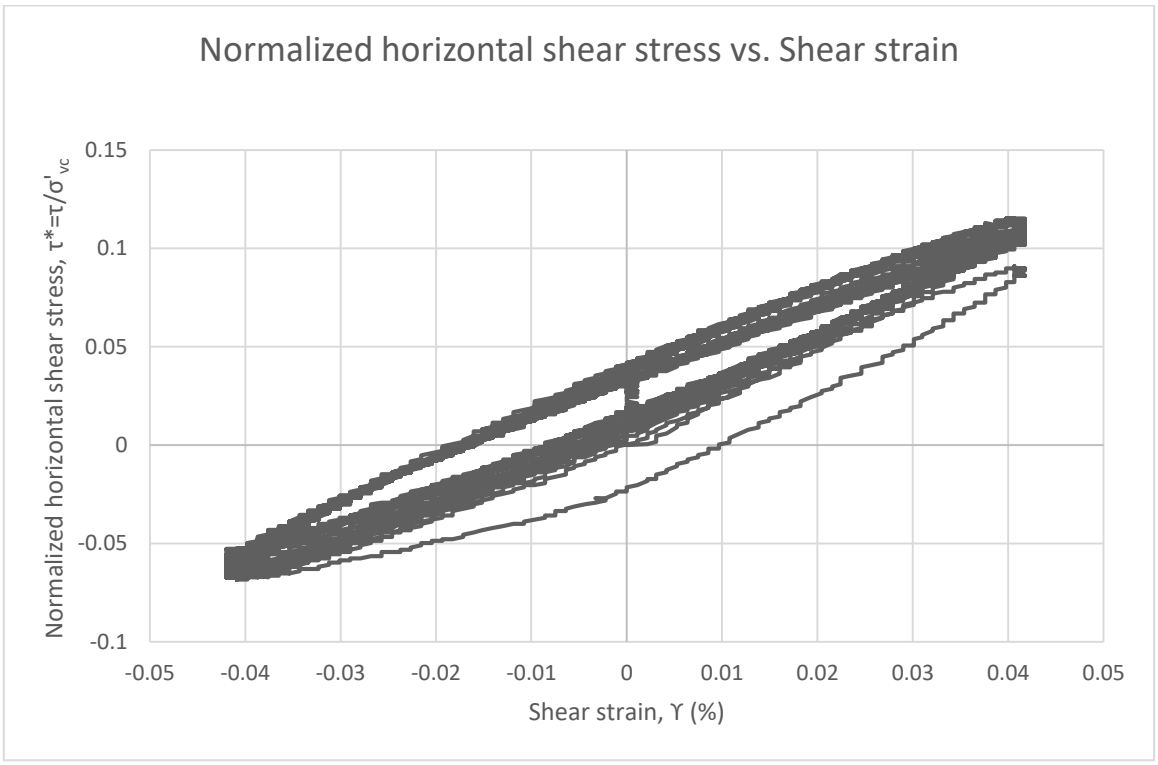

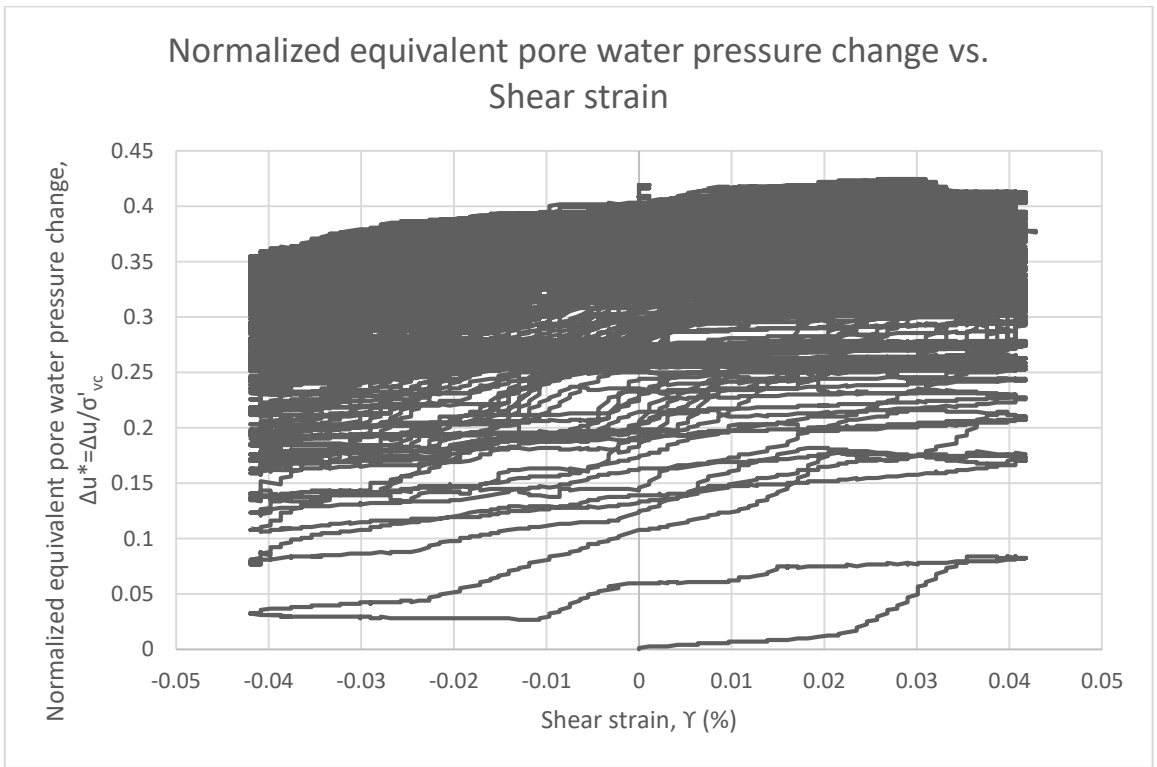

Test: 2.1; Soil: Nevada Sand; e=0.47; w=15.25%, S=87.6%
σ'_{vc}=150 (kPa); OCR=1; Υ_c=0.04%, f=0.02 Hz

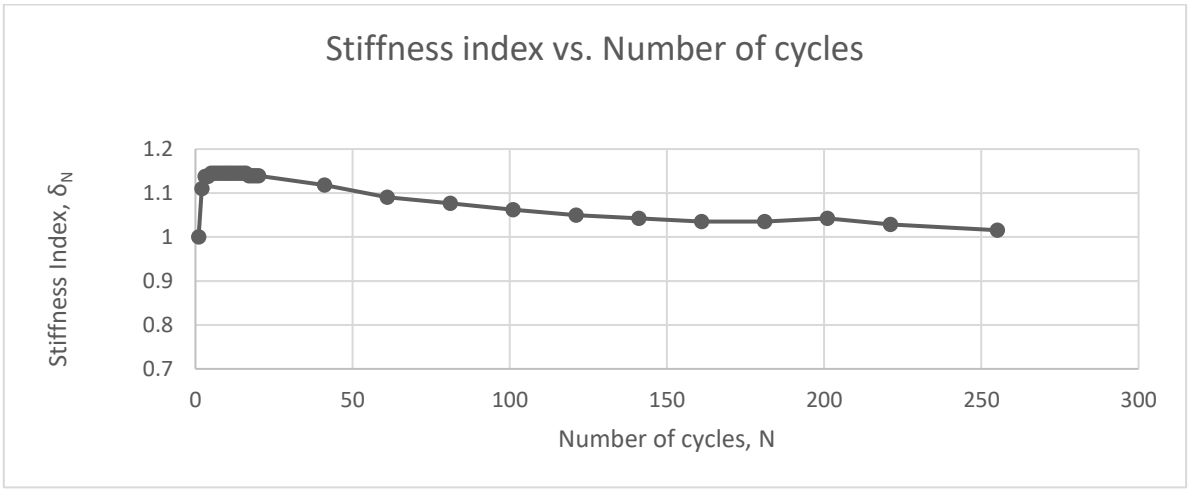

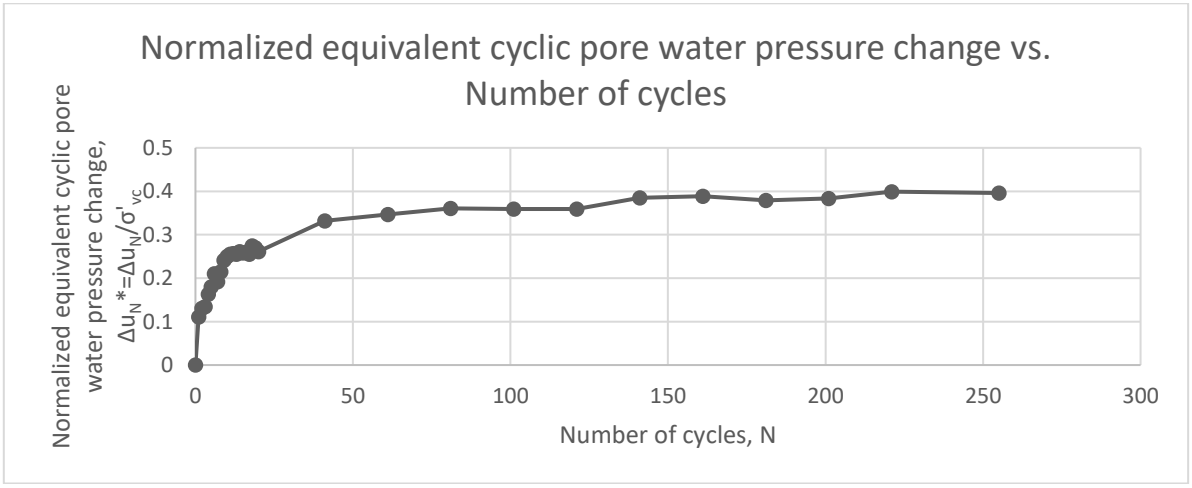

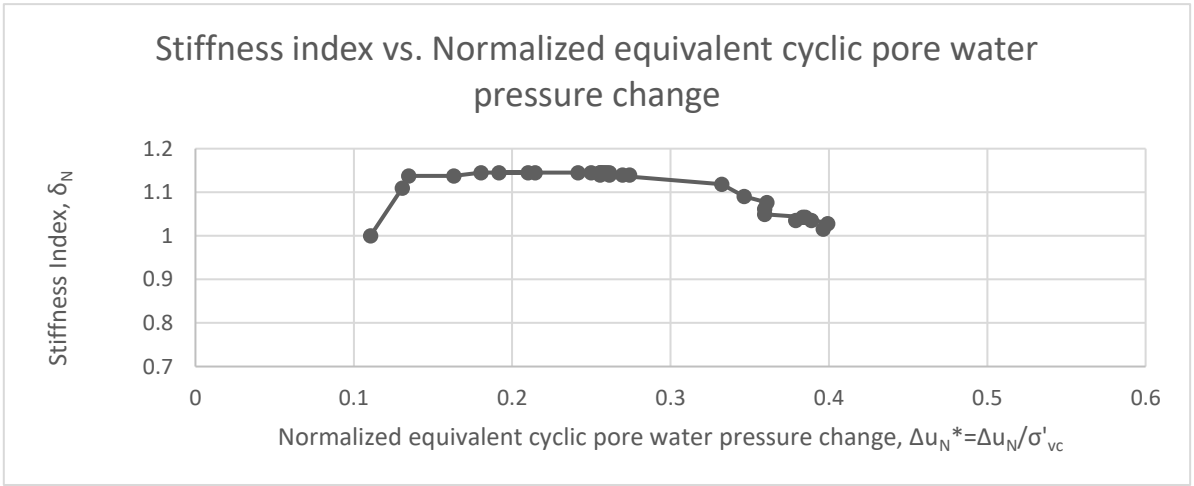

Test: 2.2; Soil: Nevada Sand; e=0.48; w=15.25%, S=85.78%
σ'_{vc}=300 (kPa); OCR=1; Υ_c=0.04%, f=0.02 Hz

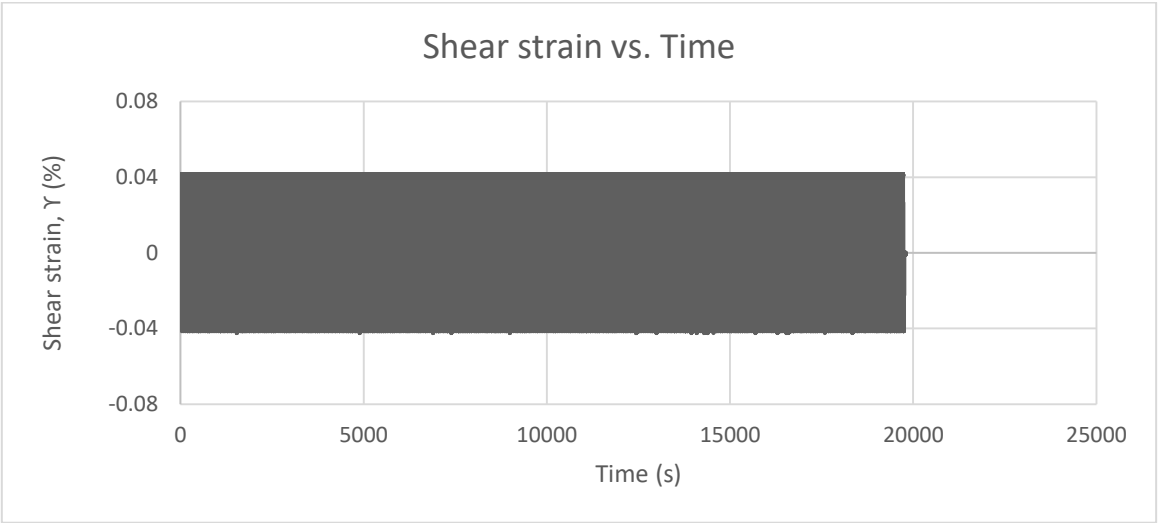

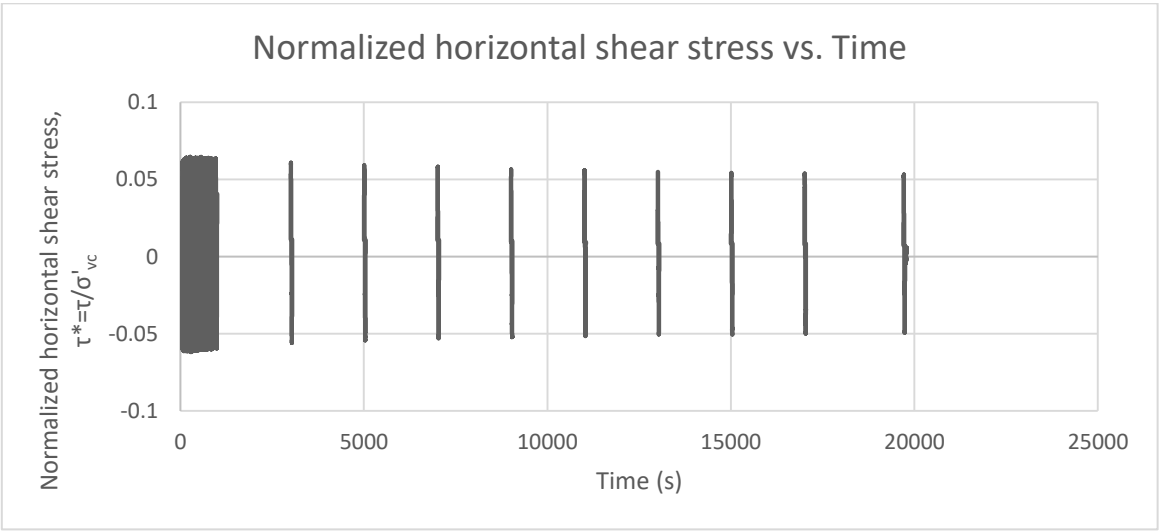

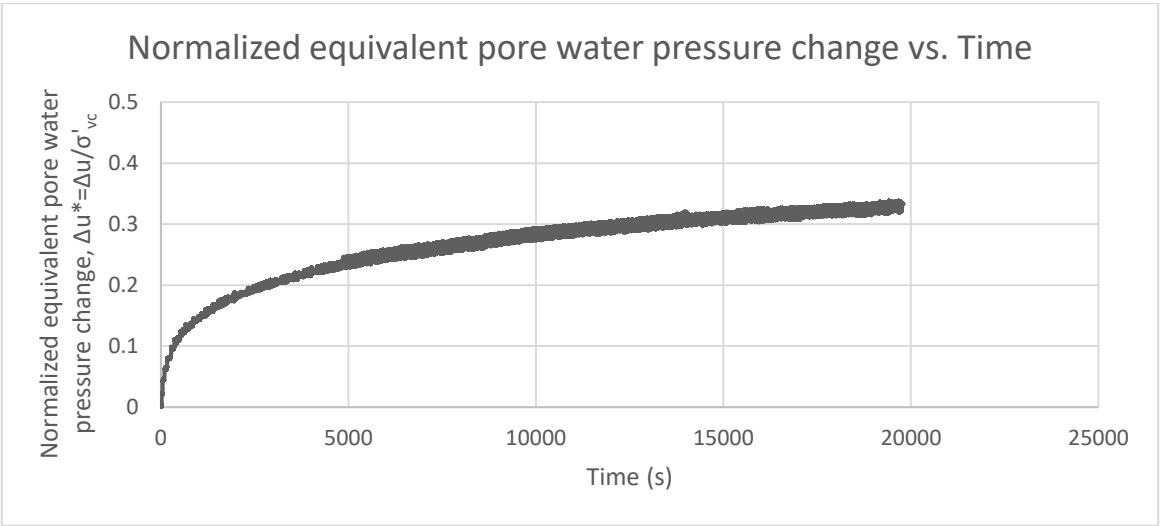

Test: 2.2; Soil: Nevada Sand; e=0.48; w=15.25%, S=85.78%
σ'_{vc}=300 (kPa); OCR=1; Υ_c=0.04%, f=0.02 Hz

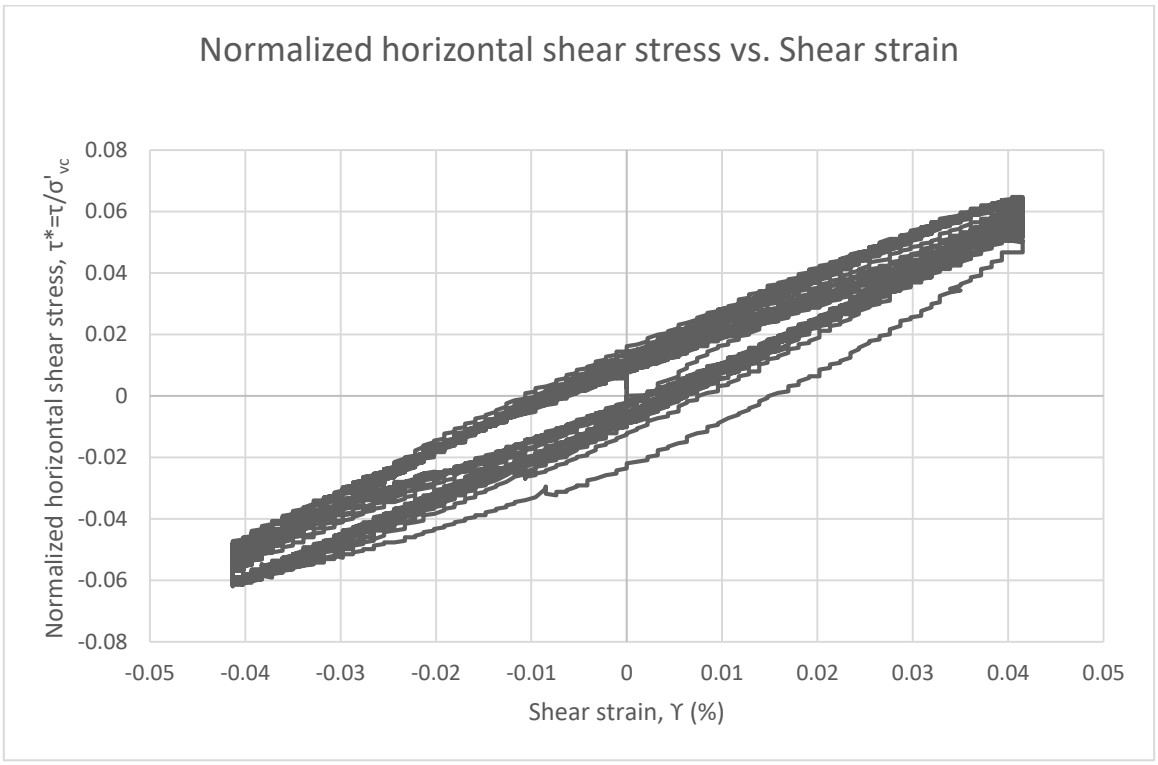

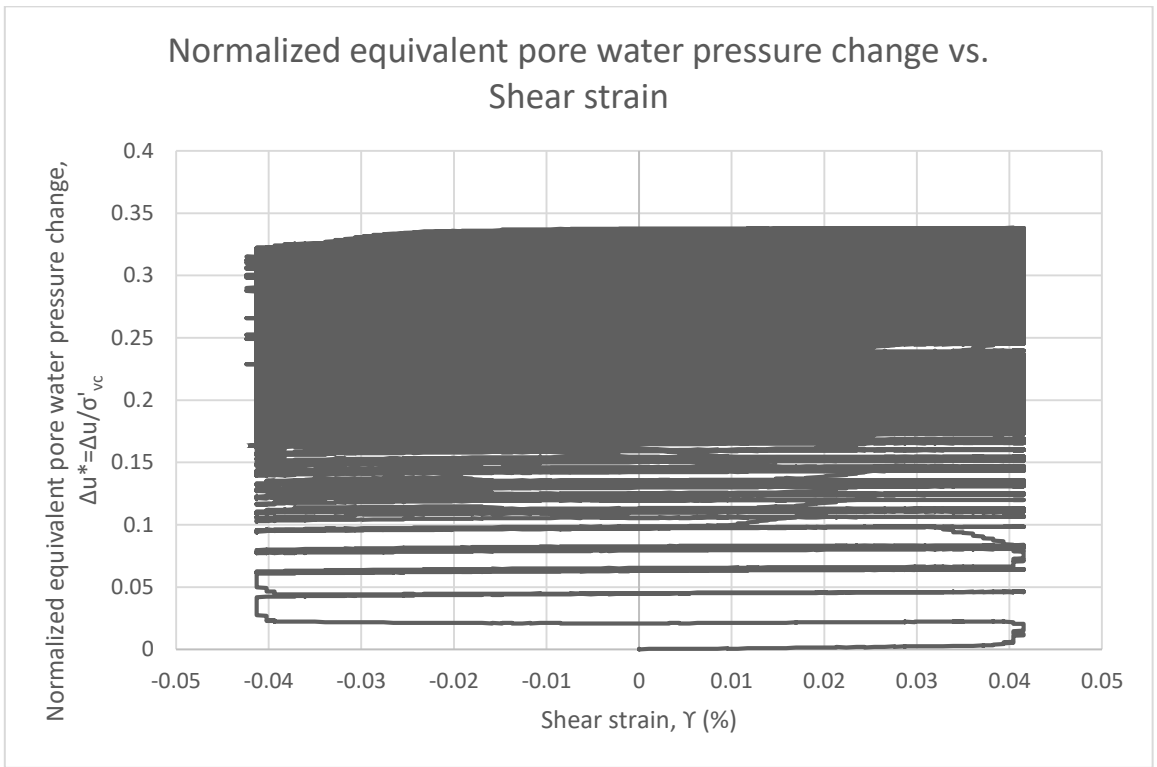

Test: 2.2; Soil: Nevada Sand; e=0.48; w=15.25%, S=85.78%
σ'_{vc}=300 (kPa); OCR=1; Υ_c=0.04%, f=0.02 Hz

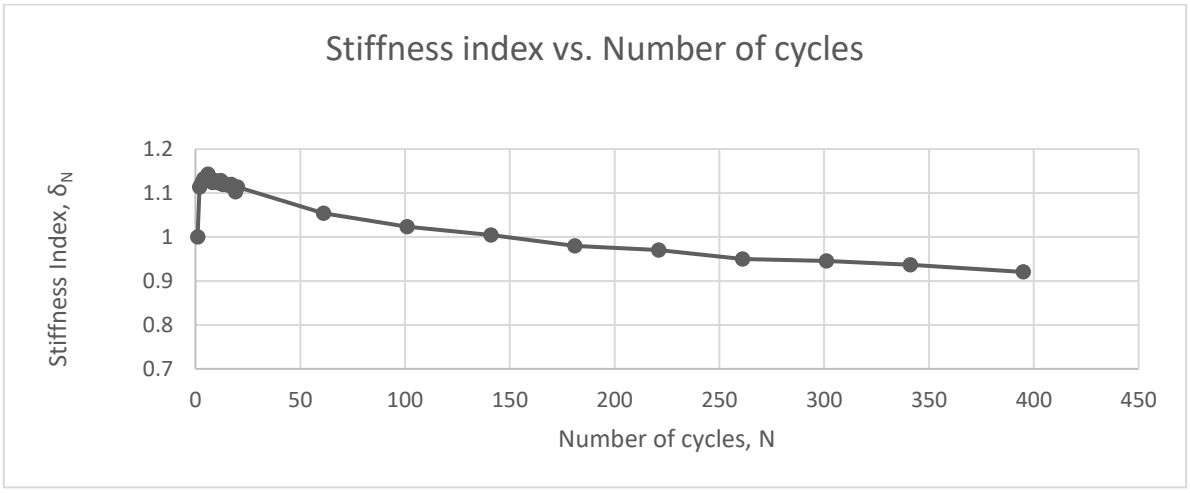

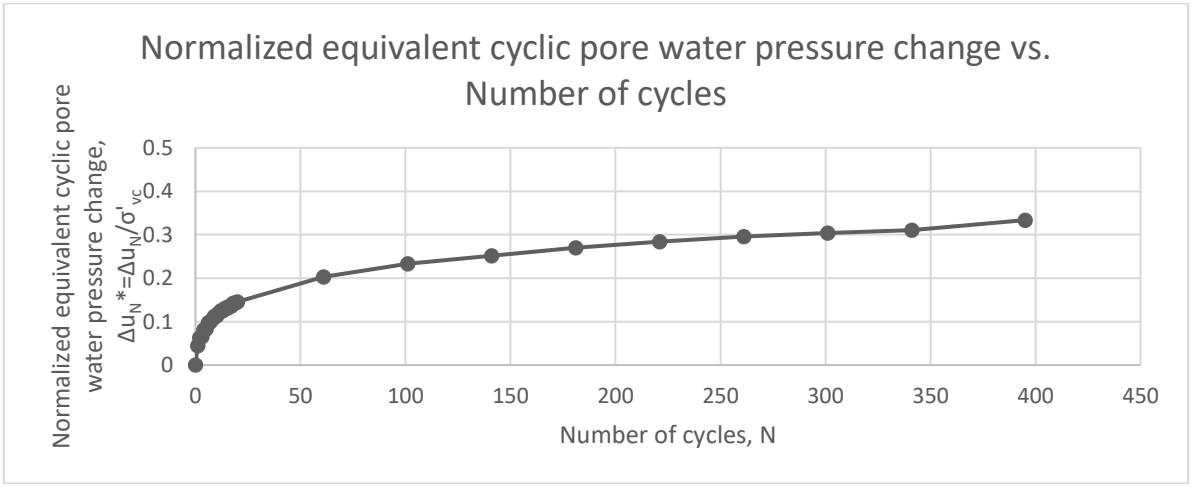

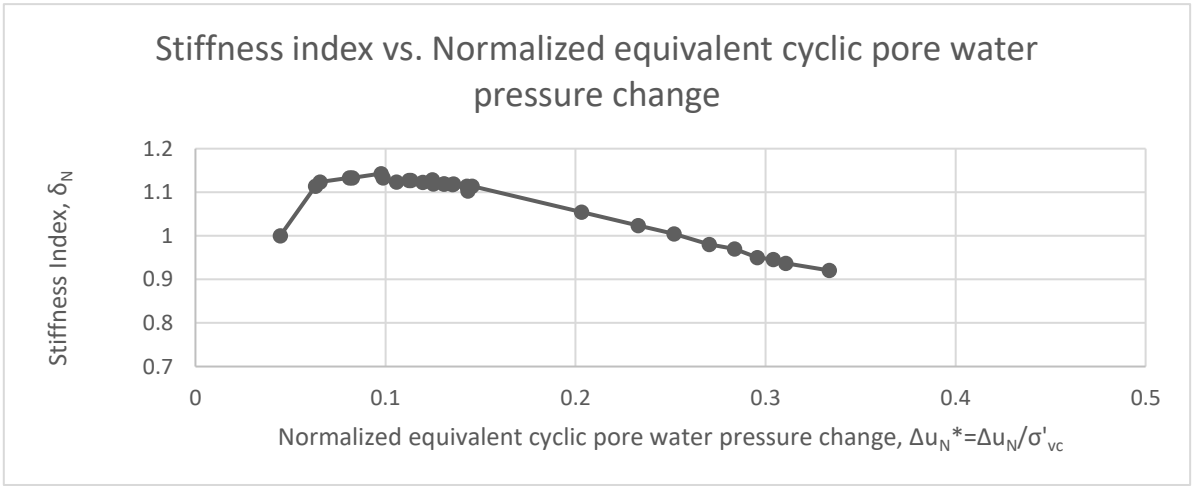

TEST 3

Test: 3.1; Soil: Nevada Sand; e=0.48; w=3.14%, S=17.66%
σ'_{vc}=150 (kPa); OCR=1; Υ_c=0.06%, f=0.02 Hz

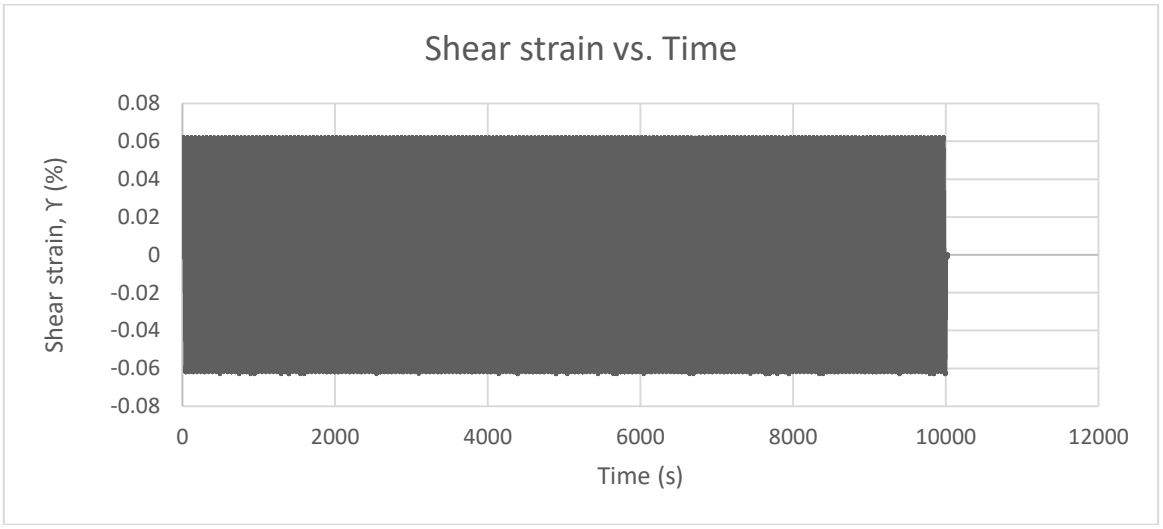

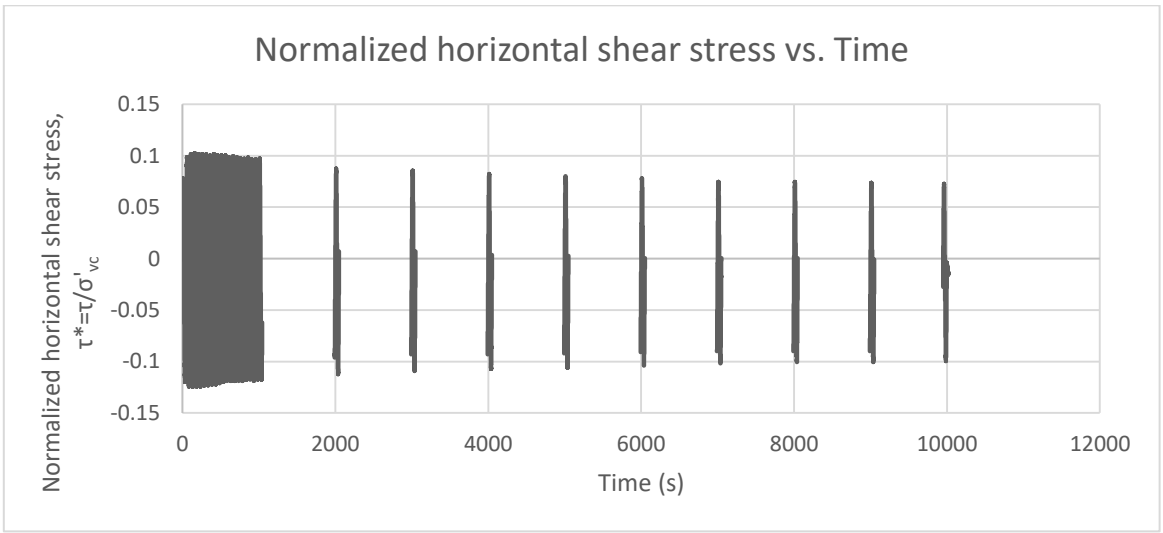

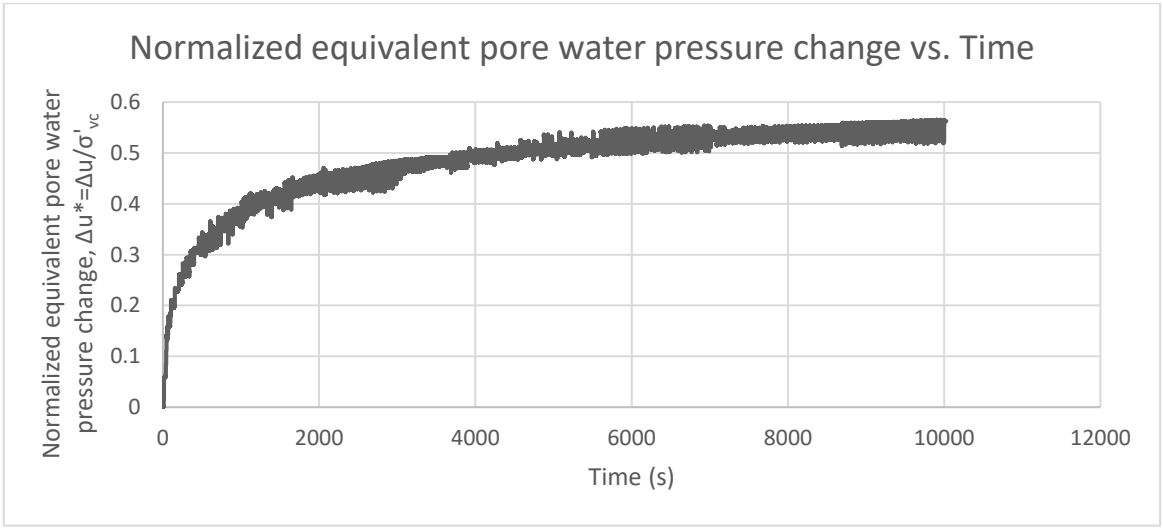

Test: 3.1; Soil: Nevada Sand; e=0.48; w=3.14%, S=17.66%
σ'_{vc}=150 (kPa); OCR=1; Υ_c=0.06%, f=0.02 Hz

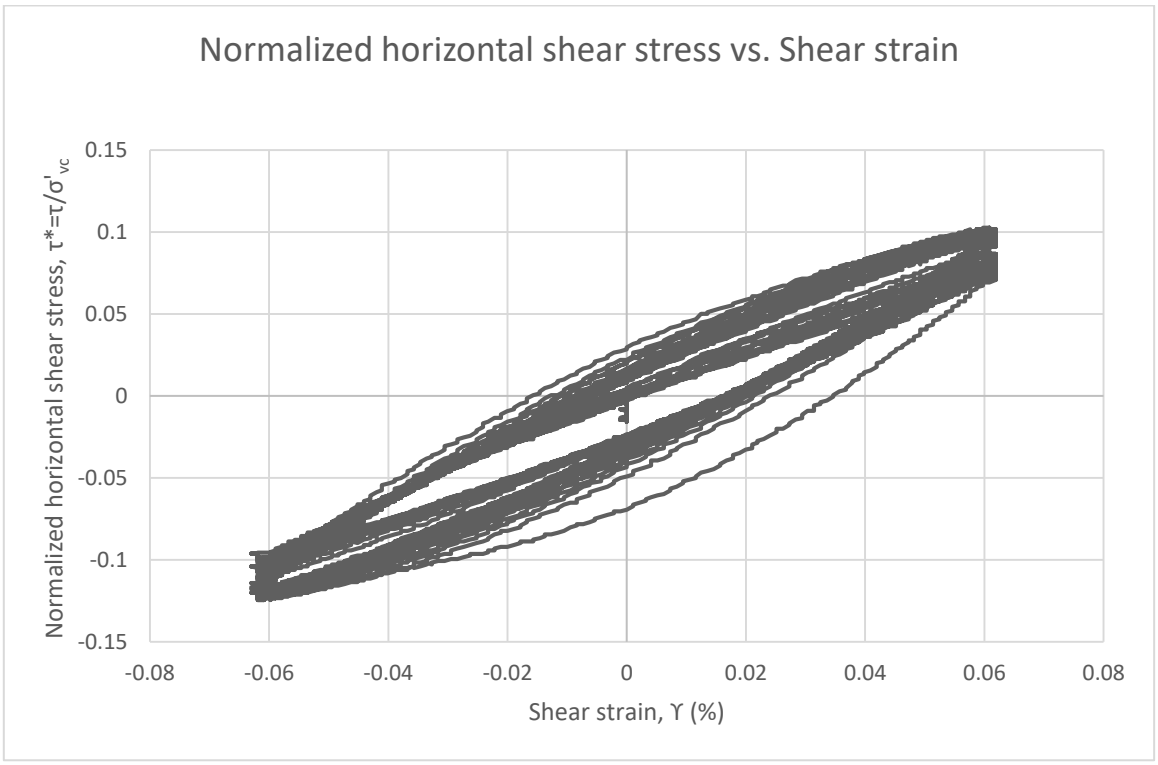

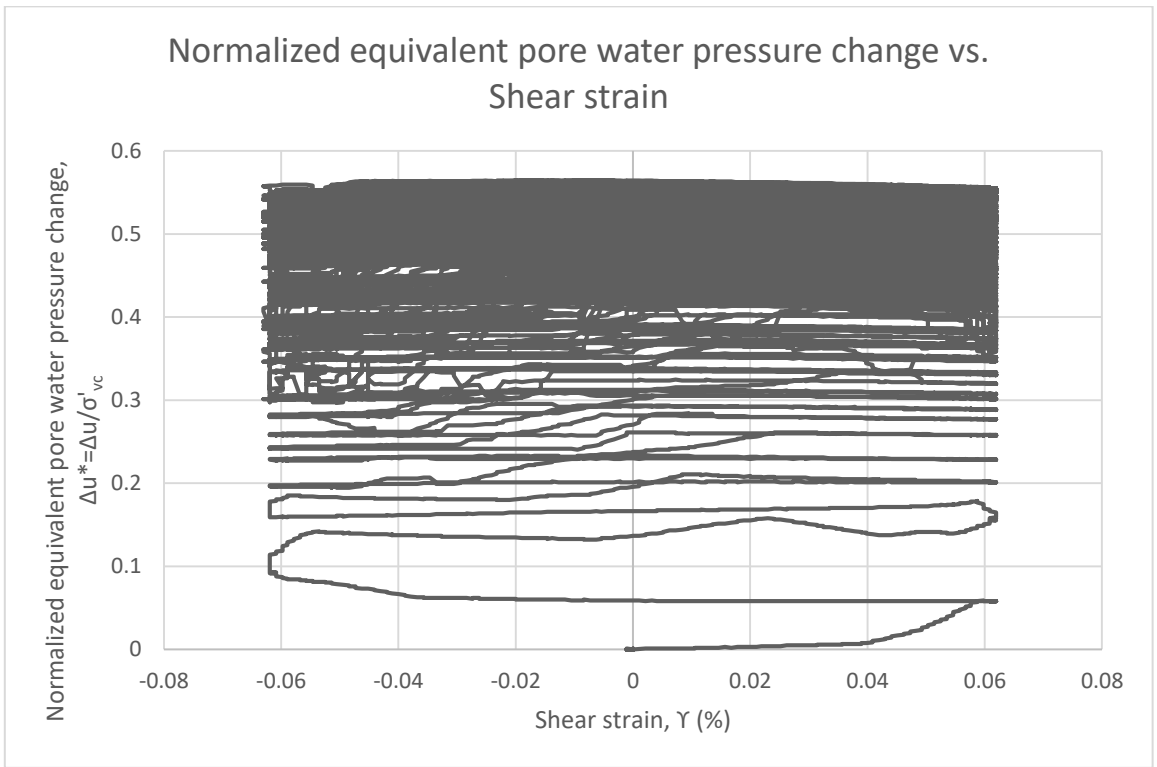

Test: 3.1; Soil: Nevada Sand; e=0.48; w=3.14%, S=17.66%
σ'_{vc}=150 (kPa); OCR=1; Υ_c=0.06%, f=0.02 Hz

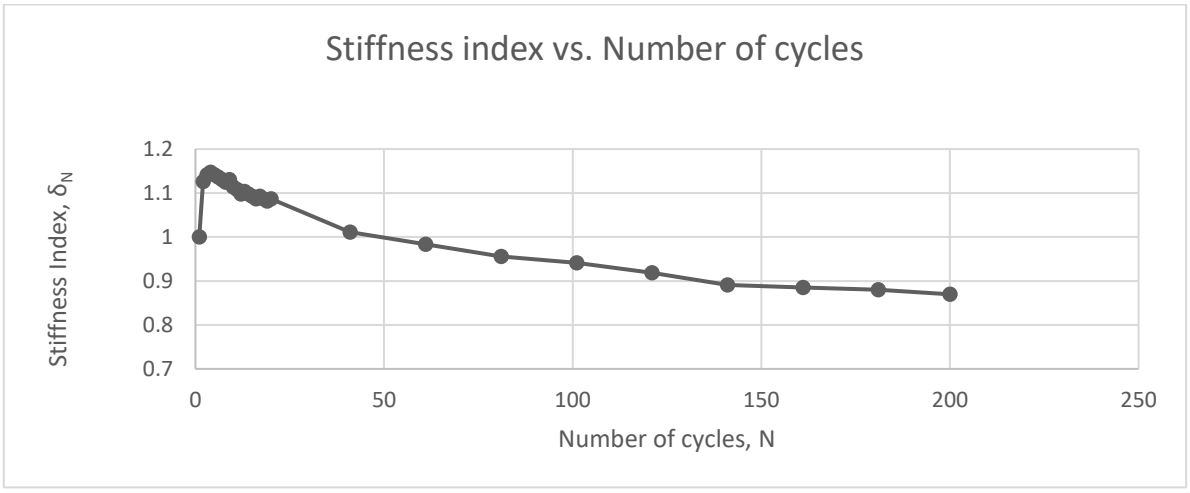

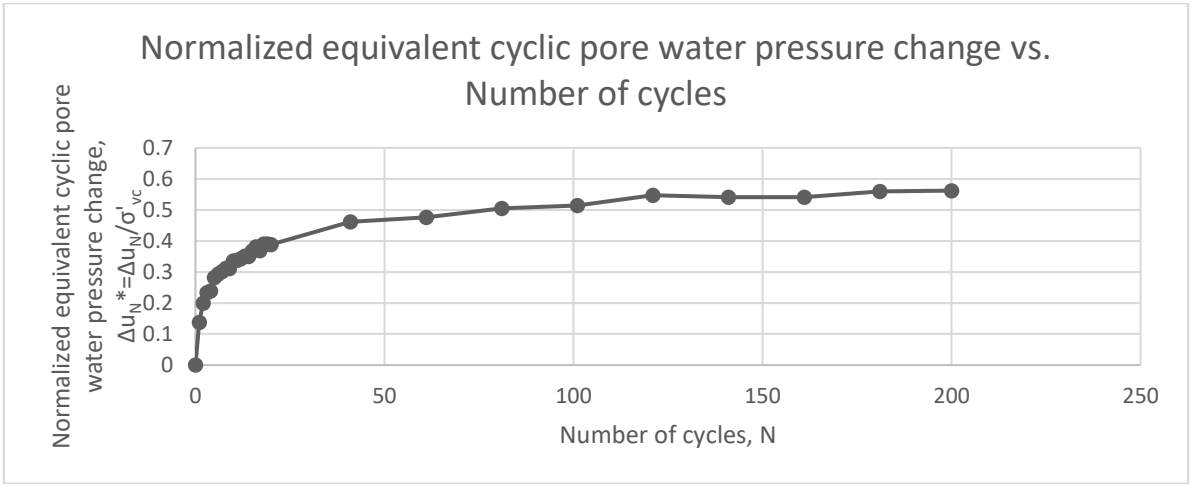

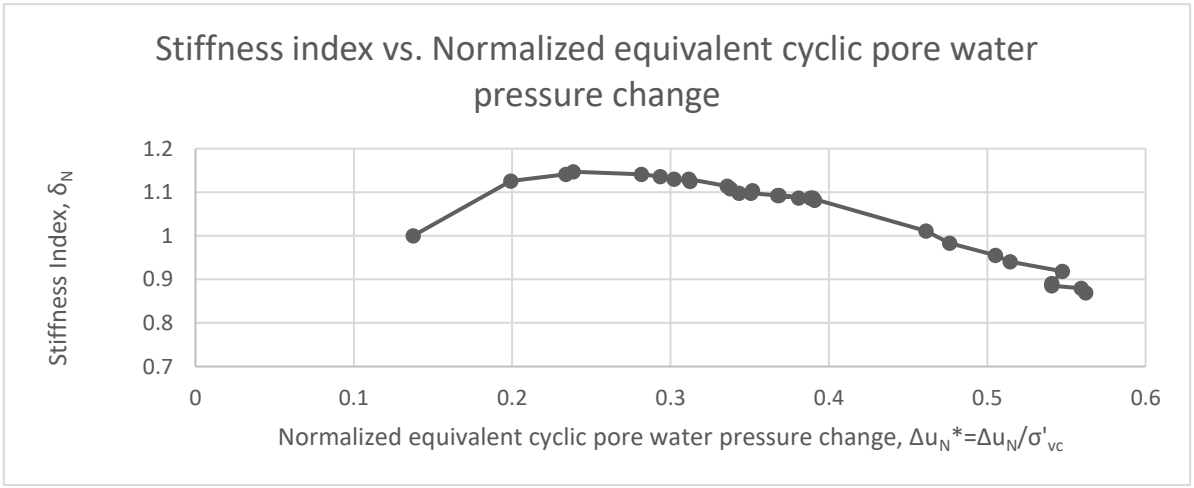

Test: 3.2; Soil: Nevada Sand; e=0.46; w=3.14%, S=18.43%
σ'_{vc}=300 (kPa); OCR=1; Υ_c=0.06%, f=0.02 Hz

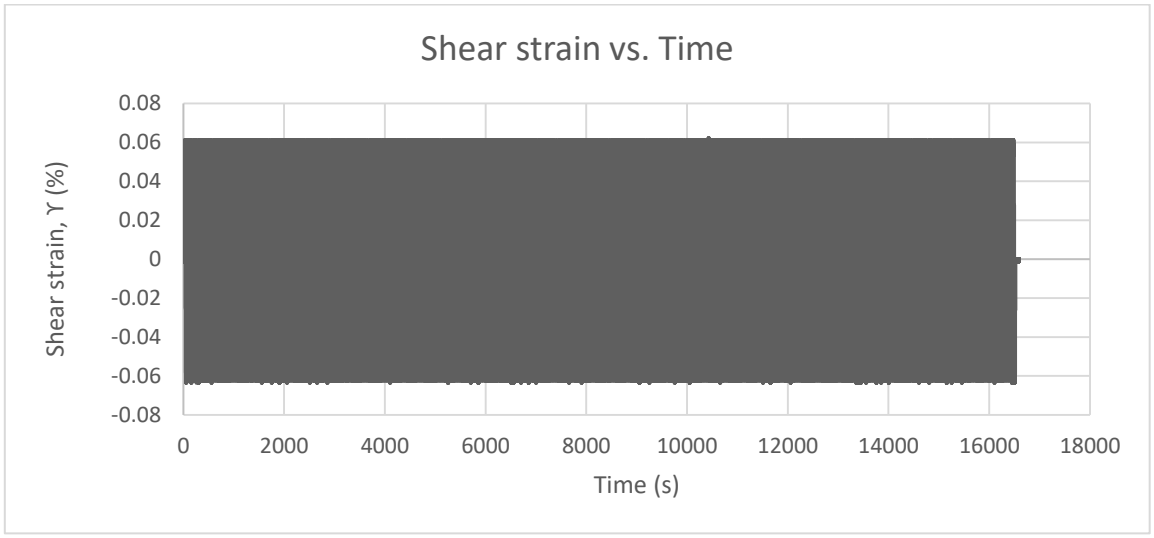

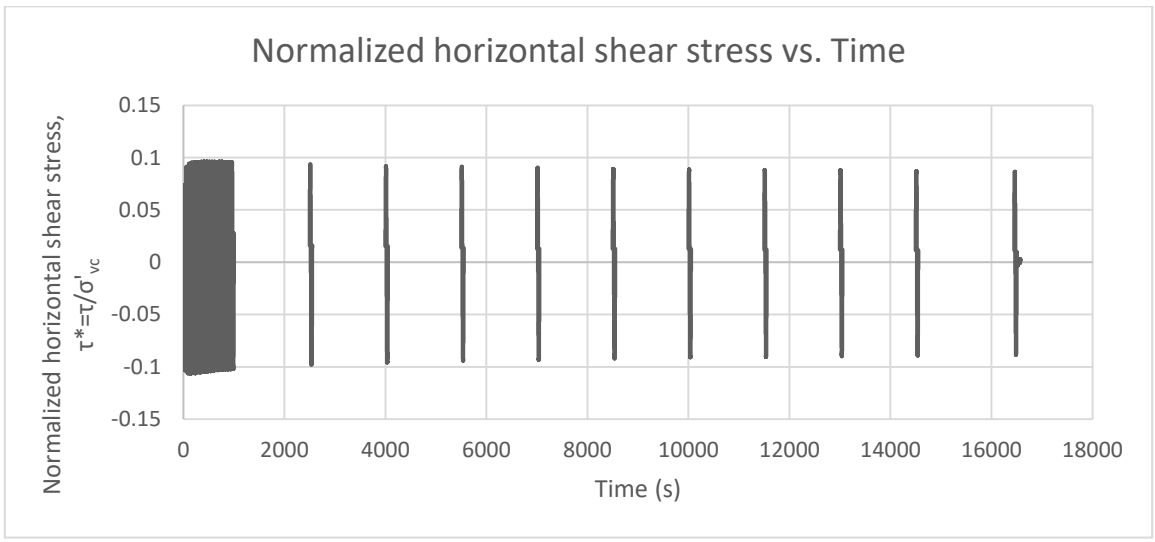

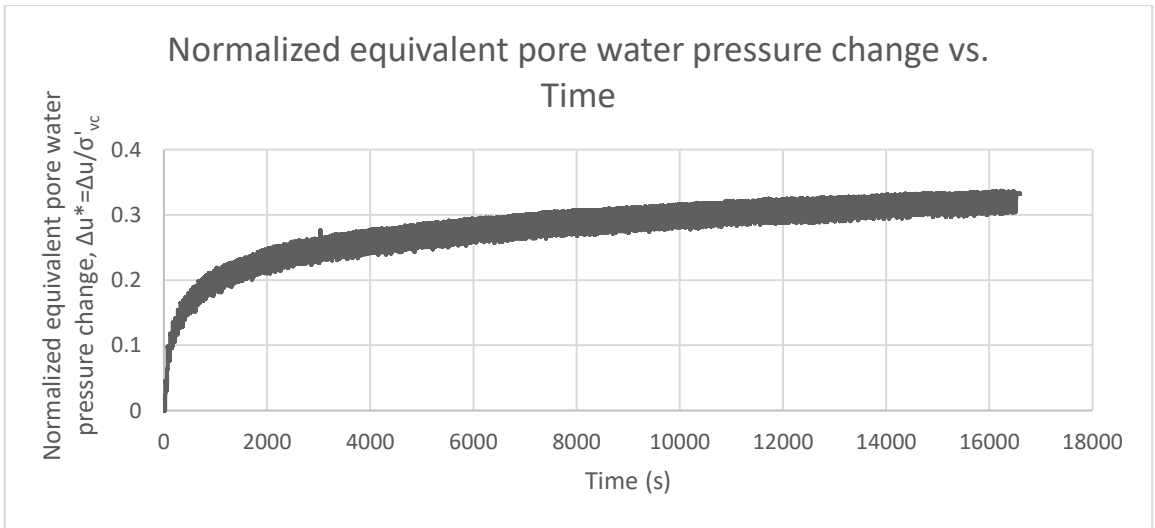

Test: 3.2; Soil: Nevada Sand; e=0.46; w=3.14%, S=18.43%
σ'_{vc}=300 (kPa); OCR=1; Υ_c=0.06%, f=0.02 Hz

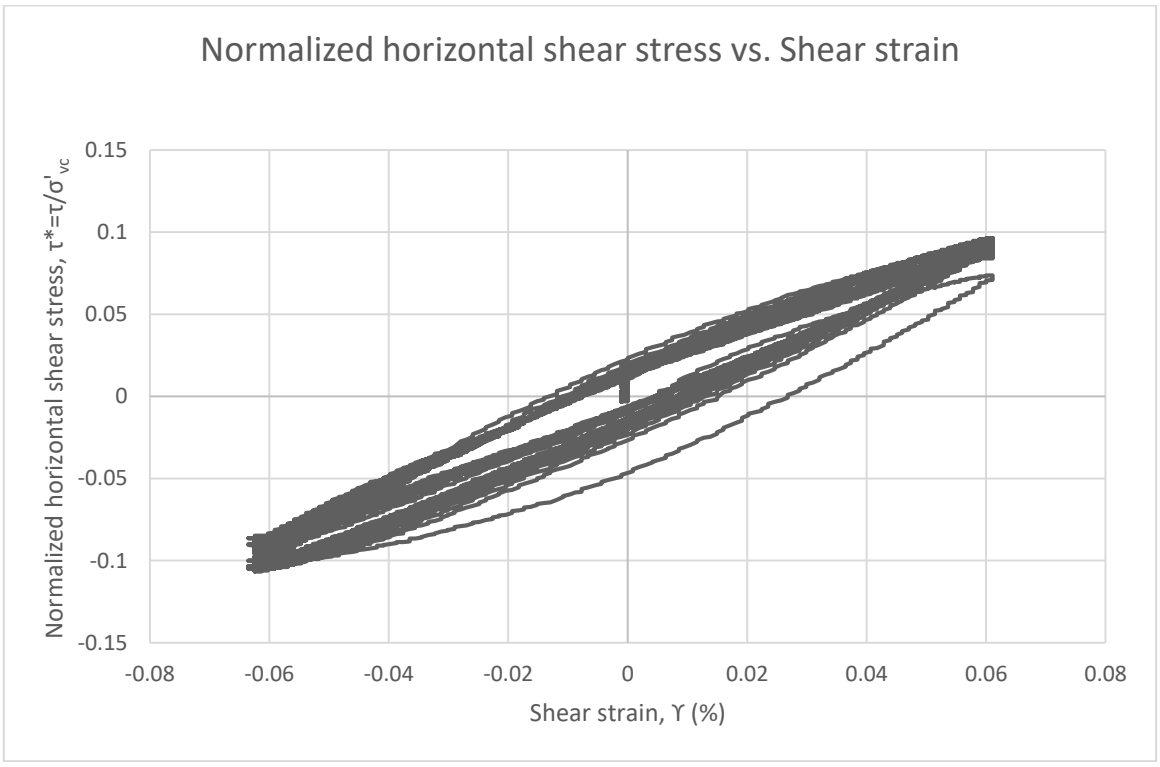

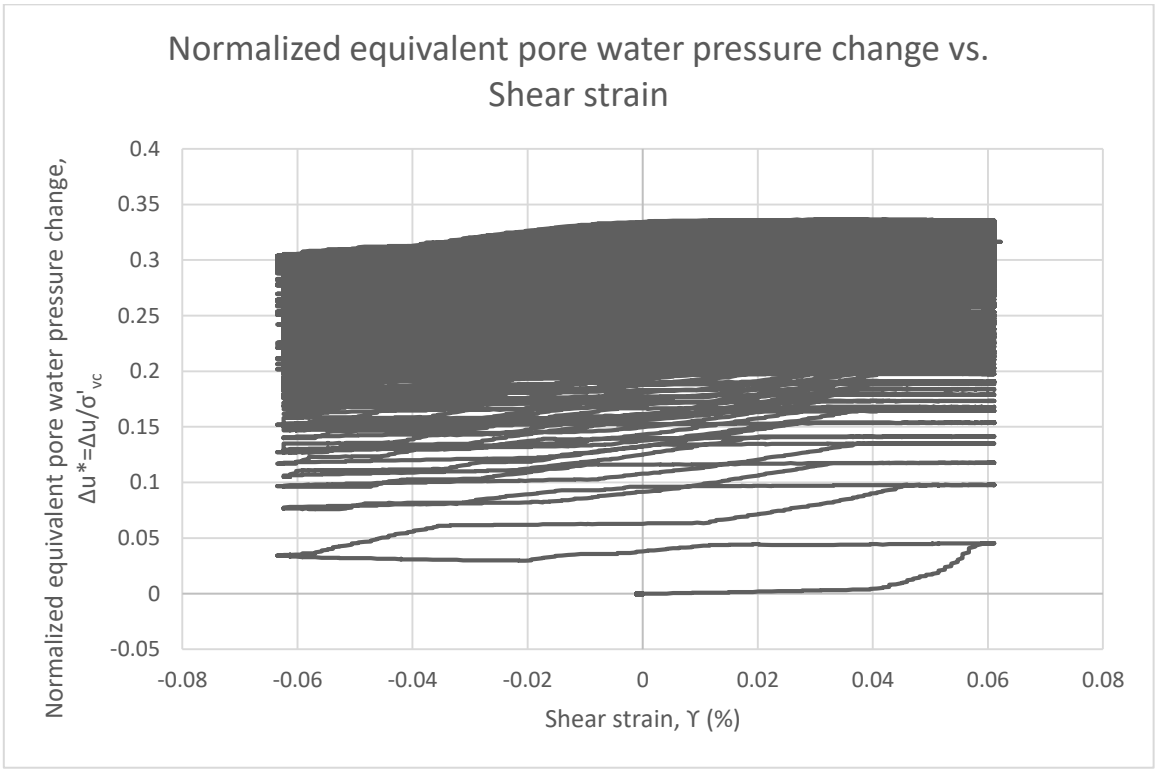

Test: 3.2; Soil: Nevada Sand; e=0.46; w=3.14%, S=18.43%
σ'_{vc}=300 (kPa); OCR=1; Υ_c=0.06%, f=0.02 Hz

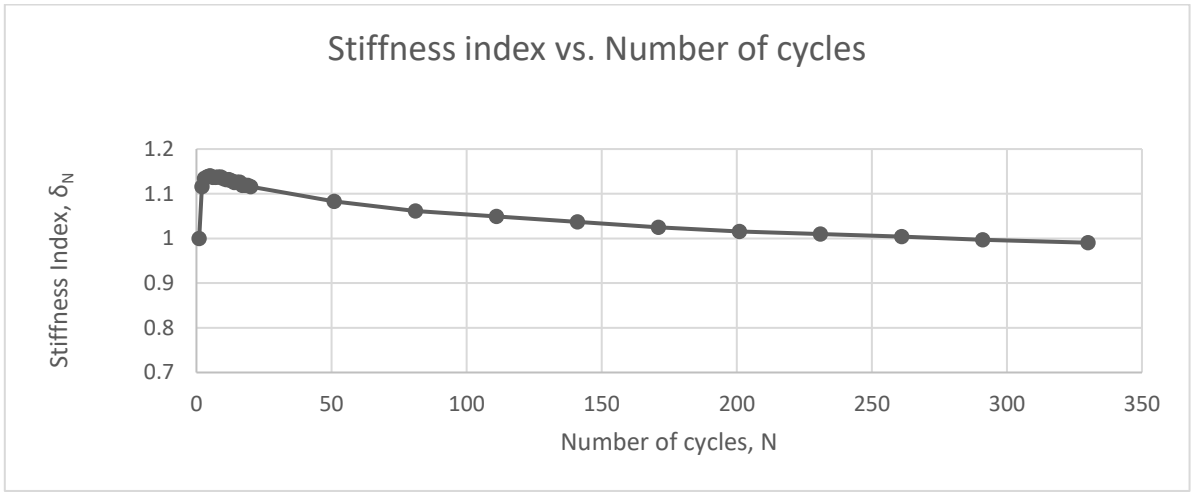

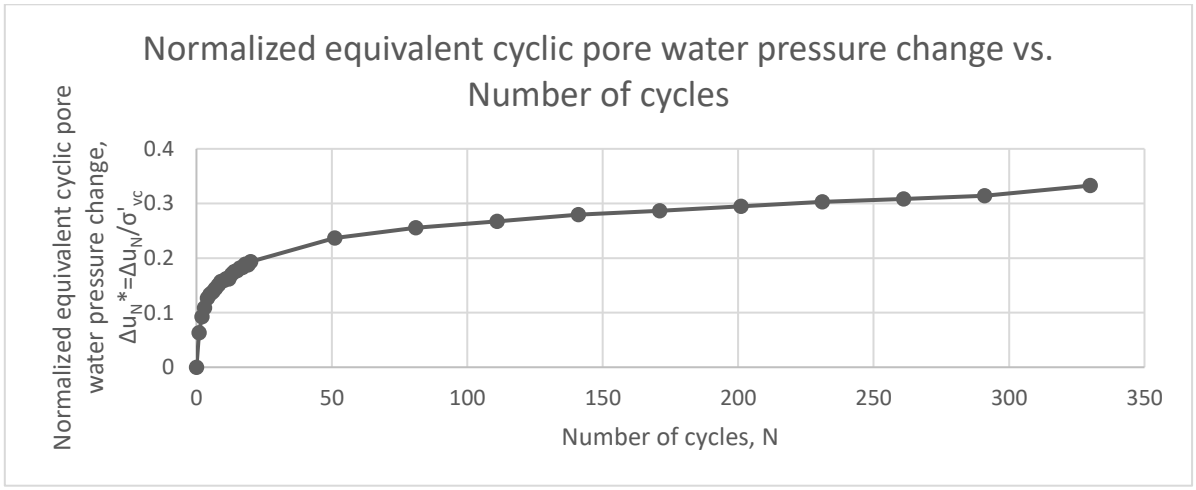

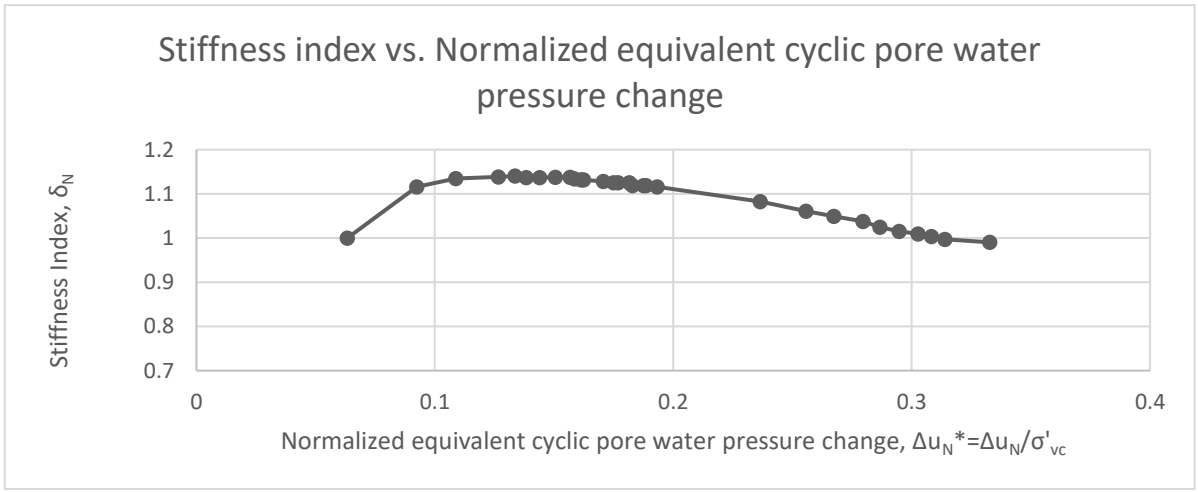

TEST 4

Test: 4.1; Soil: Nevada Sand; e=0.806; w=0%
σ'_{vc}=145 (kPa); OCR=1; Υ_c=0.08%, f=0.01 Hz

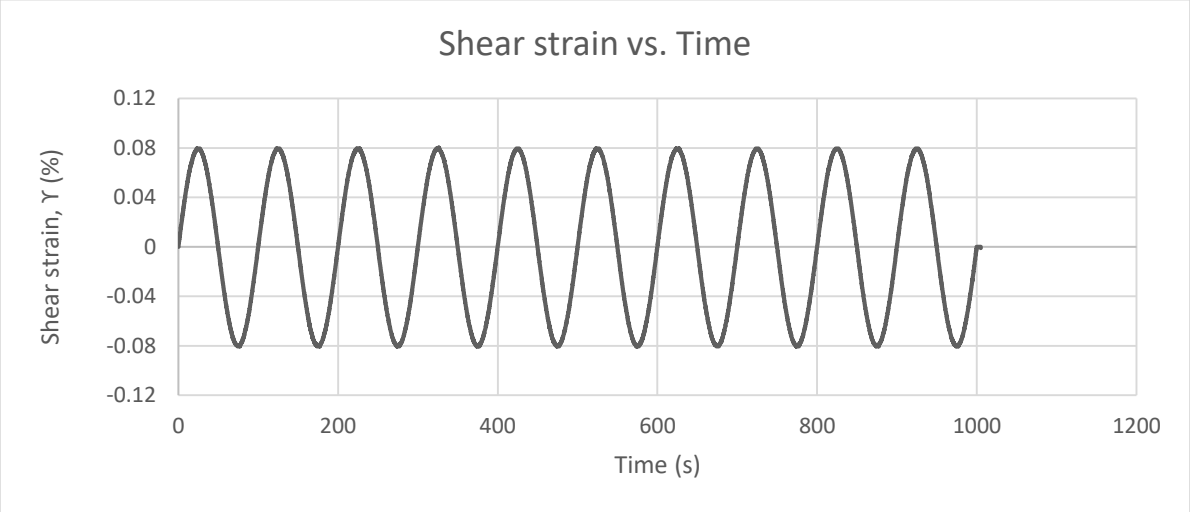

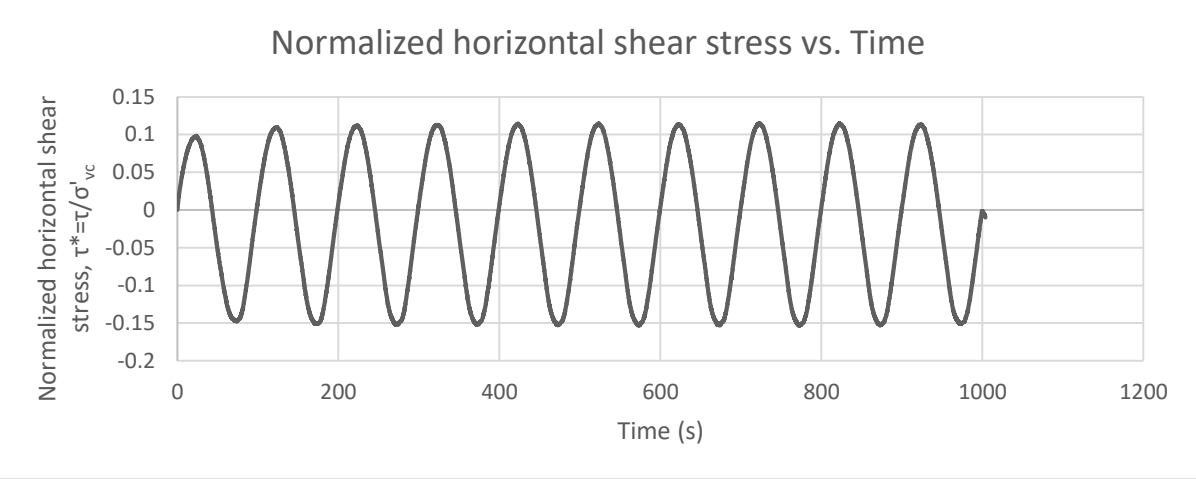

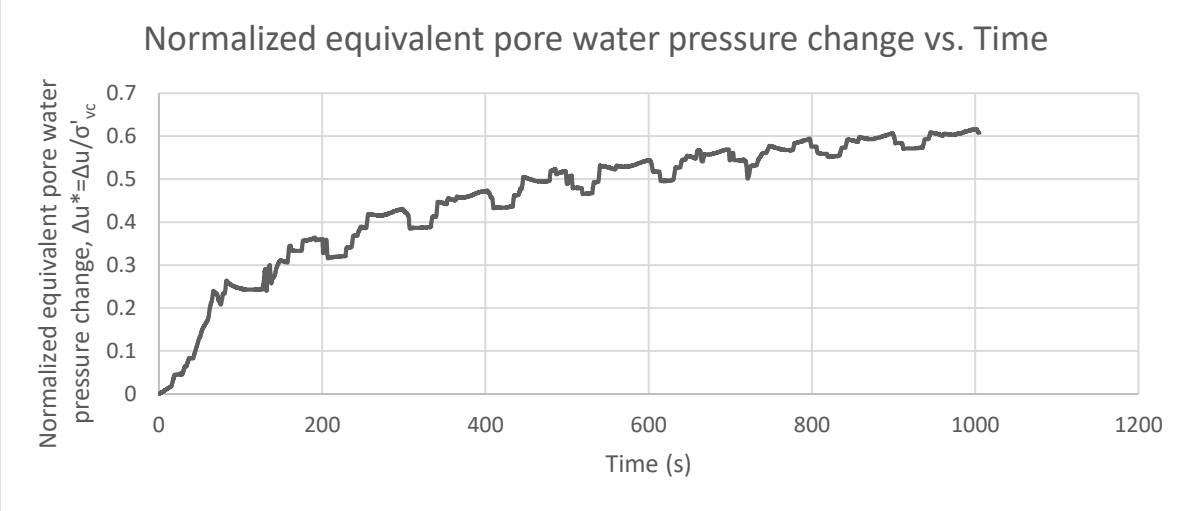

Test: 4.1; Soil: Nevada Sand; e=0.806; w=0%
σ'_{vc}=145 (kPa); OCR=1; Υ_c=0.08%, f=0.01 Hz

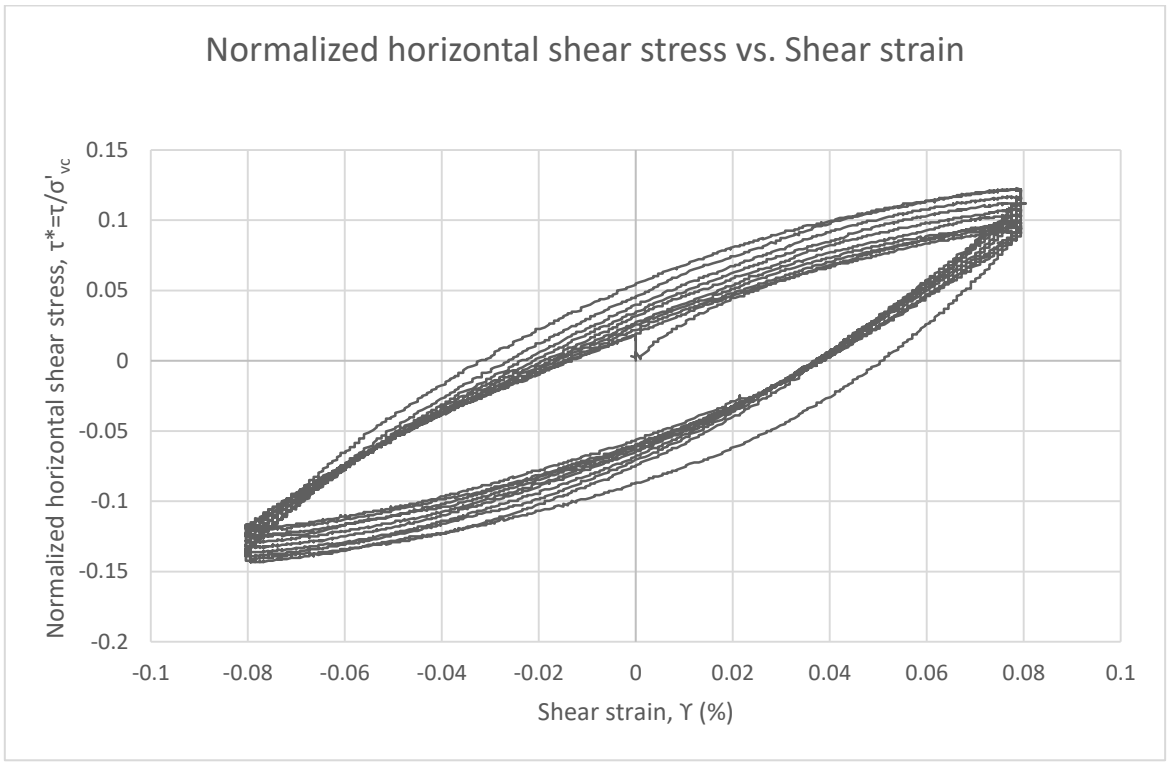

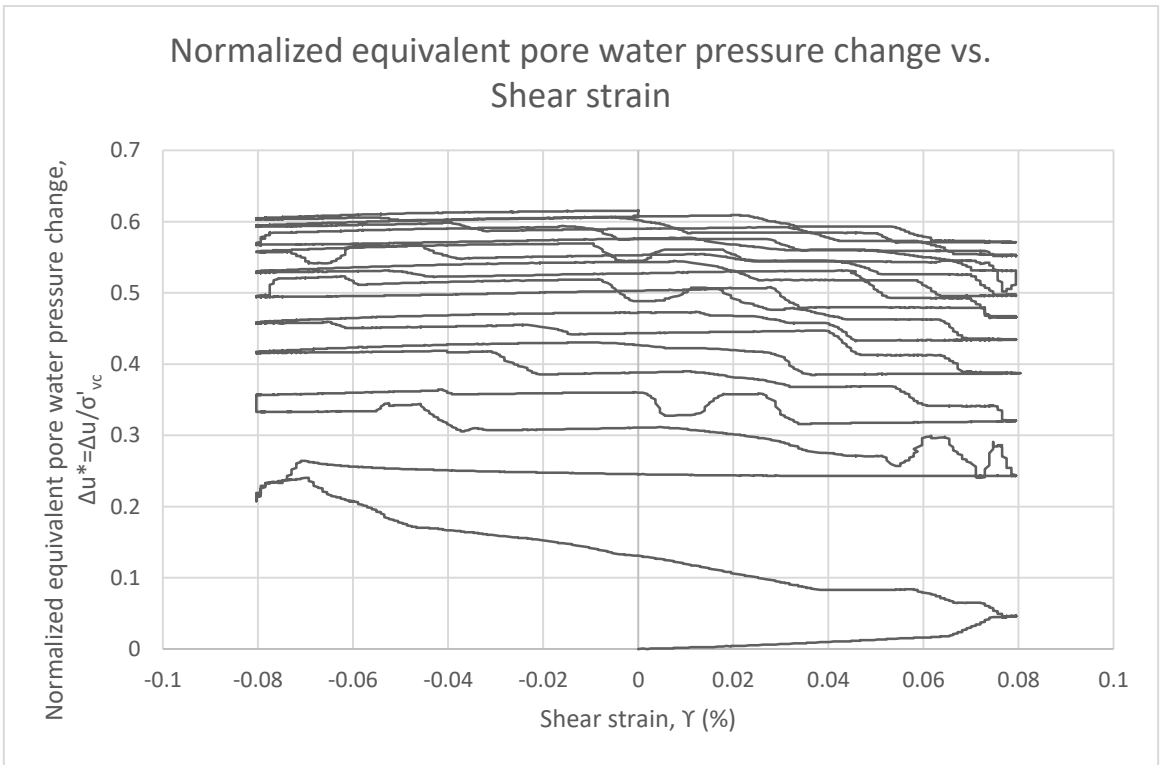

Test: 4.1; Soil: Nevada Sand; e=0.806; w=0%
σ'_{vc}=145 (kPa); OCR=1; Υ_c=0.08%, f=0.01 Hz

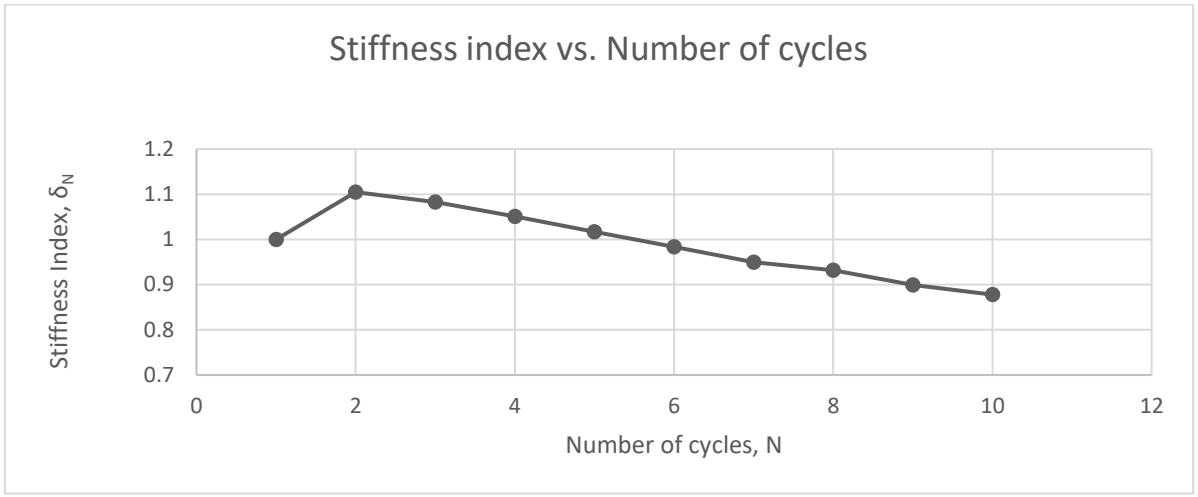

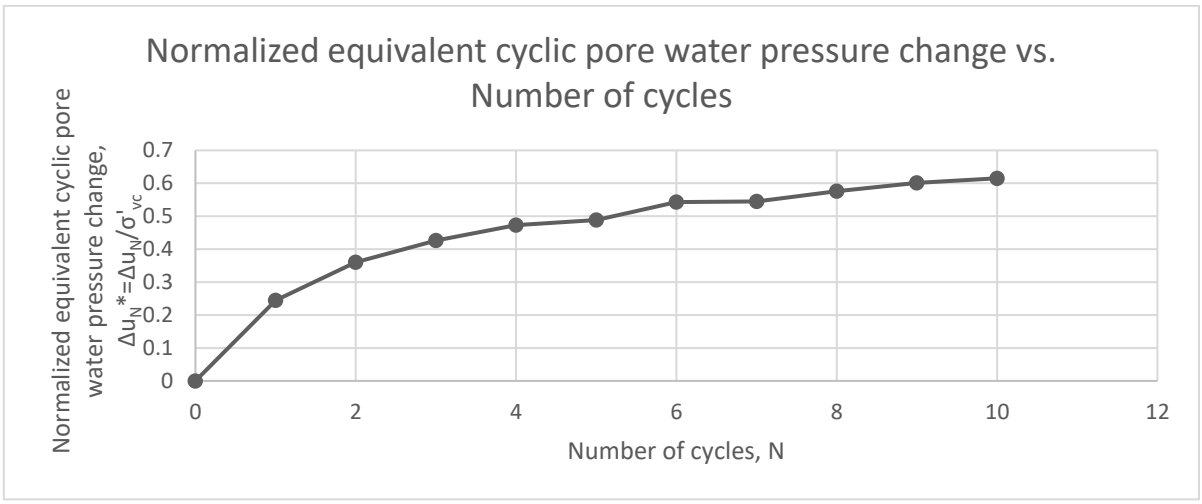

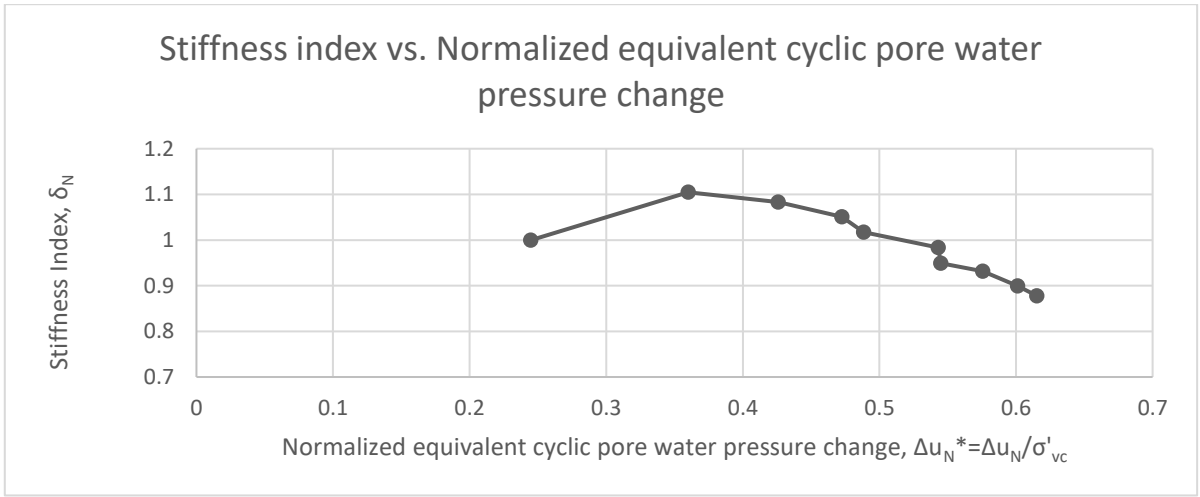

Test: 4.1; Soil: Nevada Sand; e=0.806; w=0%
σ'_{vc}=145 (kPa); OCR=1; Υ_c=0.08%, f=0.01 Hz

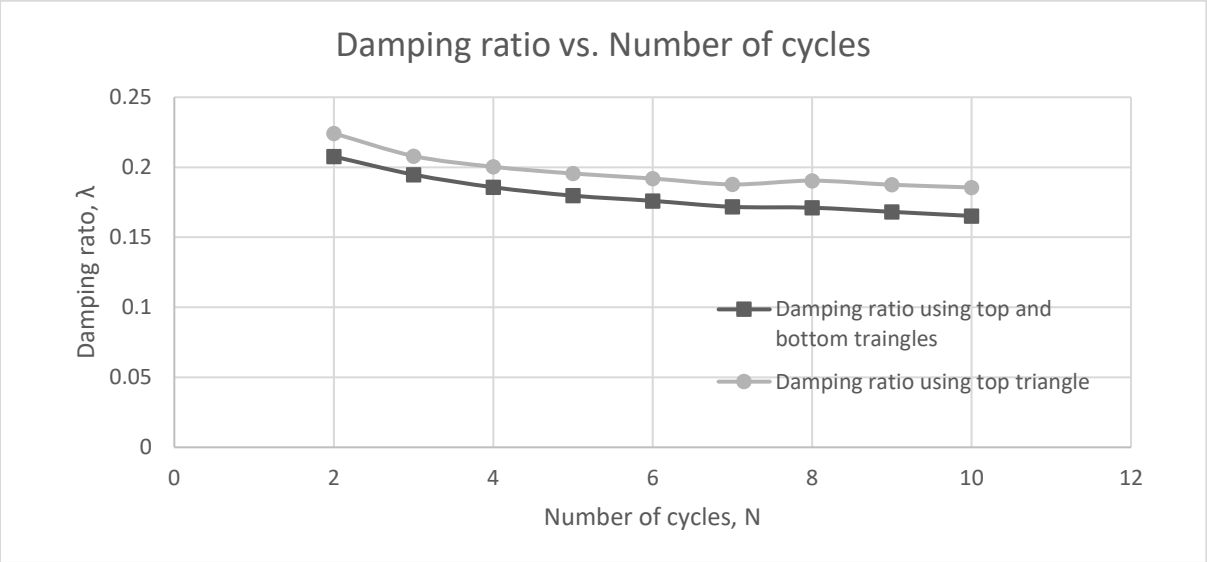

Test: 4.2; Soil: Nevada Sand; e=0.803; w=0%
σ'_{vc}=145 (kPa); OCR=1; Υ_c=0.08%, f=0.01 Hz

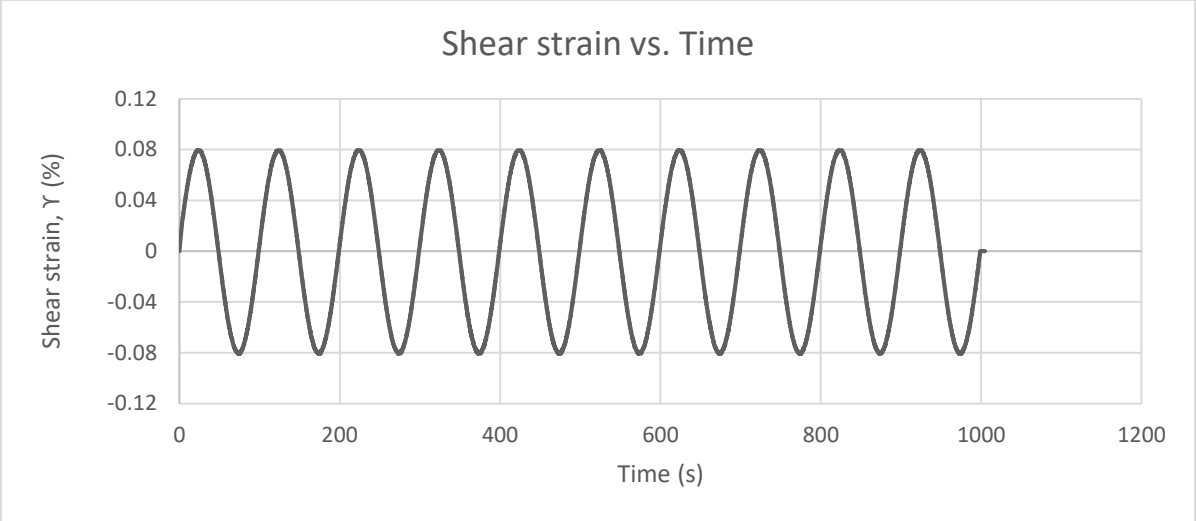

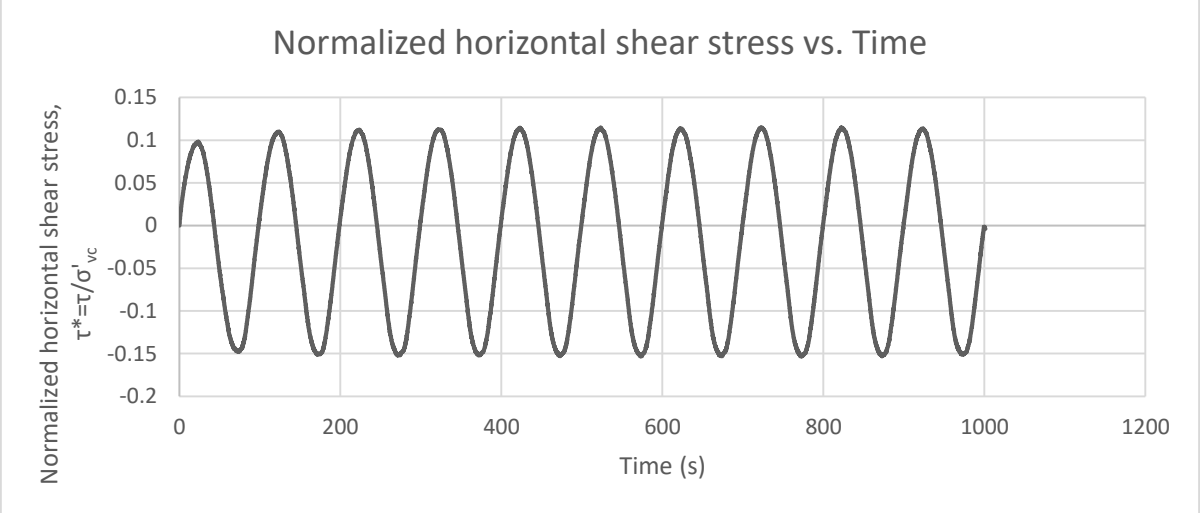

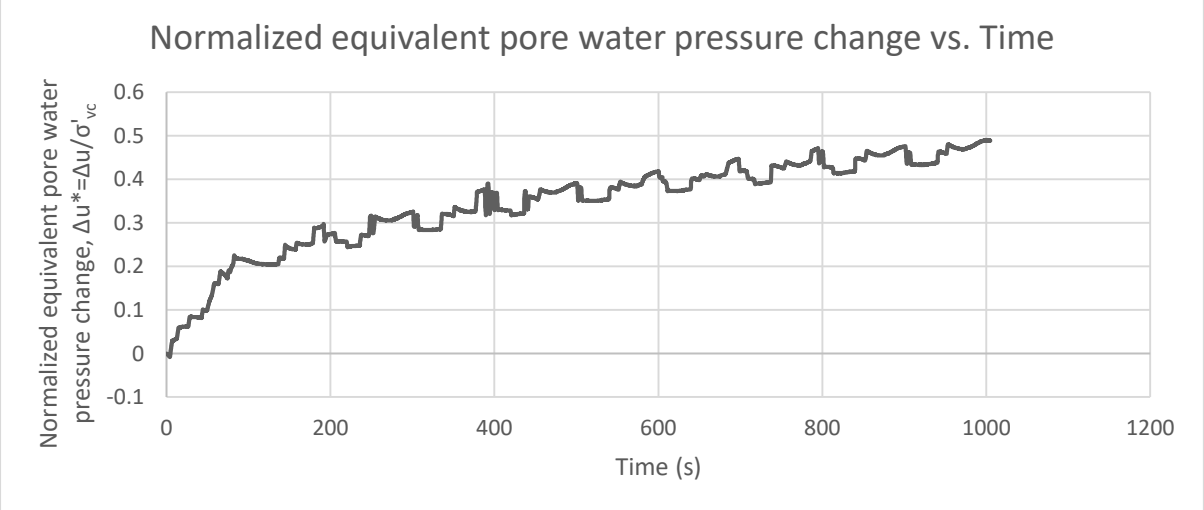

Test: 4.2; Soil: Nevada Sand; e=0.803; w=0%
σ'_{vc}=145 (kPa); OCR=1; Υ_c=0.08%, f=0.01 Hz

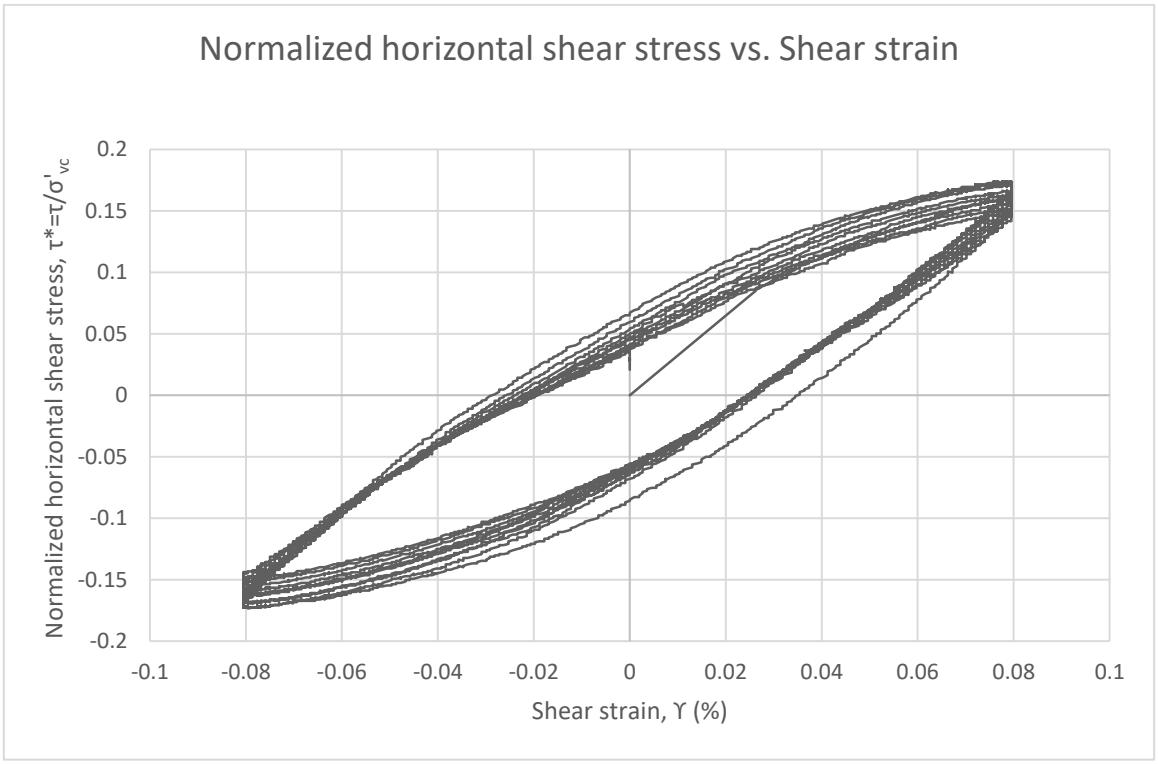

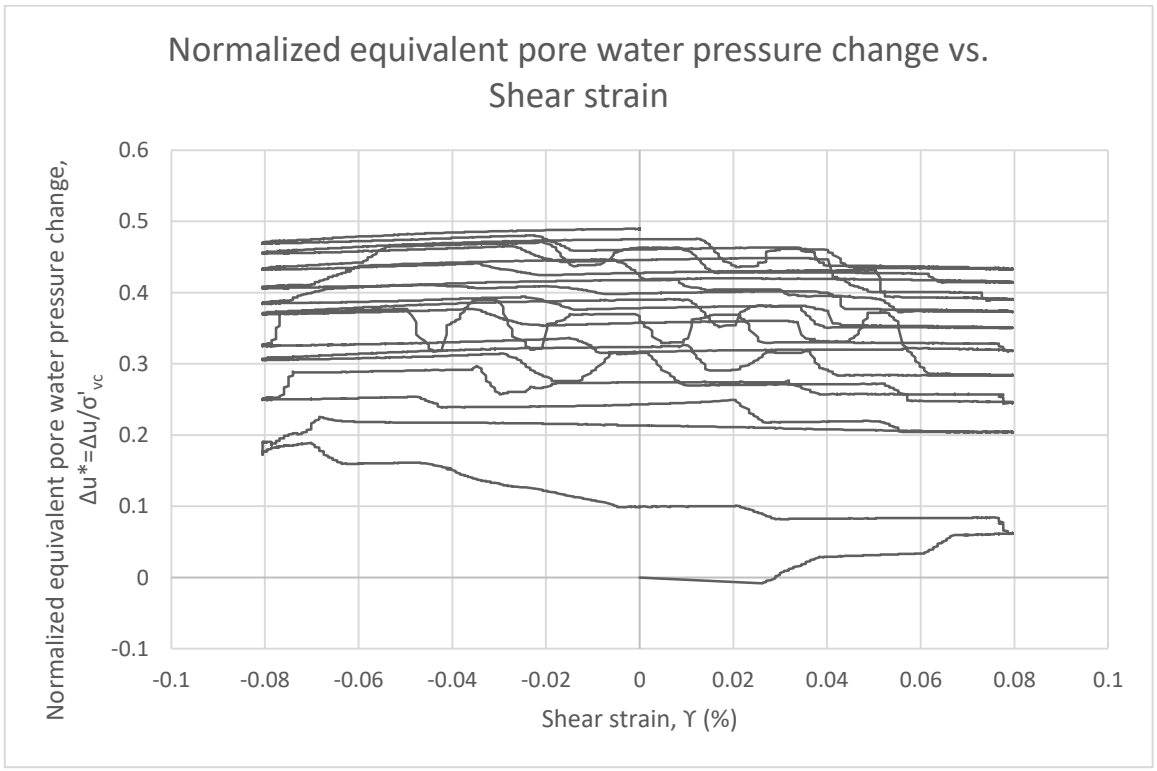

Test: 4.2; Soil: Nevada Sand; e=0.803; w=0%
σ'_{vc}=145 (kPa); OCR=1; Υ_c=0.08%, f=0.01 Hz

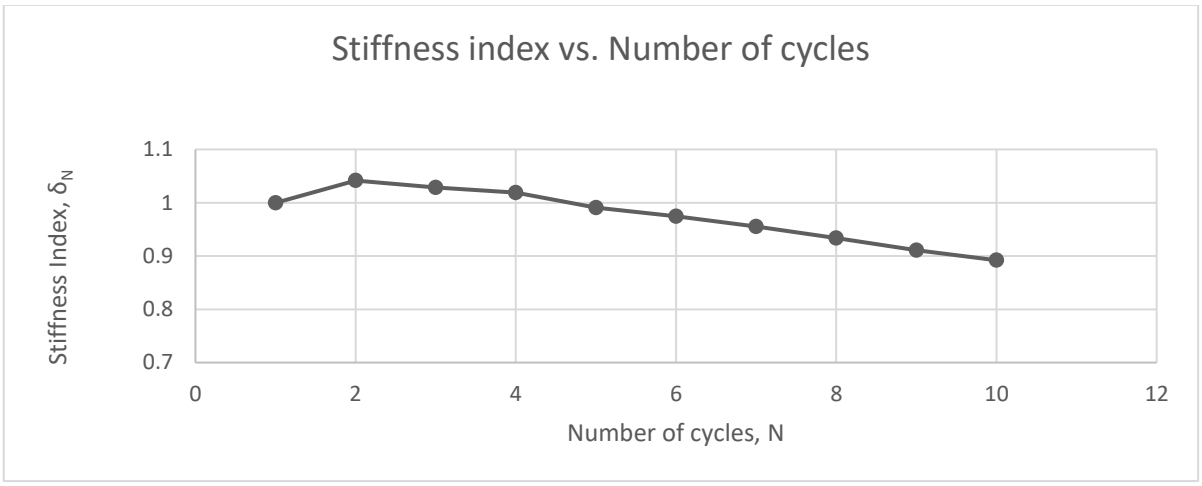

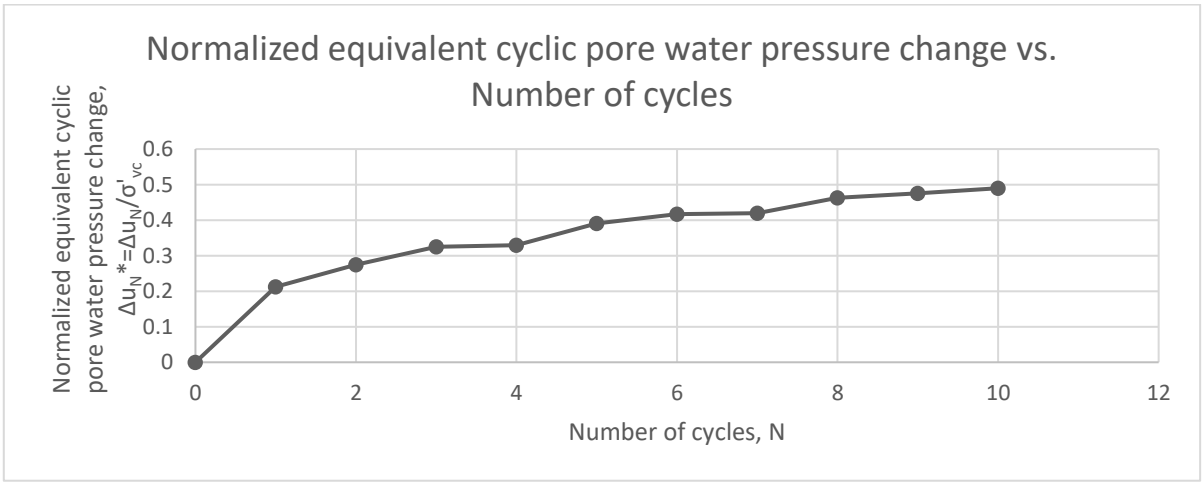

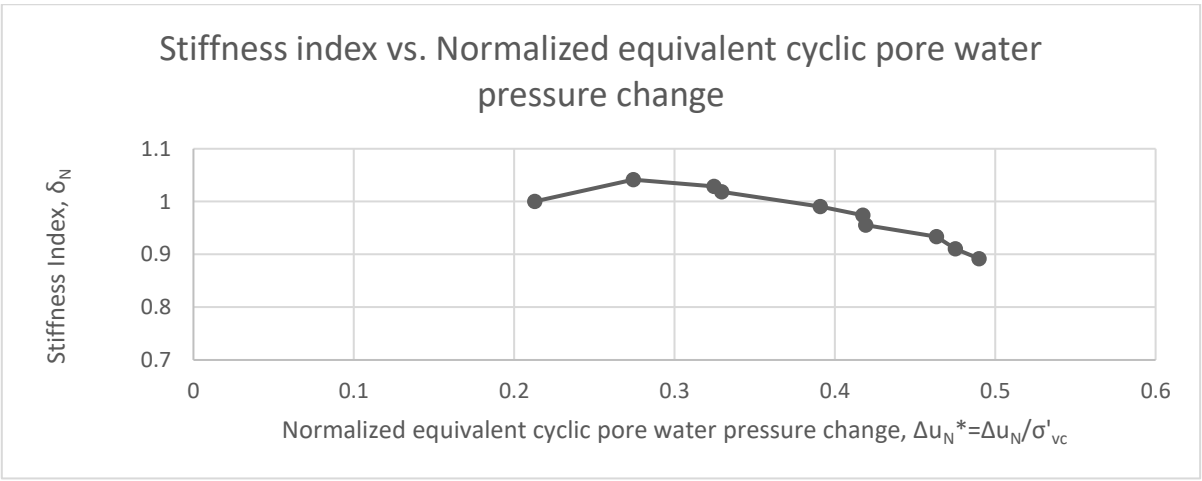

Test: 4.2; Soil: Nevada Sand; e=0.803; w=0%
σ'_{vc}=145 (kPa); OCR=1; Υ_c=0.08%, f=0.01 Hz

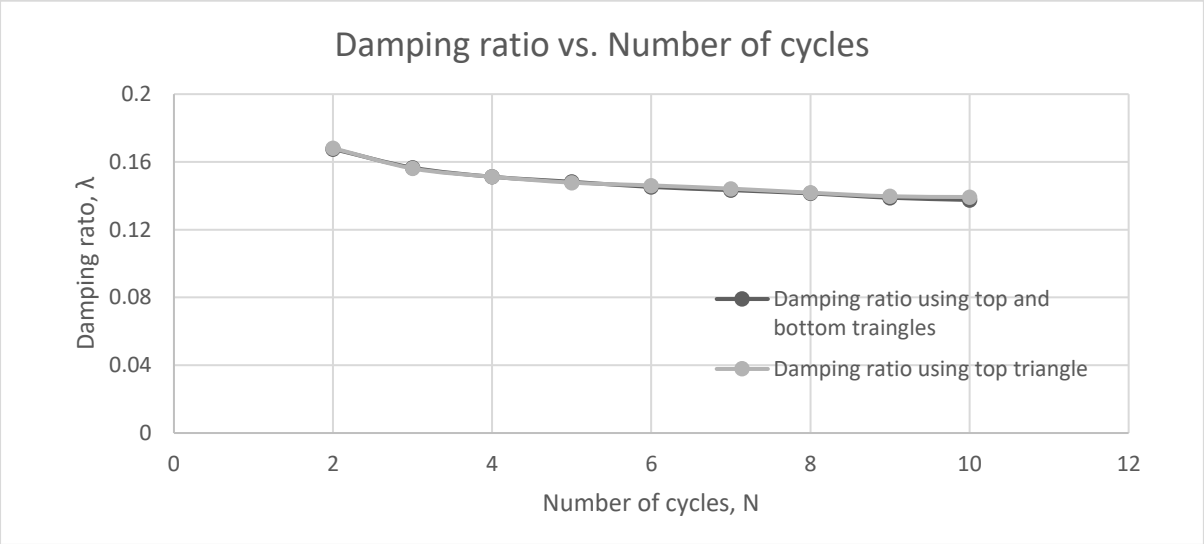

Test: 4.3; Soil: Nevada Sand; e=0.802; w=0%
σ'_{vc}=145 (kPa); OCR=1; Υ_c=0.04%, f=0.01 Hz

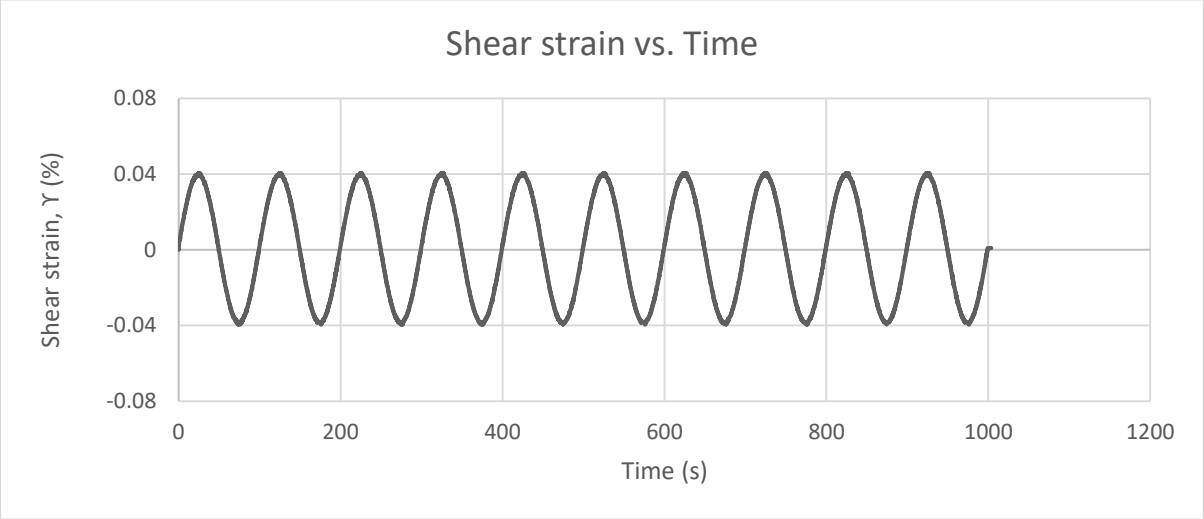

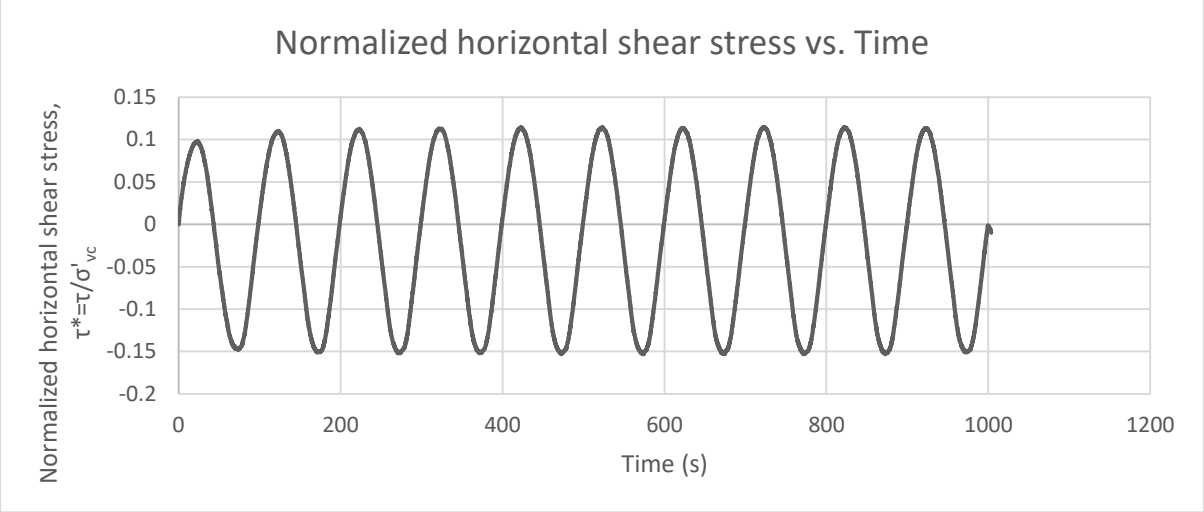

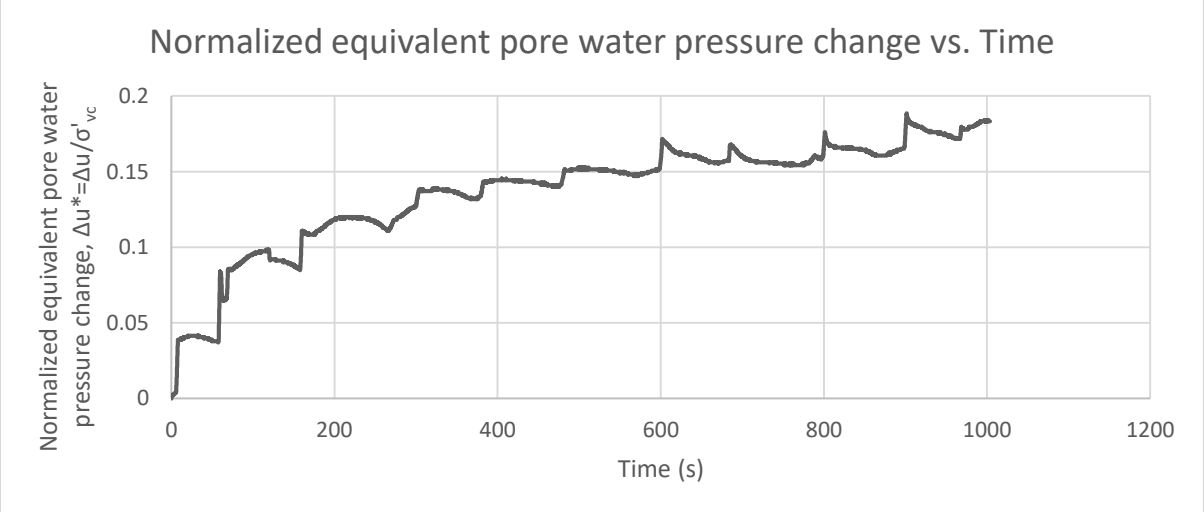

Test: 4.3; Soil: Nevada Sand; e=0.802; w=0%
σ'_{vc}=145 (kPa); OCR=1; Υ_c=0.04%, f=0.01 Hz

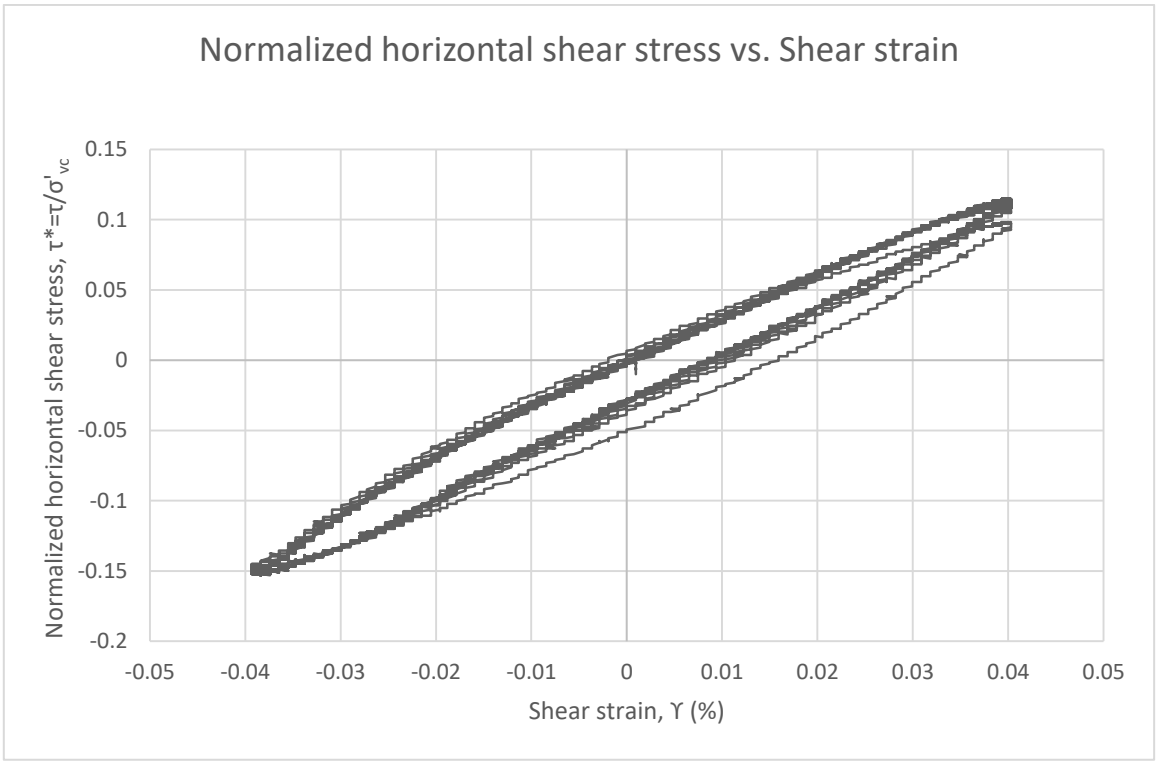

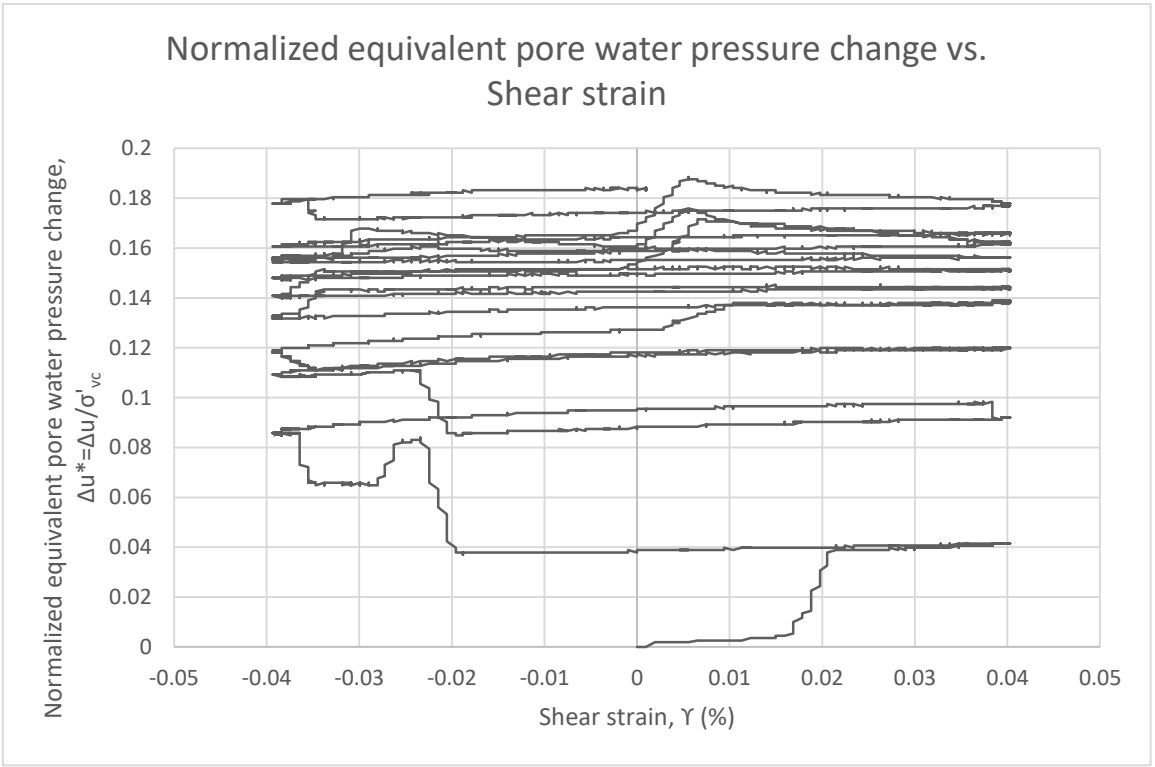

Test: 4.3; Soil: Nevada Sand; e=0.802; w=0%
σ'_{vc}=145 (kPa); OCR=1; Υ_c=0.04%, f=0.01 Hz

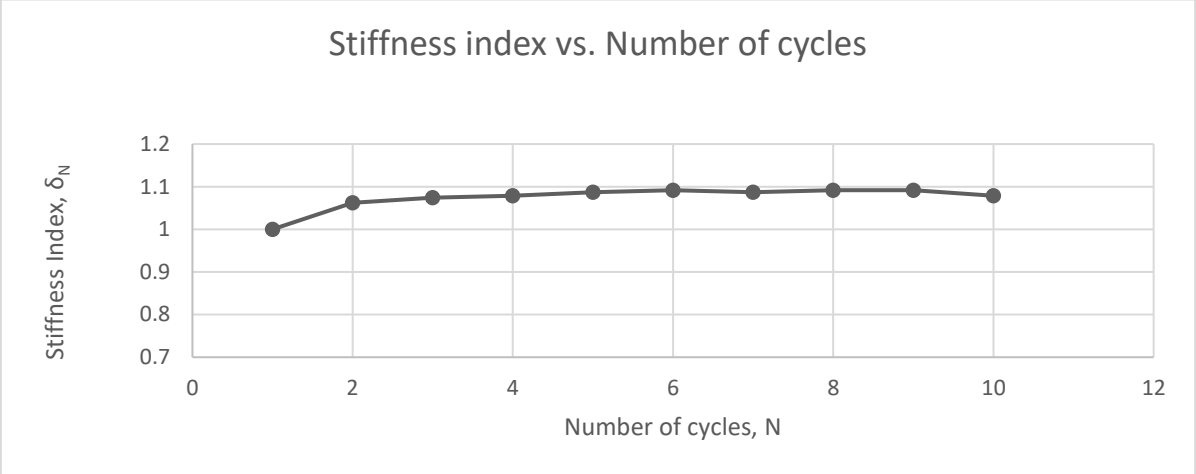

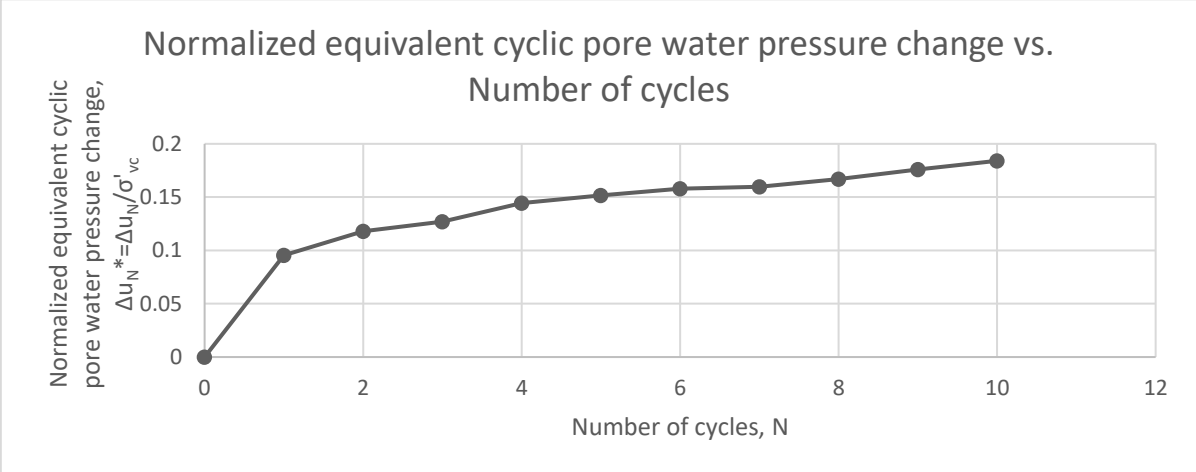

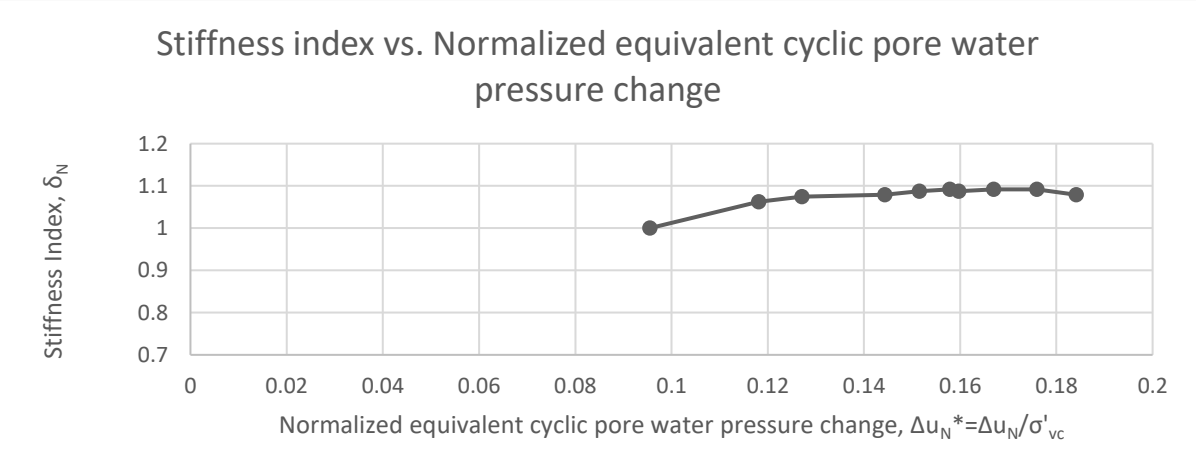

Test: 4.3; Soil: Nevada Sand; e=0.802; w=0%
σ'_{vc}=145 (kPa); OCR=1; Υ_c=0.04%, f=0.01 Hz

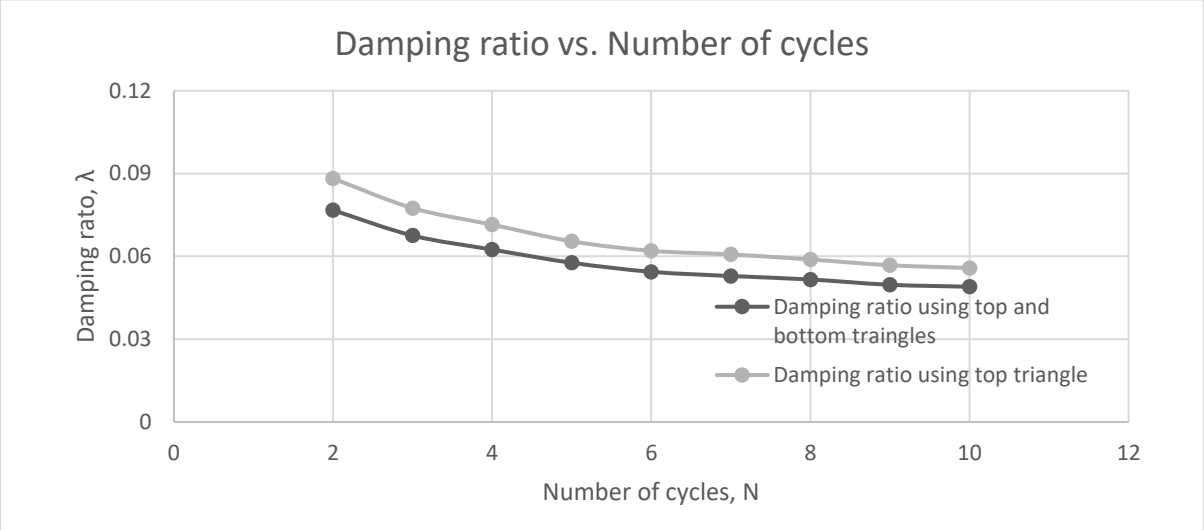

Test: 4.4; Soil: Nevada Sand; e=0.801; w=0%
σ'_{vc}=145 (kPa); OCR=1; Υ_c=0.02%, f=0.01 Hz

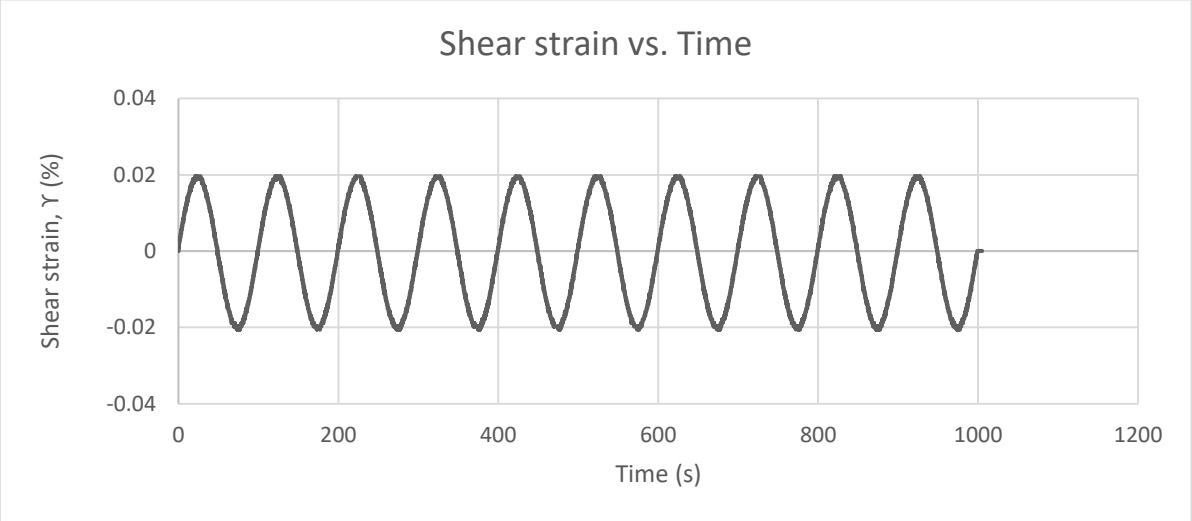

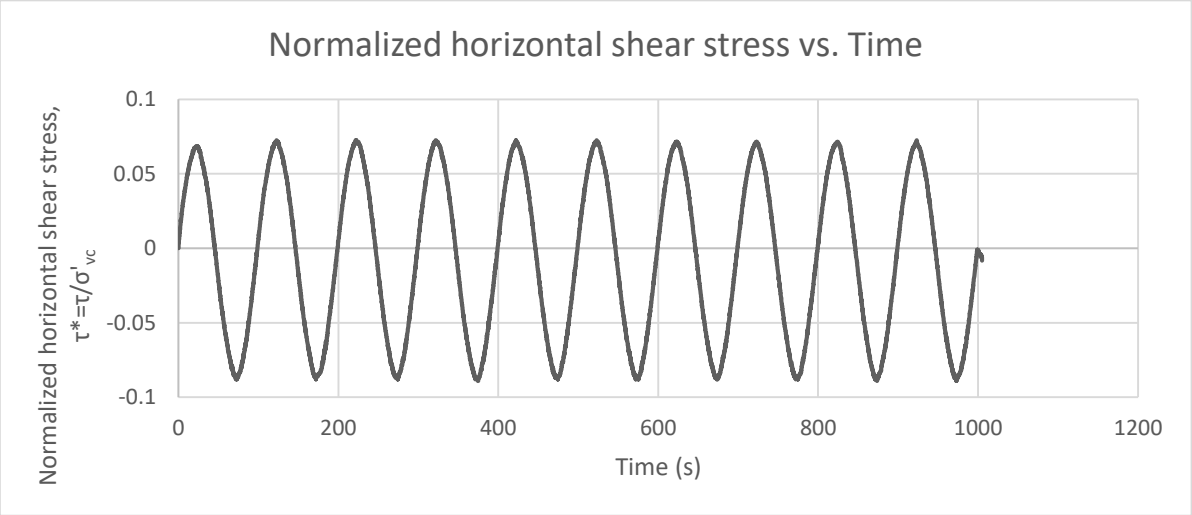

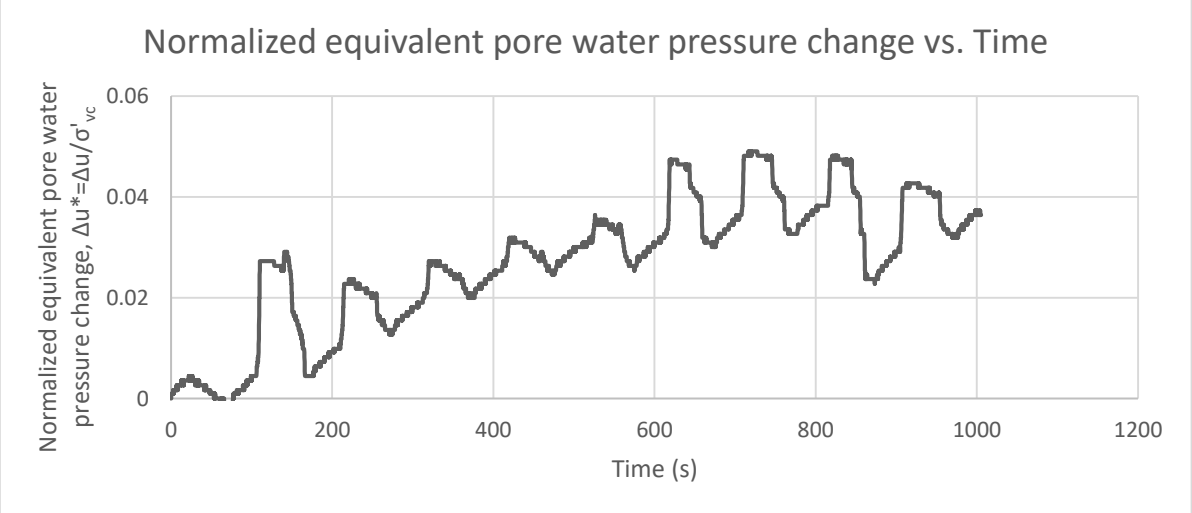

Test: 4.4; Soil: Nevada Sand; e=0.801; w=0%
σ'_{vc}=145 (kPa); OCR=1; Υ_c=0.02%, f=0.01 Hz

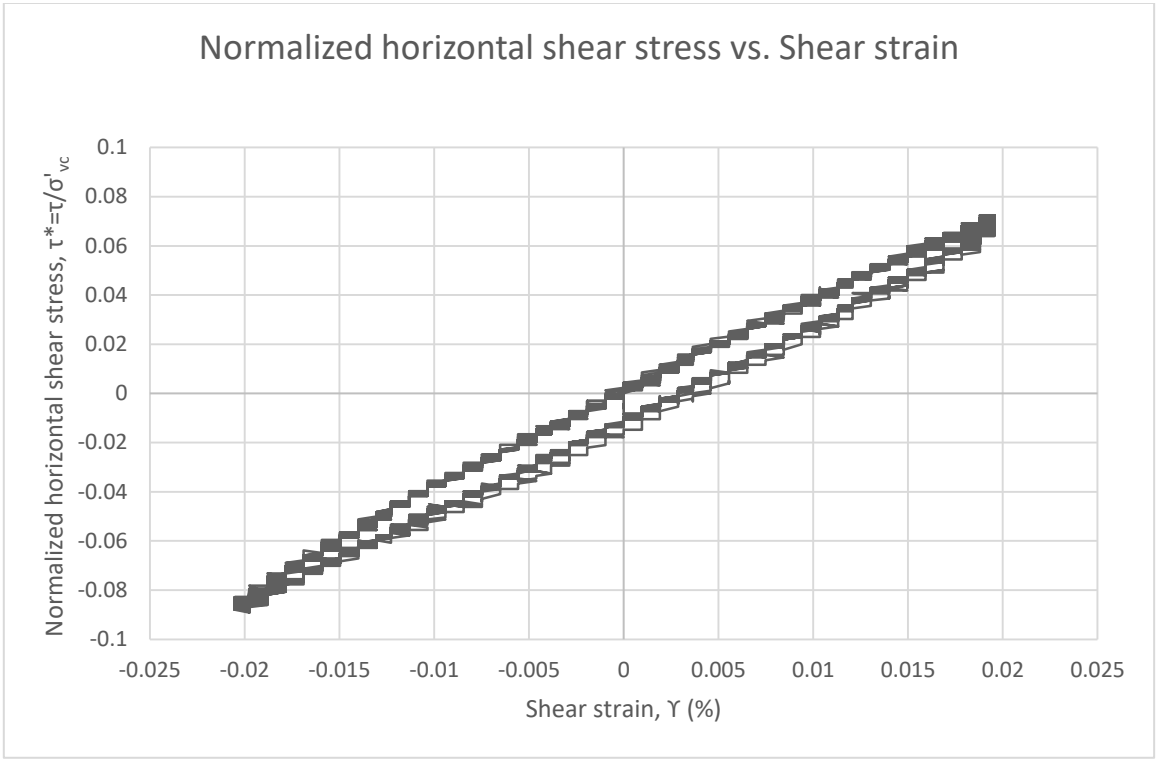

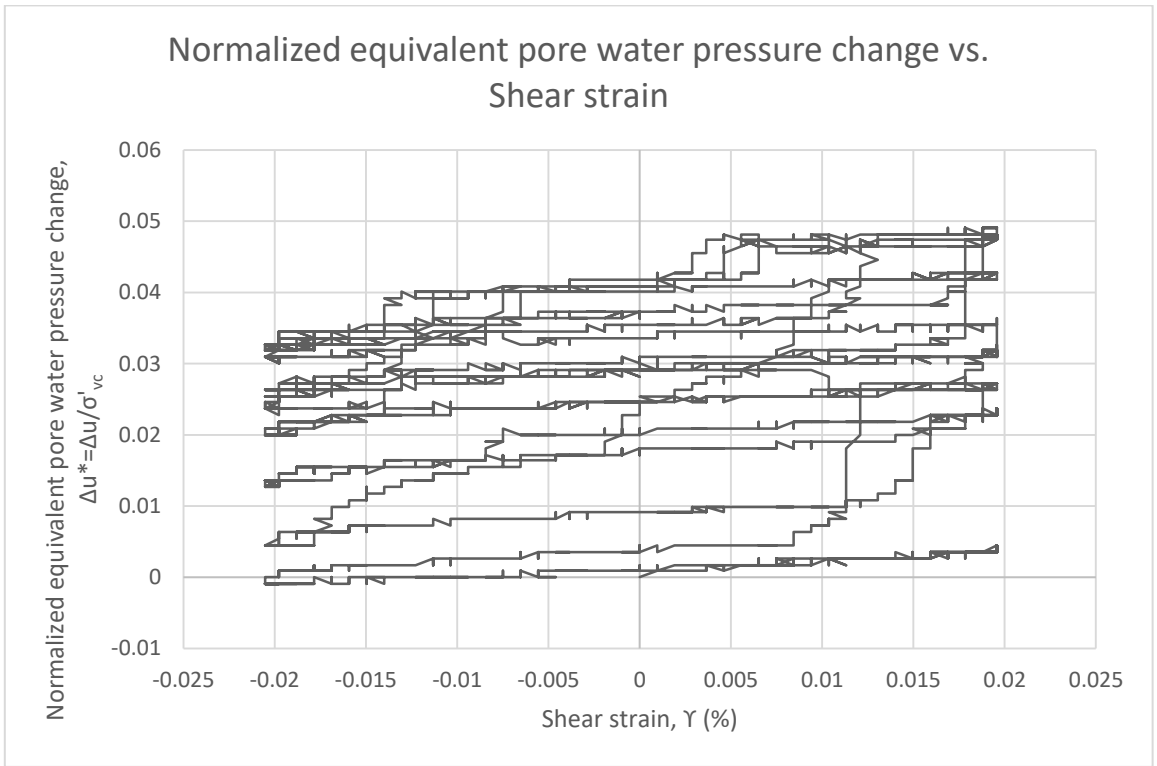

Test: 4.4; Soil: Nevada Sand; e=0.801; w=0%
σ'_{vc}=145 (kPa); OCR=1; Υ_c=0.02%, f=0.01 Hz

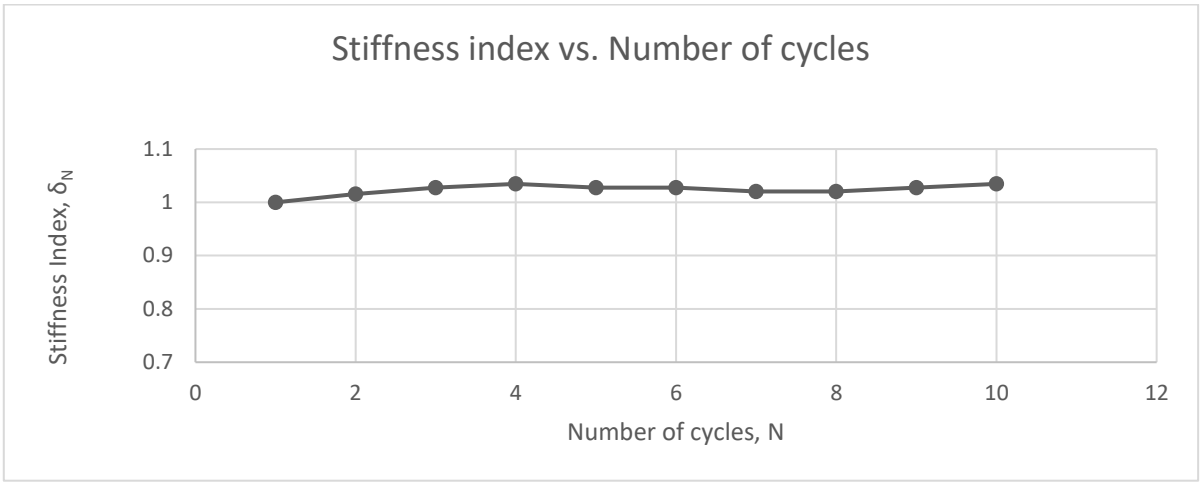

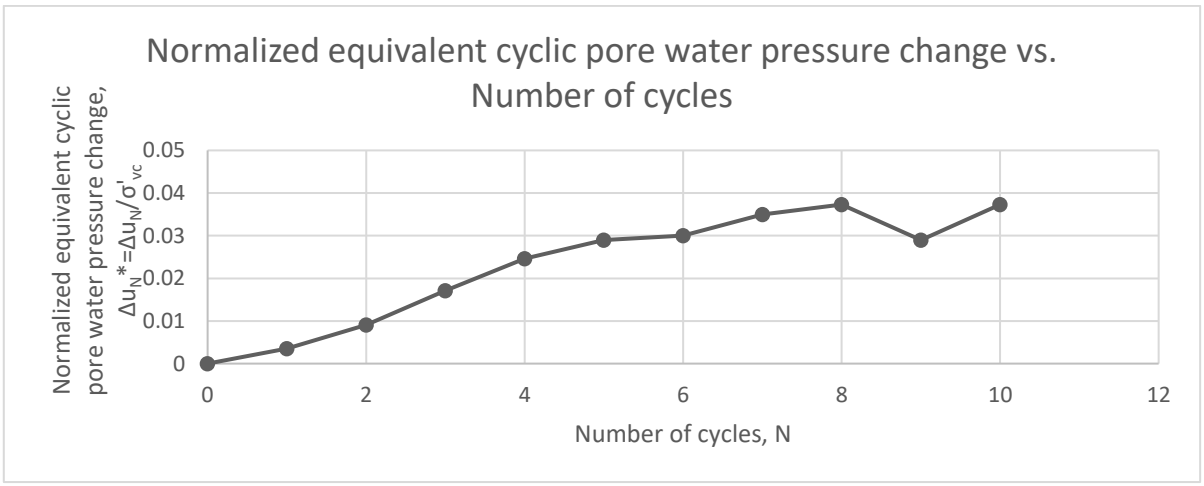

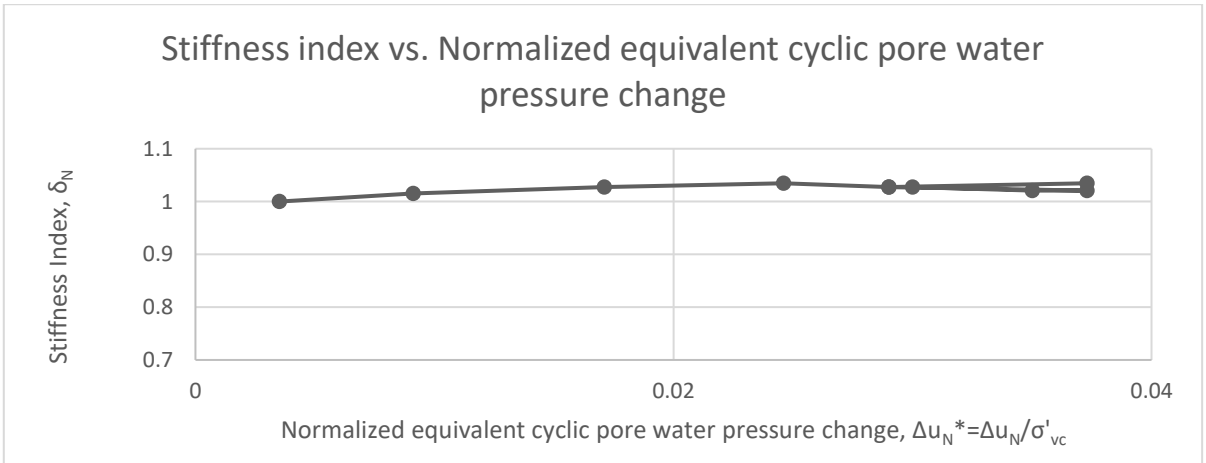

Test: 4.4; Soil: Nevada Sand; e=0.801; w=0%
σ'_{vc}=145 (kPa); OCR=1; Υ_c=0.02%, f=0.01 Hz

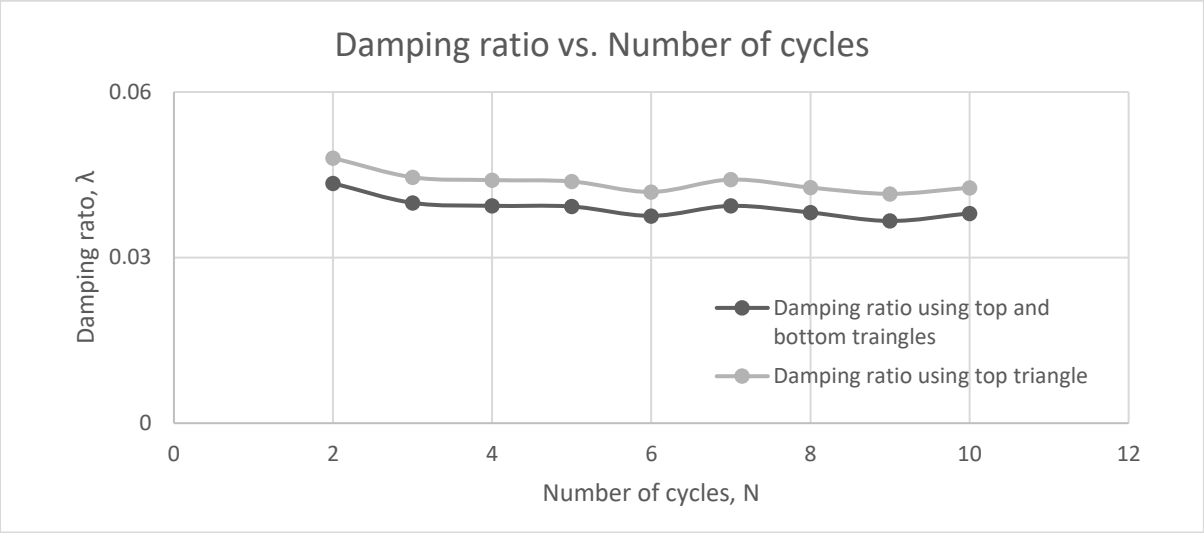

Test: 4.5; Soil: Nevada Sand; e=0.801; w=0%
σ'_{vc}=145 (kPa); OCR=1; Υ_c=0.01%, f=0.01 Hz

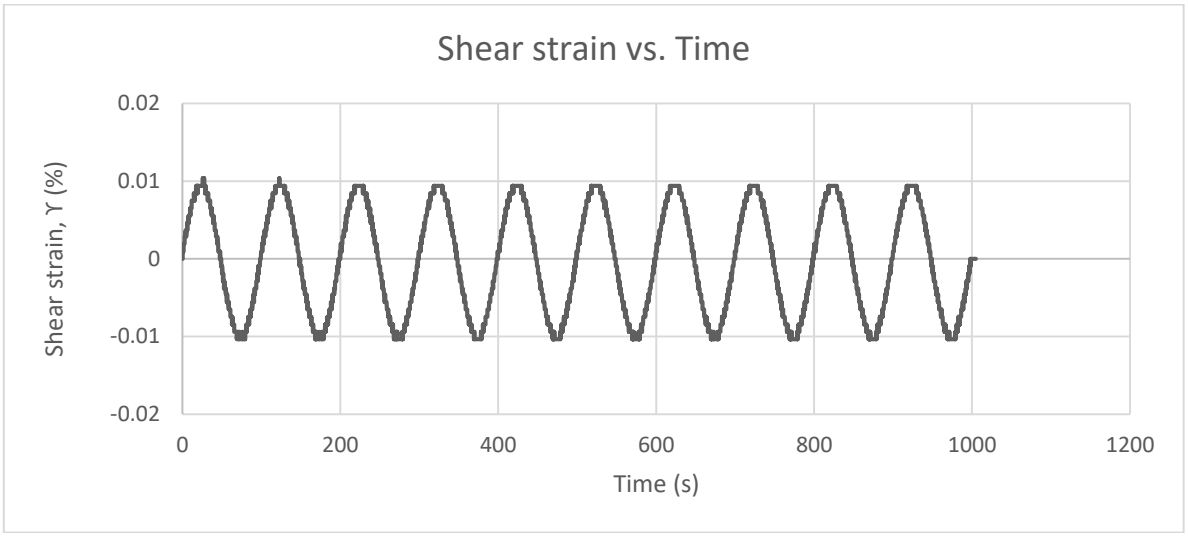

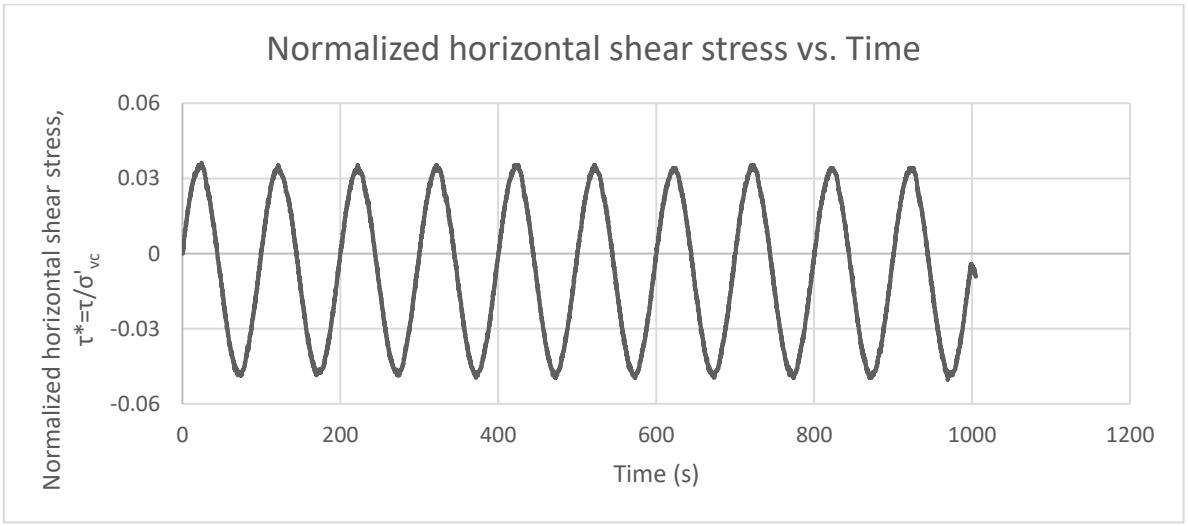

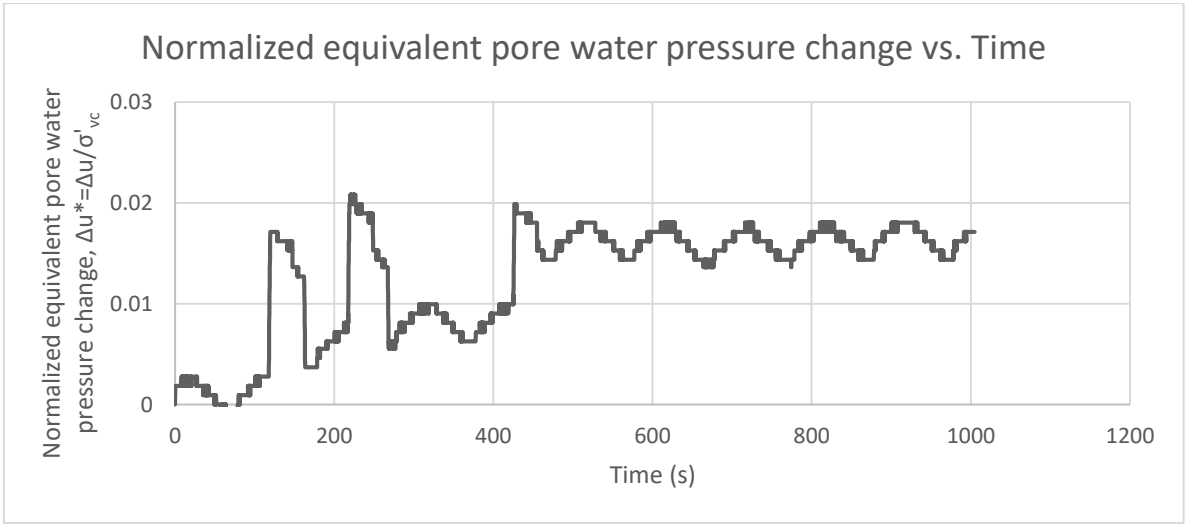

Test: 4.5; Soil: Nevada Sand; e=0.801; w=0%
σ'_{vc}=145 (kPa); OCR=1; Υ_c=0.01%, f=0.01 Hz

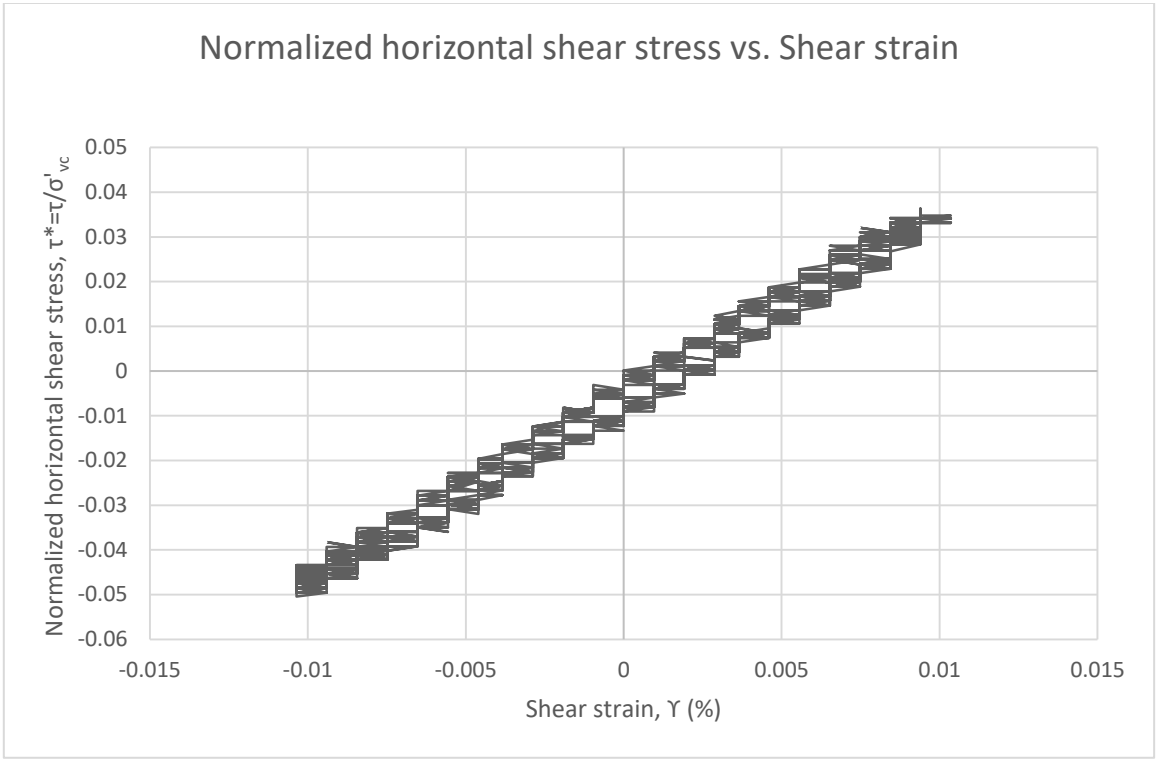

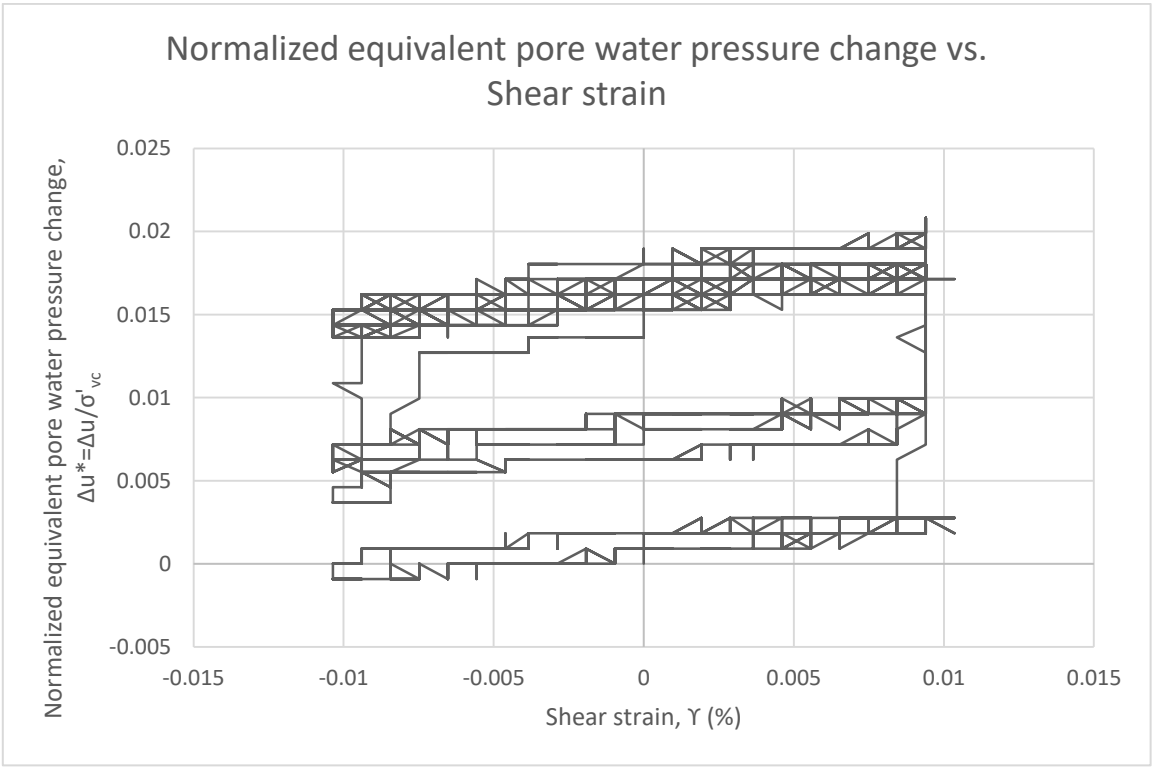

Test: 4.5; Soil: Nevada Sand; e=0.801; w=0%
σ'_{vc}=145 (kPa); OCR=1; Υ_c=0.01%, f=0.01 Hz

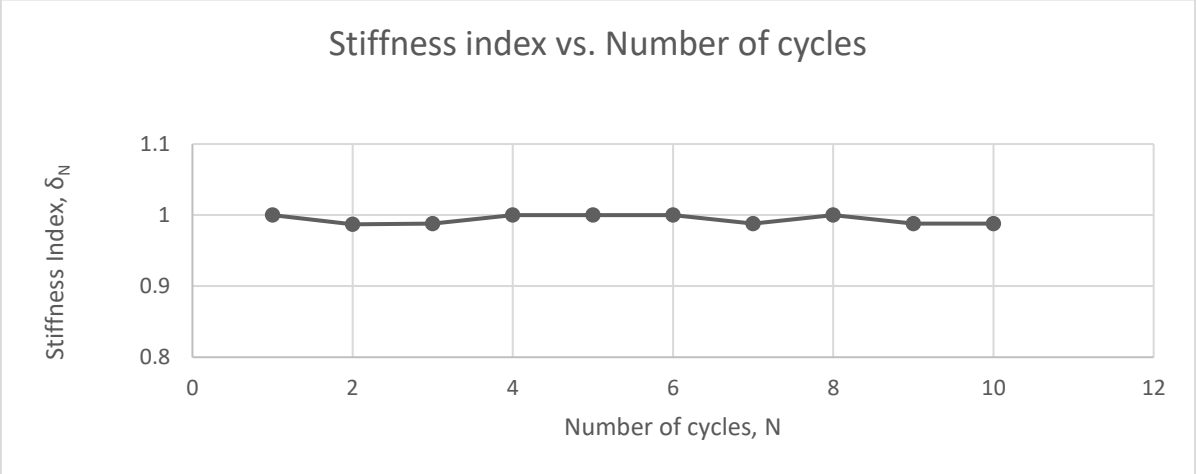

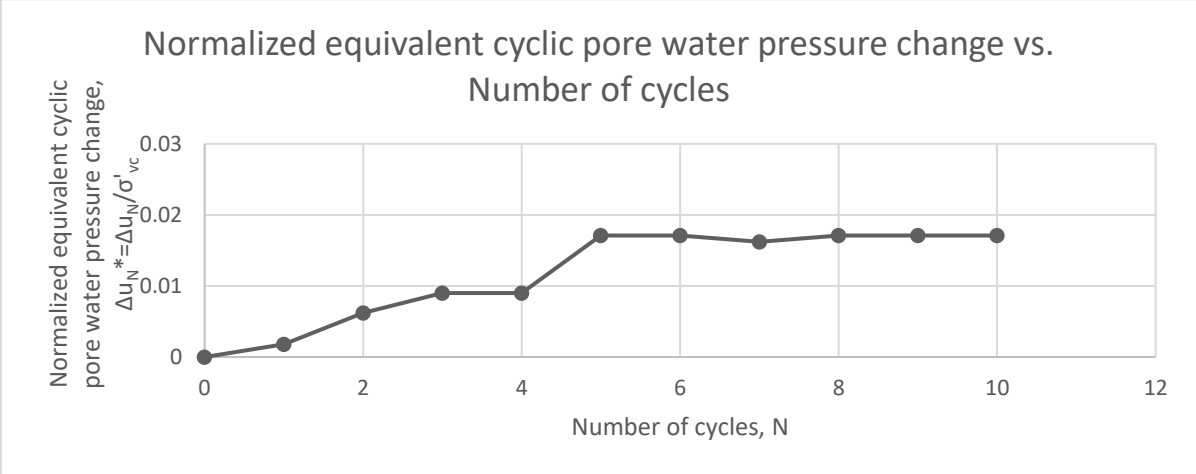

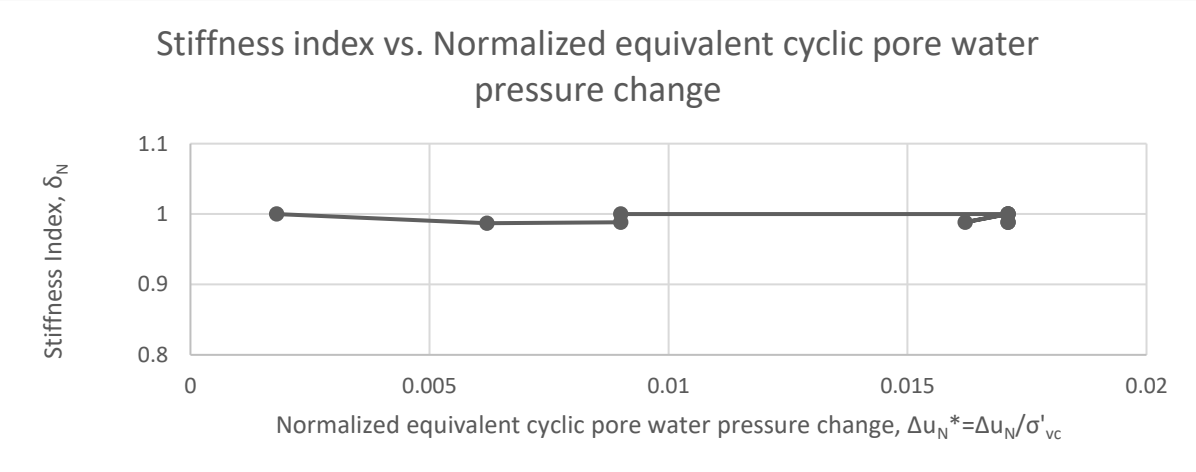

Test: 4.6; Soil: Nevada Sand; e=0.801; w=0%
σ'_{vc}=145 (kPa); OCR=1; Υ_c=0.005%, f=0.01 Hz

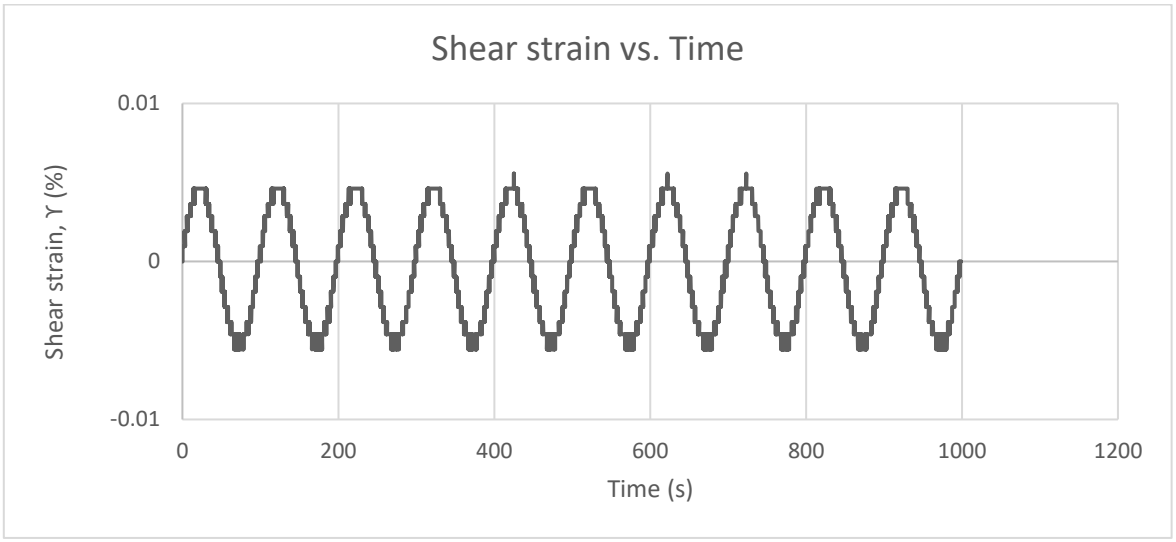

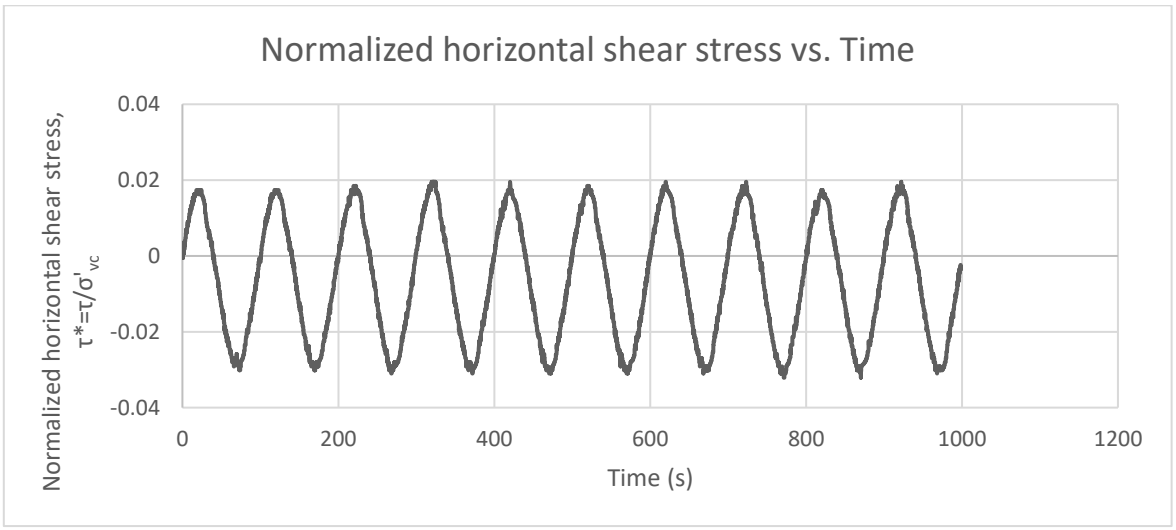

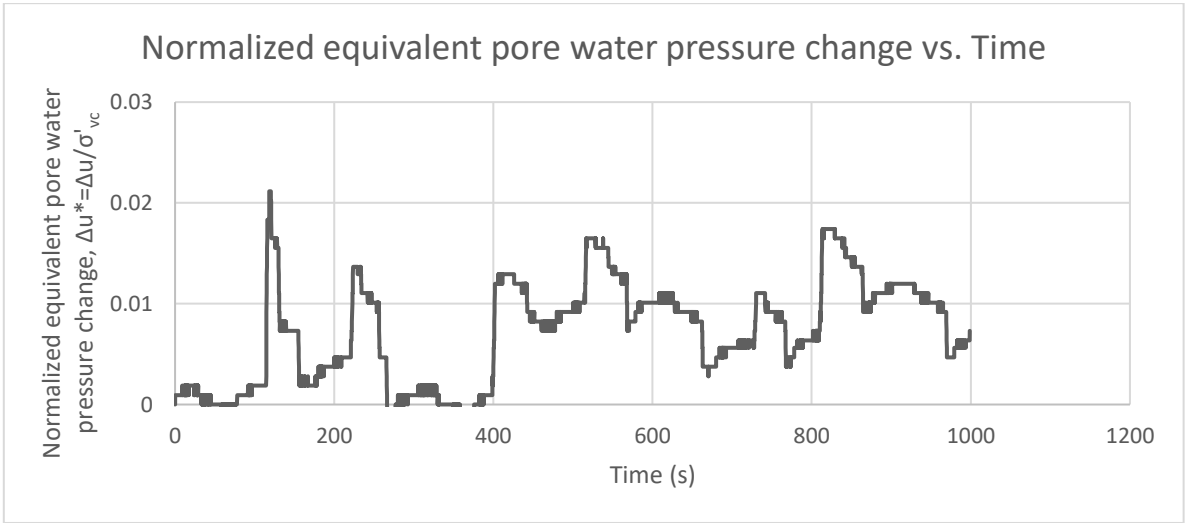

Test: 4.6; Soil: Nevada Sand; e=0.801; w=0%
σ'_{vc}=145 (kPa); OCR=1; Υ_c=0.005%, f=0.01 Hz

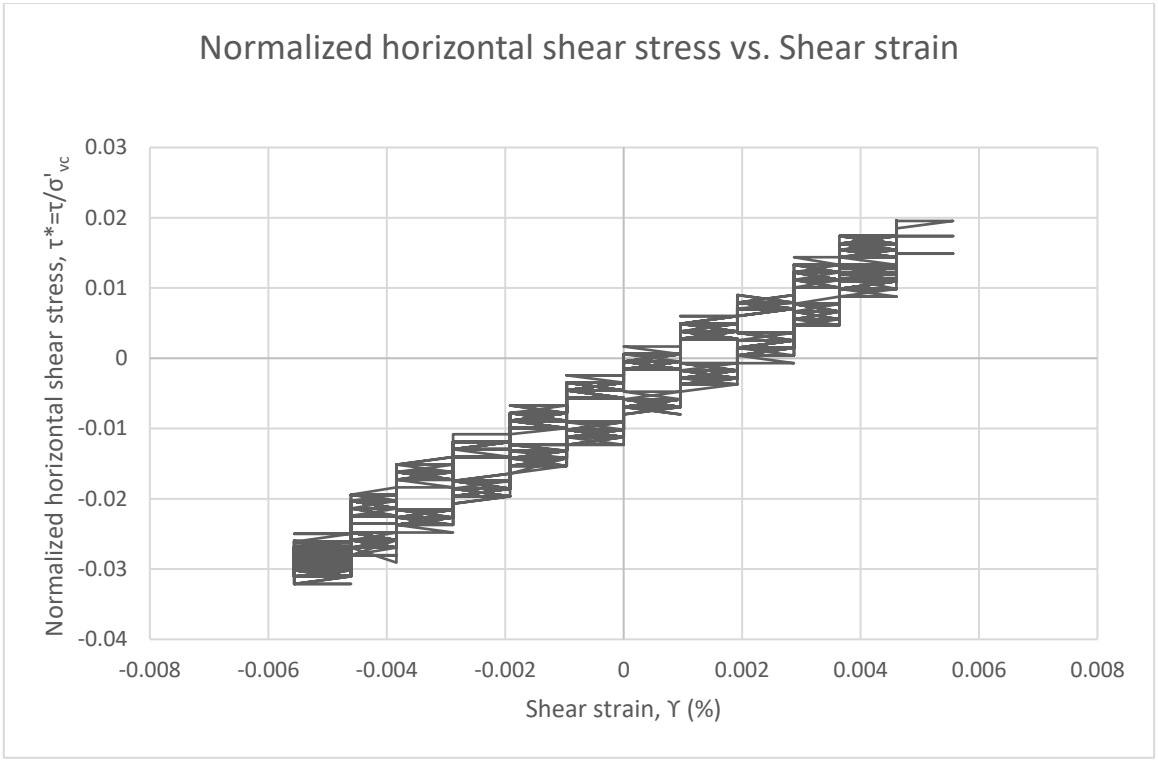

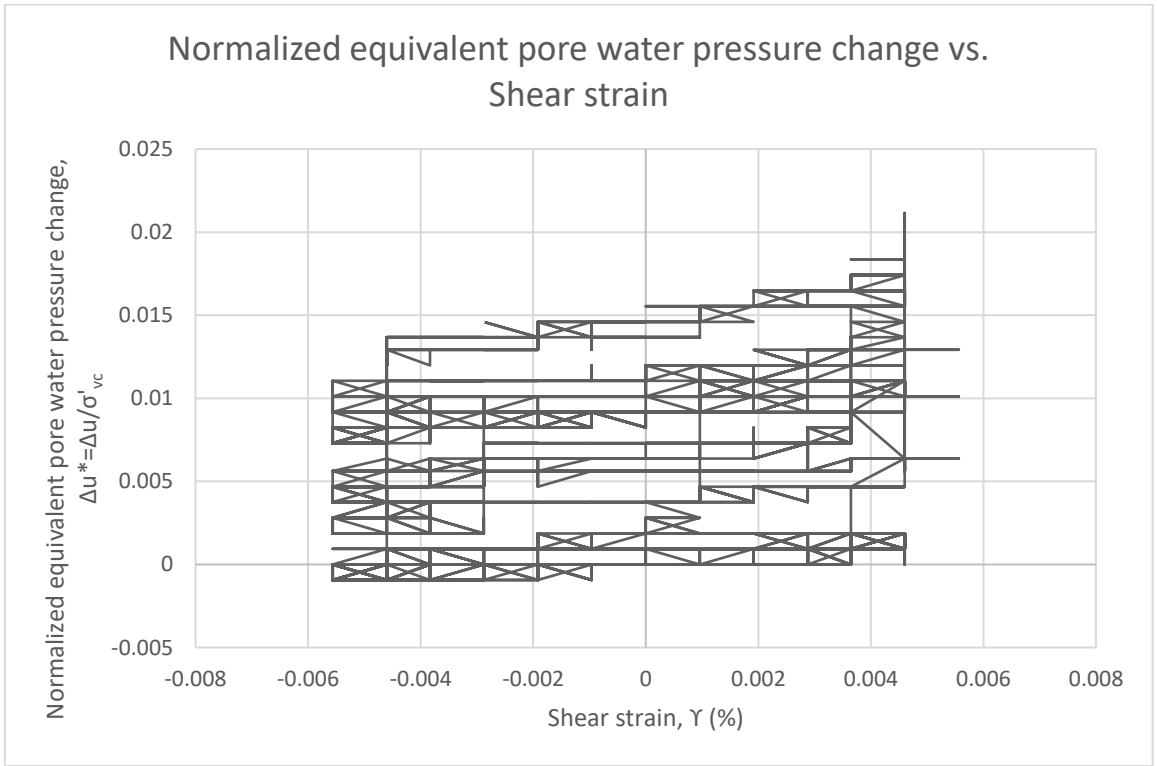

Test: 4.6; Soil: Nevada Sand; e=0.801; w=0%
σ'_{vc}=145 (kPa); OCR=1; Υ_c=0.005%, f=0.01 Hz

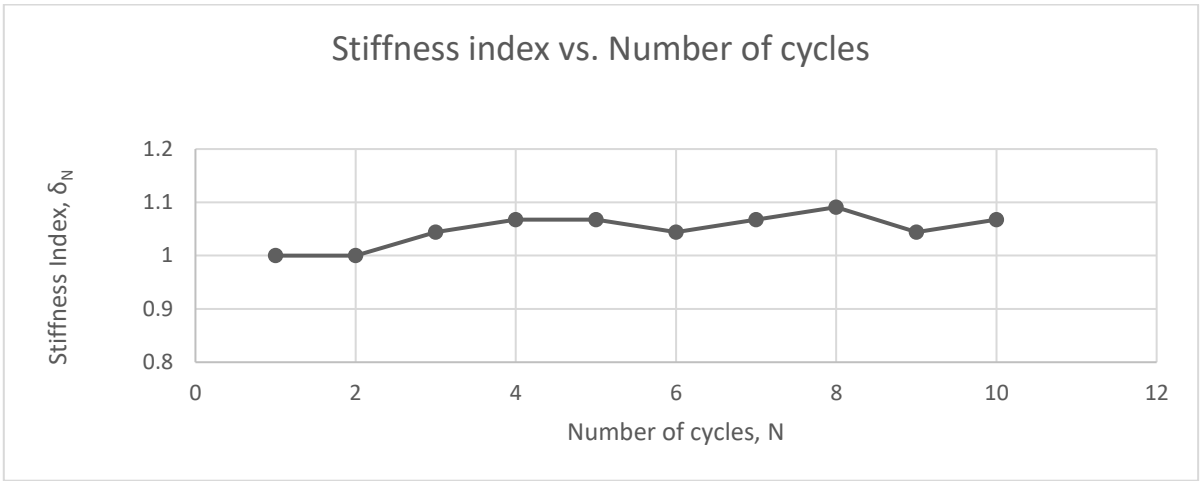

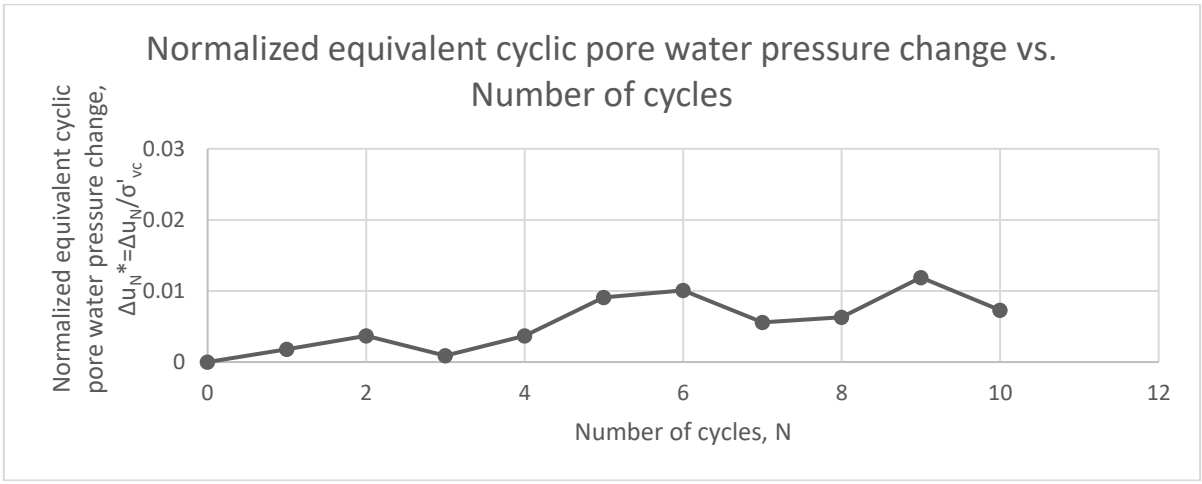

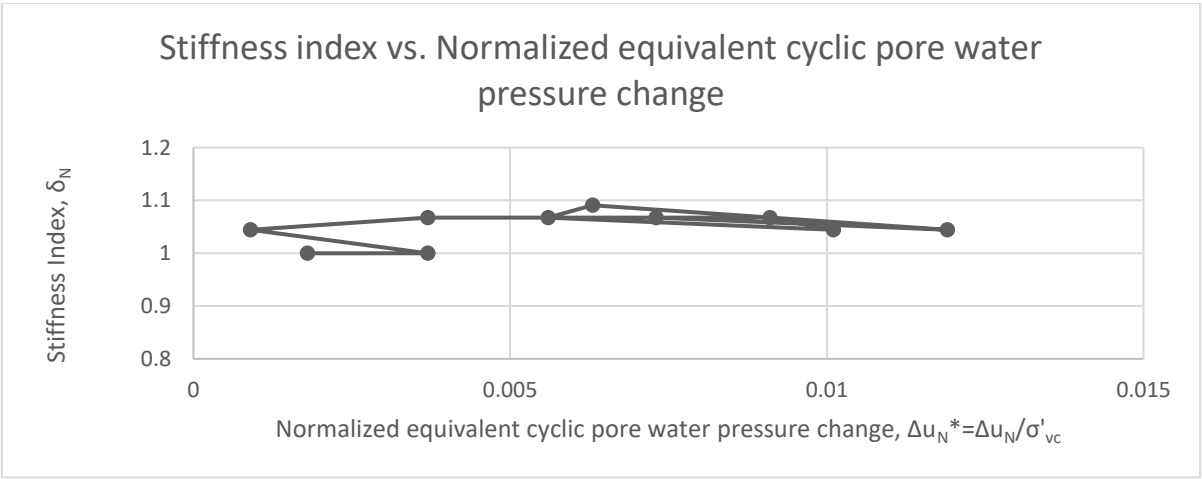

TEST 5

Test: 5.1; Soil: Nevada Sand; e=0.774; w=18.63%, S=65%
σ'_{vc}=145 (kPa); OCR=1; Υ_c=0.08%, f=0.01 Hz

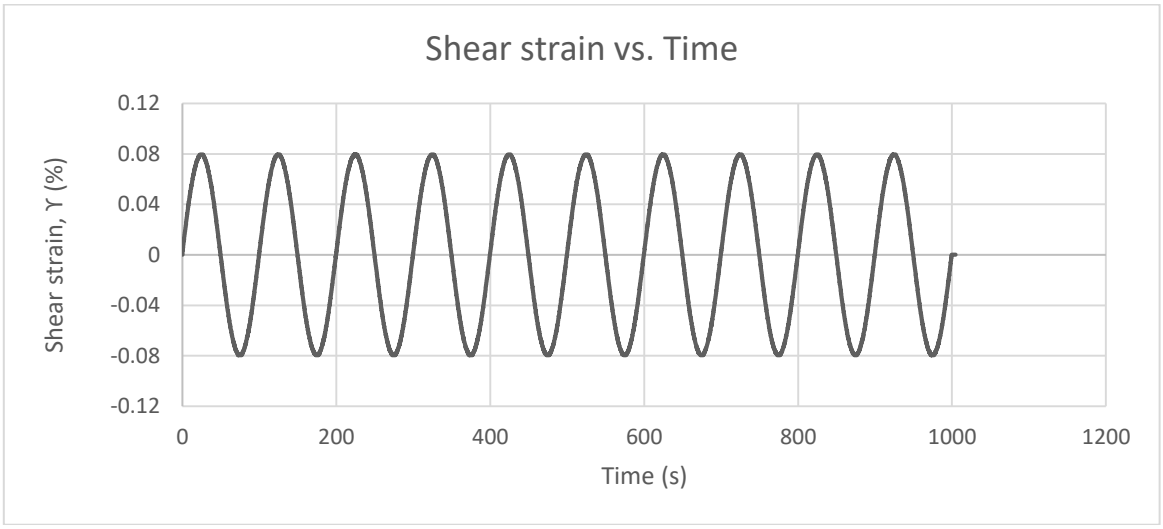

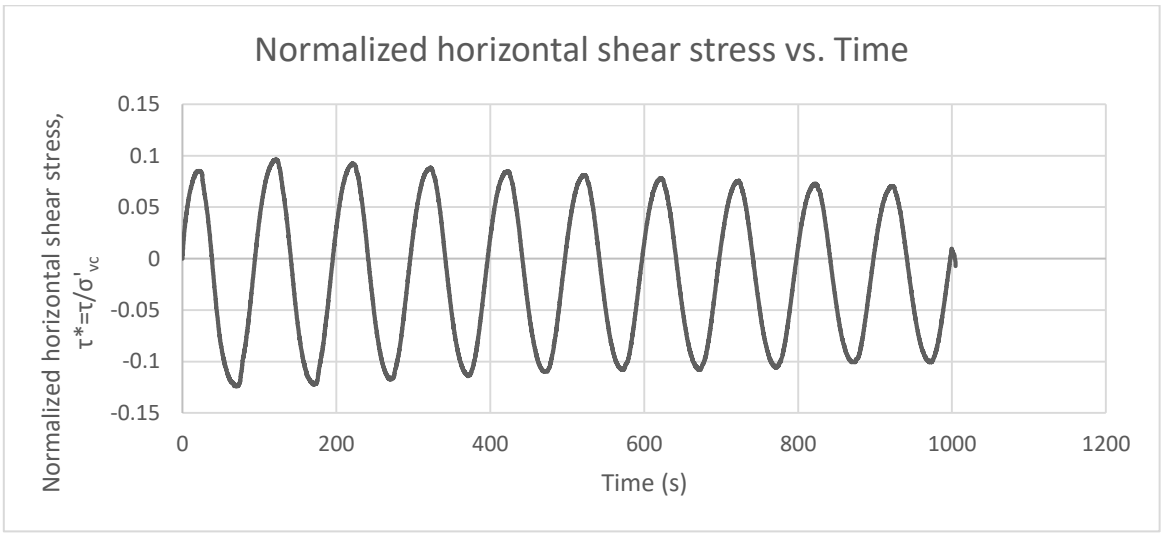

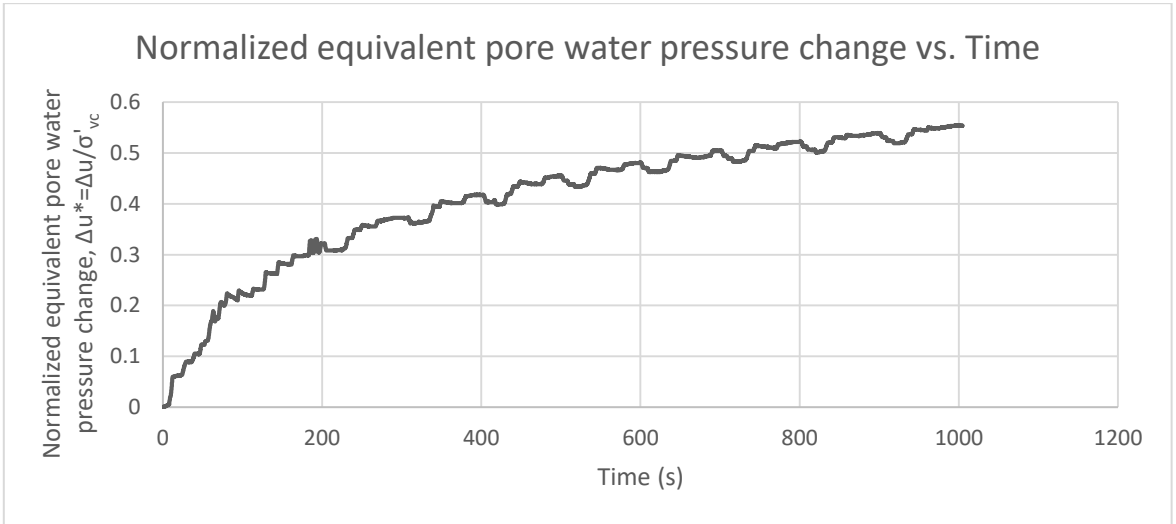

Test: 5.1; Soil: Nevada Sand; e=0.774; w=18.63%, S=65%
σ'_{vc}=145 (kPa); OCR=1; Υ_c=0.08%, f=0.01 Hz

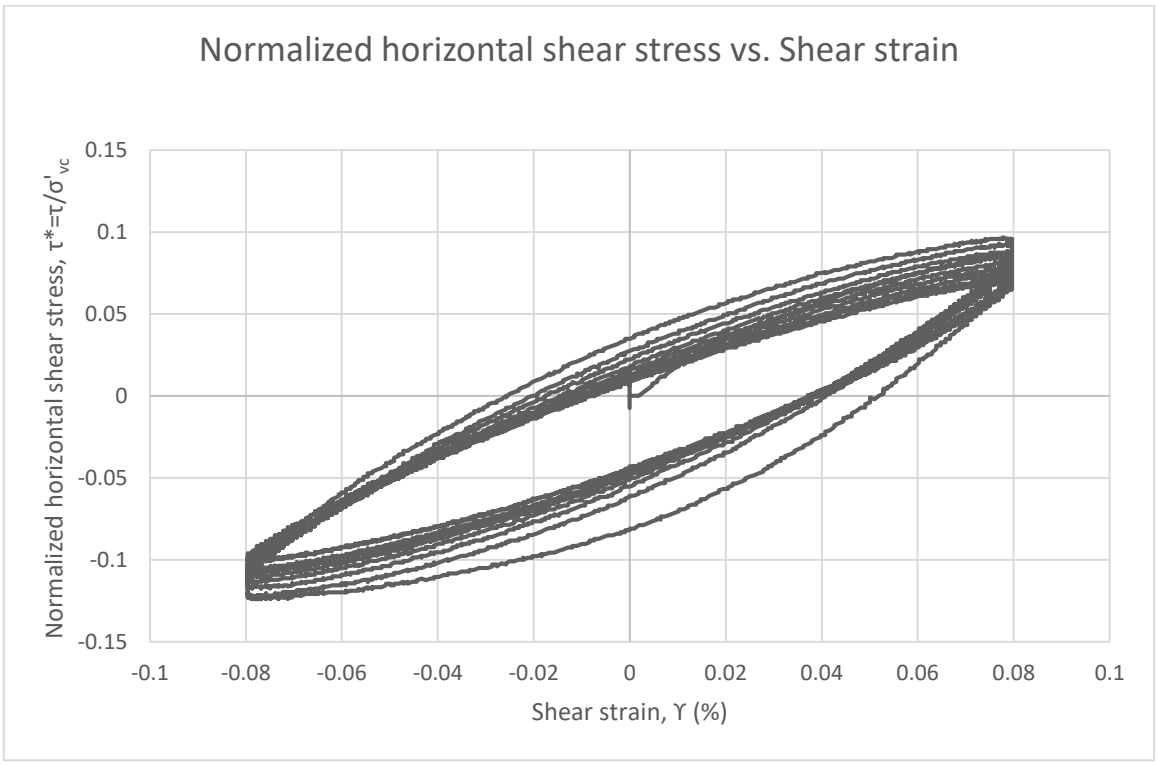

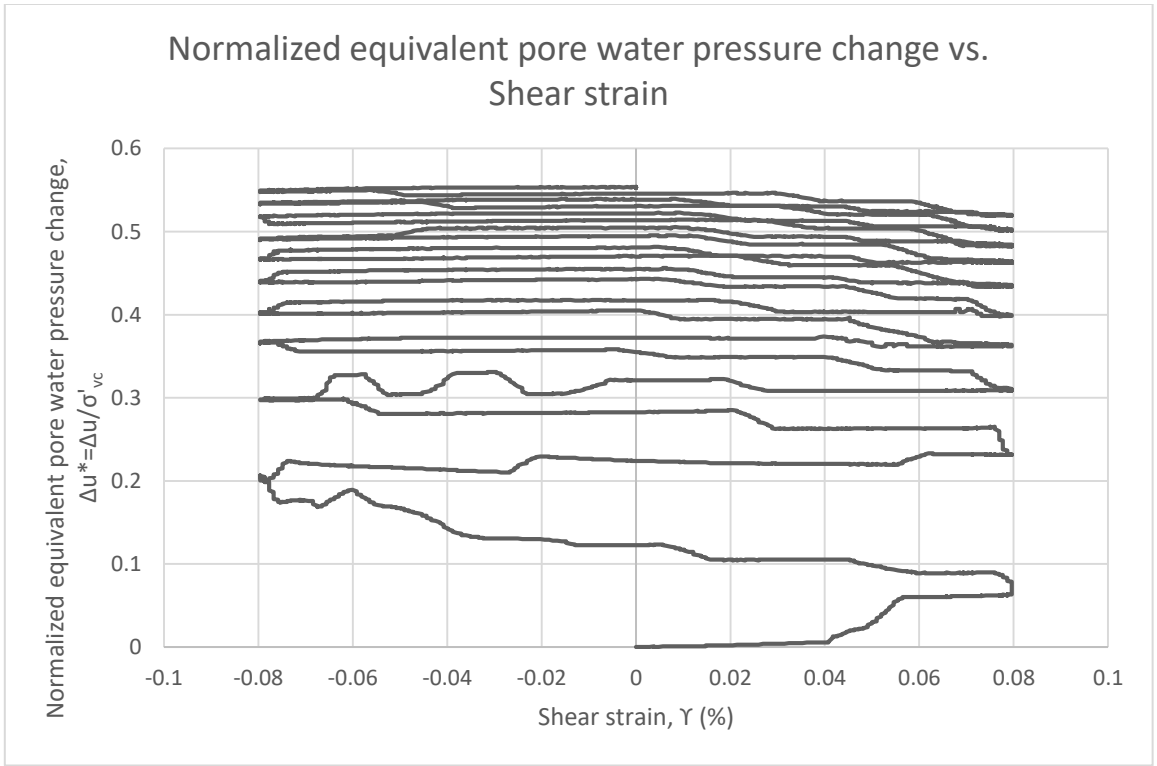

Test: 5.1; Soil: Nevada Sand; e=0.774; w=18.63%, S=65%
σ'_{vc}=145 (kPa); OCR=1; Υ_c=0.08%, f=0.01 Hz

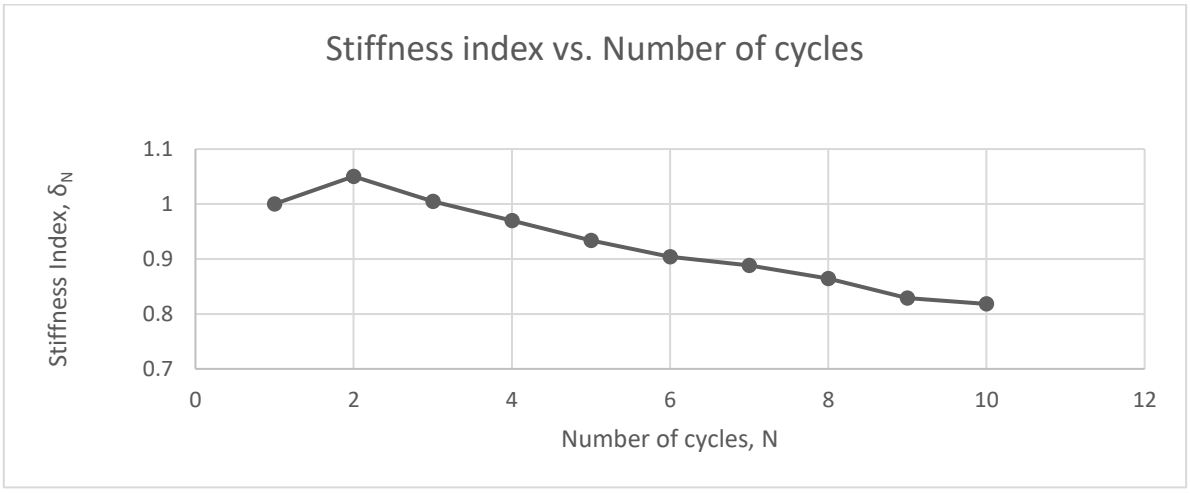

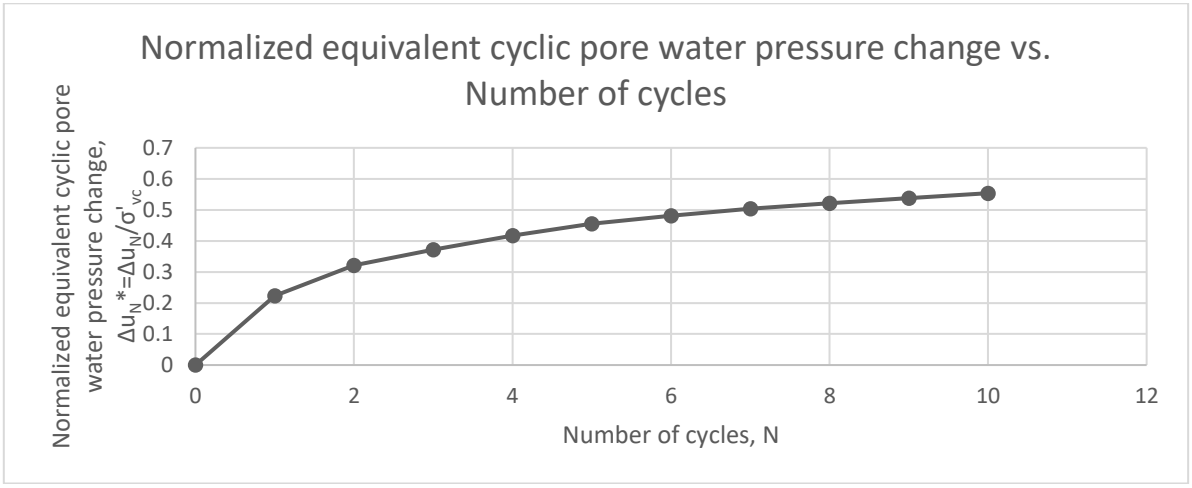

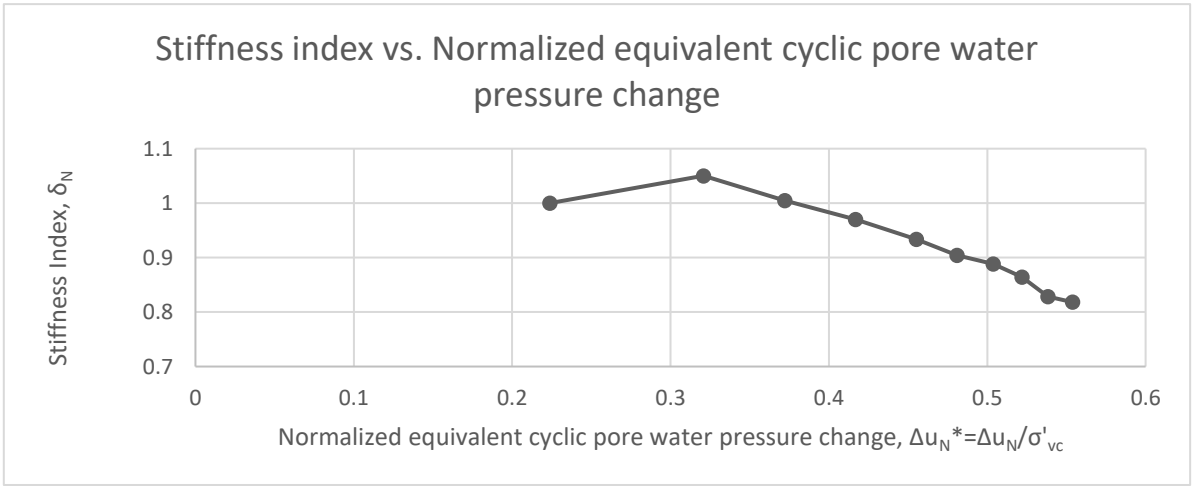

Test: 5.1; Soil: Nevada Sand; e=0.774; w=18.63%, S=65%
σ'_{vc}=145 (kPa); OCR=1; Υ_c=0.08%, f=0.01 Hz

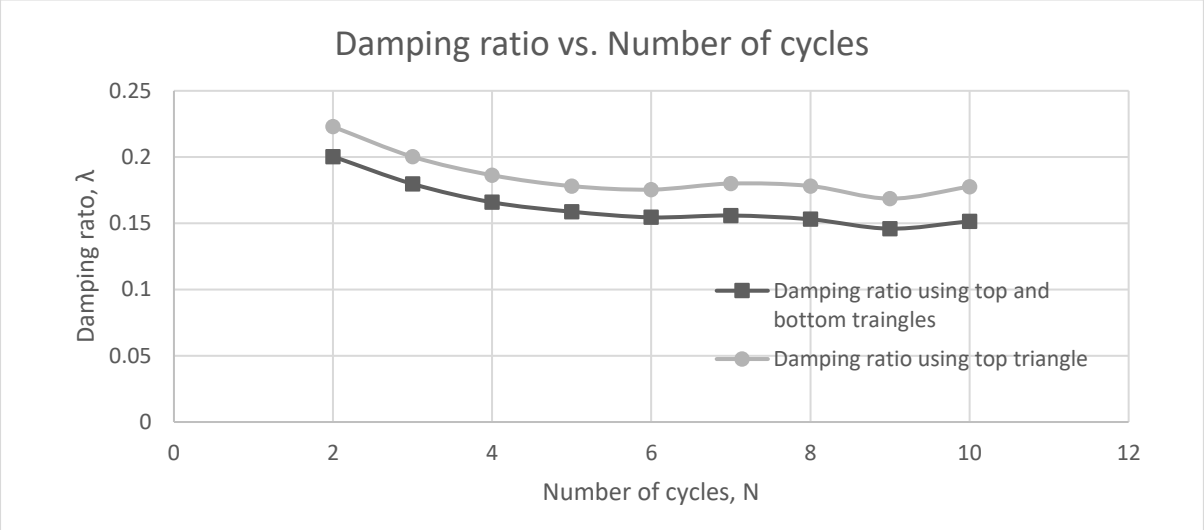

Test: 5.2; Soil: Nevada Sand; e=0.771; w=18.63%, S=65%
σ'_{vc}=145 (kPa); OCR=1; Υ_c=0.08%, f=0.01 Hz

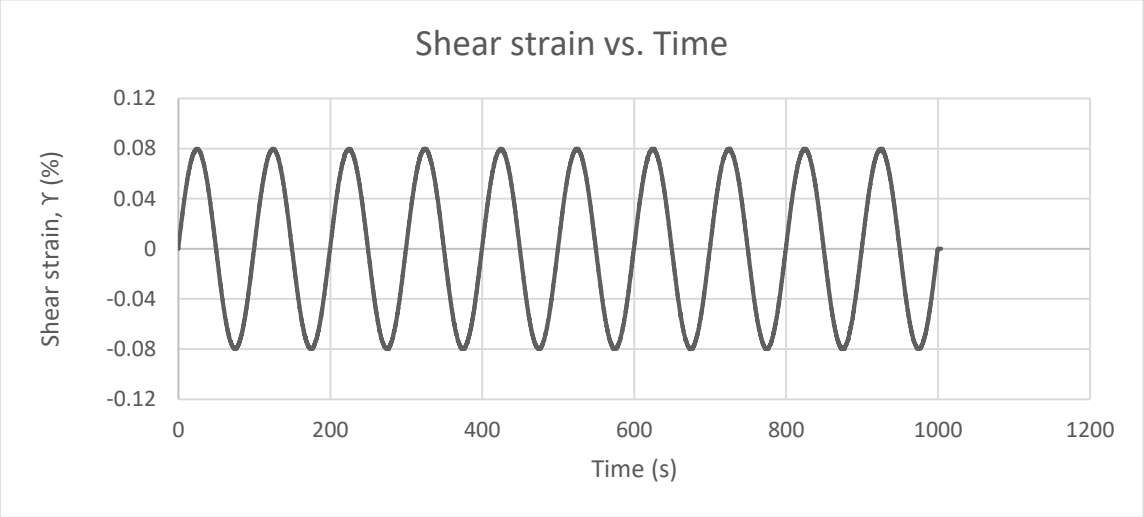

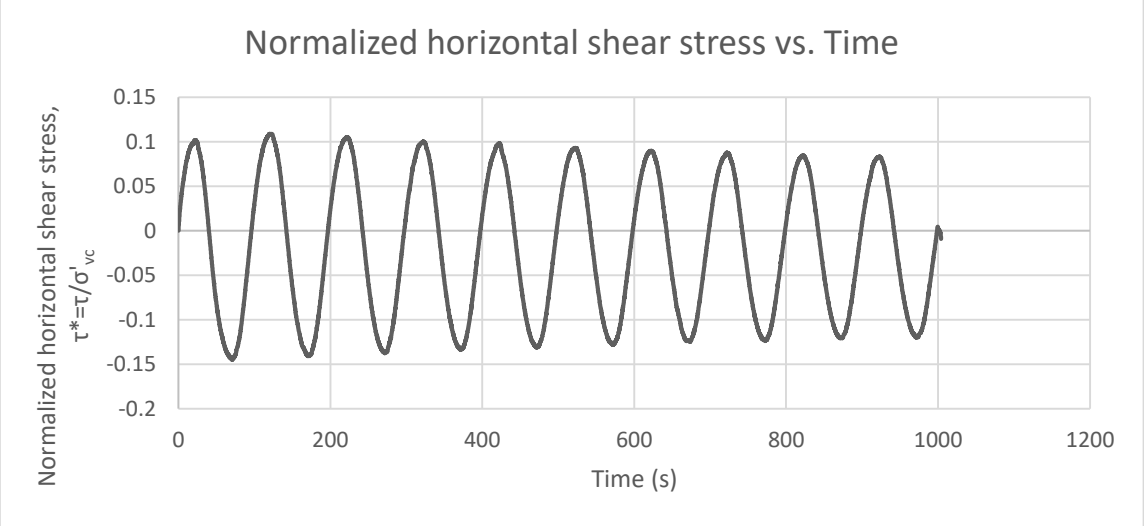

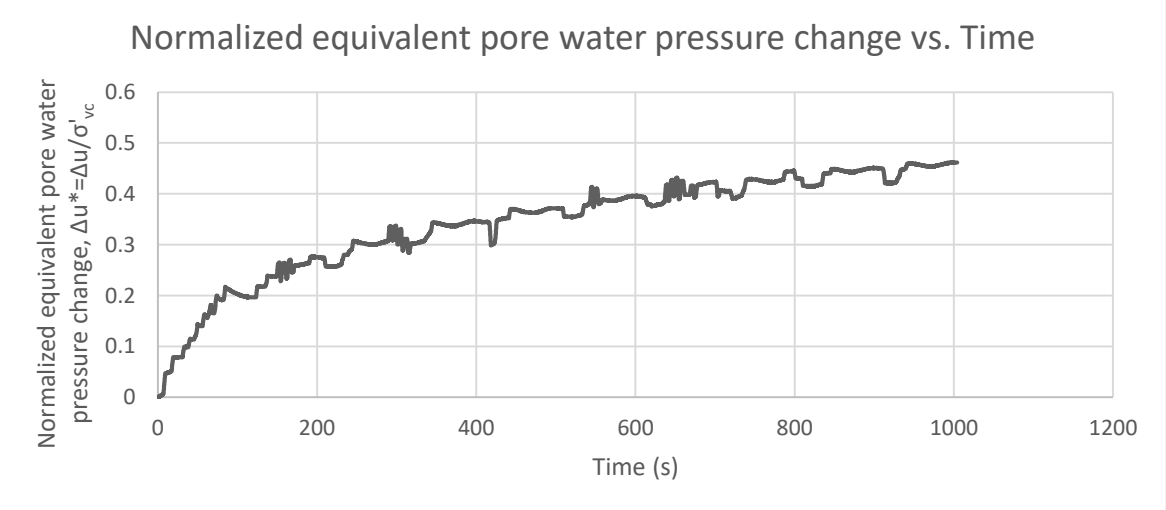

Test: 5.2; Soil: Nevada Sand; e=0.771; w=18.63%, S=65%
σ'_{vc}=145 (kPa); OCR=1; Υ_c=0.08%, f=0.01 Hz

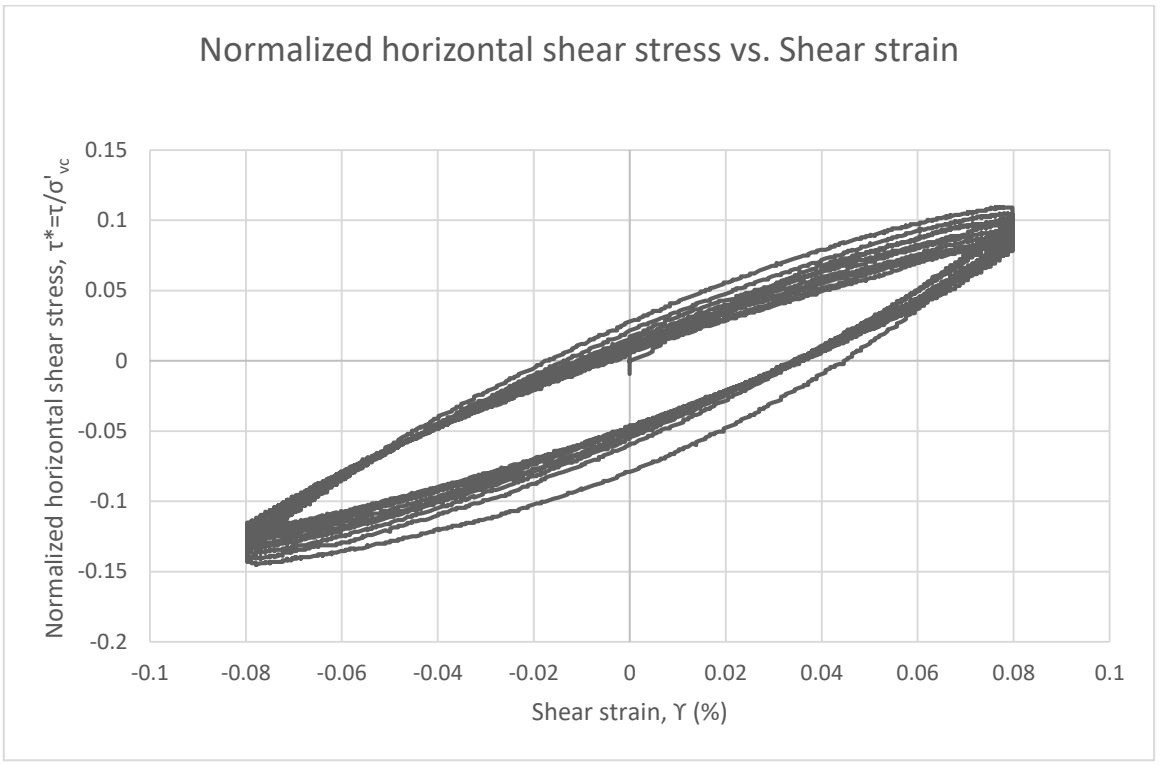

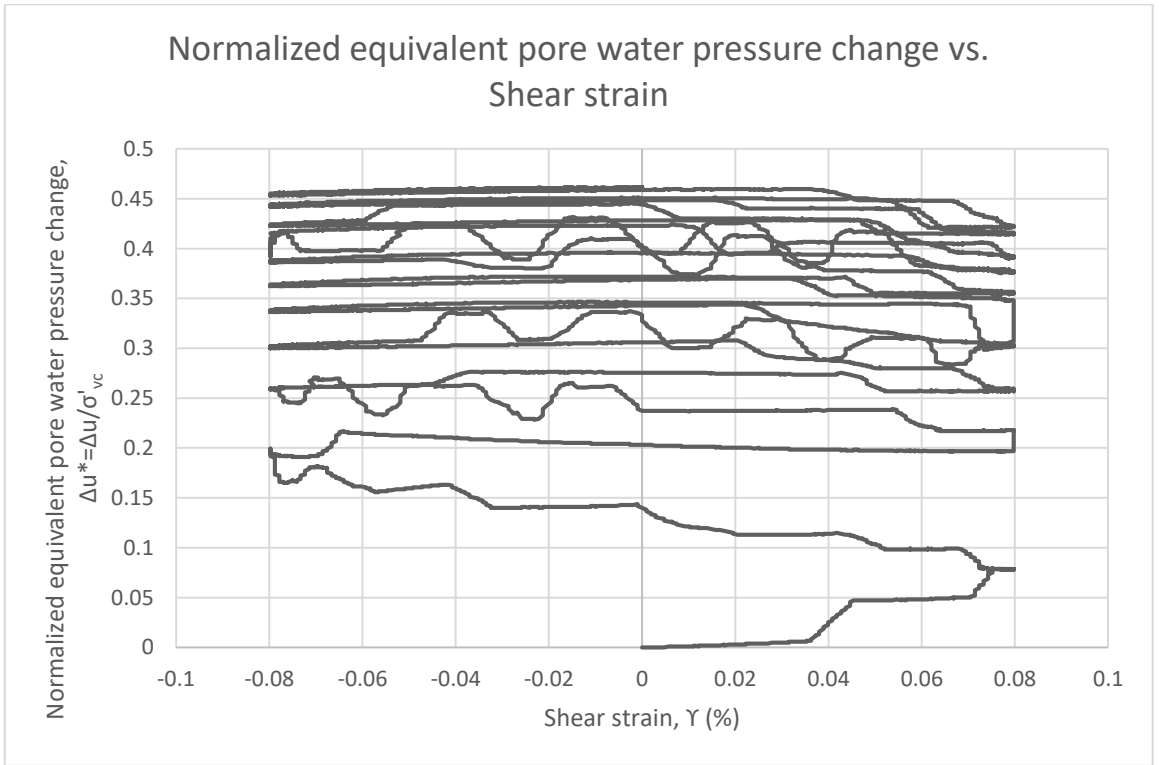

Test: 5.2; Soil: Nevada Sand; e=0.771; w=18.63%, S=65%
σ'_{vc}=145 (kPa); OCR=1; Υ_c=0.08%, f=0.01 Hz

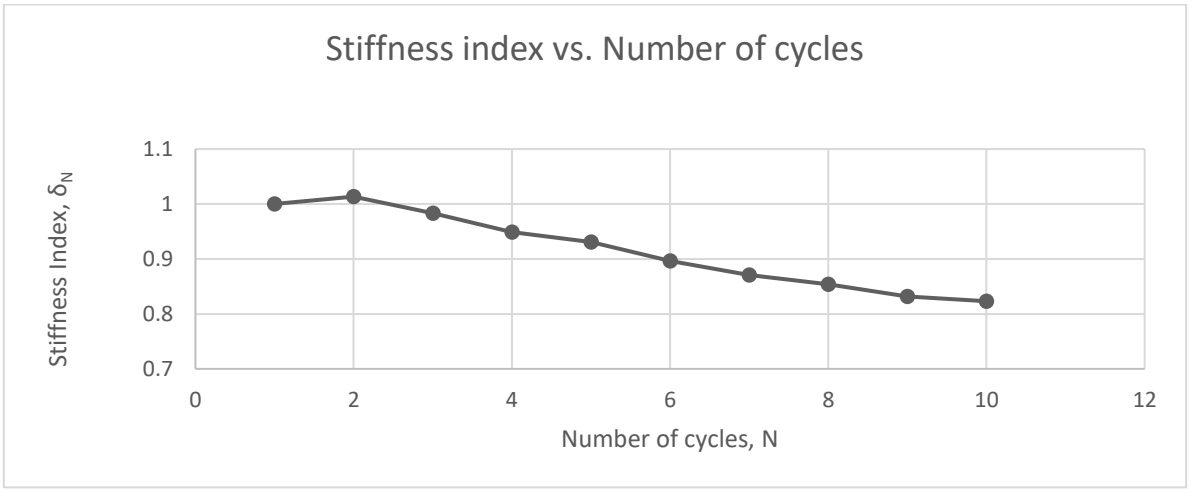

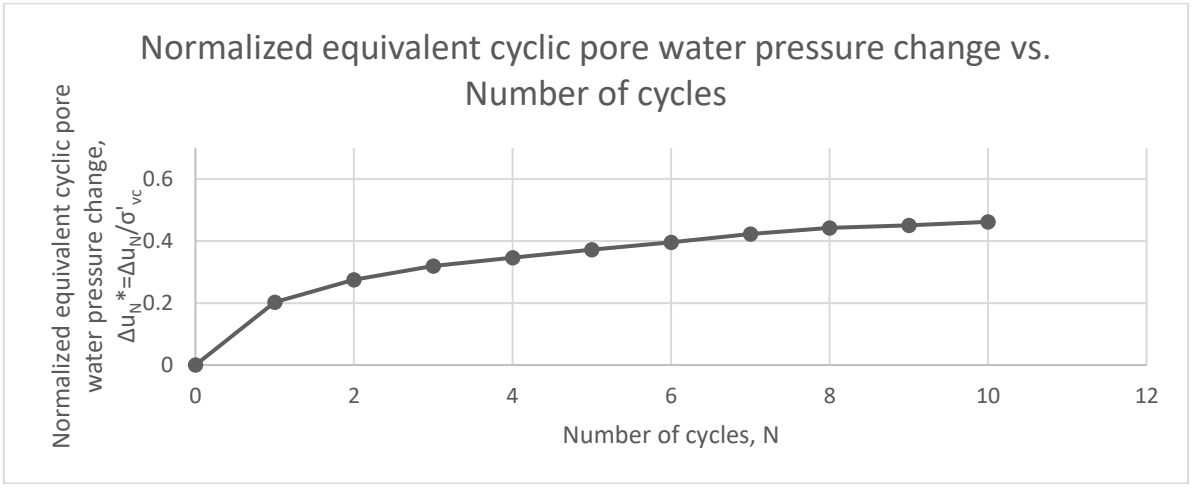

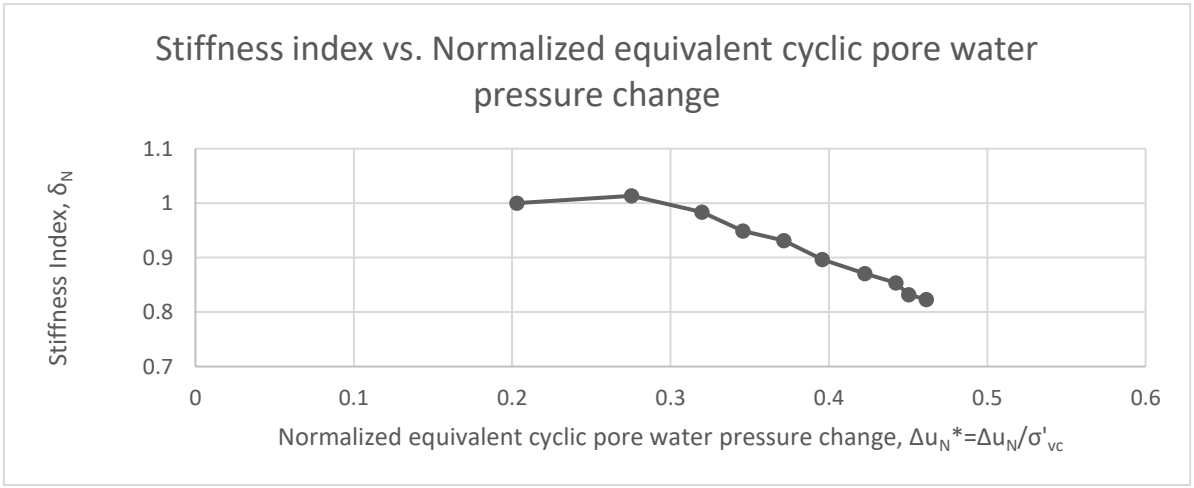

Test: 5.2; Soil: Nevada Sand; e=0.771; w=18.63%, S=65%
σ'_{vc}=145 (kPa); OCR=1; Υ_c=0.08%, f=0.01 Hz

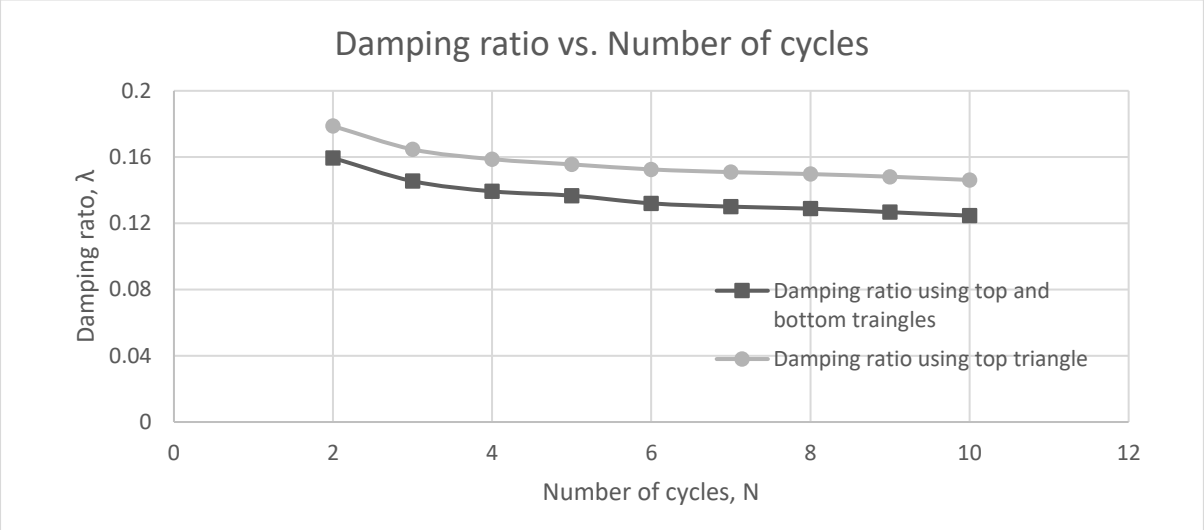

Test: 5.3; Soil: Nevada Sand; e=0.771; w=18.63%, S=65%
σ'_{vc}=145 (kPa); OCR=1; Υ_c=0.04%, f=0.01 Hz

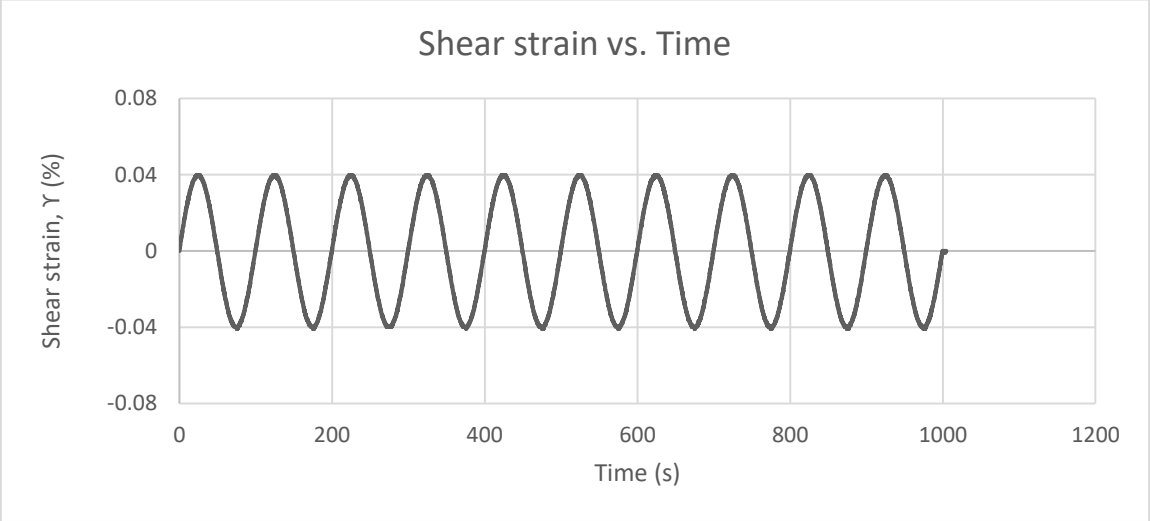

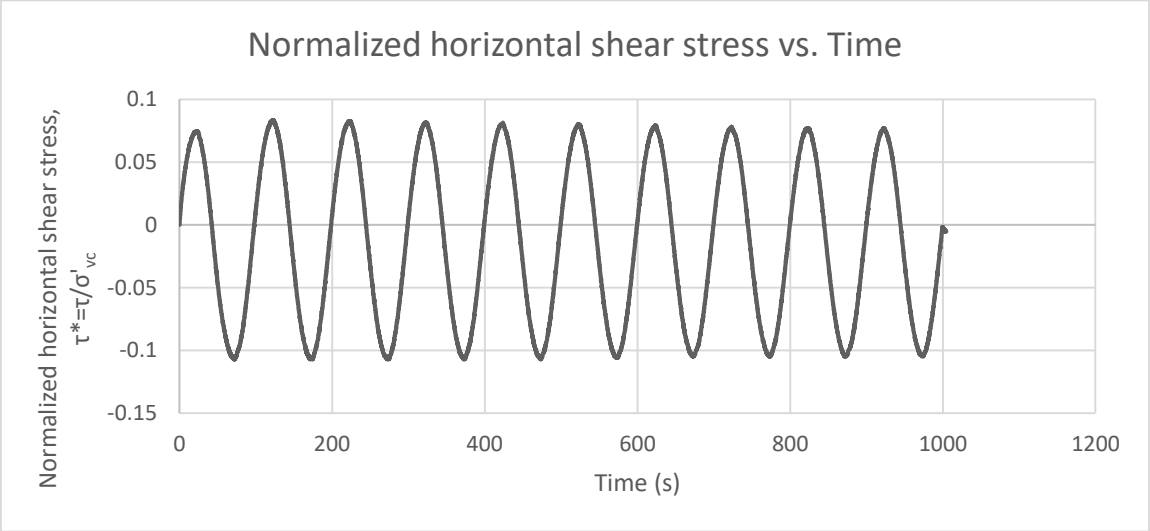

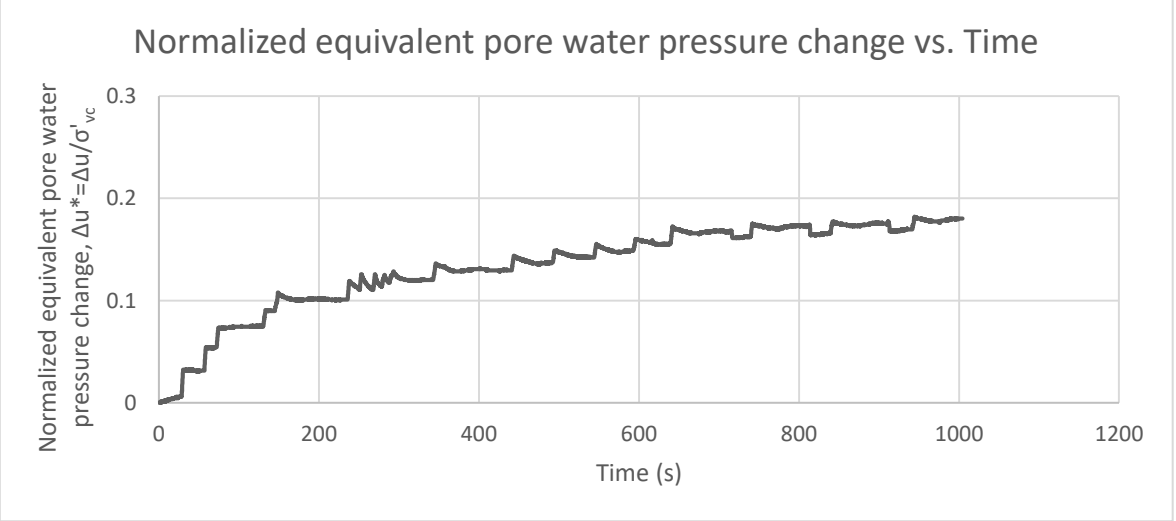

Test: 5.3; Soil: Nevada Sand; e=0.771; w=18.63%, S=65%
σ'_{vc}=145 (kPa); OCR=1; Υ_c=0.04%, f=0.01 Hz

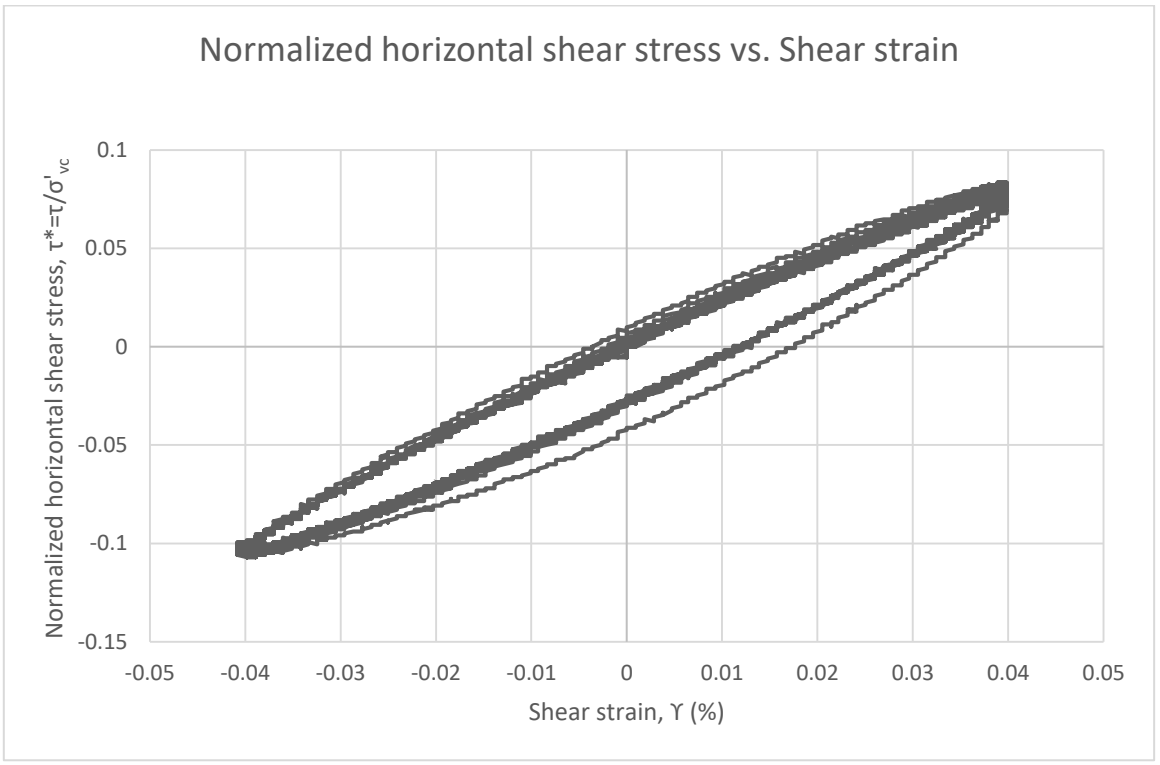

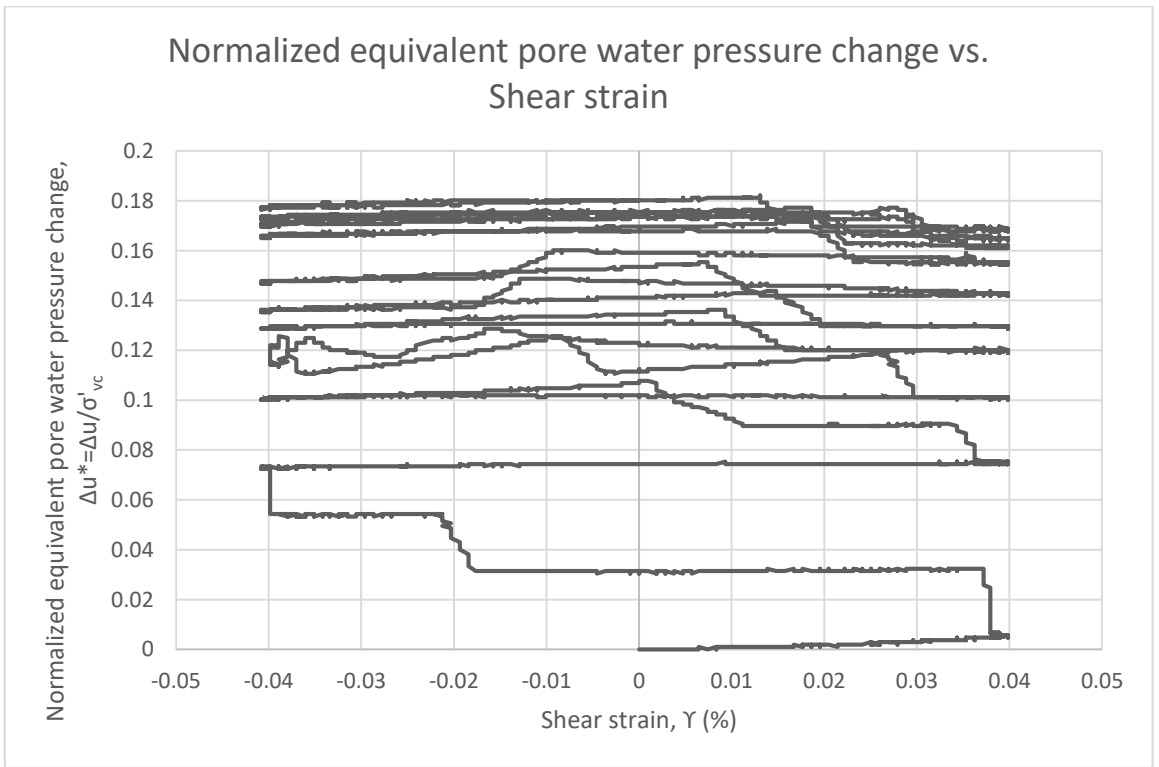

Test: 5.3; Soil: Nevada Sand; e=0.771; w=18.63%, S=65%
σ'_{vc}=145 (kPa); OCR=1; Υ_c=0.04%, f=0.01 Hz

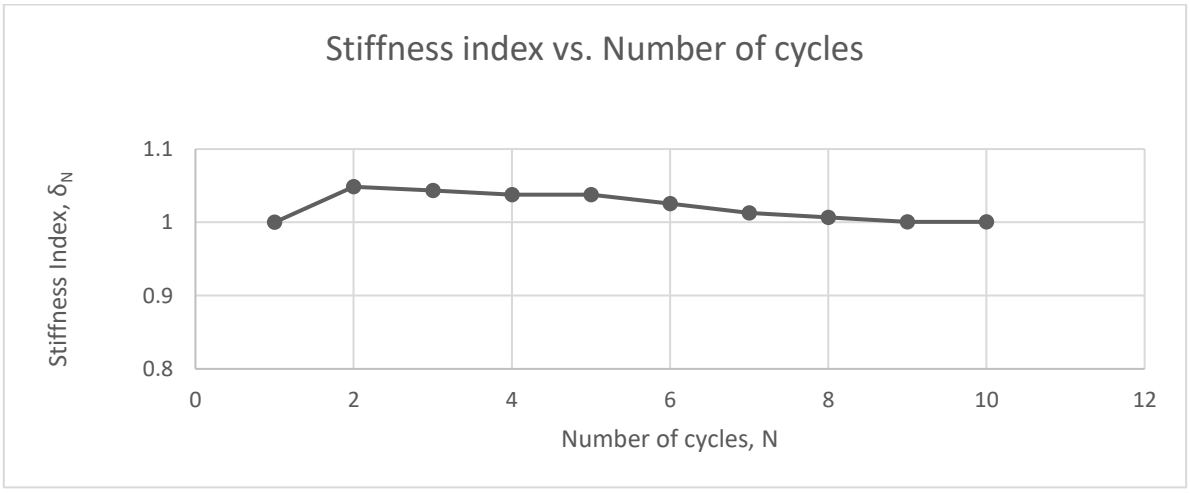

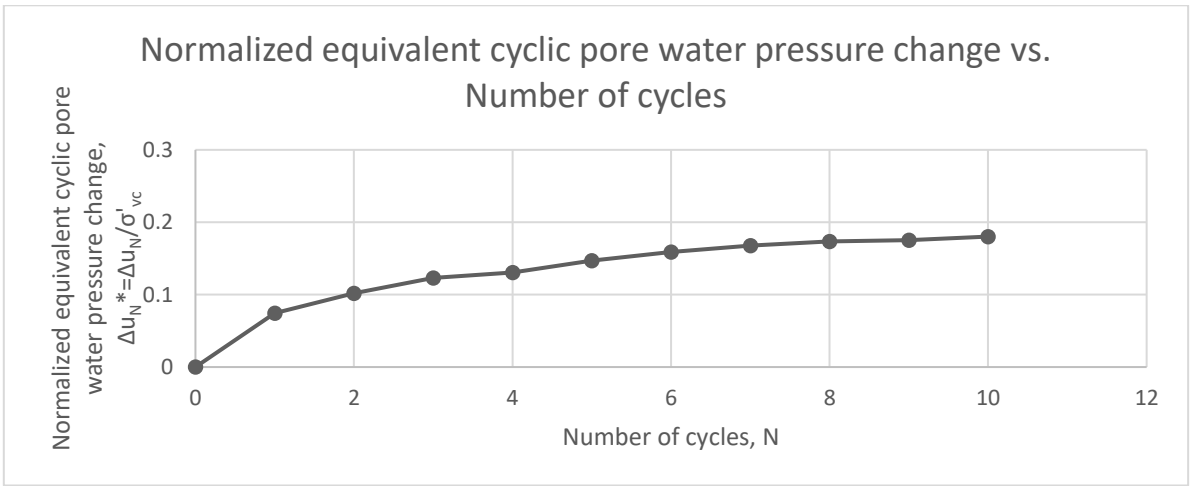

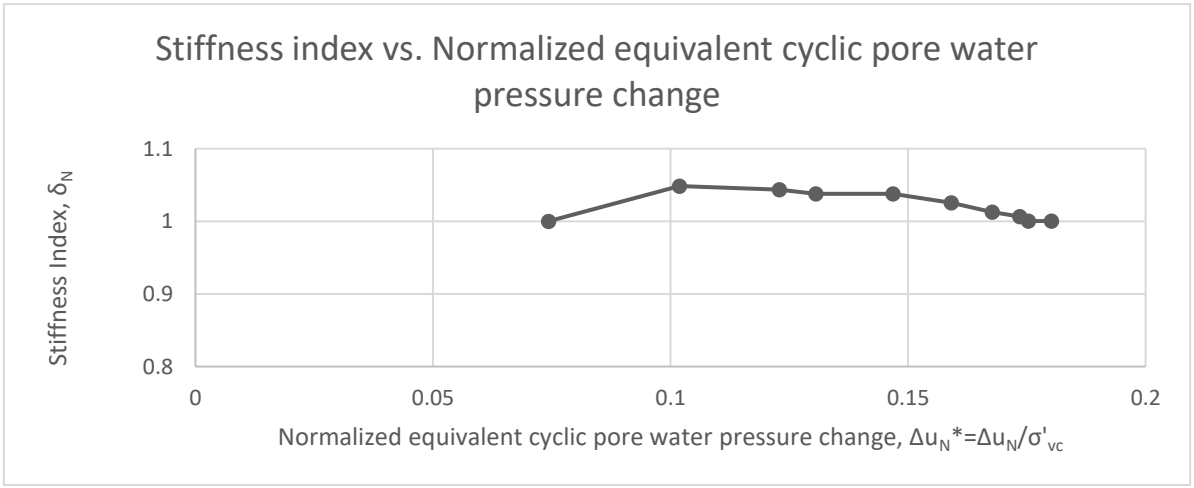

Test: 5.3; Soil: Nevada Sand; e=0.771; w=18.63%, S=65%
σ'_{vc}=145 (kPa); OCR=1; Υ_c=0.04%, f=0.01 Hz

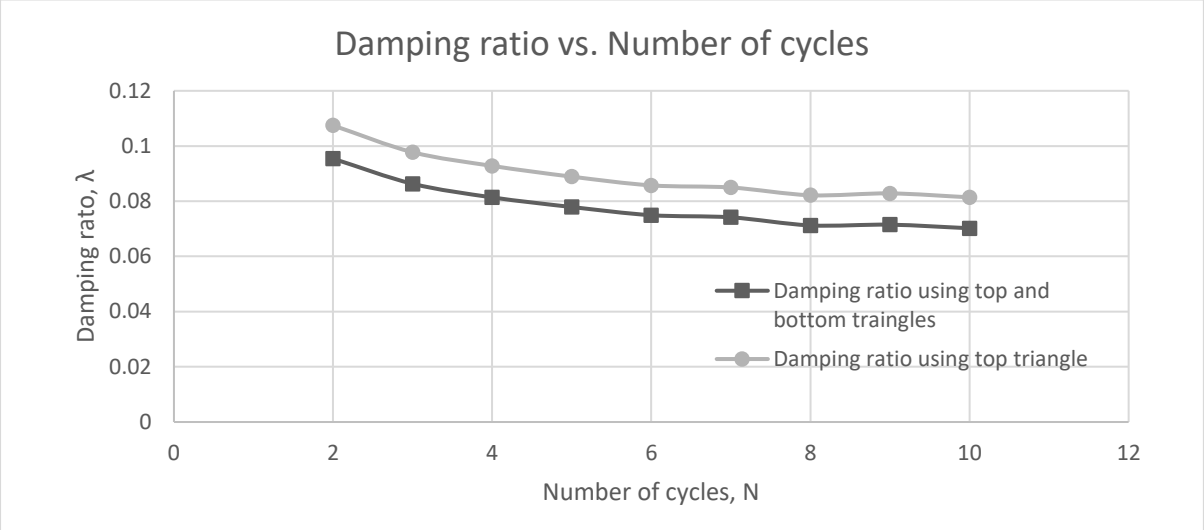

Test: 5.4; Soil: Nevada Sand; e=0.771; w=18.63%, S=65%
σ'_{vc}=145 (kPa); OCR=1; Υ_c=0.02%, f=0.01 Hz

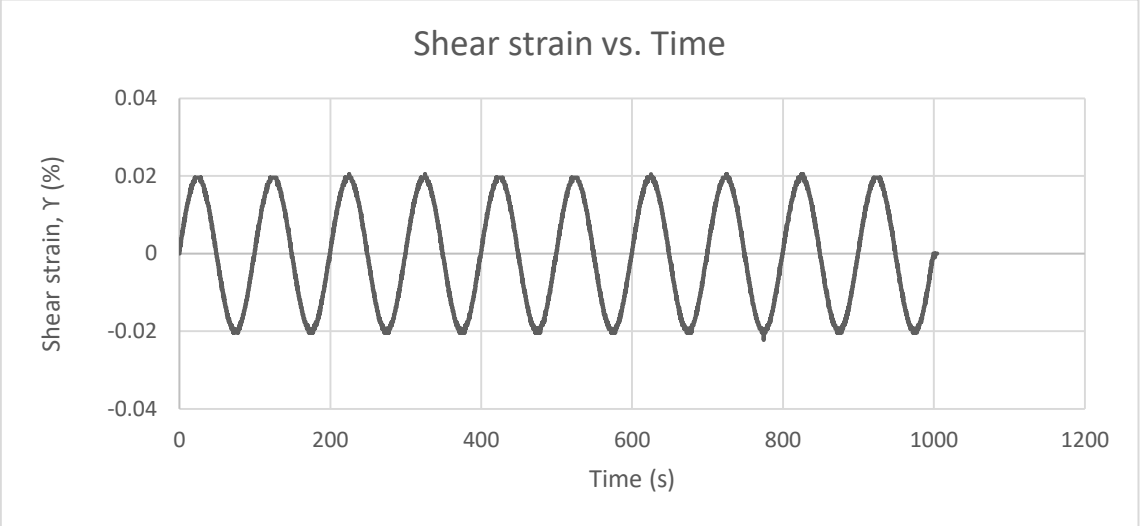

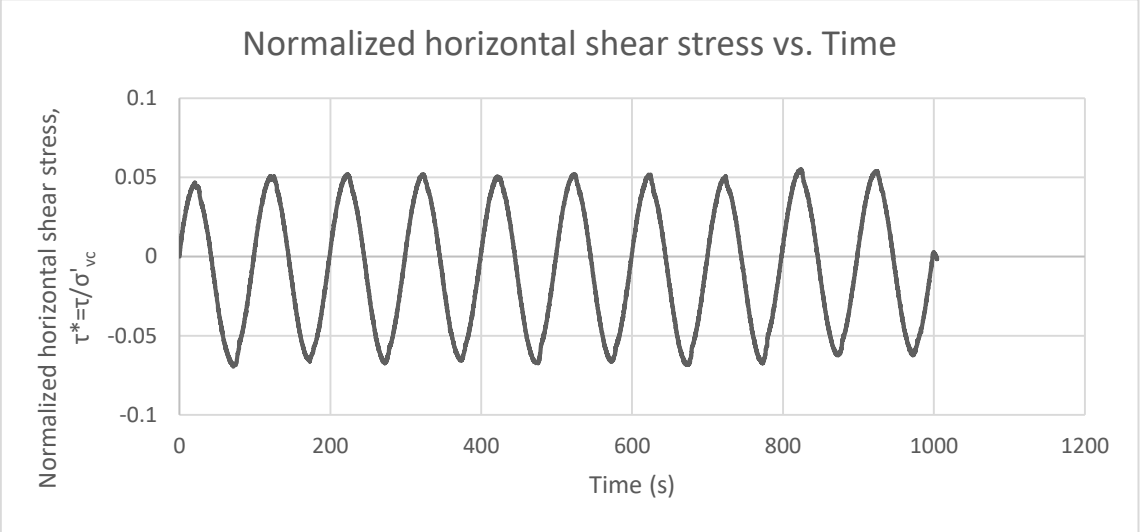

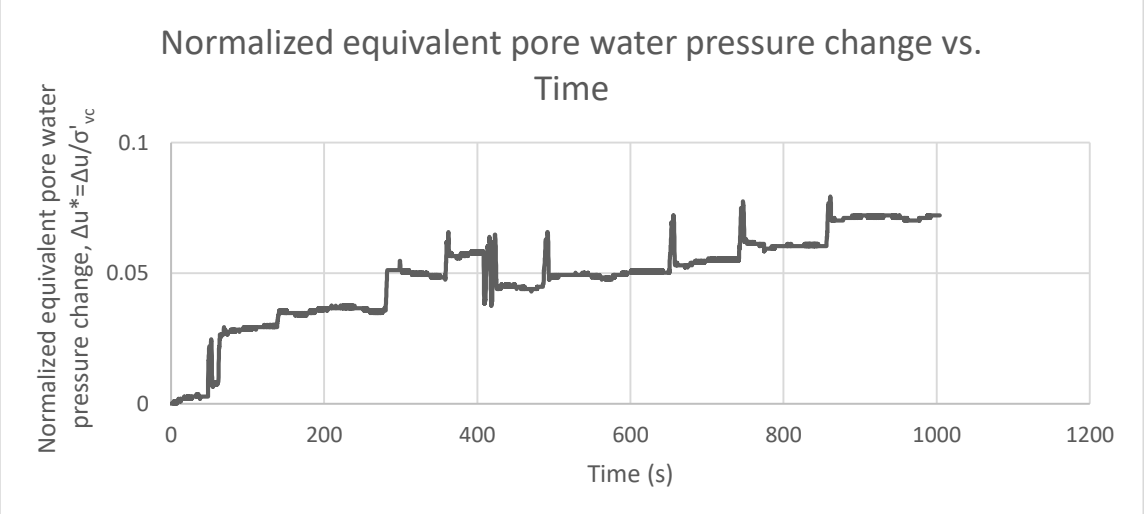

Test: 5.4; Soil: Nevada Sand; e=0.771; w=18.63%, S=65%
σ'_{vc}=145 (kPa); OCR=1; Υ_c=0.02%, f=0.01 Hz

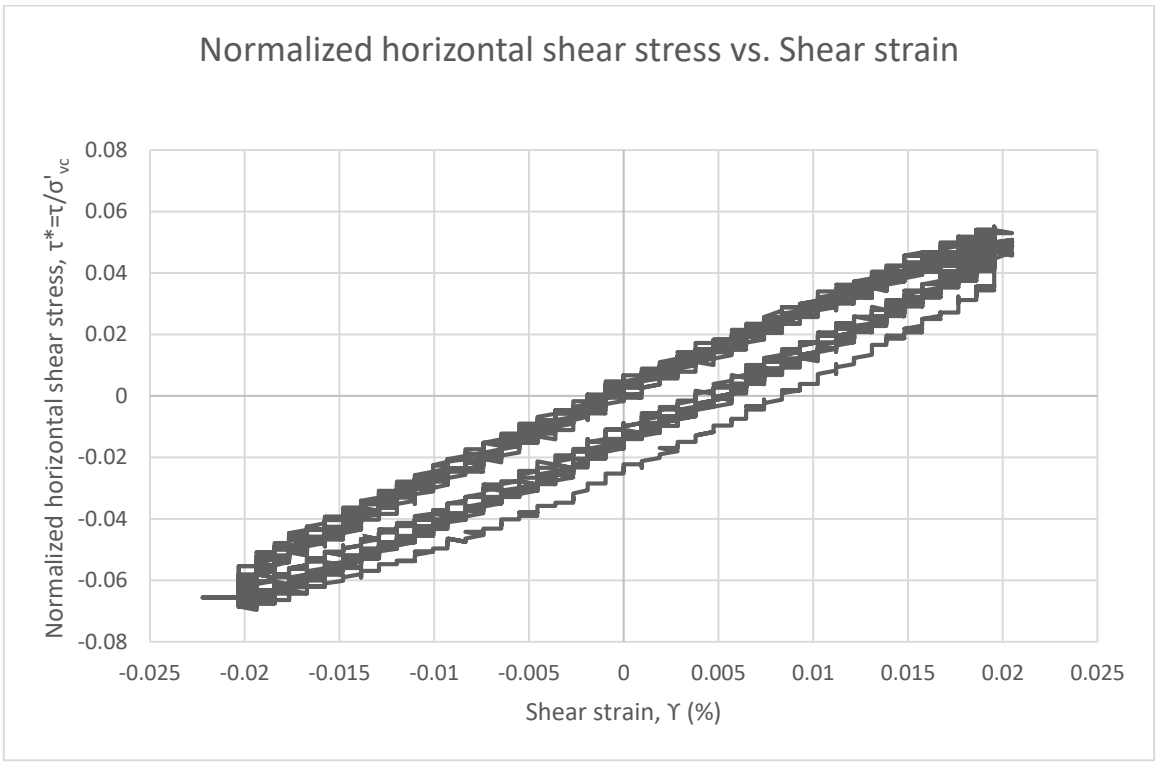

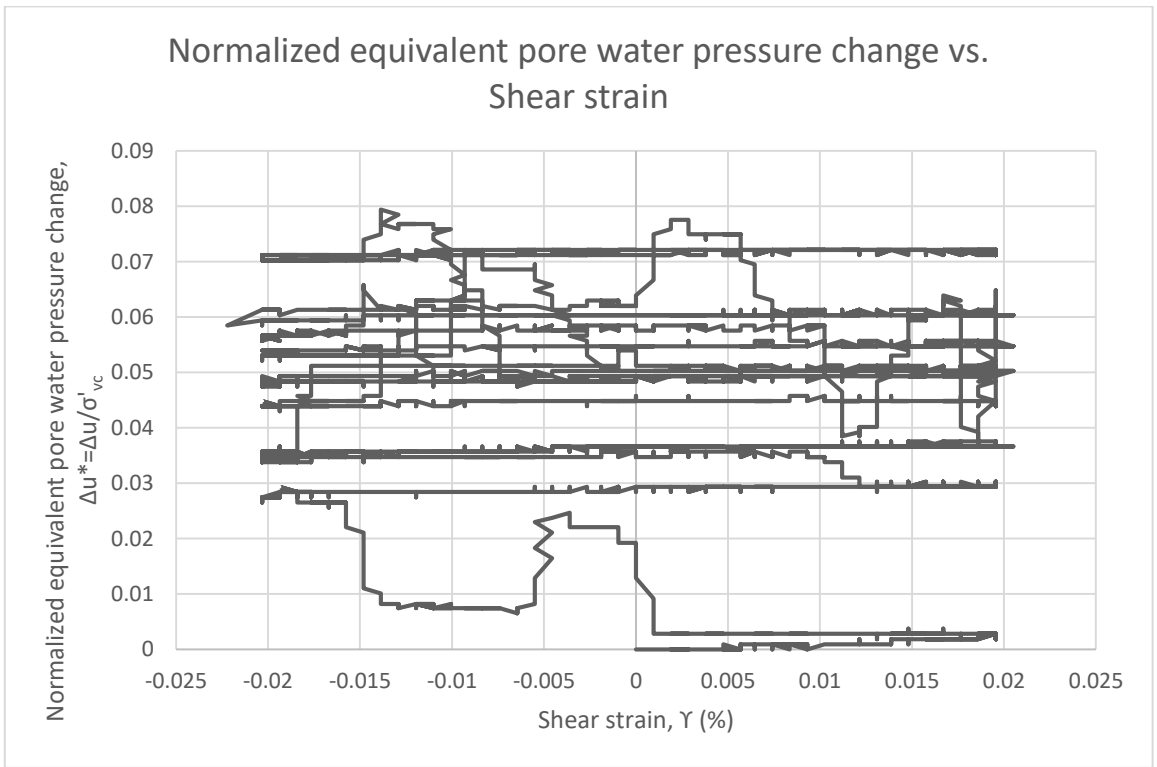

Test: 5.4; Soil: Nevada Sand; e=0.771; w=18.63%, S=65%
σ'_{vc}=145 (kPa); OCR=1; Υ_c=0.02%, f=0.01 Hz

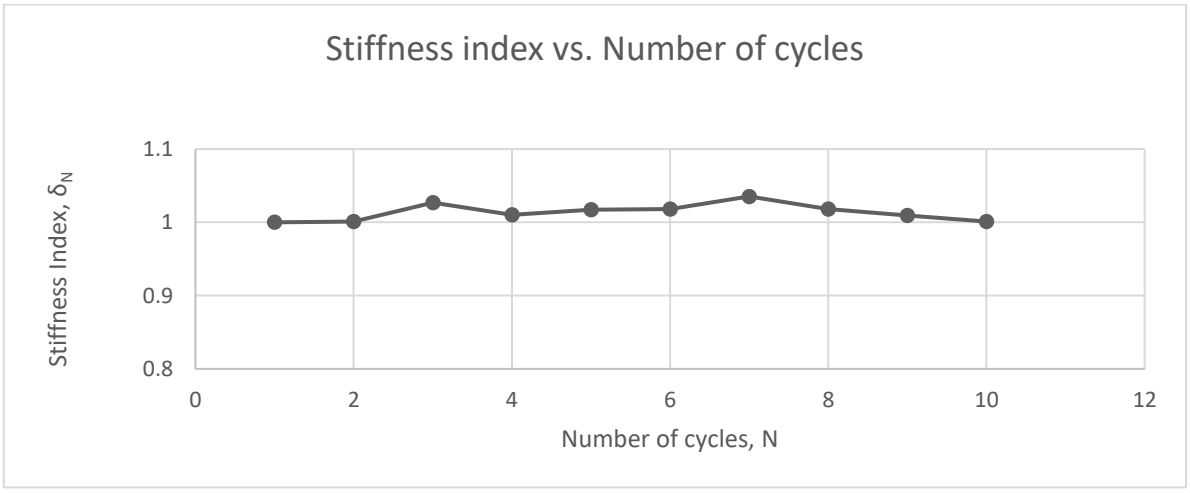

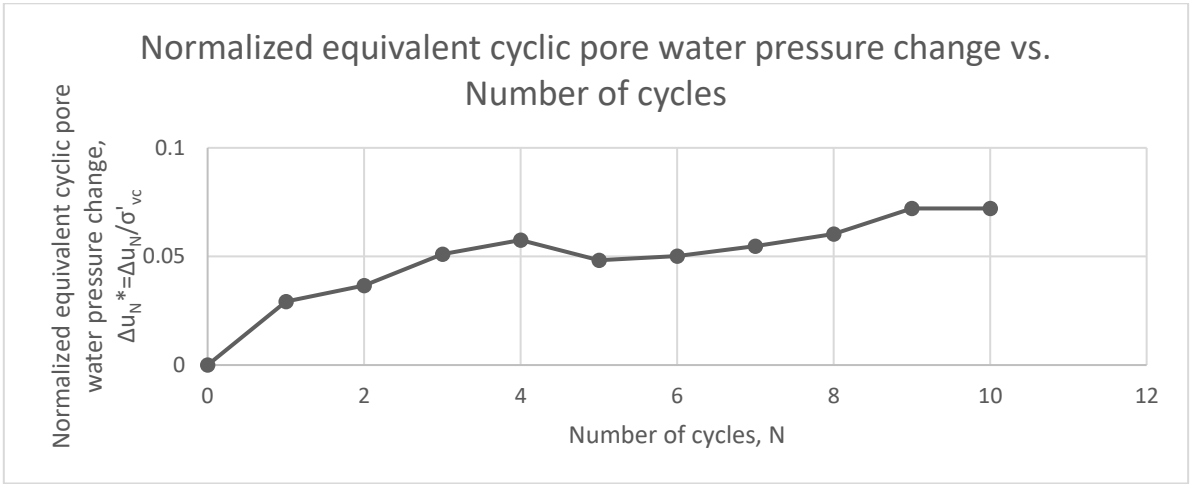

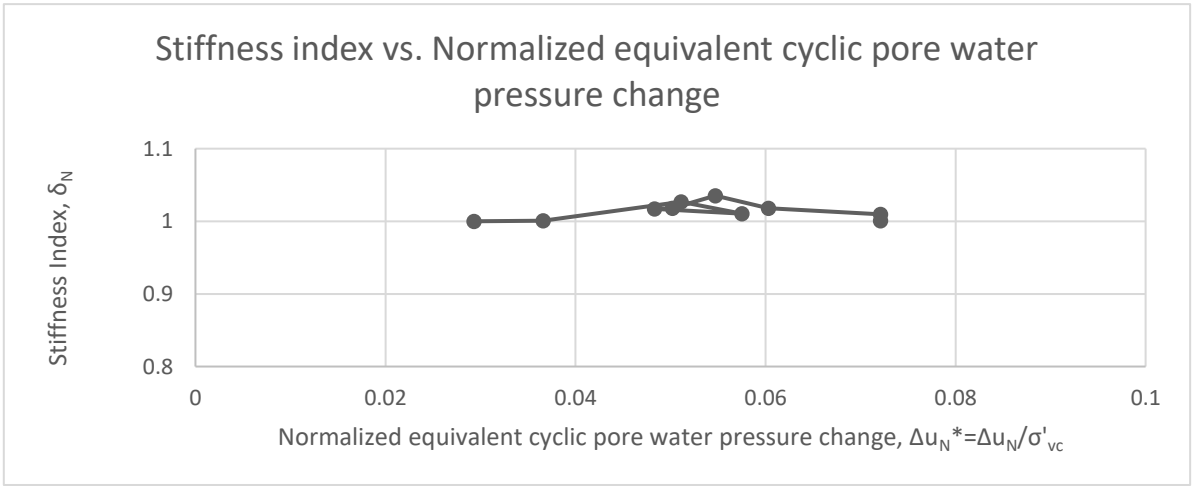

Test: 5.4; Soil: Nevada Sand; e=0.771; w=18.63%, S=65%
σ'_{vc}=145 (kPa); OCR=1; Υ_c=0.02%, f=0.01 Hz

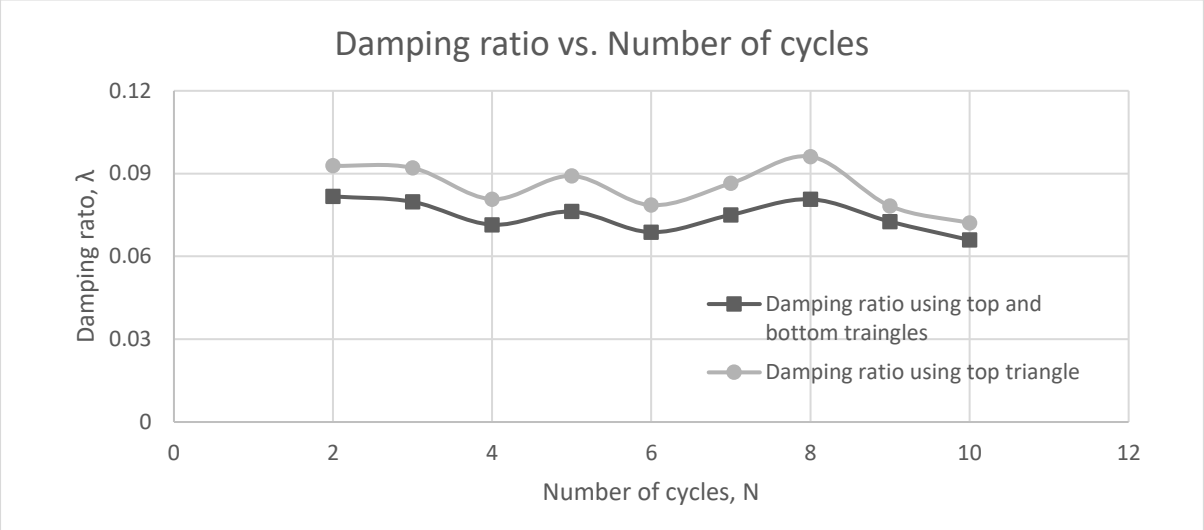

Test: 5.5; Soil: Nevada Sand; e=0.771; w=18.63%, S=65%
σ'_{vc}=145 (kPa); OCR=1; Υ_c=0.01%, f=0.01 Hz

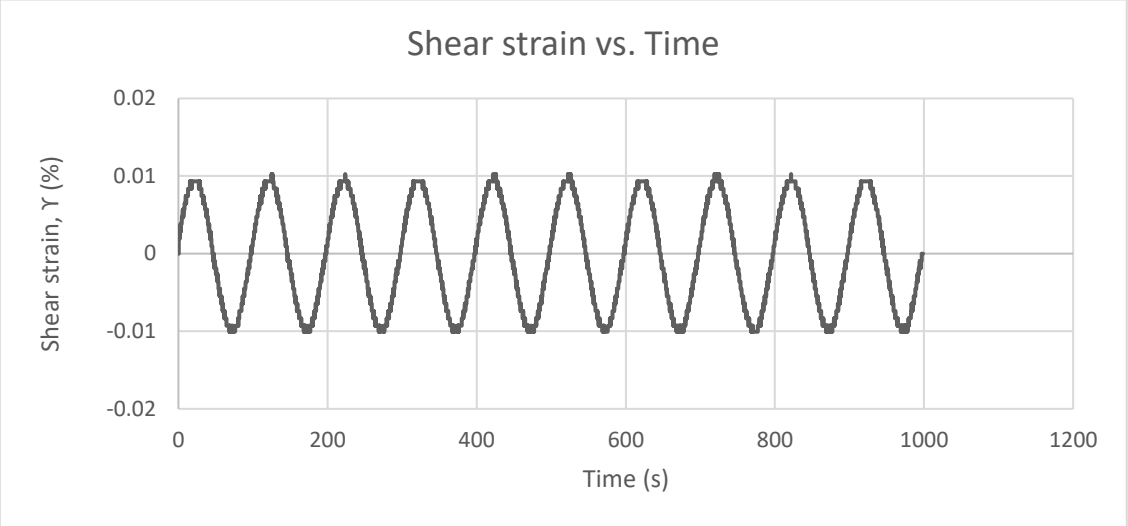

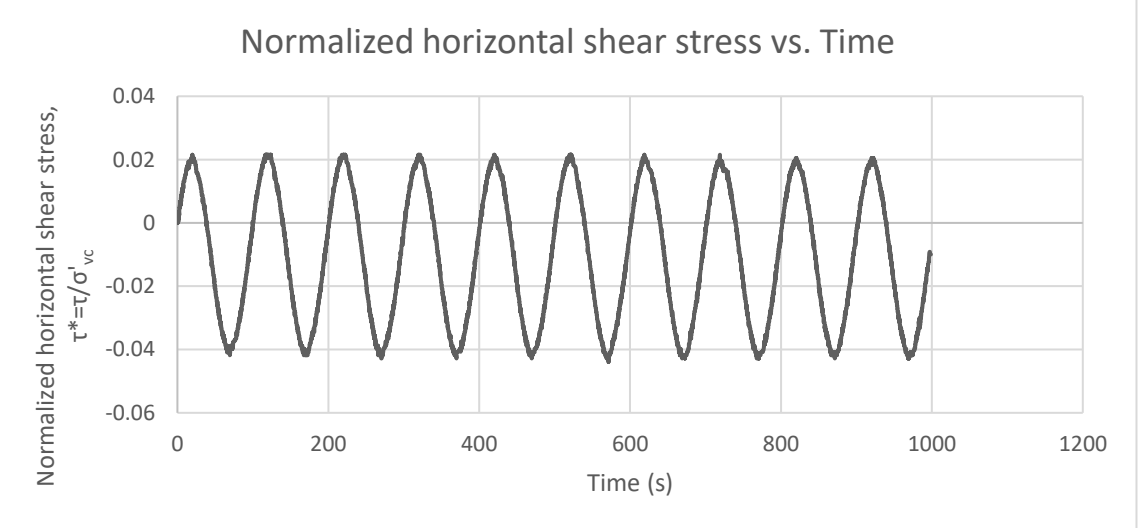

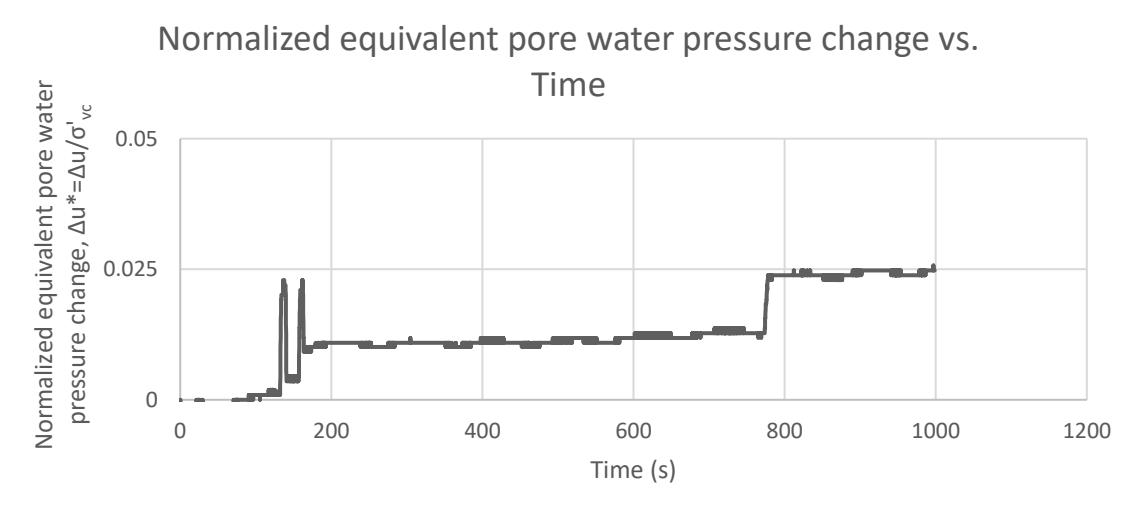

Test: 5.5; Soil: Nevada Sand; e=0.771; w=18.63%, S=65%
σ'_{vc}=145 (kPa); OCR=1; Υ_c=0.01%, f=0.01 Hz

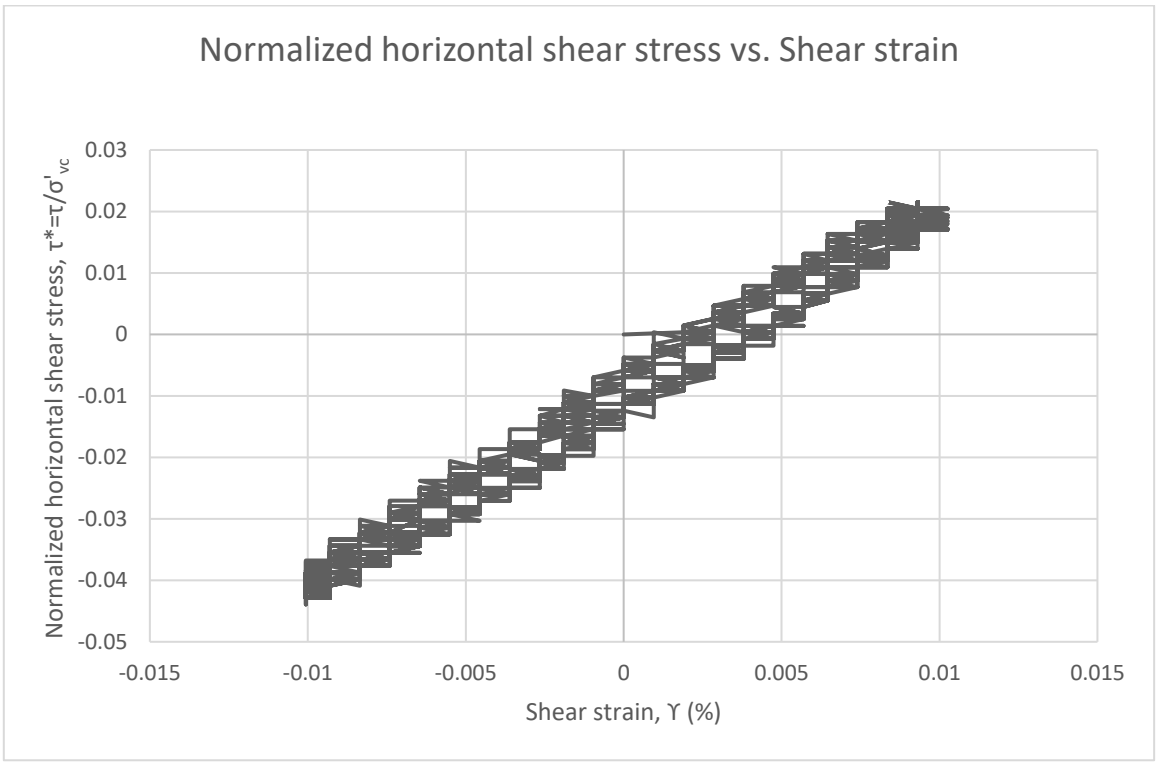

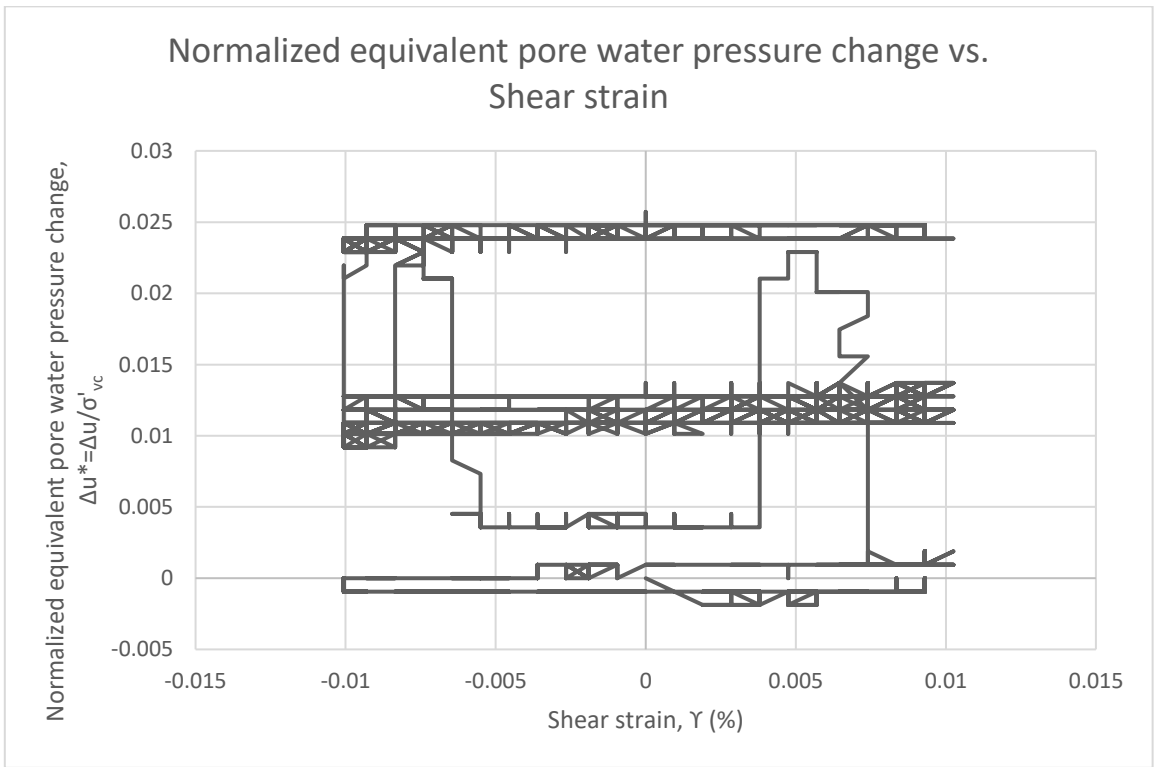

Test: 5.5; Soil: Nevada Sand; e=0.771; w=18.63%, S=65%
σ'_{vc}=145 (kPa); OCR=1; Υ_c=0.01%, f=0.01 Hz

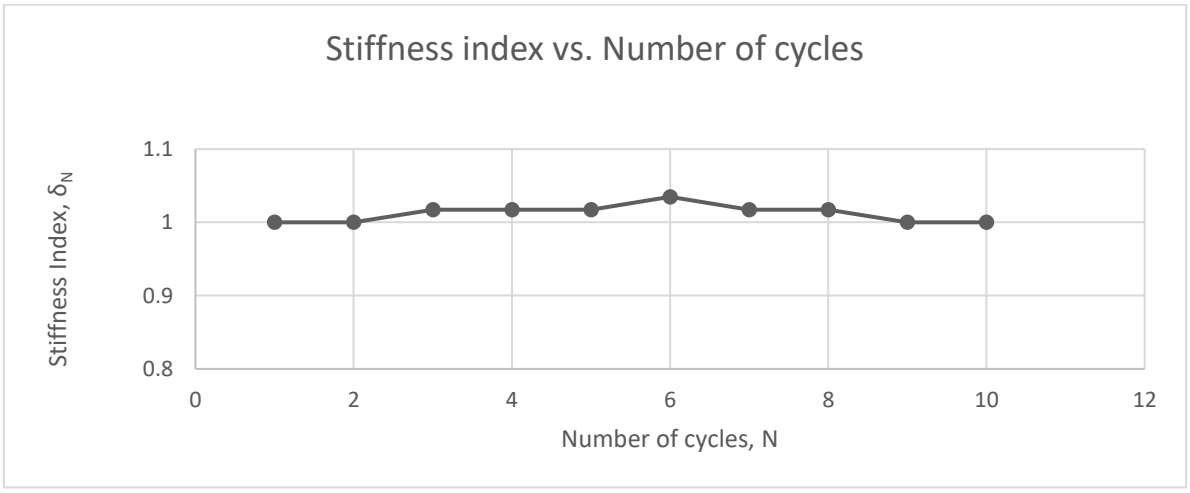

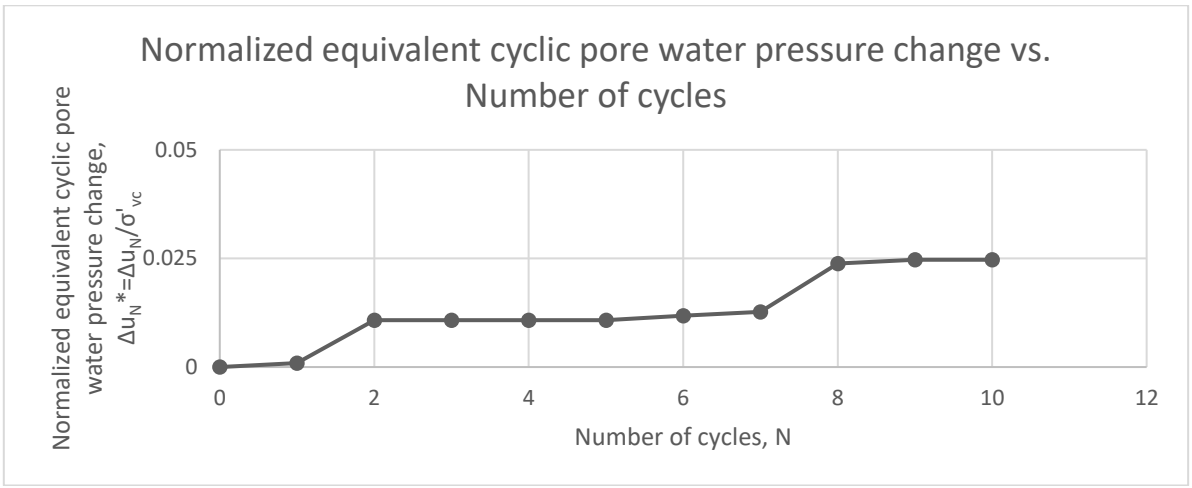

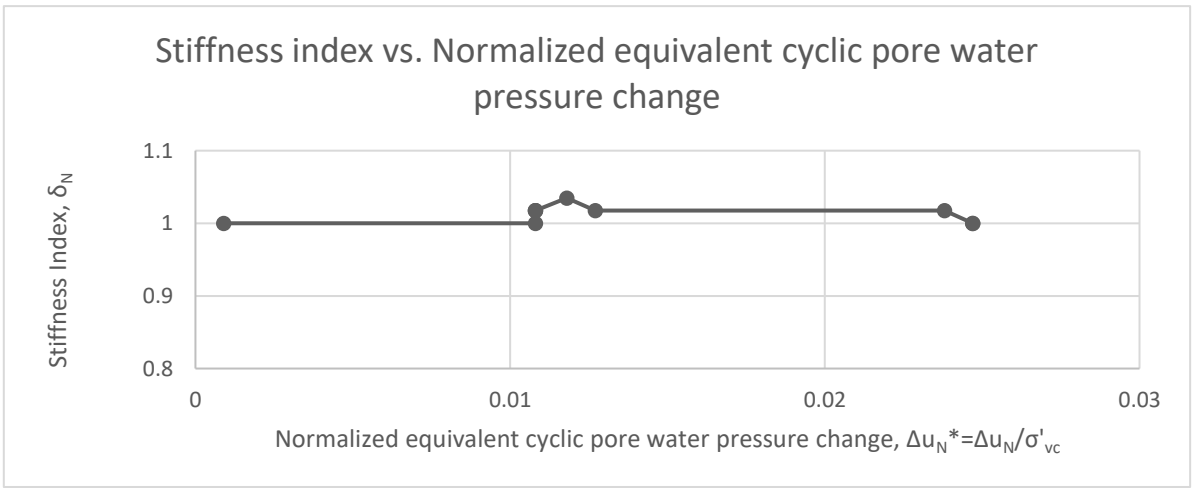

Test: 5.6; Soil: Nevada Sand; e=0.771; w=18.63%, S=65%
σ'_{vc}=145 (kPa); OCR=1; Υ_c=0.005%, f=0.01 Hz

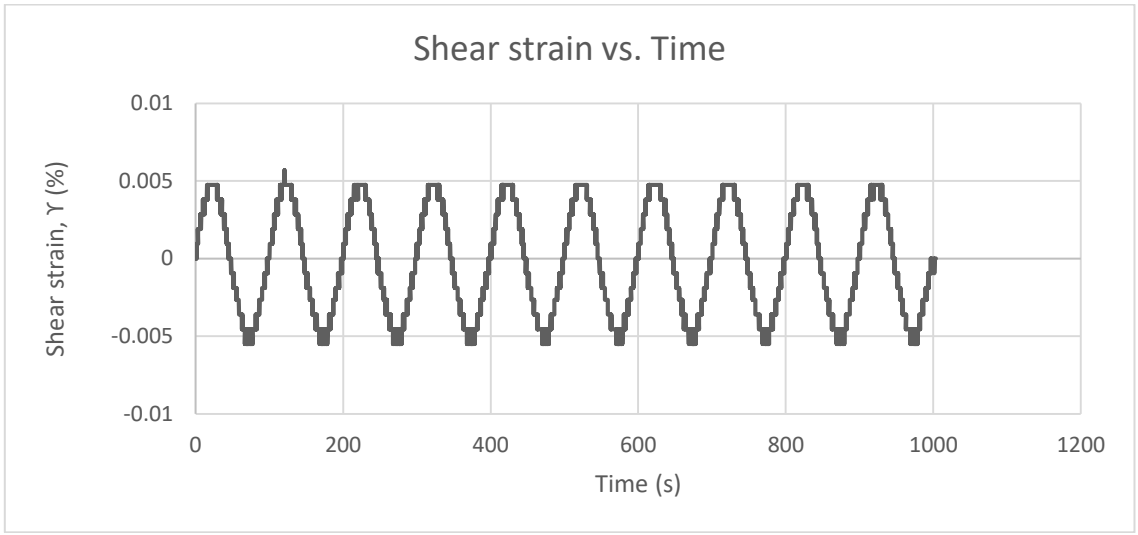

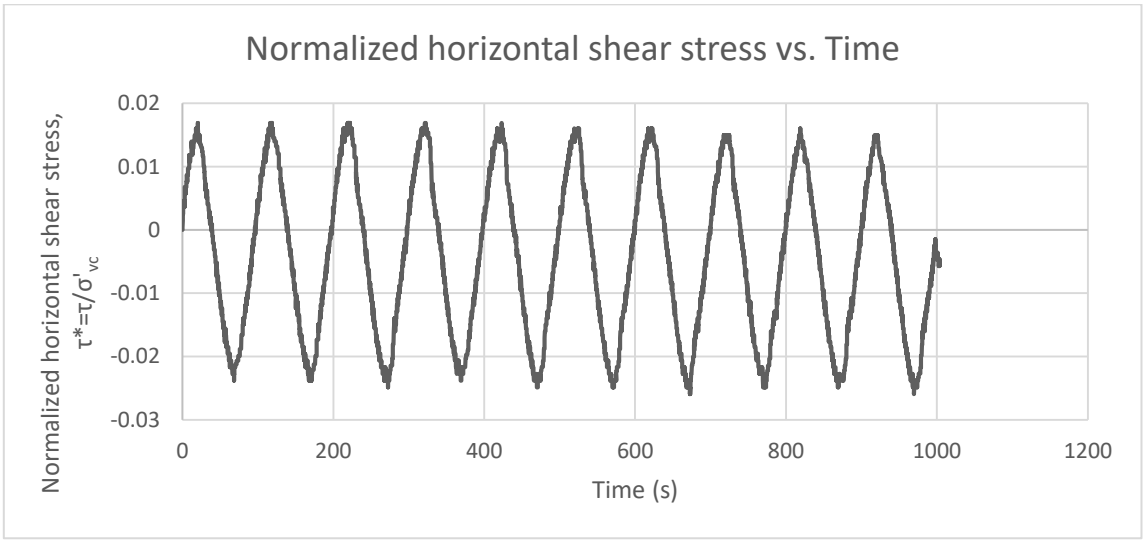

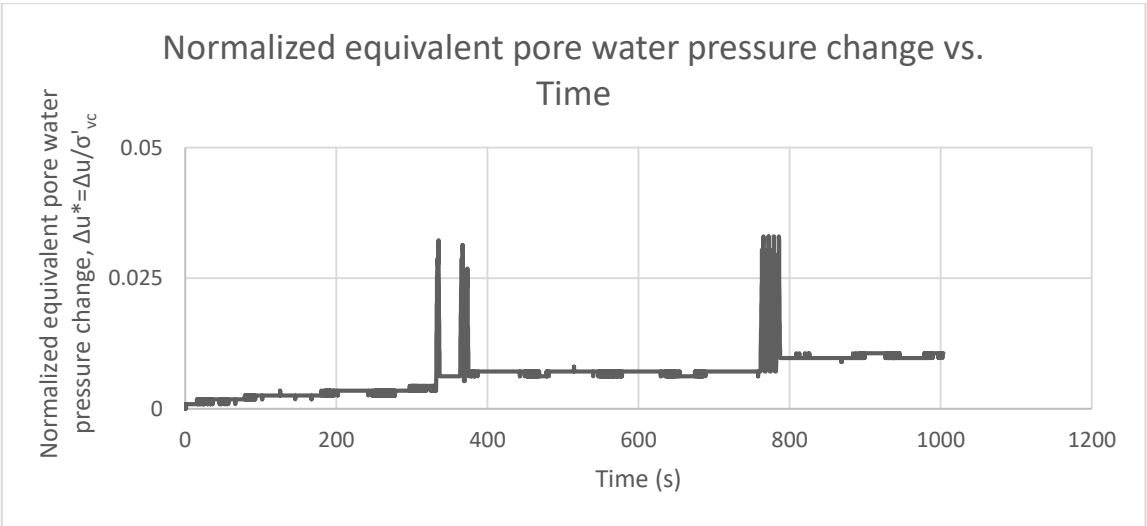

Test: 5.6; Soil: Nevada Sand; e=0.771; w=18.63%, S=65%
σ'_{vc}=145 (kPa); OCR=1; Υ_c=0.005%, f=0.01 Hz

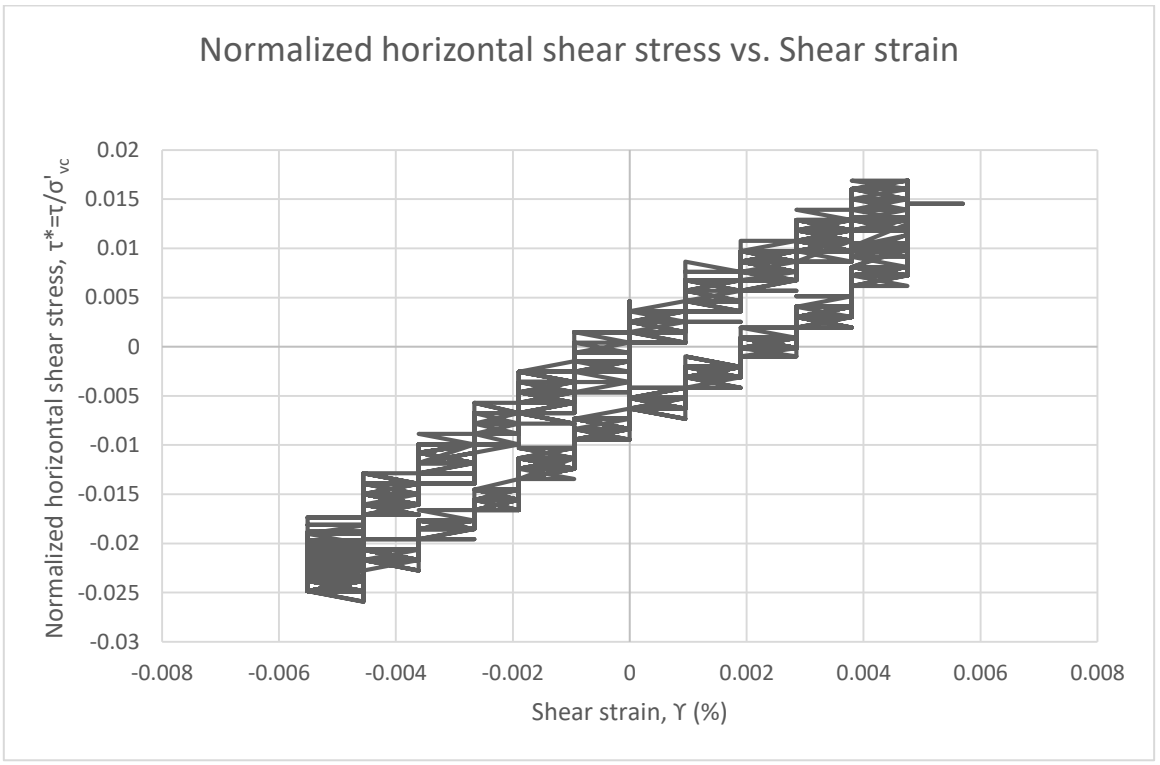

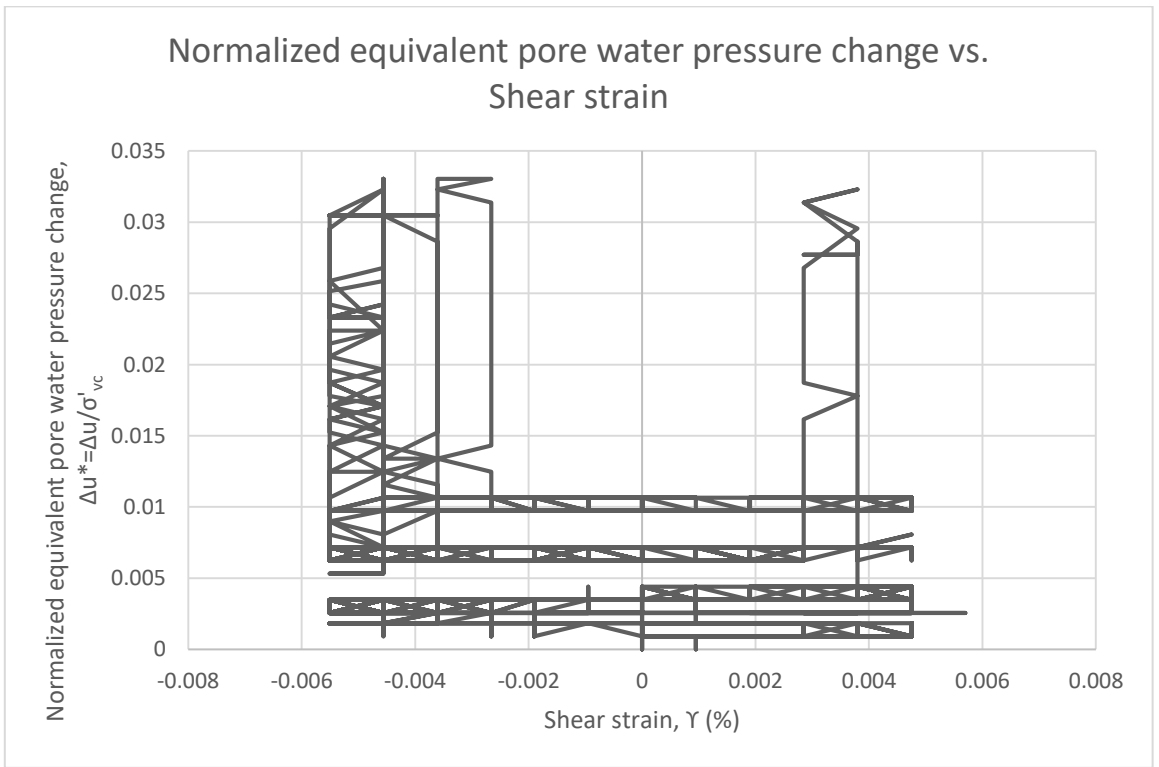

Test: 5.6; Soil: Nevada Sand; e=0.771; w=18.63%, S=65%
σ'_{vc}=145 (kPa); OCR=1; Υ_c=0.005%, f=0.01 Hz

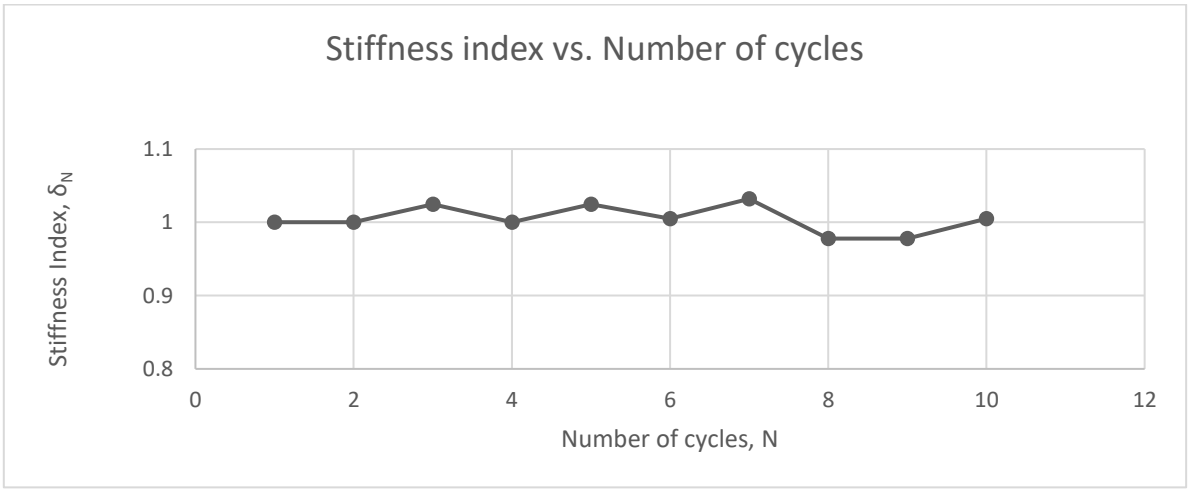

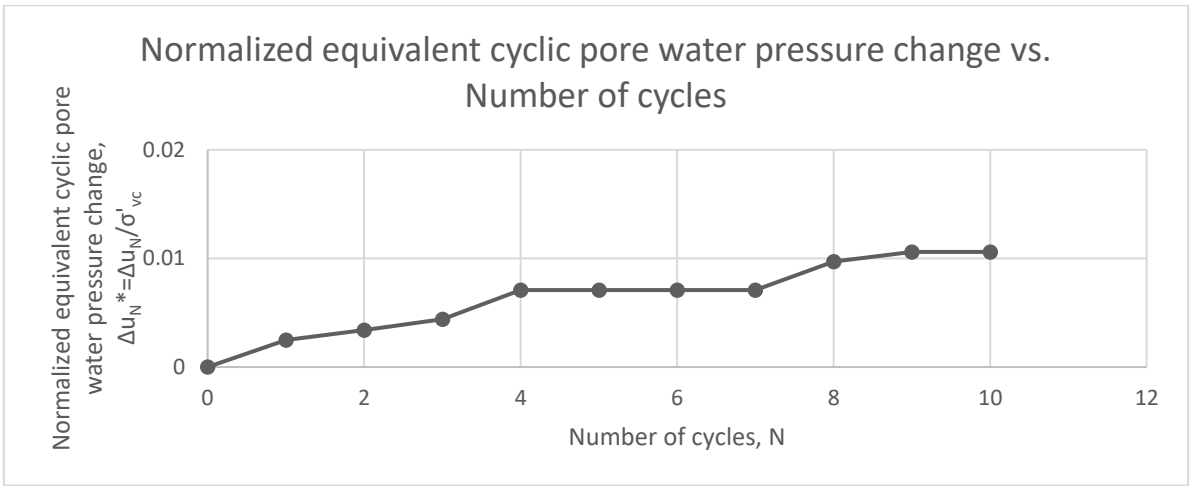

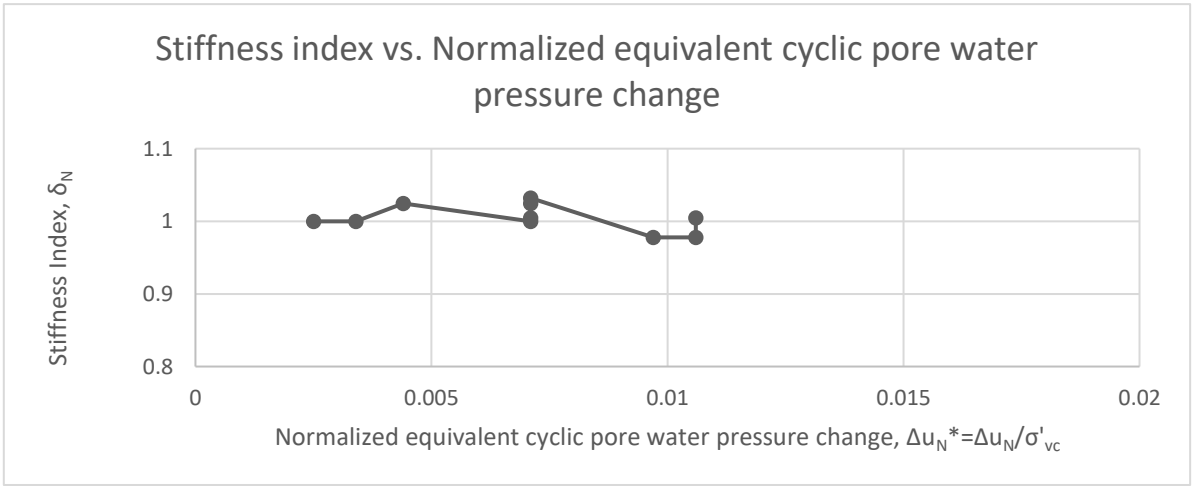

TEST 6

Test: 6.1; Soil: Nevada Sand; e=0.641; w=0%
σ'_{vc}=150 (kPa); OCR=1; Υ_c=0.08%, f=0.01 Hz

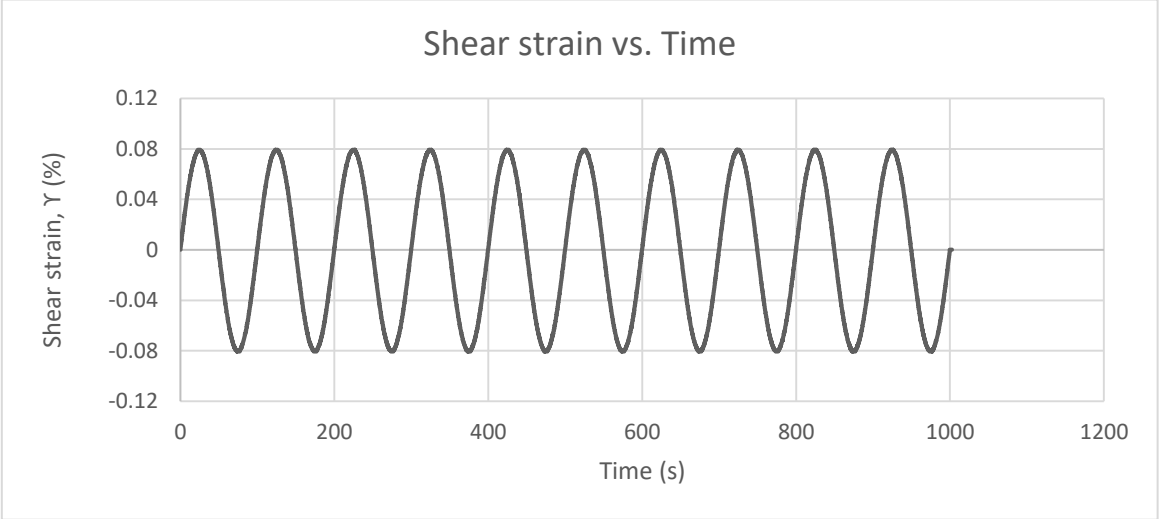

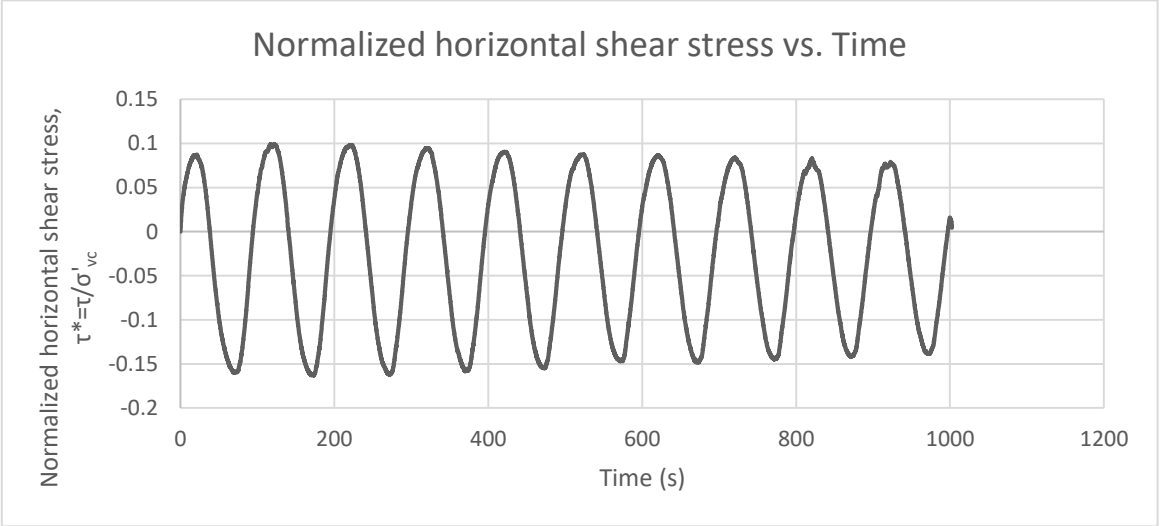

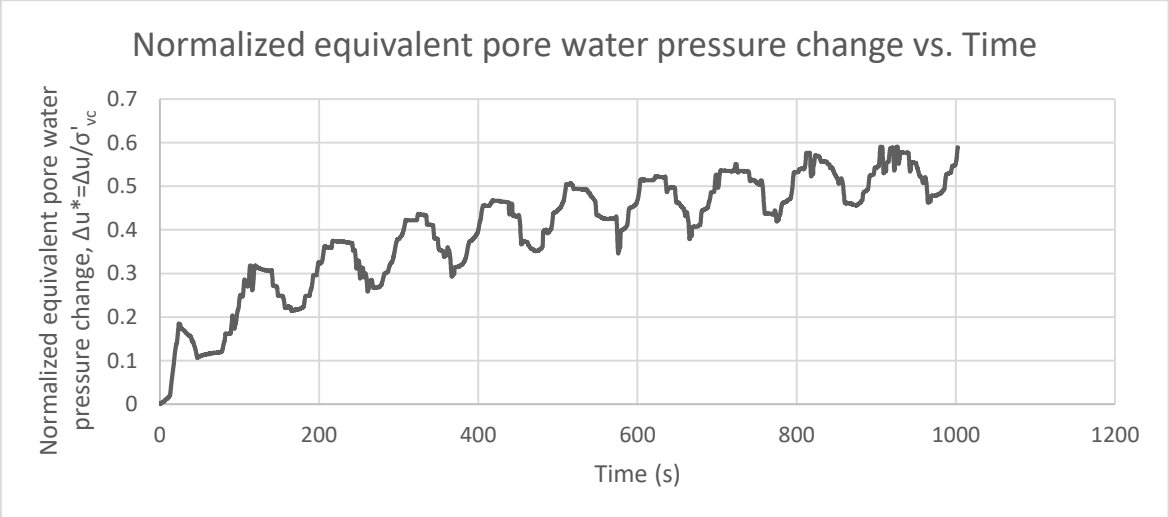

Test: 6.1; Soil: Nevada Sand; e=0.641; w=0%
σ'_{vc}=150 (kPa); OCR=1; Υ_c=0.08%, f=0.01 Hz

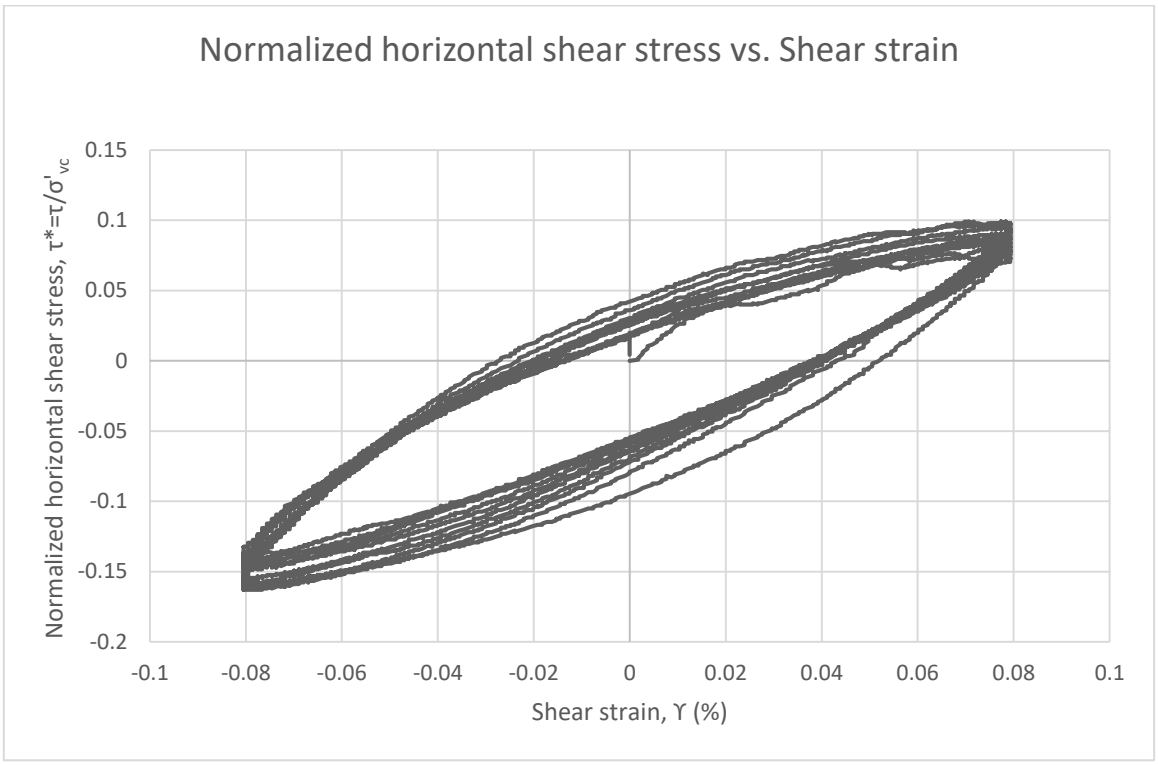

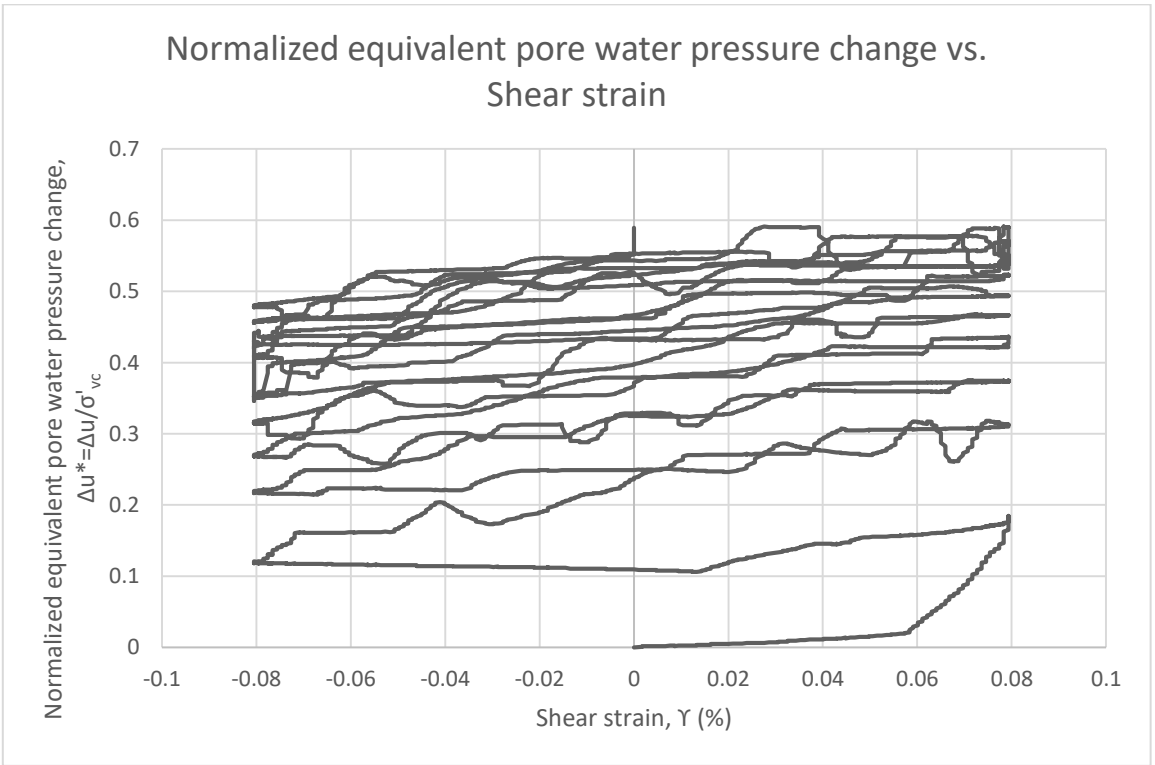

Test: 6.1; Soil: Nevada Sand; e=0.641; w=0%
σ'_{vc}=150 (kPa); OCR=1; Υ_c=0.08%, f=0.01 Hz

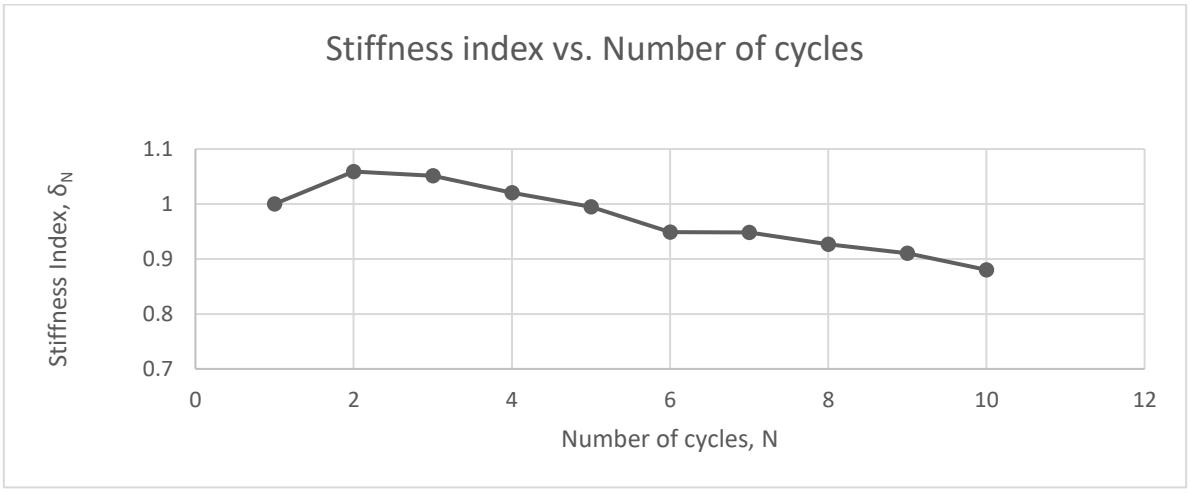

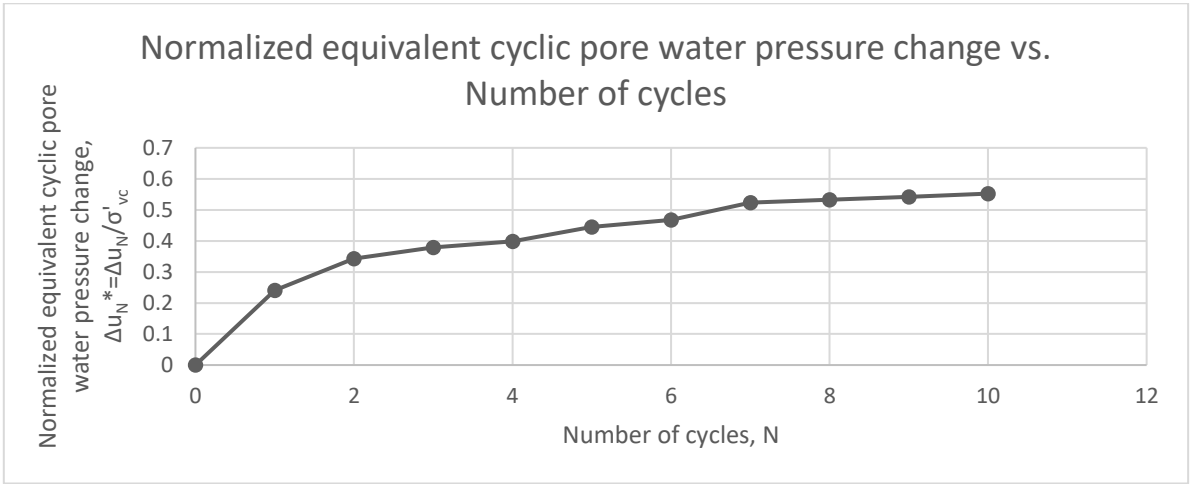

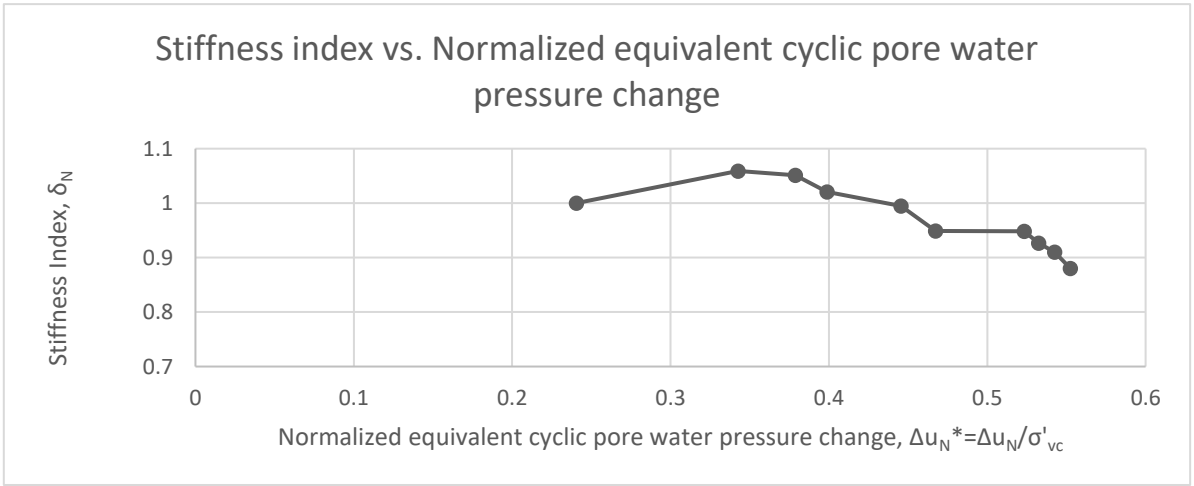

Test: 6.1; Soil: Nevada Sand; e=0.641; w=0%
σ'_{vc}=150 (kPa); OCR=1; Υ_c=0.08%, f=0.01 Hz

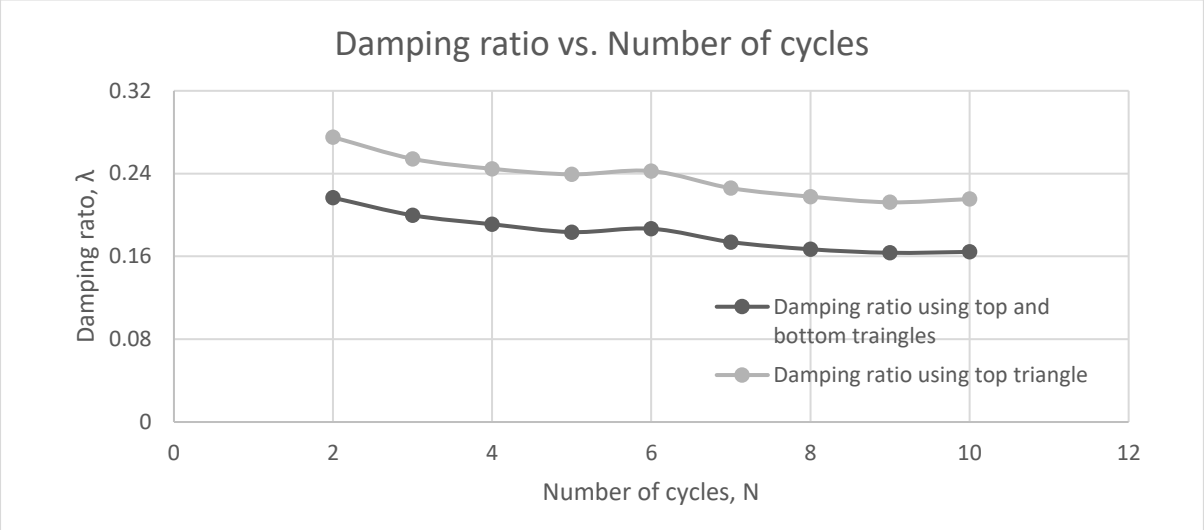

Test: 6.2; Soil: Nevada Sand; e=0.64; w=0%
σ'_{vc}=150 (kPa); OCR=1; f=0.01 Hz

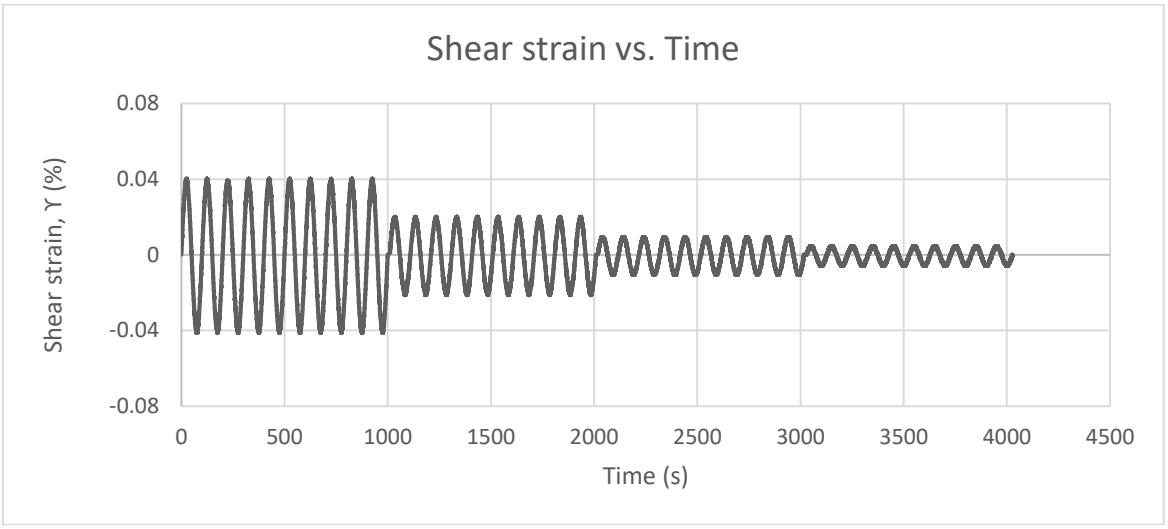

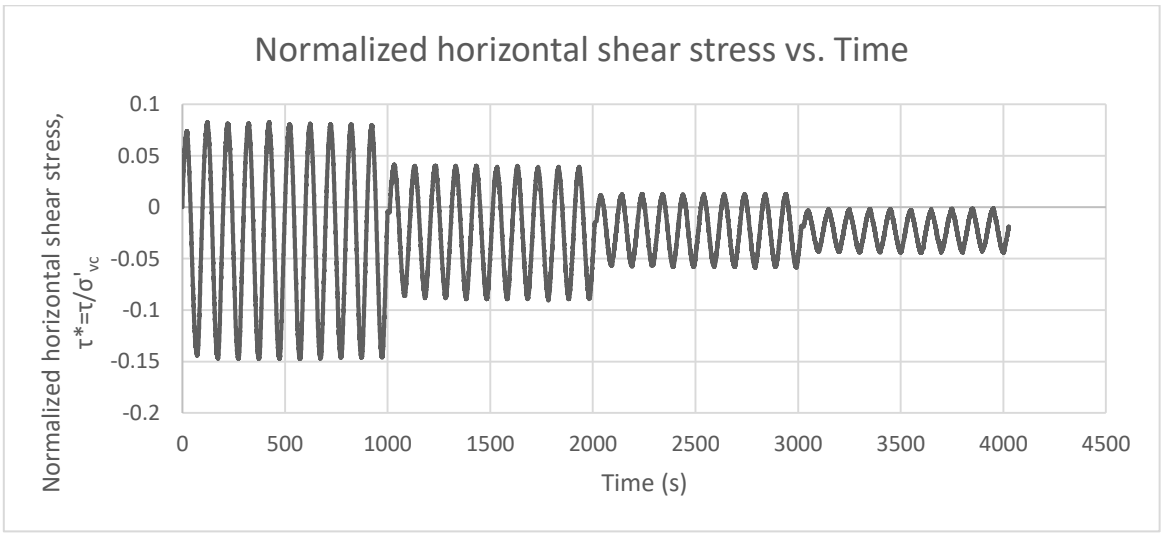

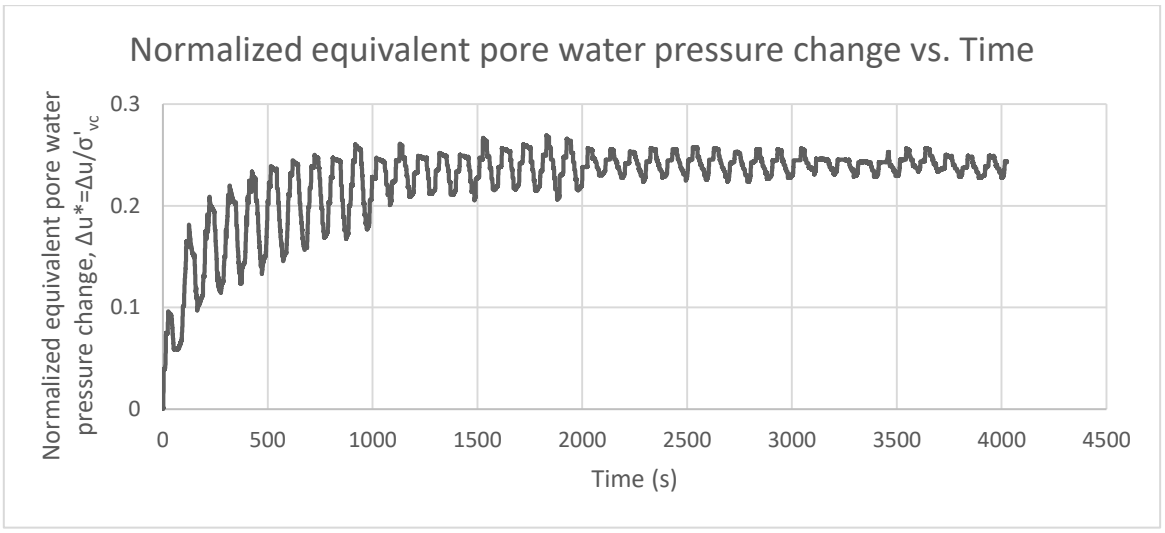

Test: 6.2; Soil: Nevada Sand; e=0.64; w=0%
σ'_{vc}=150 (kPa); OCR=1; f=0.01 Hz

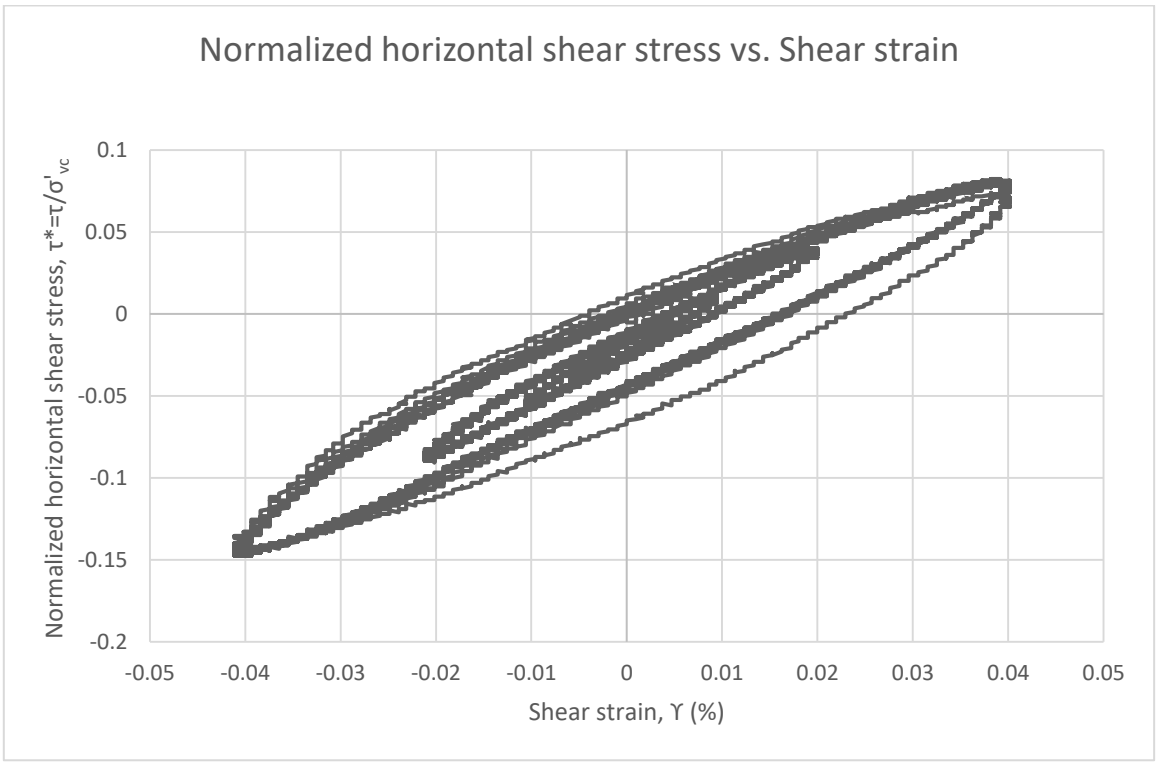

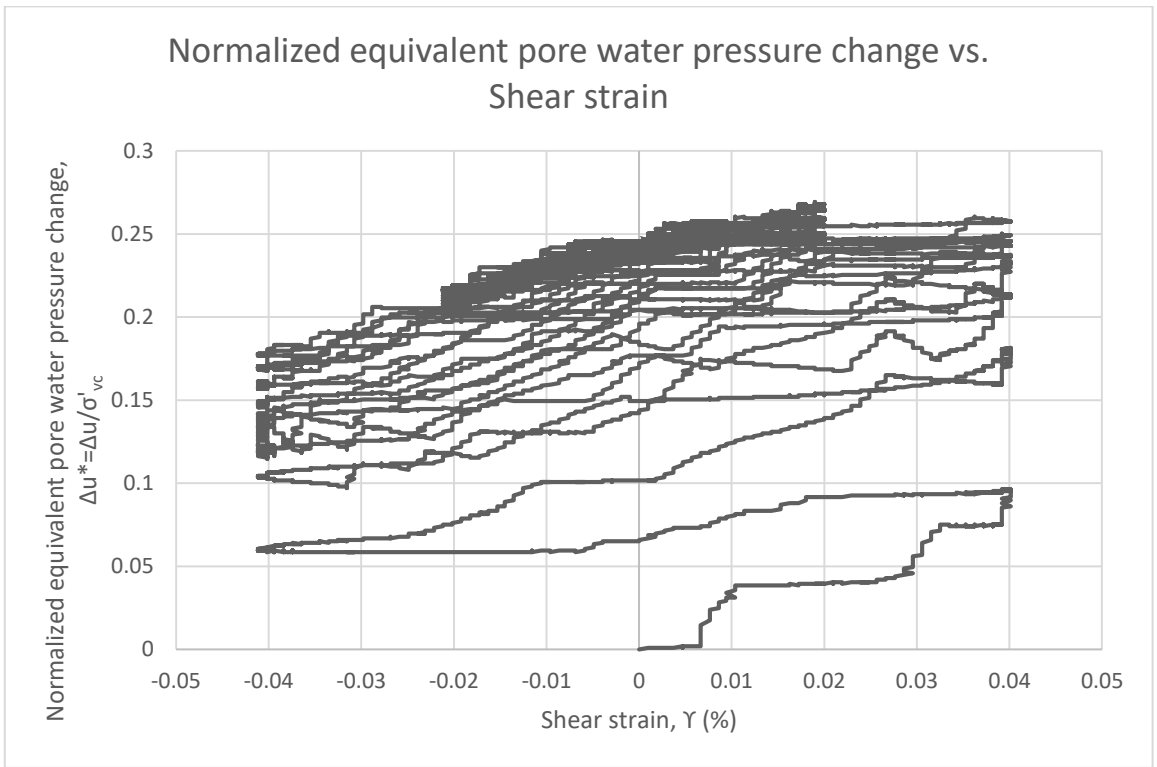

Test: 6.2; Soil: Nevada Sand; e=0.64; w=0%
σ'_{vc}=150 (kPa); OCR=1; f=0.01 Hz

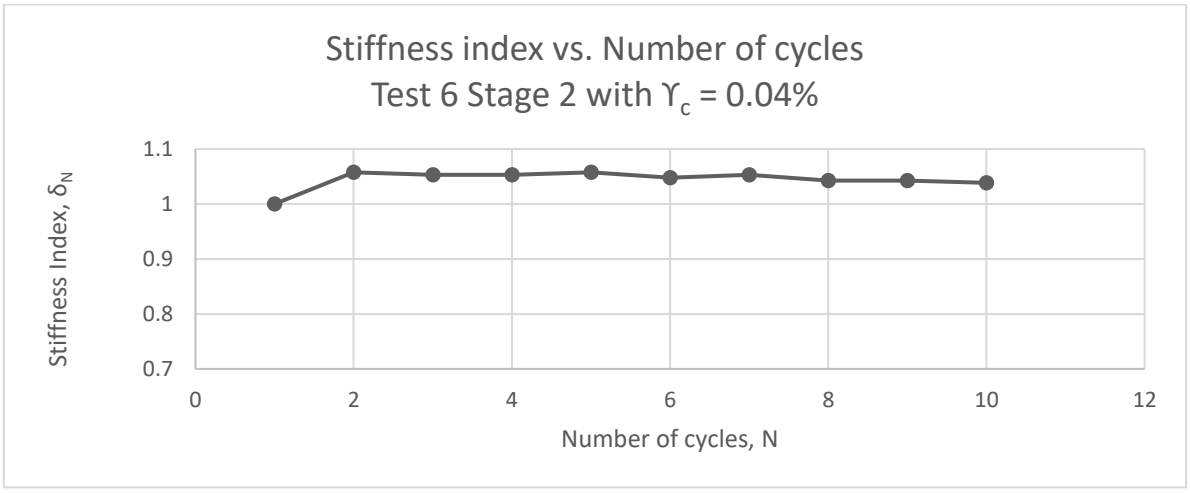

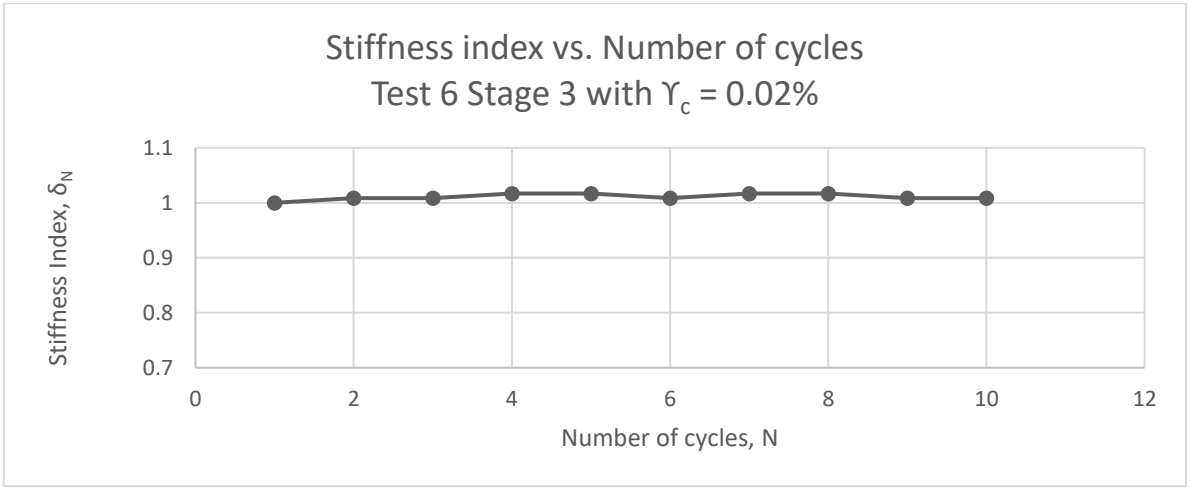

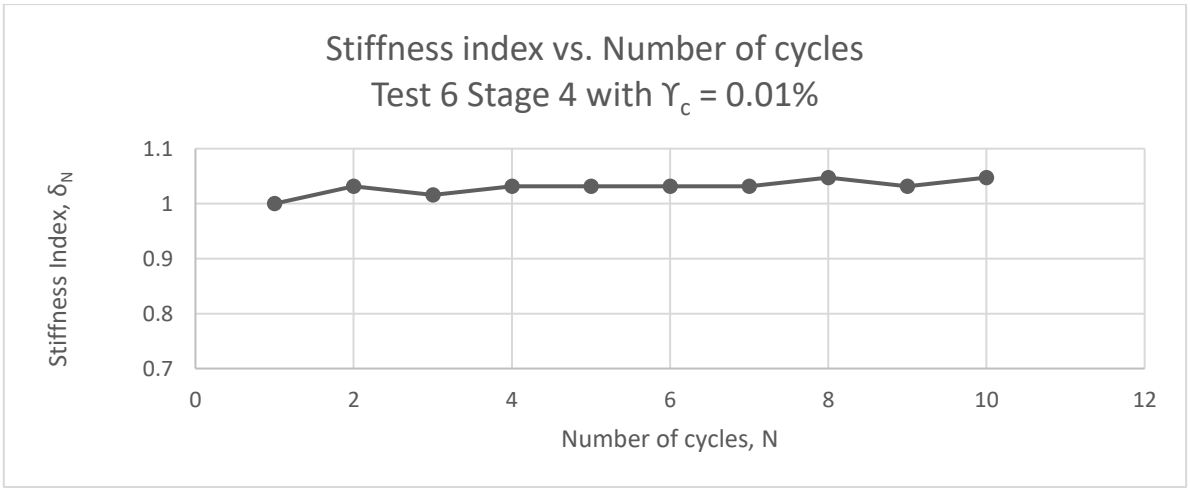

Test: 6.2; Soil: Nevada Sand; e=0.64; w=0%
σ'_{vc}=150 (kPa); OCR=1; f=0.01 Hz

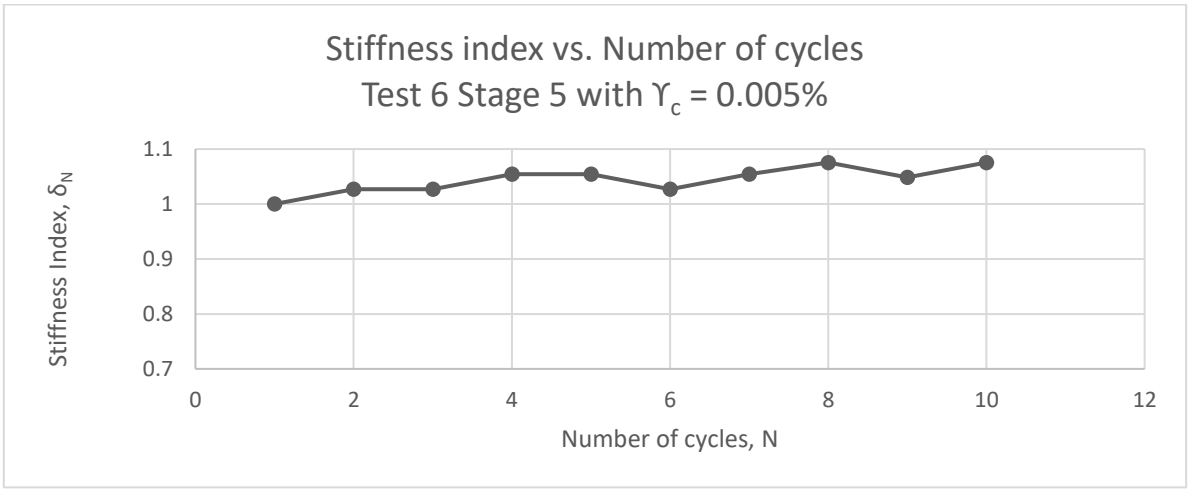

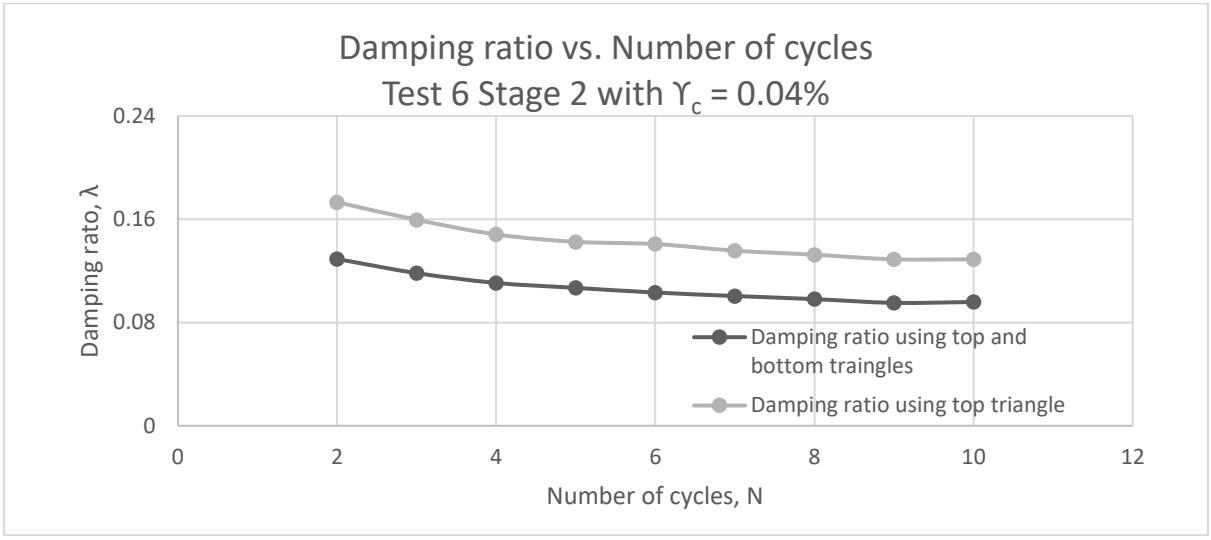

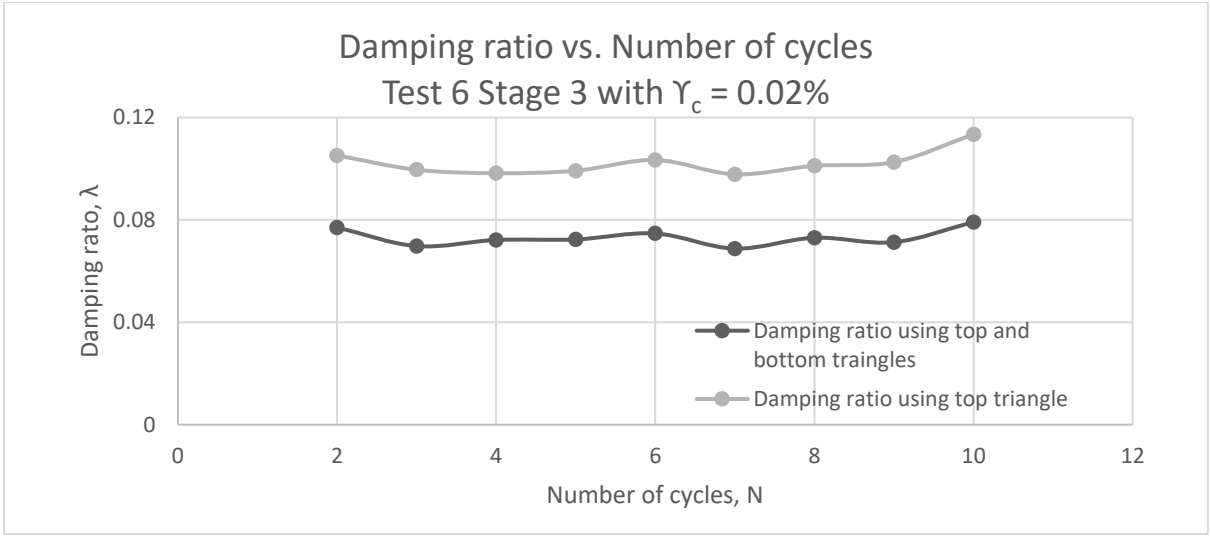

TEST 7

Test: 7; Soil: Nevada Sand; e=0.63; w=0%
σ'_{vc}=220 (kPa); OCR=1; f=0.1 Hz

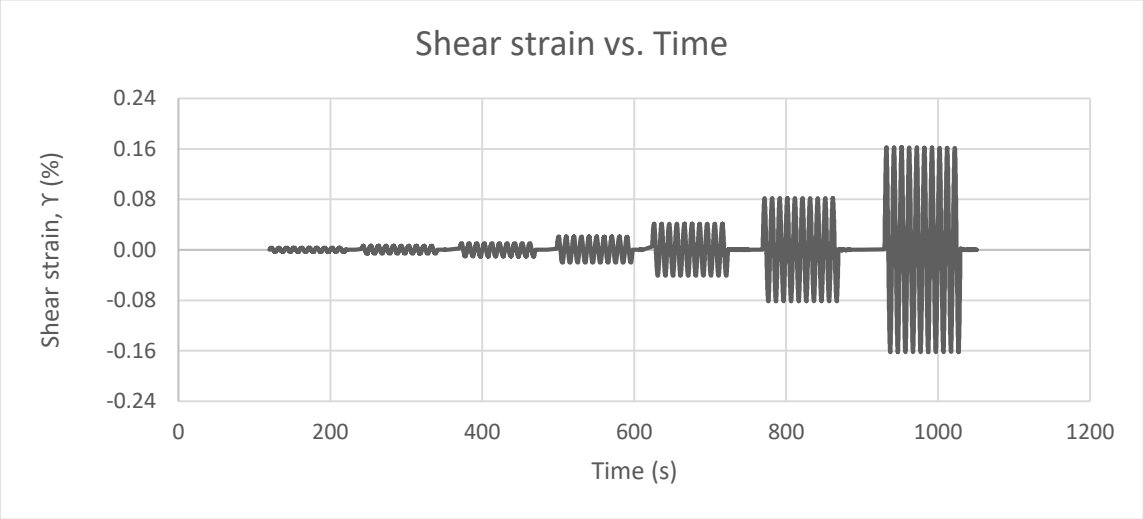

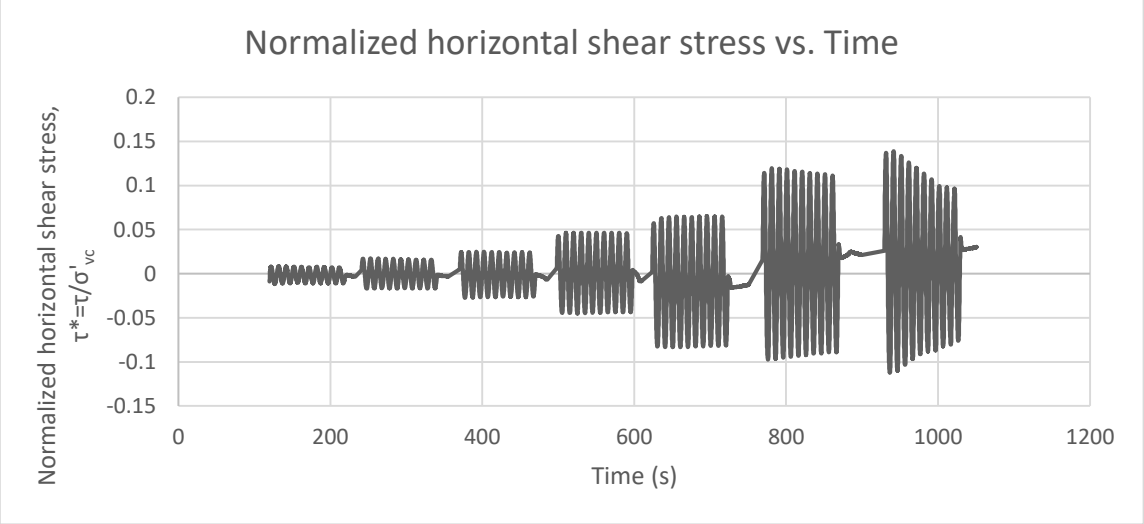

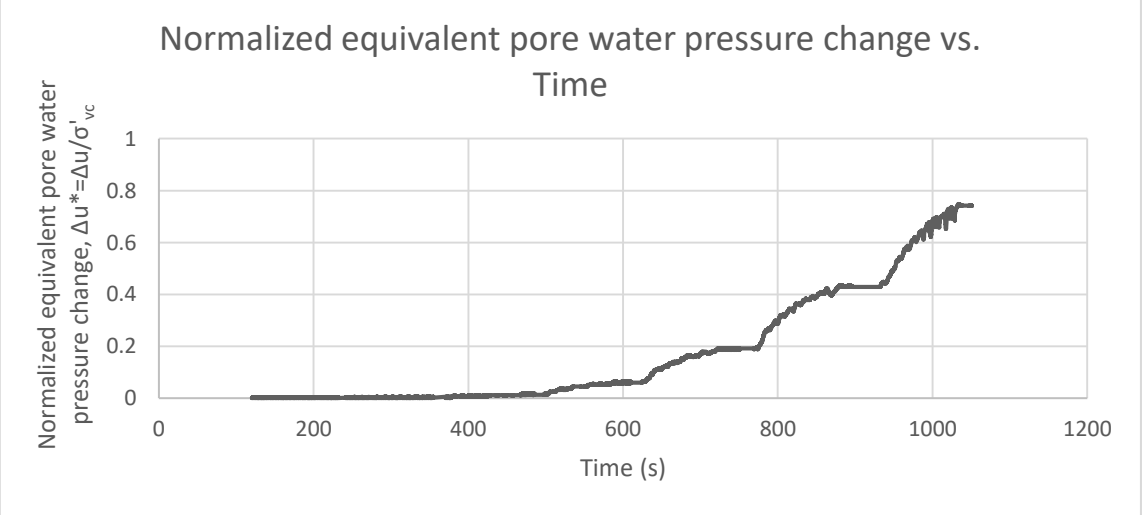

Test: 7; Soil: Nevada Sand; e=0.63; w=0%
σ'_{vc}=220 (kPa); OCR=1; f=0.1 Hz

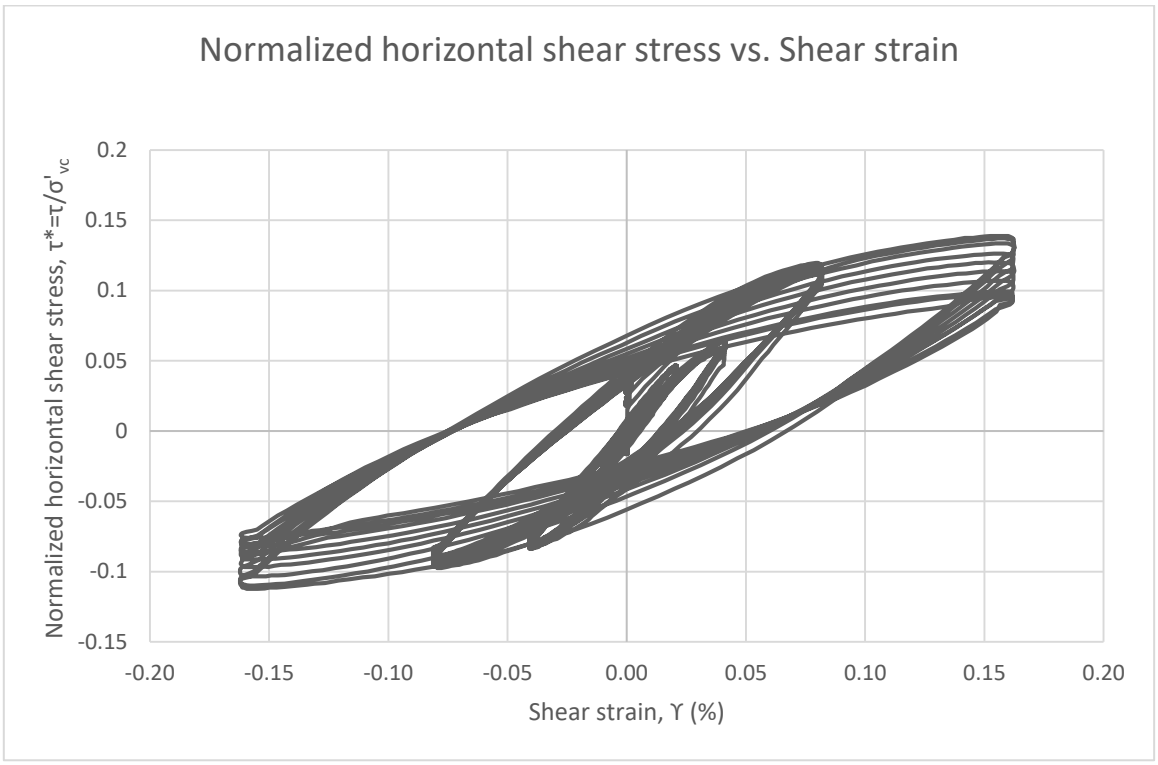

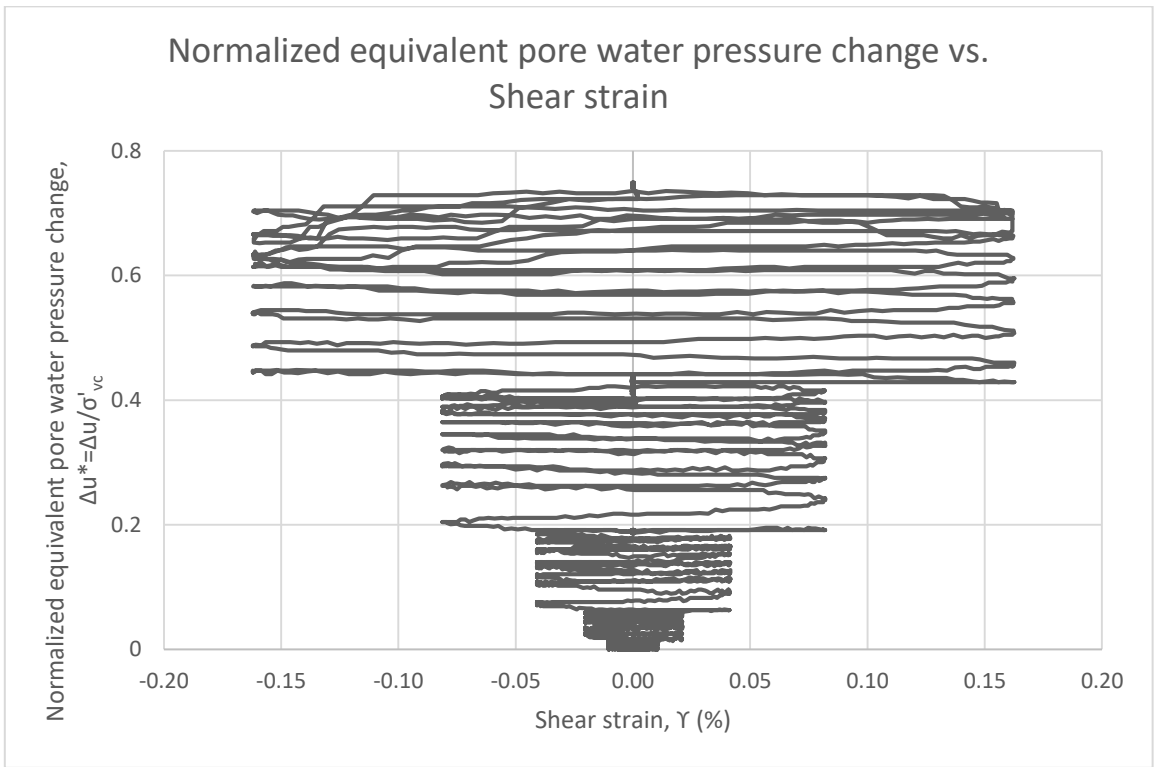

Test: 7; Soil: Nevada Sand; e=0.63; w=0%
σ'_{vc}=220 (kPa); OCR=1; f=0.1 Hz

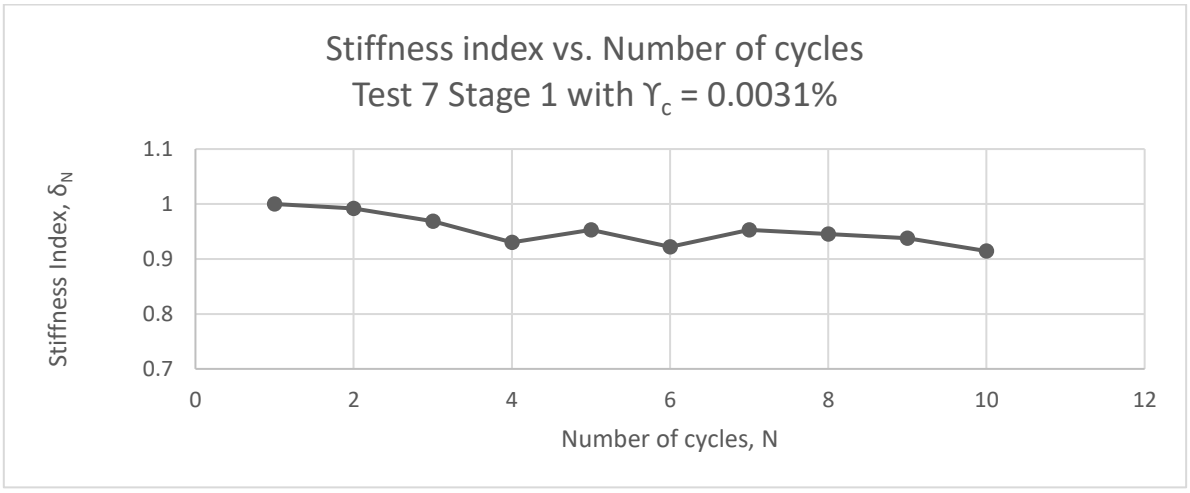

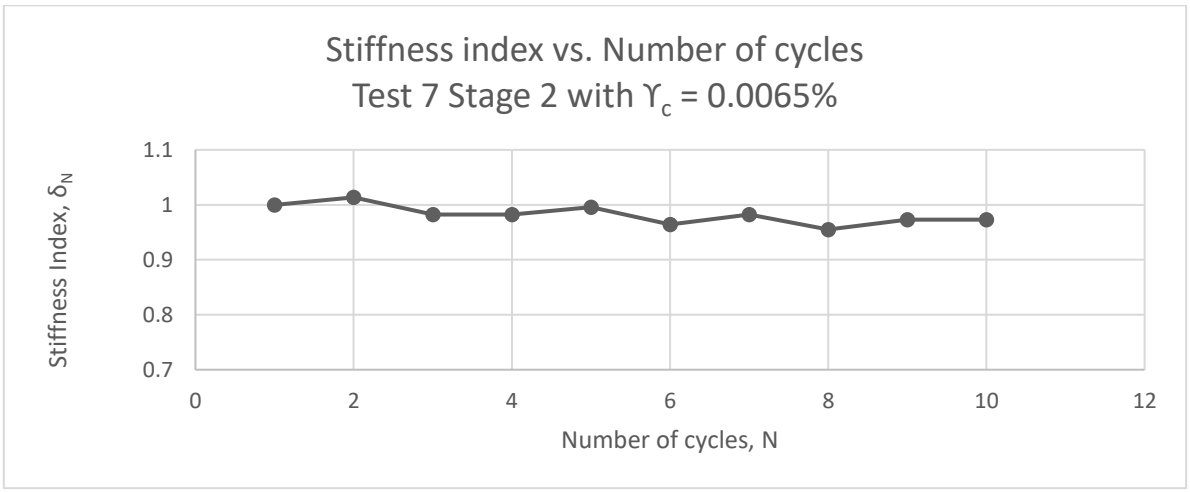

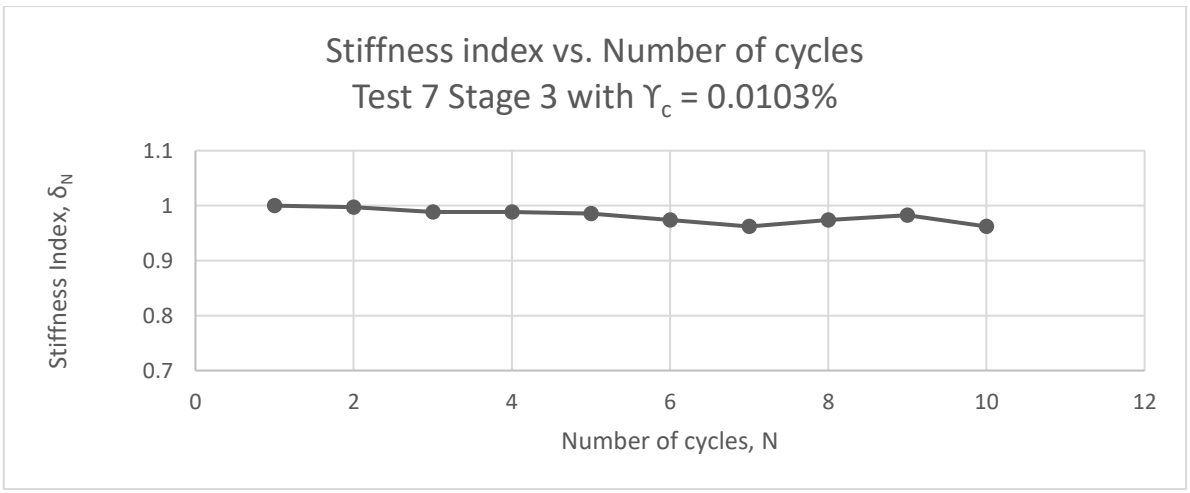

Test: 7; Soil: Nevada Sand; e=0.63; w=0%
σ'_{vc}=220 (kPa); OCR=1; f=0.1 Hz

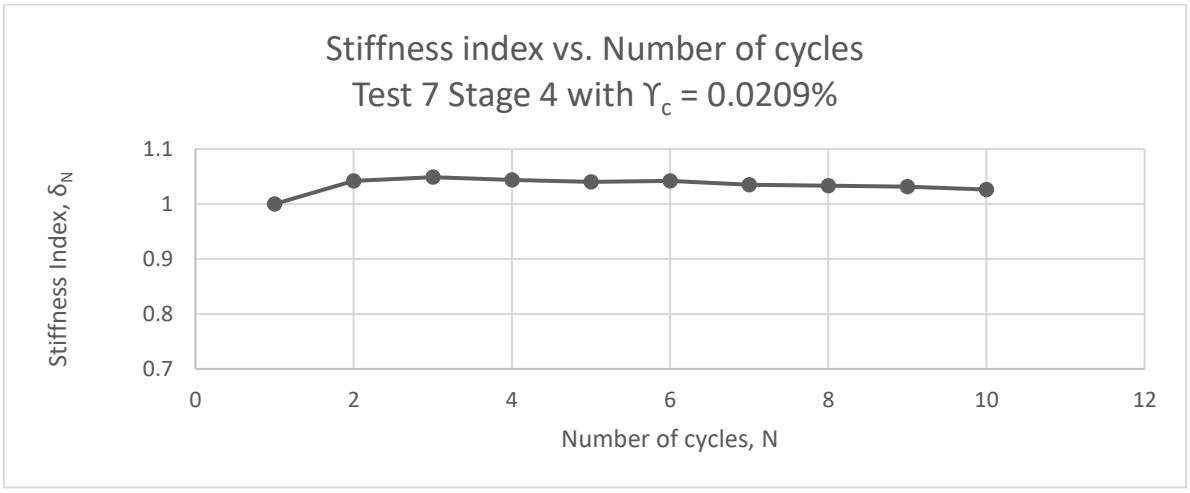

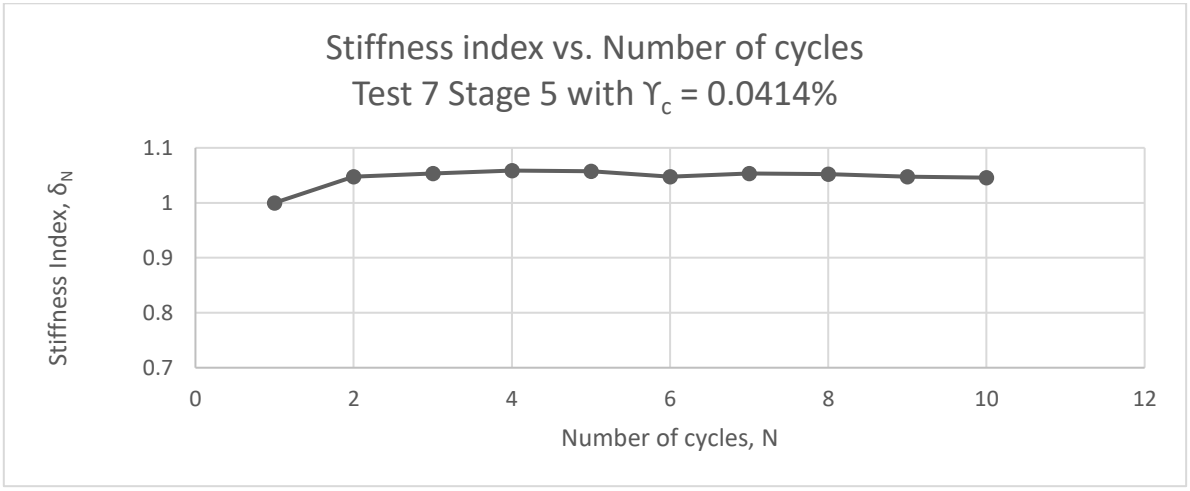

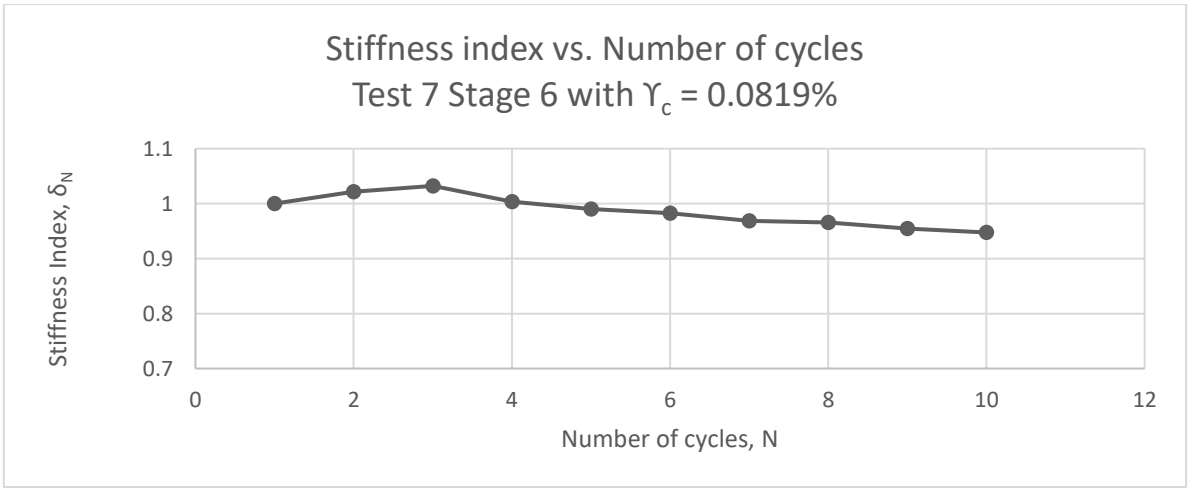

Test: 7; Soil: Nevada Sand; e=0.63; w=0%
σ'_{vc}=220 (kPa); OCR=1; f=0.1 Hz

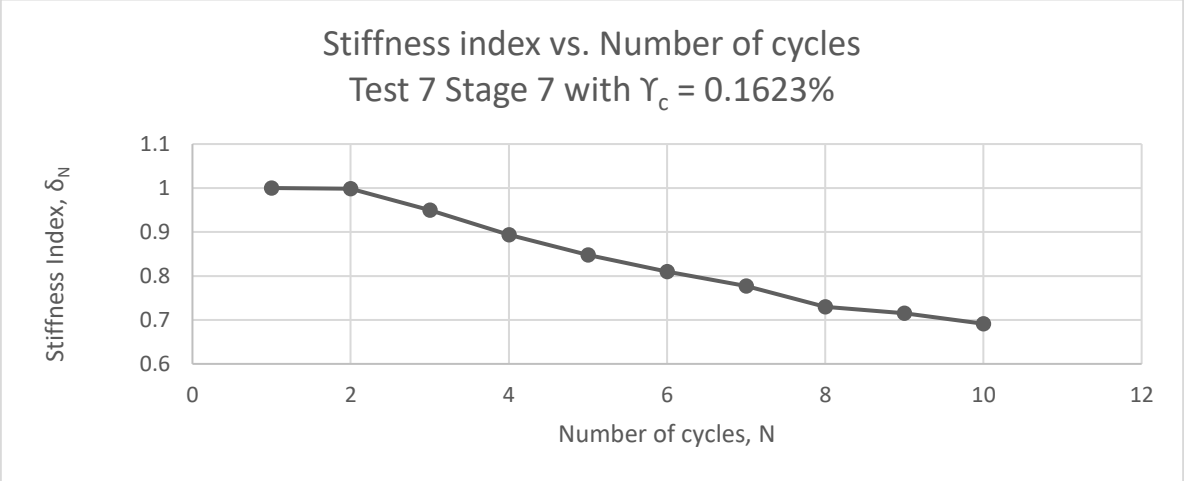

TEST 8

Test: 8; Soil: Nevada Sand; e=0.63; w=0%
σ'_{vc}=145 (kPa); OCR=1; f=0.01 Hz

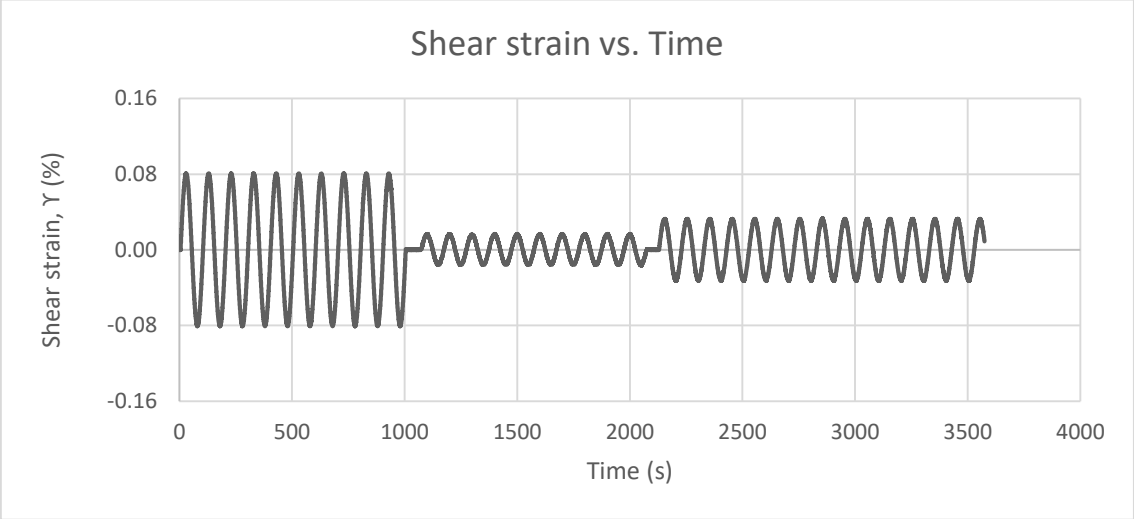

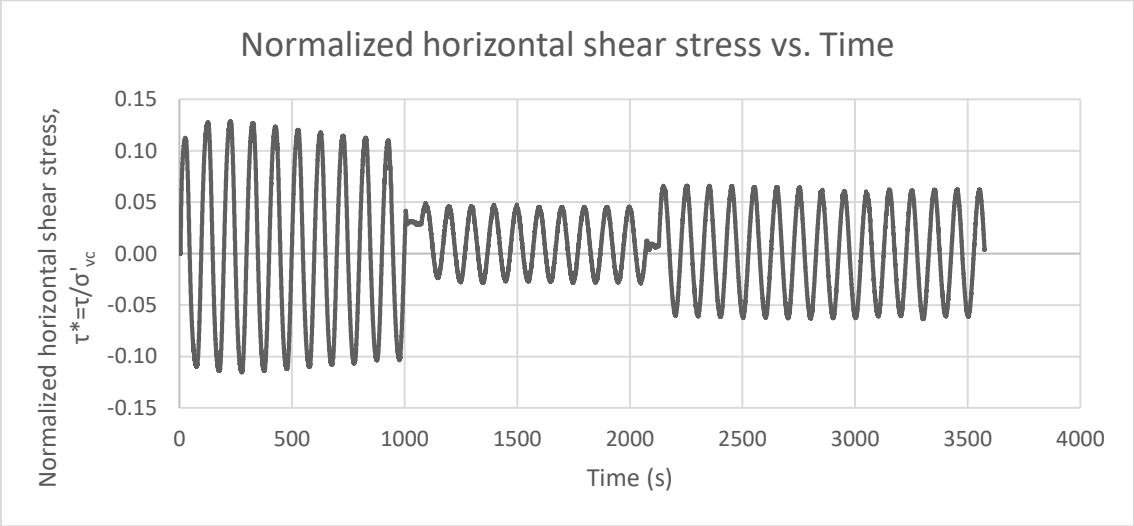

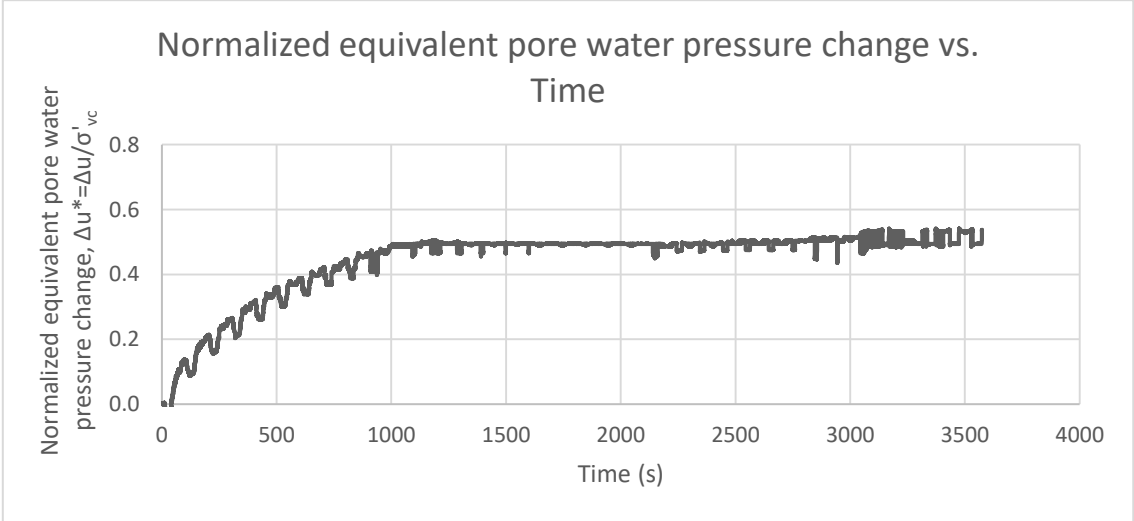

Test: 8; Soil: Nevada Sand; e=0.63; w=0%
σ'_{vc}=145 (kPa); OCR=1; f=0.01 Hz

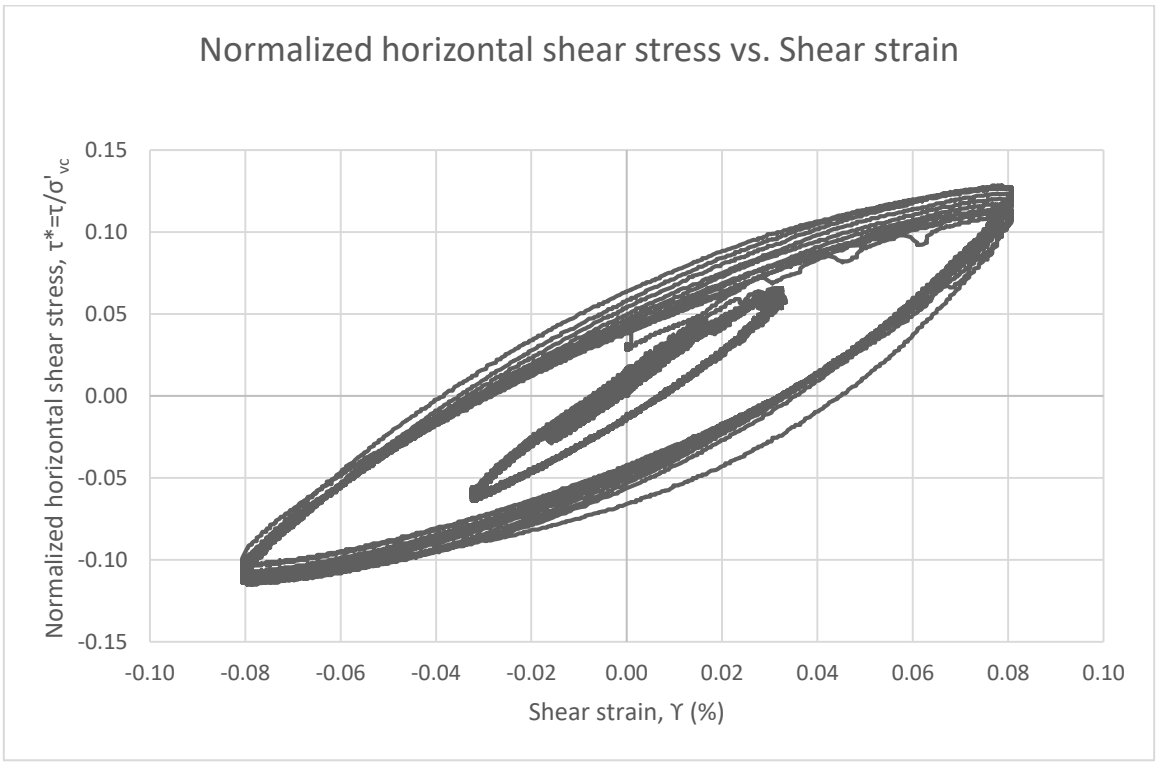

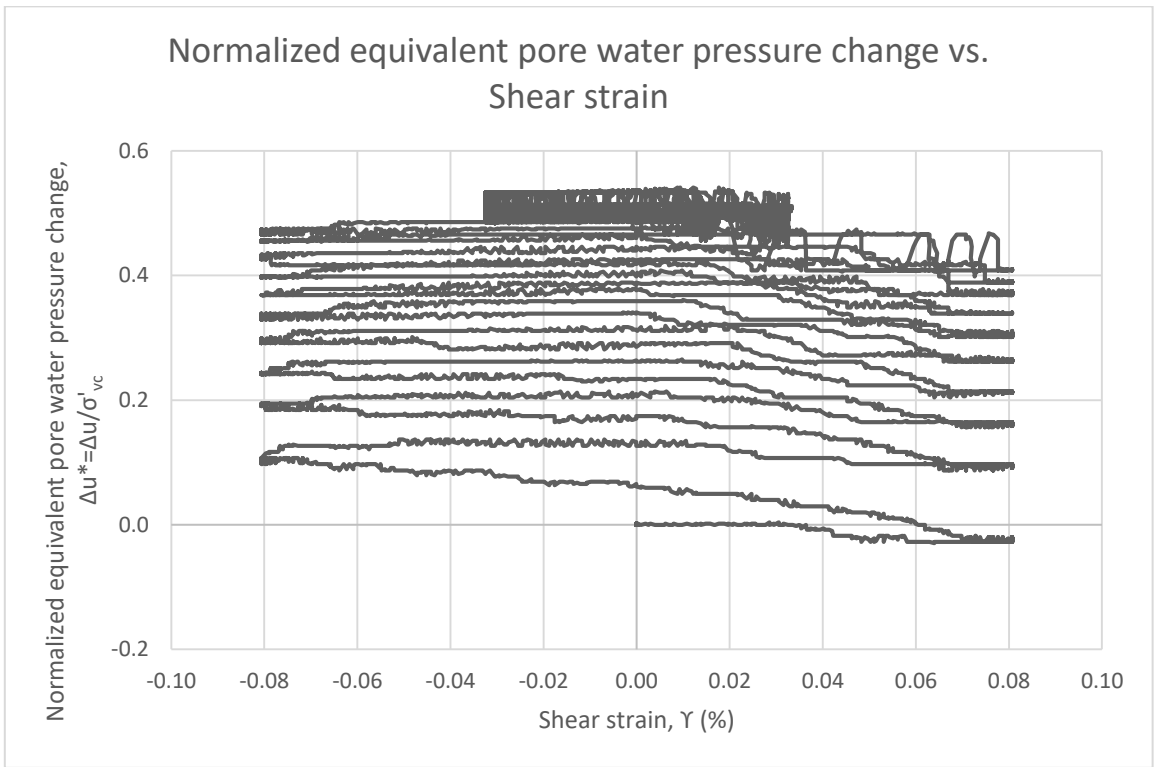

Test: 8; Soil: Nevada Sand; e=0.63; w=0%
σ'_{vc}=145 (kPa); OCR=1; f=0.01 Hz

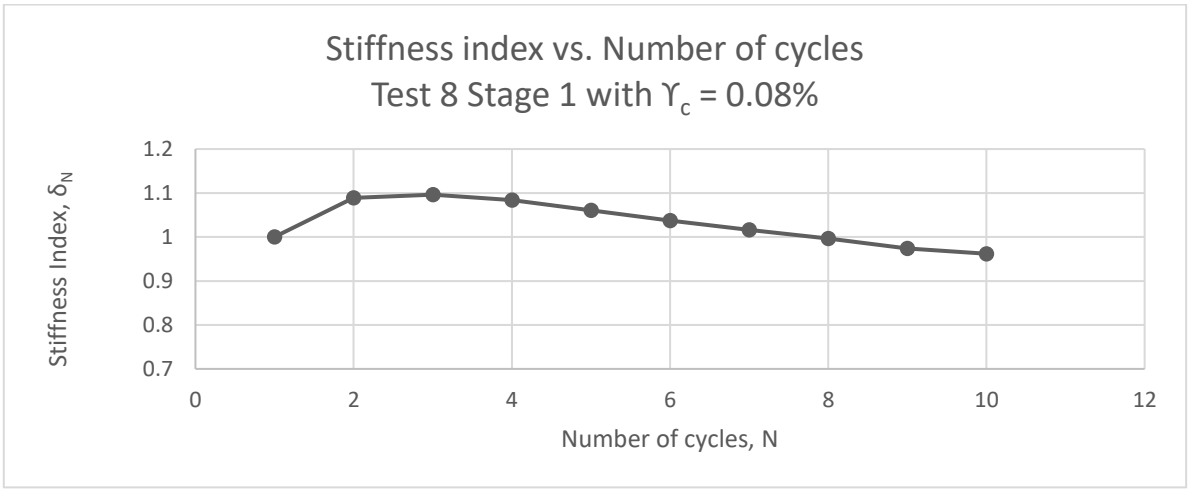

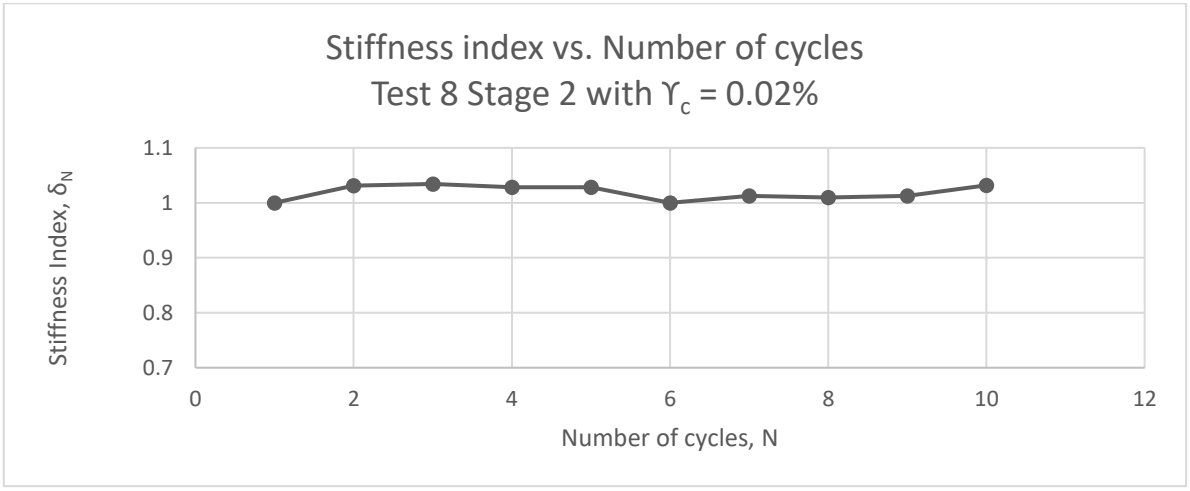

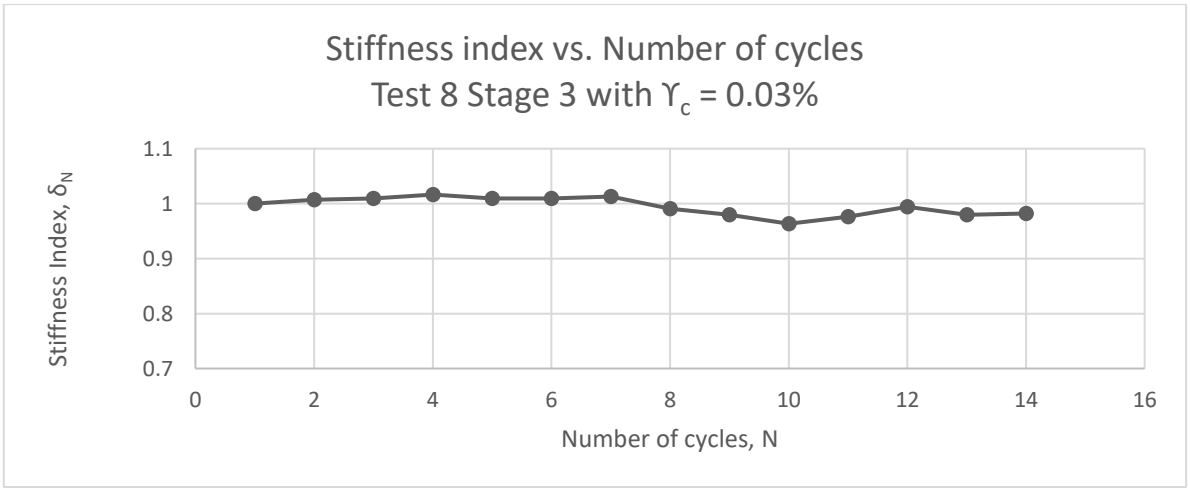

Test: 8; Soil: Nevada Sand; e=0.63; w=0%
σ'_{vc}=145 (kPa); OCR=1; f=0.01 Hz

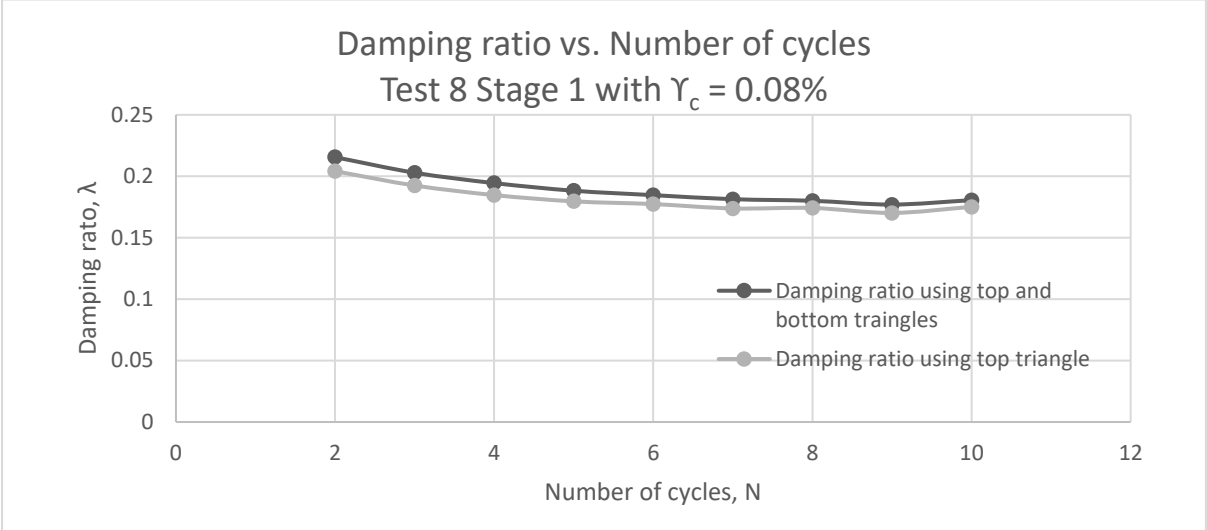

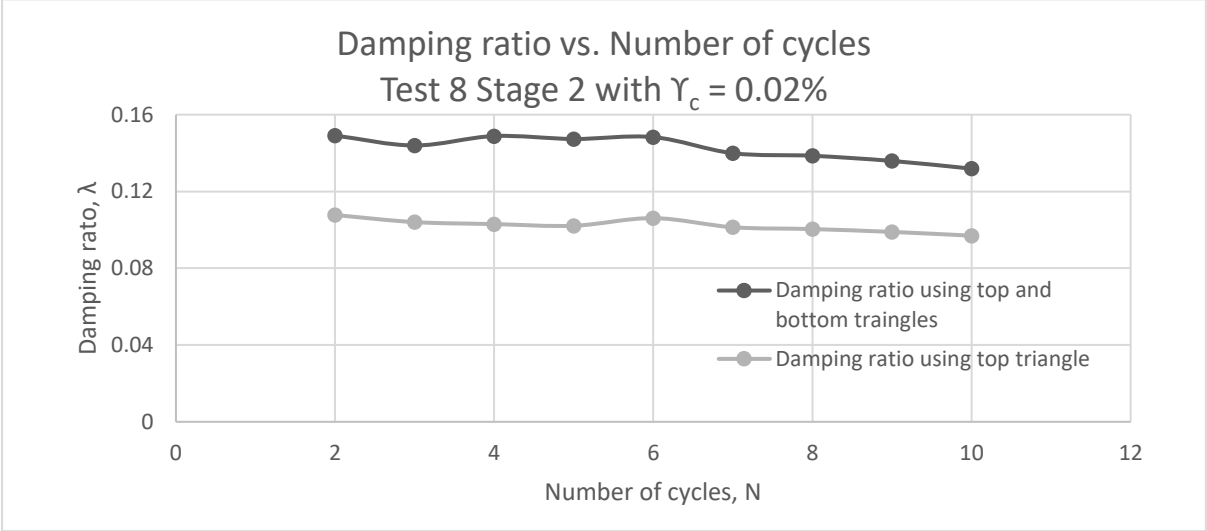

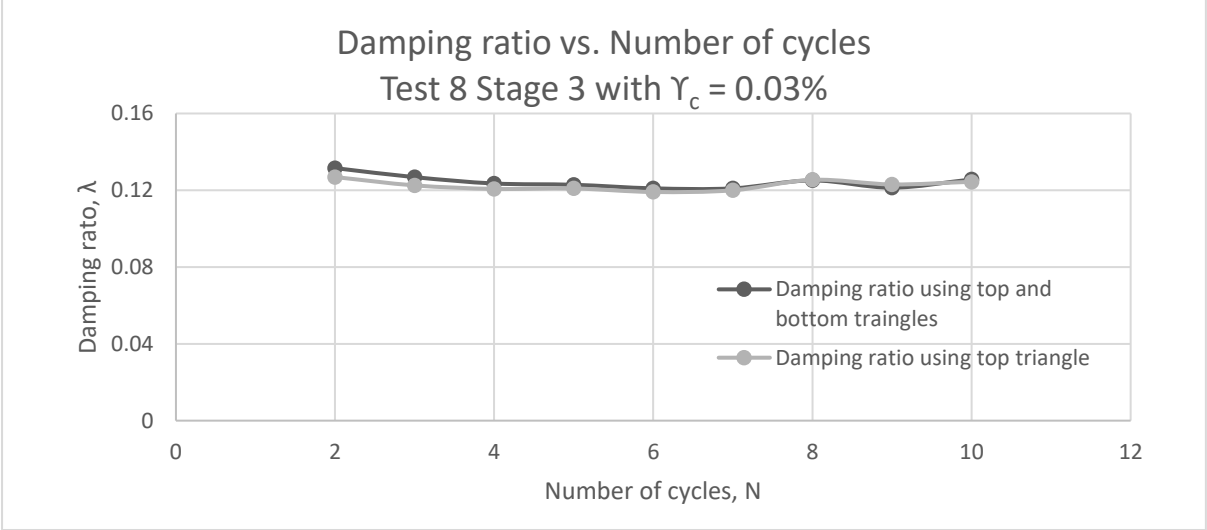

TEST 9

Test: 9; Soil: Toyoura Sand; e=0.71; w=0%
σ'_{vc}=146 (kPa); OCR=1; f=0.01 Hz

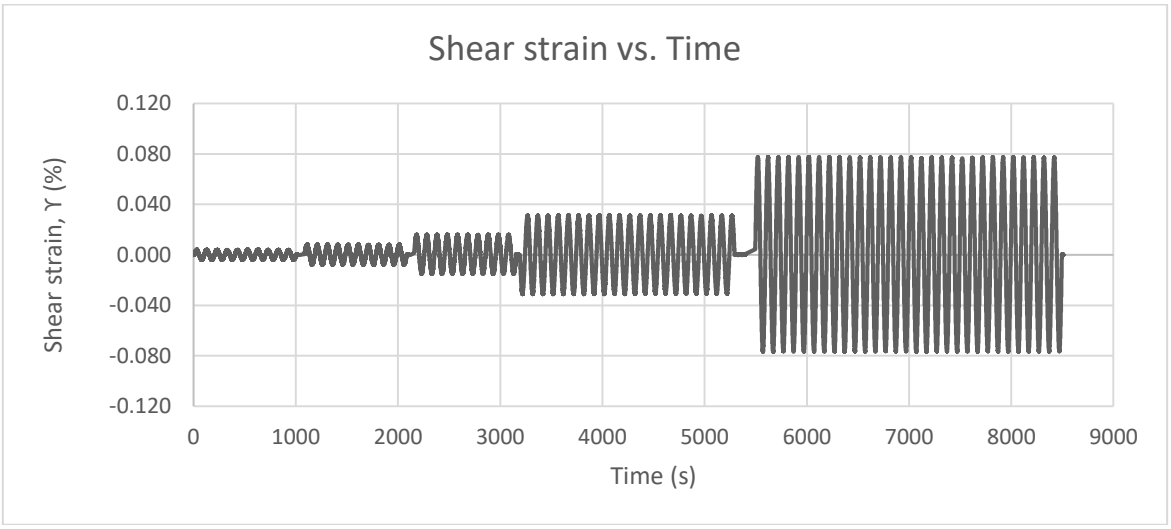

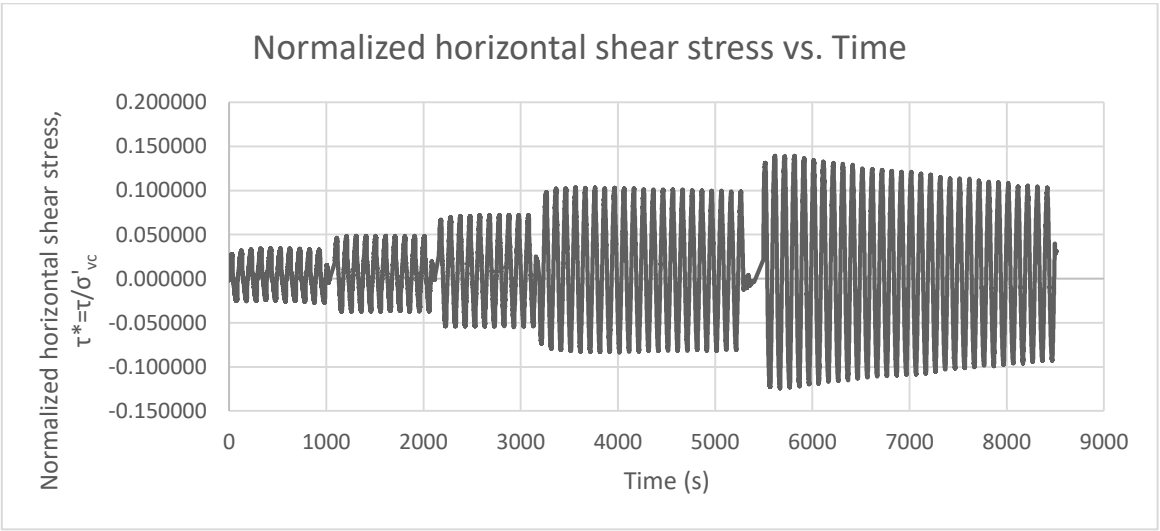

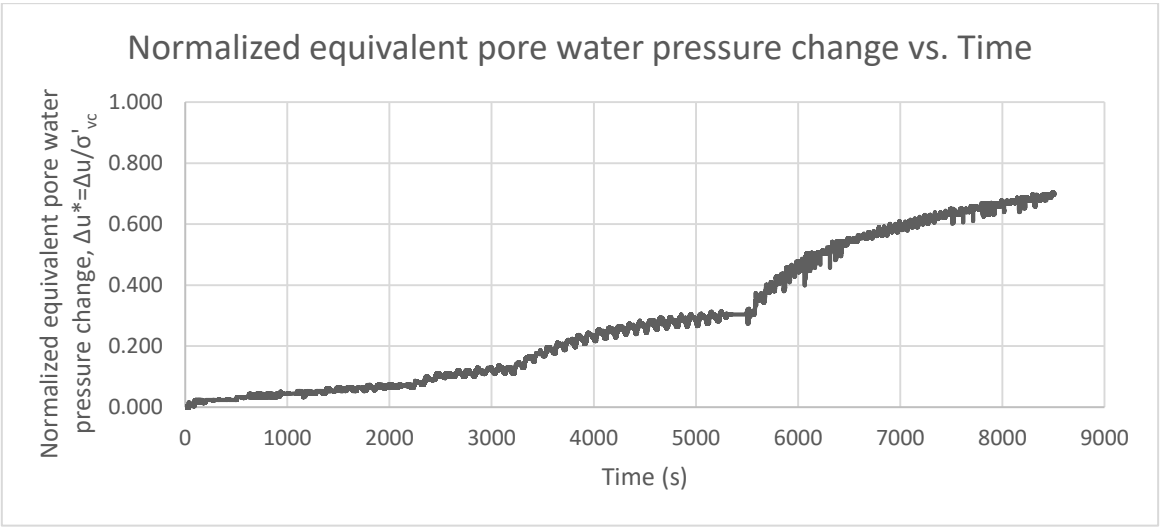

Test: 9; Soil: Toyoura Sand; e=0.71; w=0%
σ'_{vc}=146 (kPa); OCR=1; f=0.01 Hz

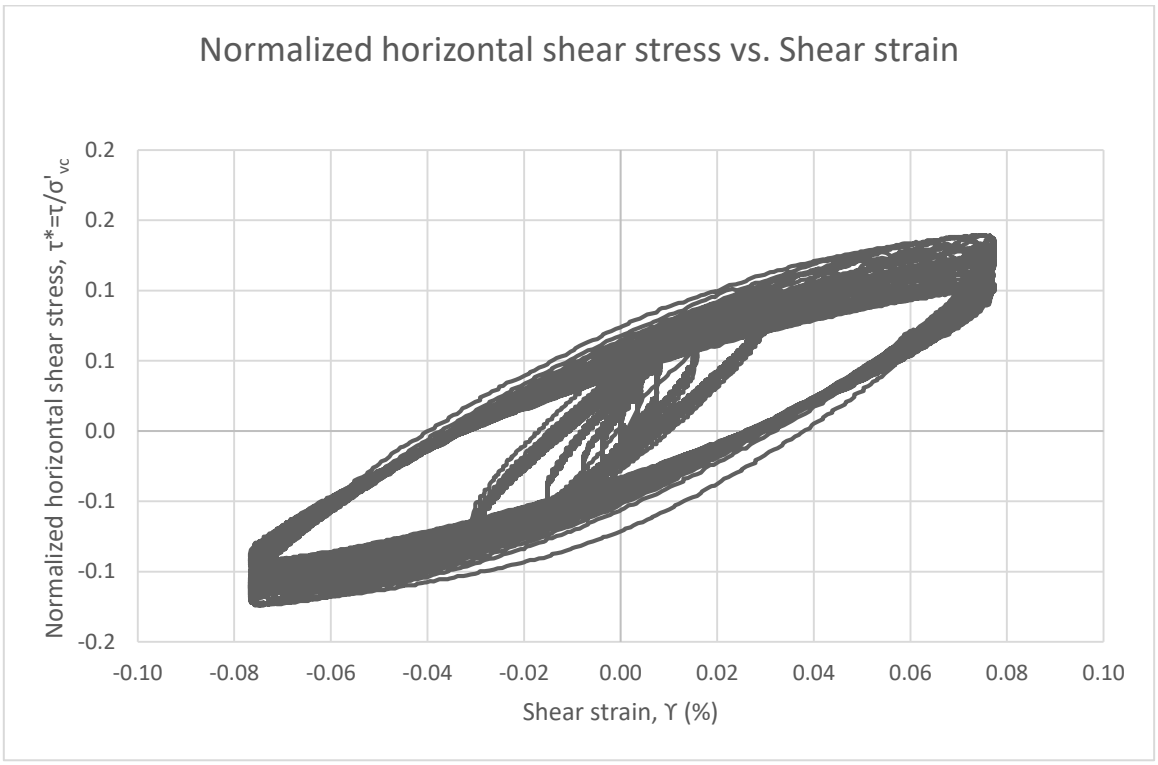

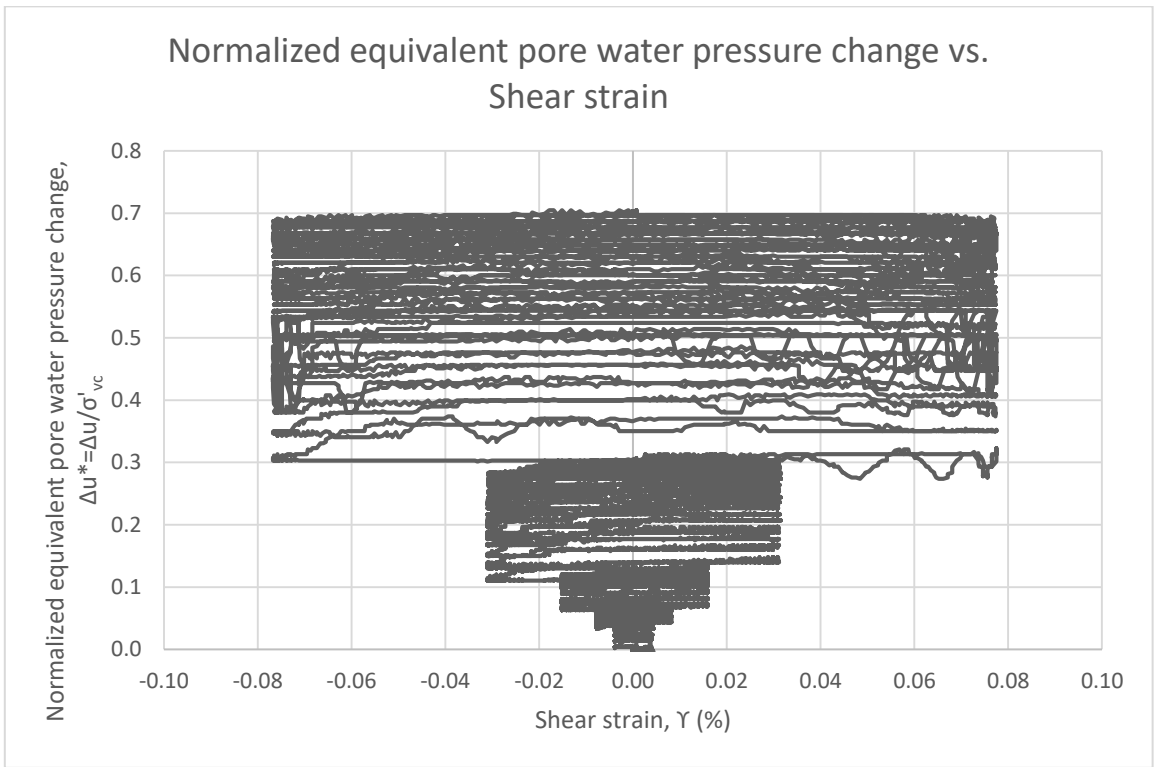

Test: 9; Soil: Toyoura Sand; e=0.71; w=0%
σ'_{vc}=146 (kPa); OCR=1; f=0.01 Hz

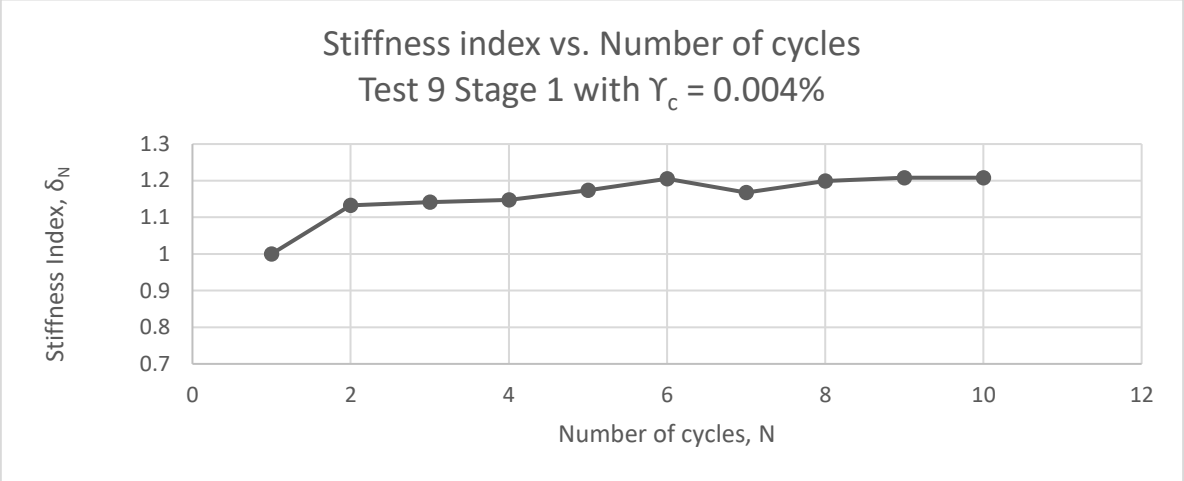

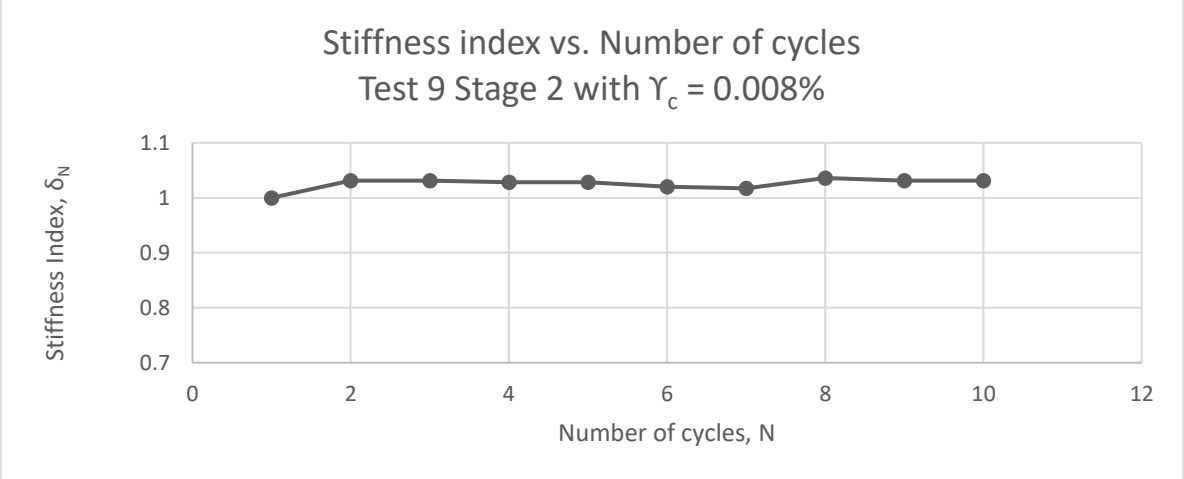

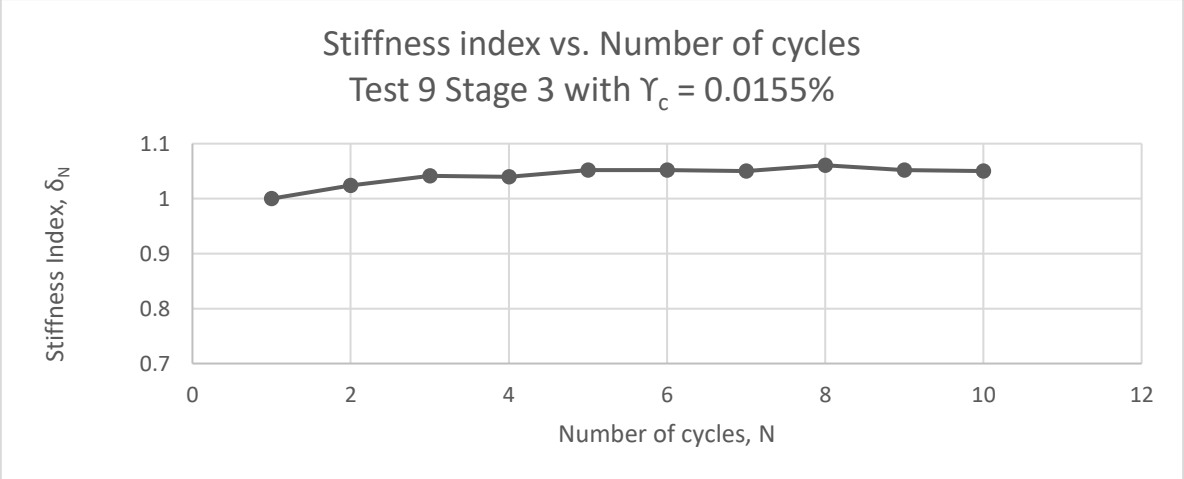

Test: 9; Soil: Toyoura Sand; e=0.71; w=0%
σ'_{vc}=146 (kPa); OCR=1; f=0.01 Hz

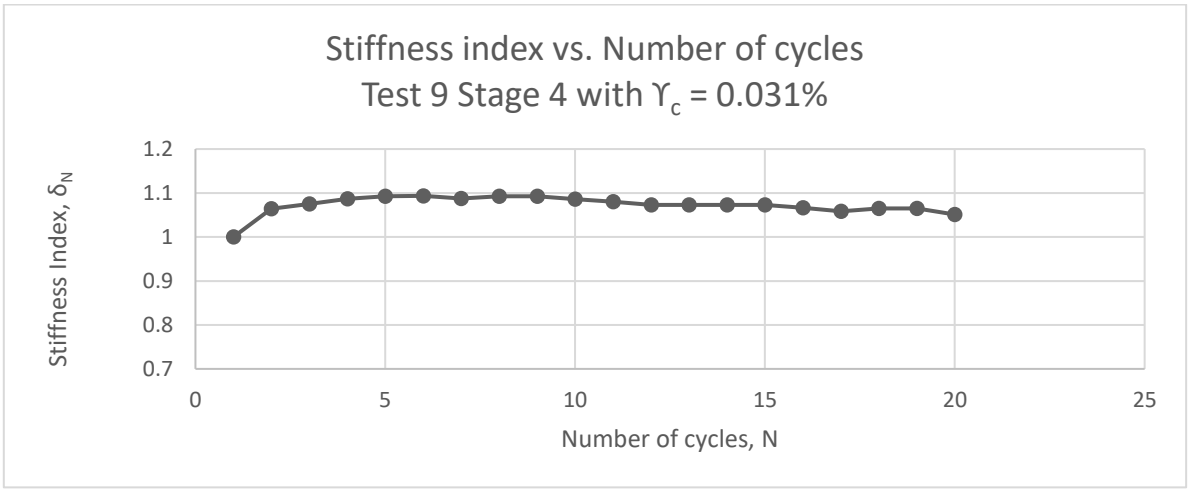

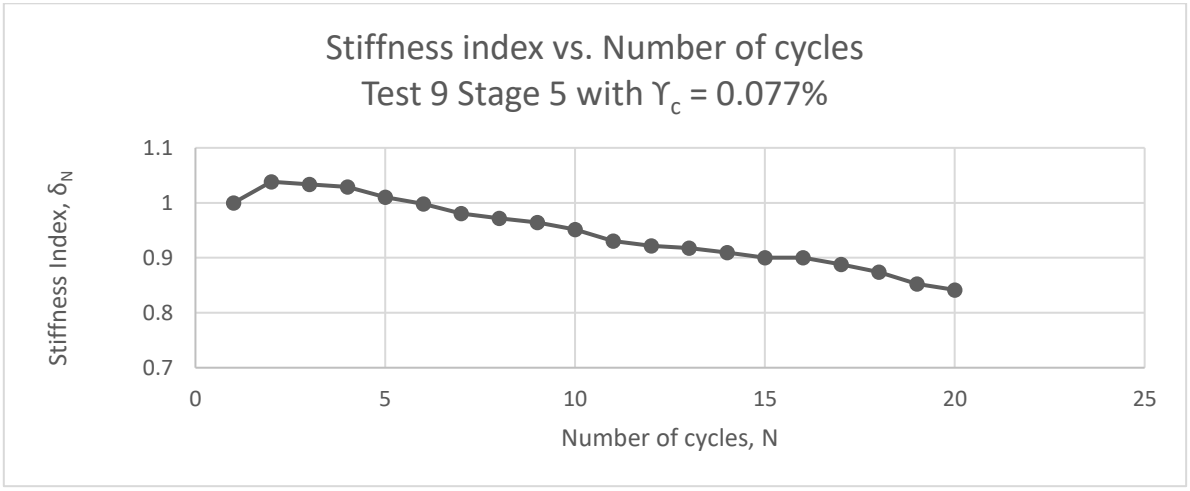

TEST 10

Test: 10; Soil: Red Coarse Sand; e=0.63; w=0%
σ'_{vc}=152 (kPa); OCR=1; f=0.01 Hz

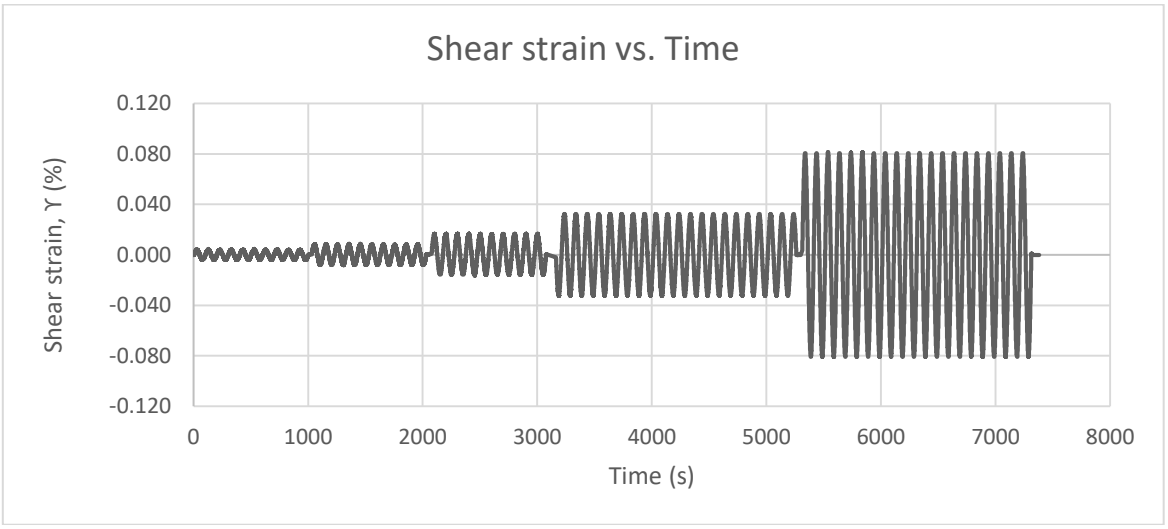

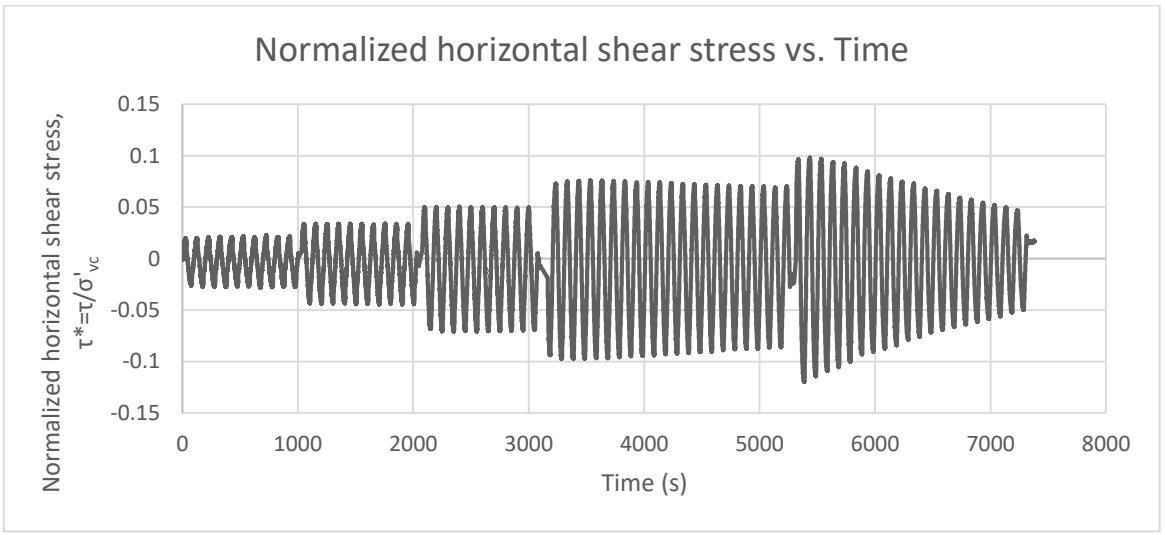

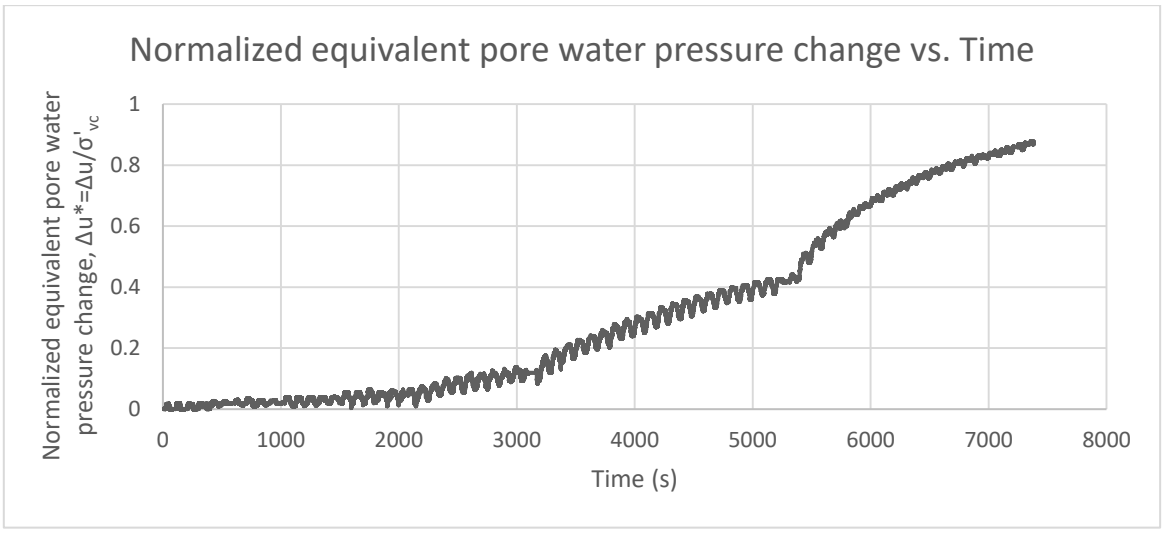

Test: 10; Soil: Red Coarse Sand; e=0.63; w=0%
σ'_{vc}=152 (kPa); OCR=1; f=0.01 Hz

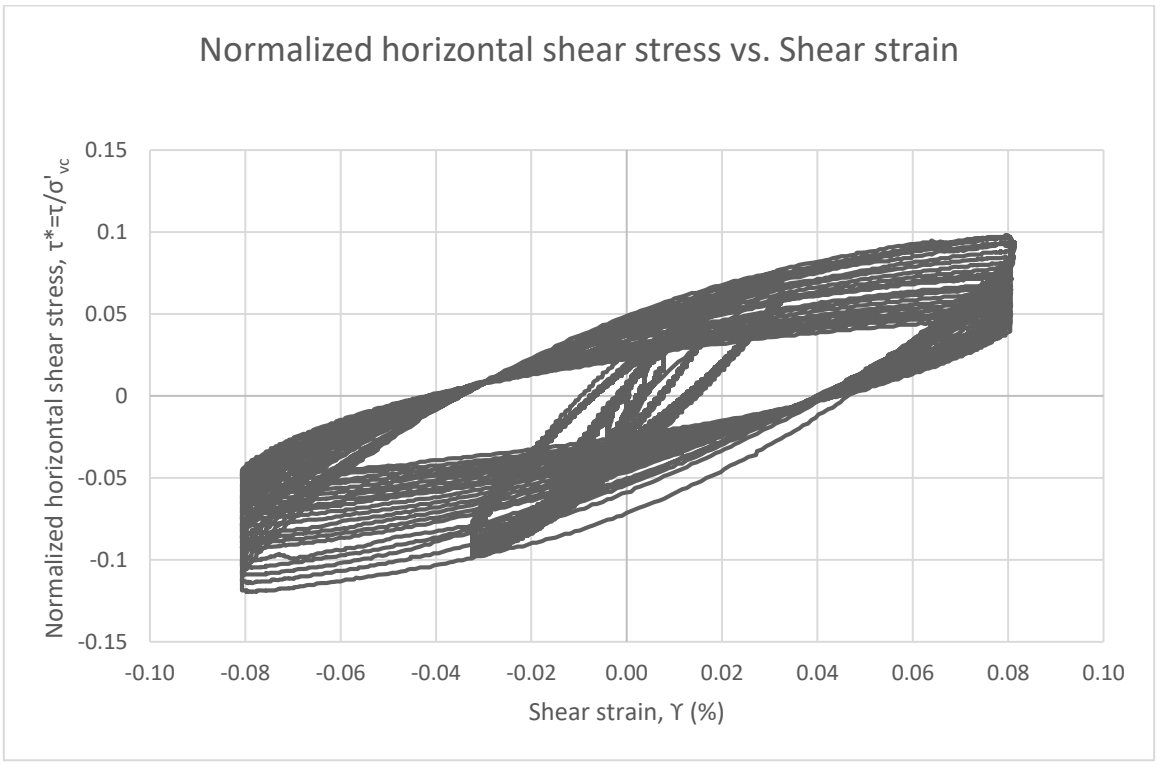

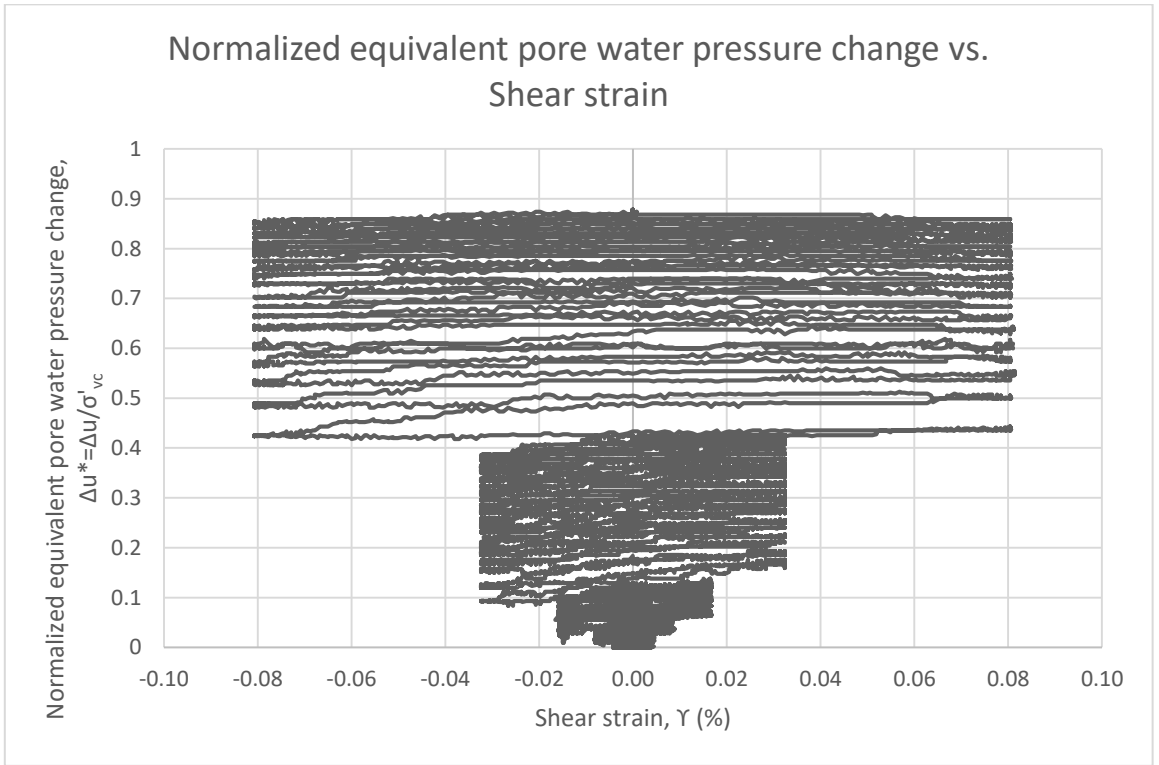

Test: 10; Soil: Red Coarse Sand; e=0.63; w=0%
σ'_{vc}=152 (kPa); OCR=1; f=0.01 Hz

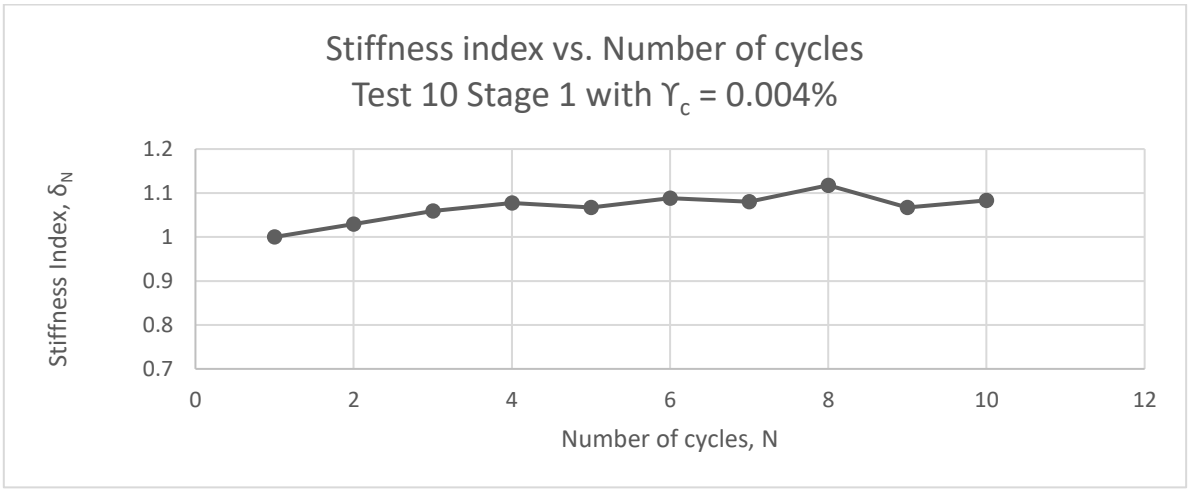

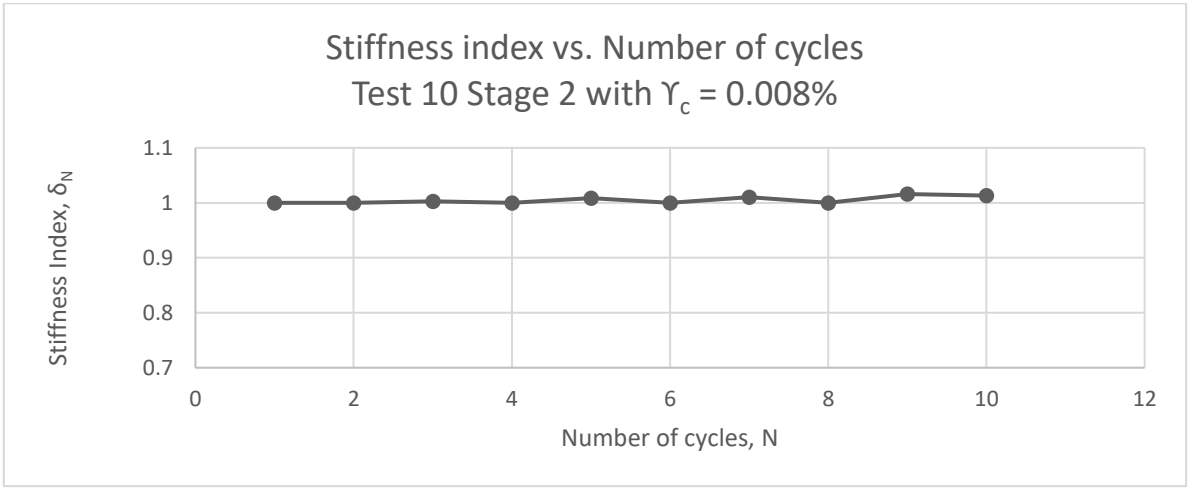

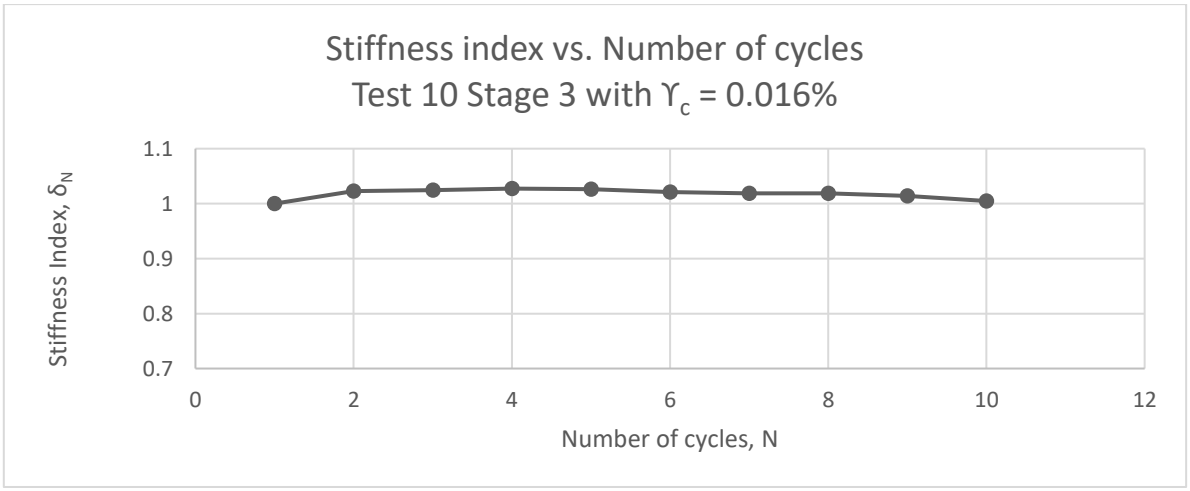

Test: 10; Soil: Red Coarse Sand; e=0.63; w=0%
σ'_{vc}=152 (kPa); OCR=1; f=0.01 Hz

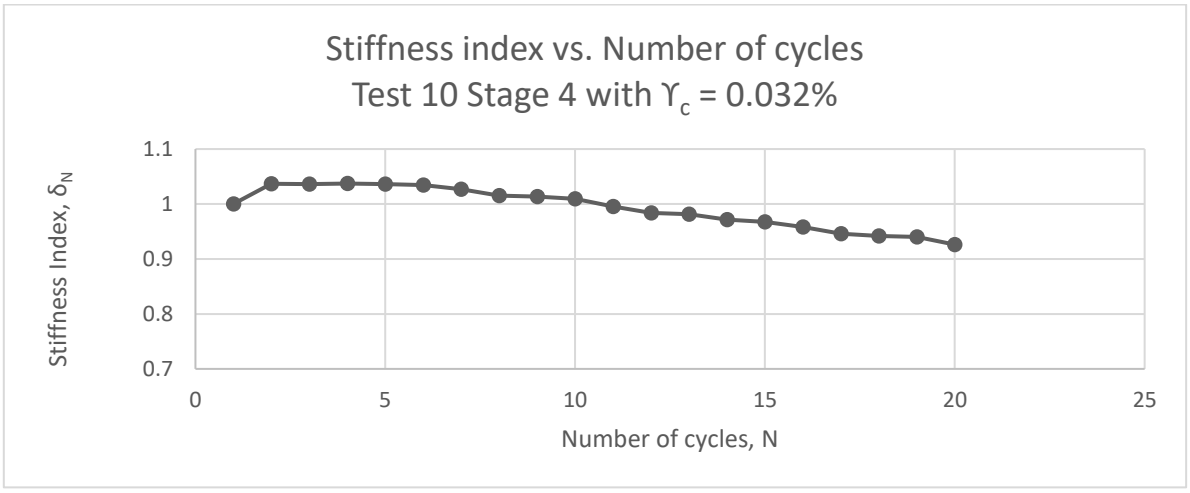

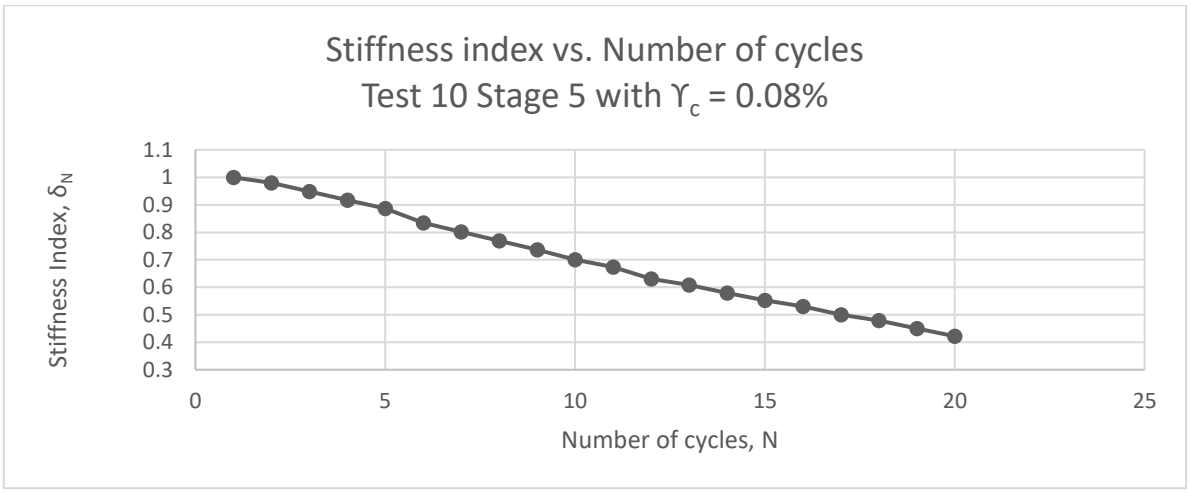

TEST 11

Test: 11; Soil: Nevada Sand; e=0.6; w=0%
σ'_{vc}=156.5 (kPa); OCR=1; $\tau_c=0.08\sigma'_{vc}$, f=0.01 Hz

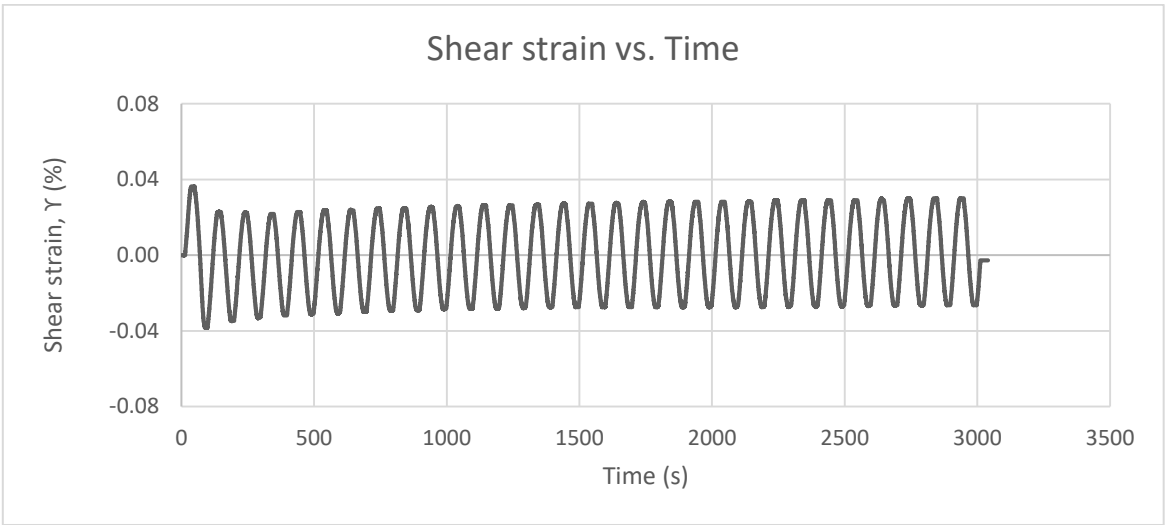

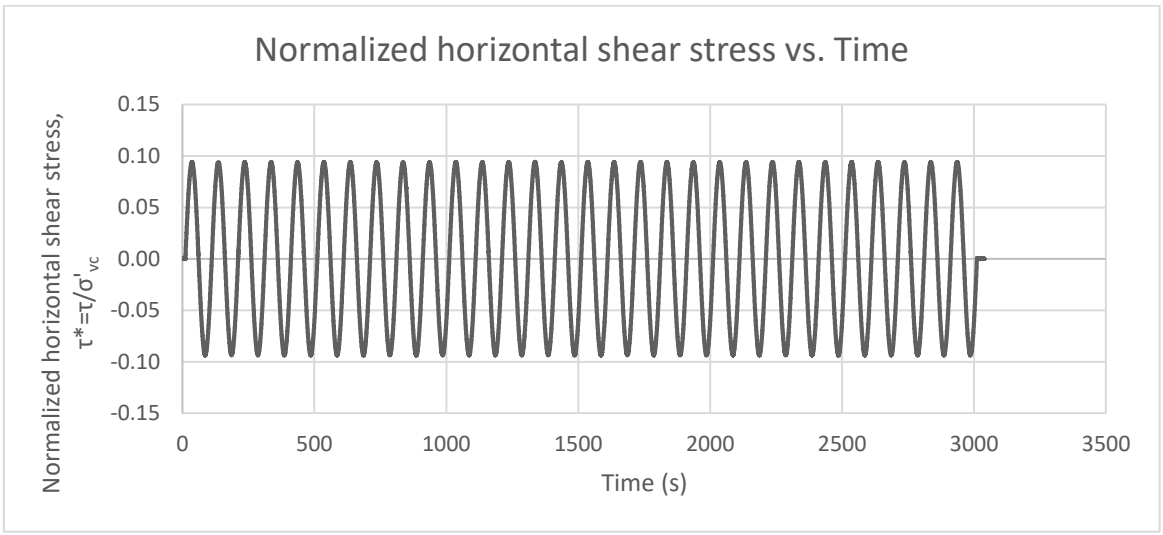

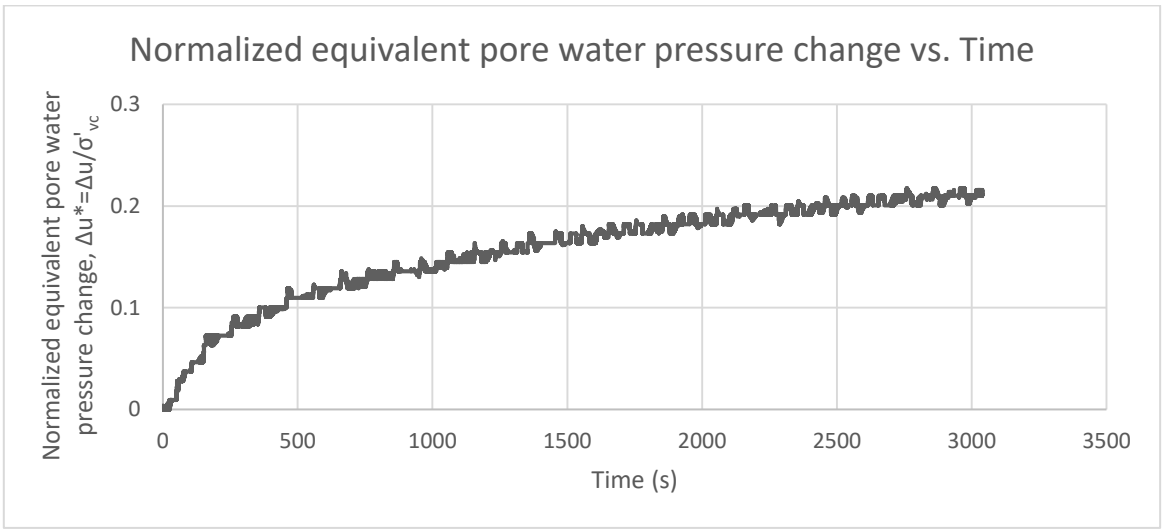

Test: 11; Soil: Nevada Sand; e=0.6; w=0%
σ'_{vc}=156.5 (kPa); OCR=1; $\tau_c=0.08\sigma'_{vc}$, f=0.01 Hz

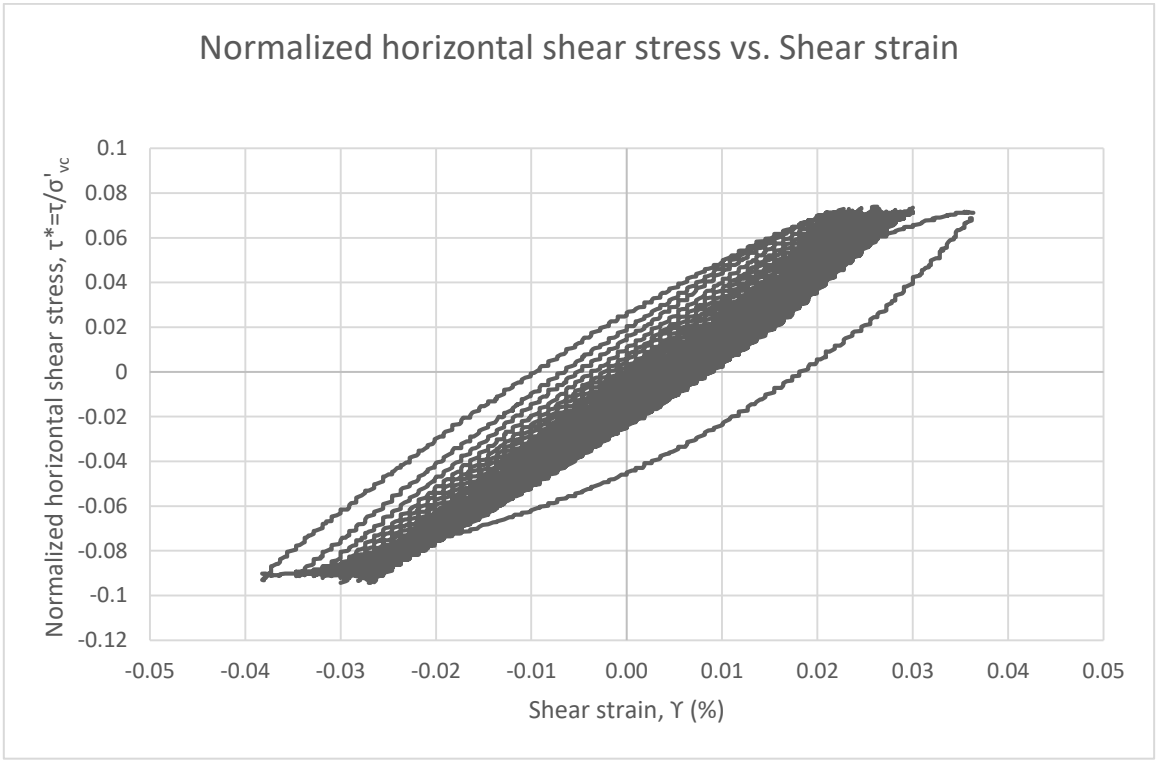

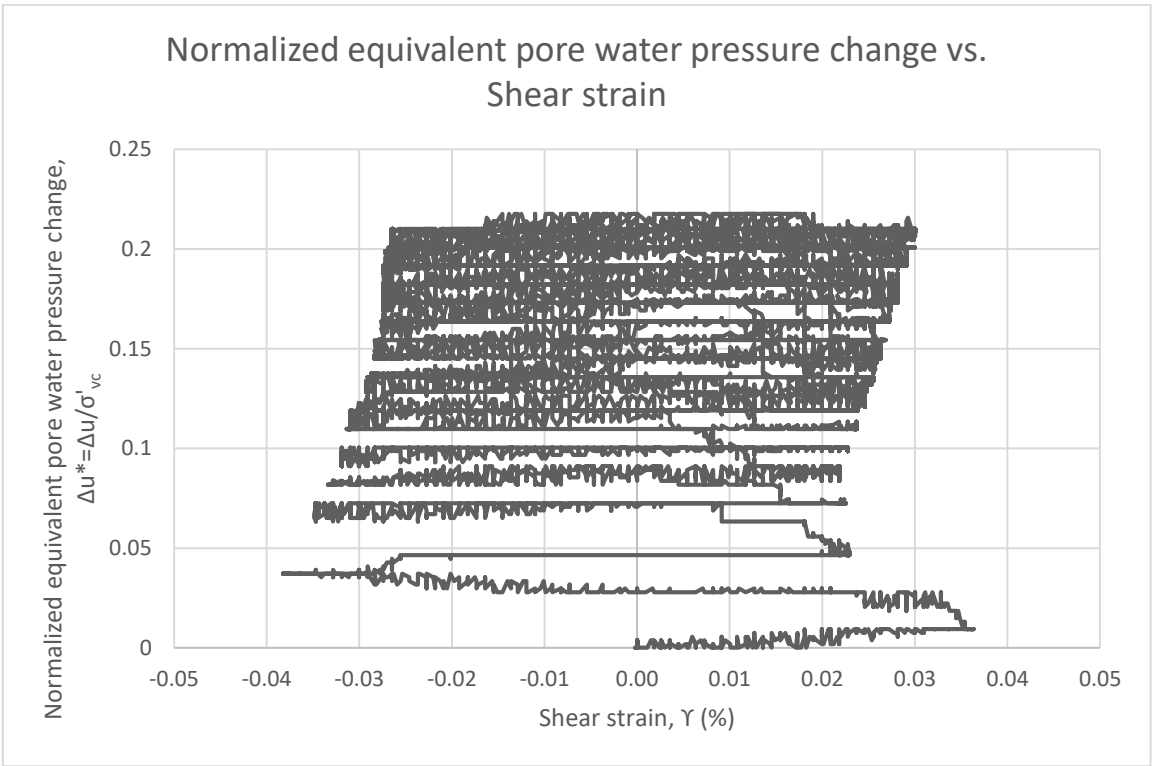

Test: 11; Soil: Nevada Sand; e=0.6; w=0%
σ'_{vc}=156.5 (kPa); OCR=1; $\tau_c=0.08\sigma'_{vc}$, f=0.01 Hz

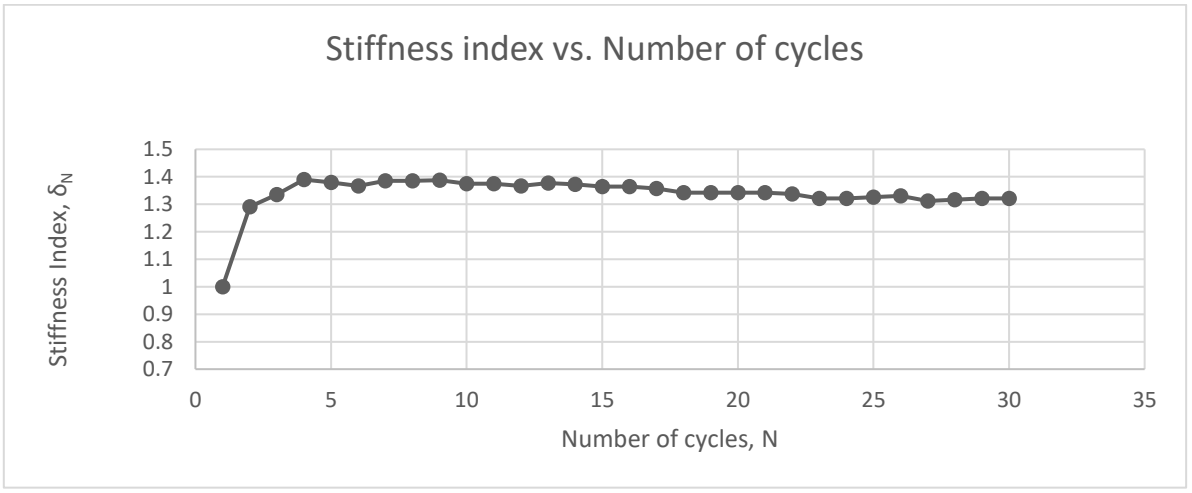

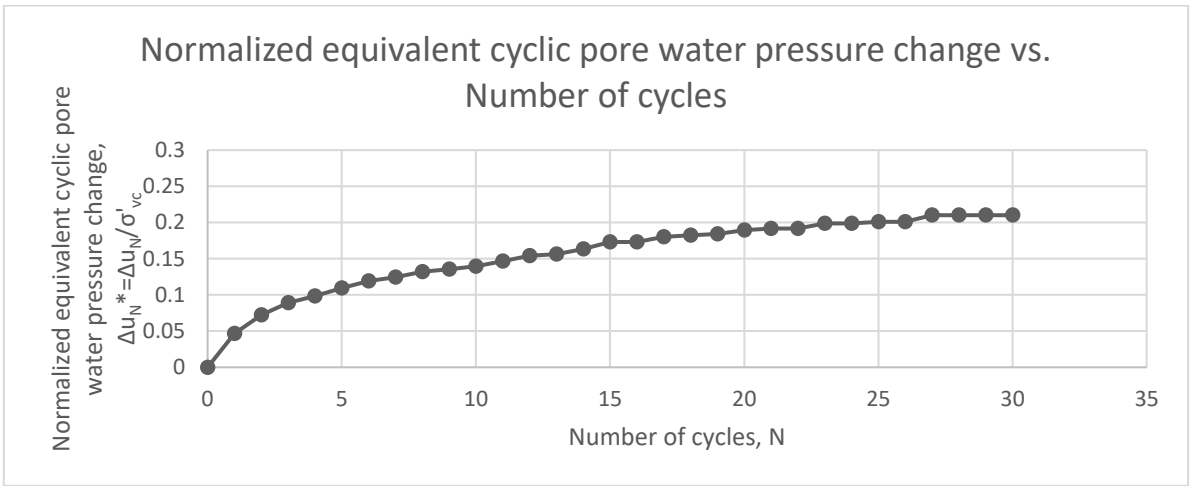

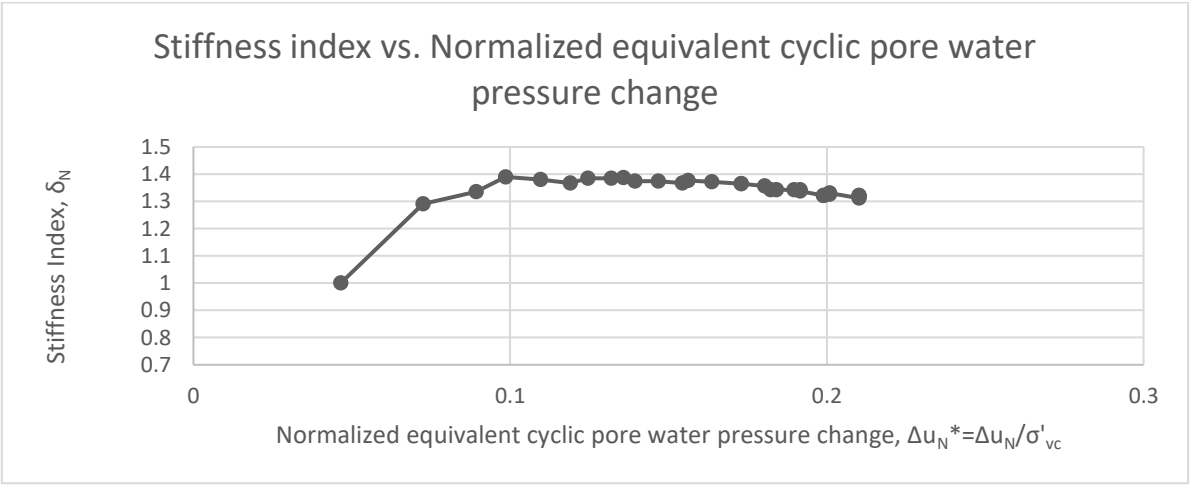

TEST 12

Test: 12; Soil: Nevada Sand; e=0.63; w=0%
σ'_{vc}=162 (kPa); OCR=1; $\tau_c=0.1\sigma'_{vc}$, f=0.01 Hz

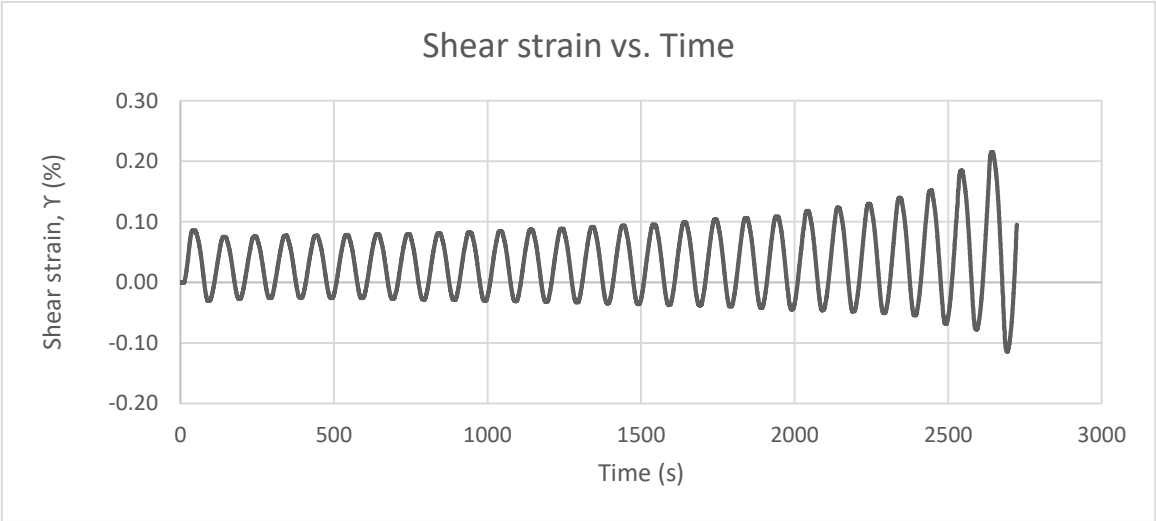

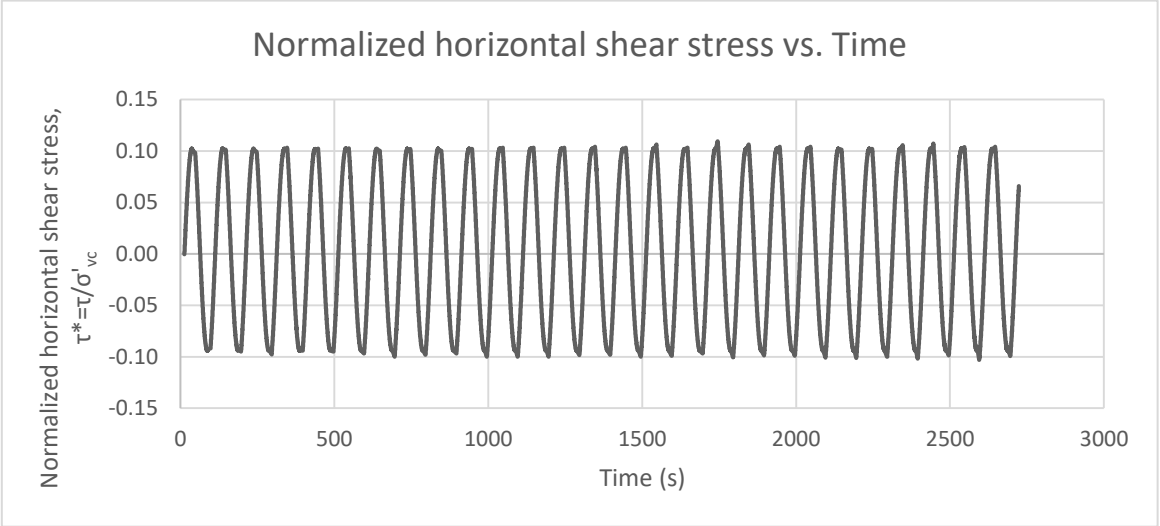

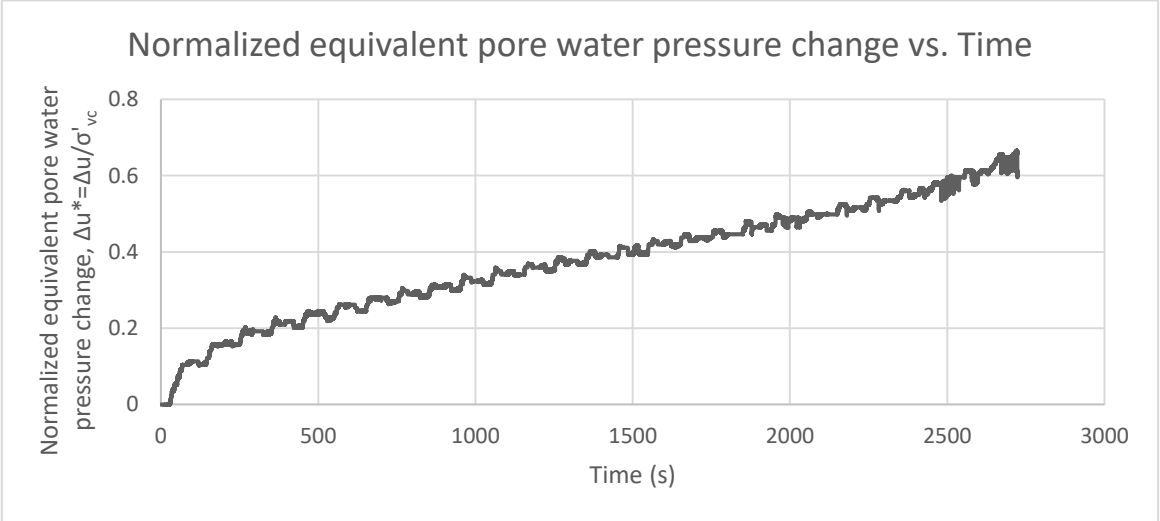

Test: 12; Soil: Nevada Sand; e=0.63; w=0%
σ'_{vc}=162 (kPa); OCR=1; $\tau_c=0.1\sigma'_{vc}$, f=0.01 Hz

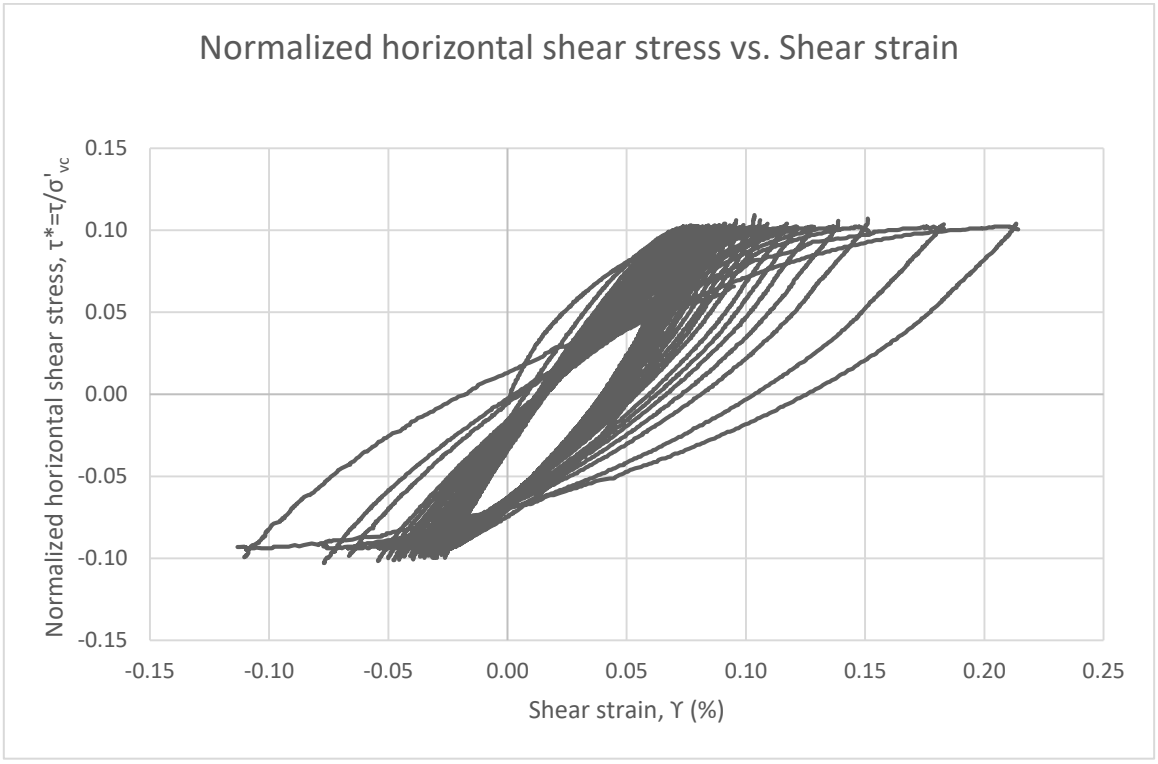

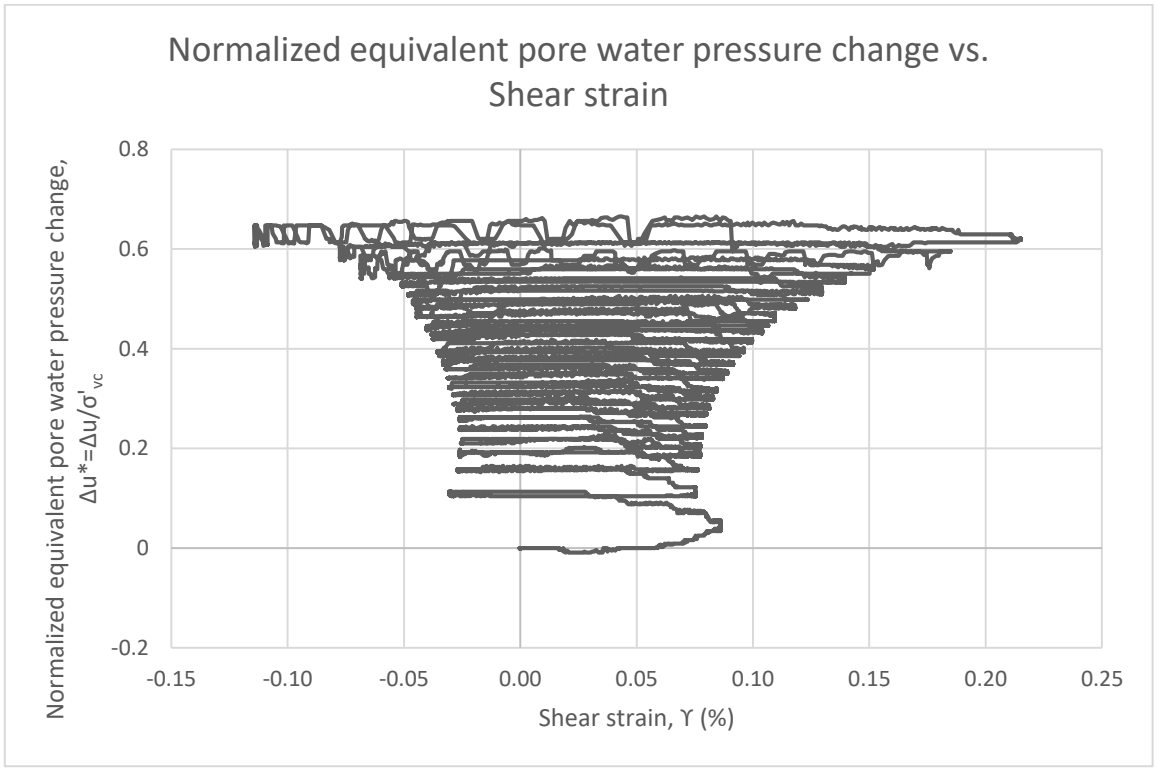

Test: 12; Soil: Nevada Sand; e=0.63; w=0%
σ'_{vc}=162 (kPa); OCR=1; $\tau_c=0.1\sigma'_{vc}$, f=0.01 Hz

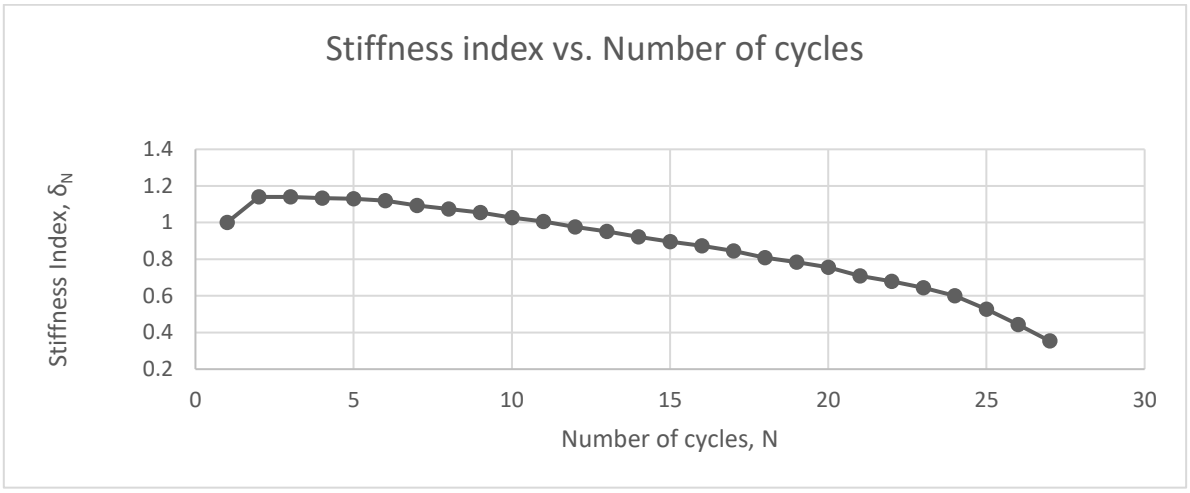

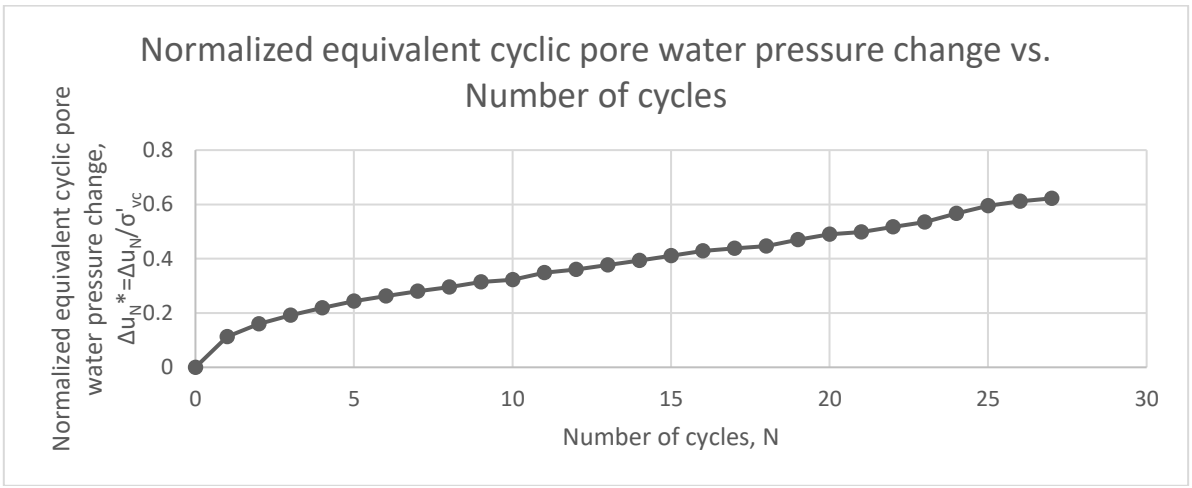

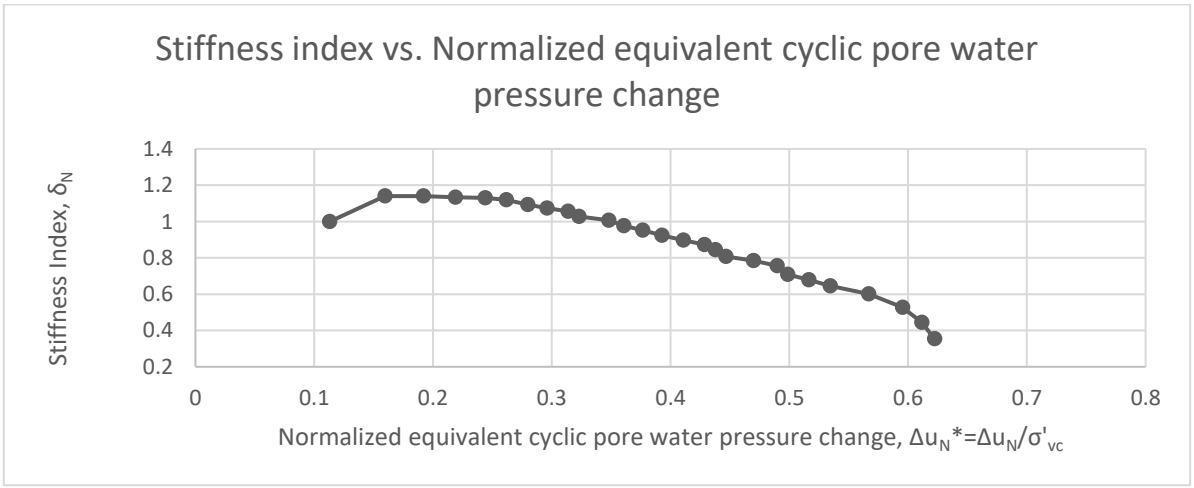

8. Analysis and comparison of the test results on cyclic pore water pressure buildup and stiffness change

In this chapter the test results are analyzed to examine whether and to what extent they agree with the findings by Mortezaie (2012) and Vucetic and Mortezaie (2015) for various testing conditions. That is, if they agree with the trends shown in Figures 1.4 through 1.6.

The cyclic shear strain amplitudes, Υ_c, in the tests analyzed here range from 0.0032% to 0.16%. However, in all but two tests/stages γ_c was 0.08% or less. The two exceptions are the last stage 7 of Test 7 with Υ_c=0.163% and the end of the cyclic stress-controlled Test 12 when Υ_c reached around 0.16%. In some stages Υ_c was below the threshold shear strain for cyclic pore water pressure buildup $\Upsilon_{tp}\approx$0.01, but in most of them it was above. Accordingly, to analyze systematically how the stiffness index δ_N of sand changes with the number of cycles, N, and how it is related to the increase of the cyclic pore water pressure Δu_N, the test results are divided in the following groups with respect to amplitude Υ_c:

- Tests with Υ_c<0.01%, i.e., the tests with Υ_c below the cyclic threshold shear strain $\Upsilon_{tp}\approx$0.01% below which the cyclic pore water pressure practically does not build up.
- Tests with Υ_c=0.01%, i.e., at the cyclic threshold shear strain $\Upsilon_{tp}\approx$0.01% when extremely small cyclic pore water pressure may or may not build up.
- Tests with Υ_c=0.016% when very small cyclic pore water pressure builds up.
- Tests with Υ_c=0.02% when small cyclic pore water pressure builds up.
- Tests with Υ_c=0.03% when small cyclic pore water pressure builds up
- Tests with Υ_c=0.04% when small to moderate cyclic pore water pressure builds up.
- Tests with Υ_c=0.06% when moderate to significant cyclic pore pressure builds up.
- Tests with Υ_c=0.08% when significant cyclic pore water pressure builds up.
- Cyclic stress-controlled tests

Tests with Υ_c<0.01%

Figure 8.1(a) shows the stiffness index, δ_N, with the number of cycles, N, the normalized cyclic pore water pressure buildup, Δu_N*, with N that is negligibly small, and the relationship between δ_N and Δu_N* for the cyclic stages (cyclic tests) when the specimens were consolidated prior to cyclic shearing with Υ_c smaller than 0.01%. For the stages when there was no reconsolidation δ_N versus N is shown in Figure 8.1(b). The legends in the plots indicate the test and stage number, whether specimen was dry or saturated, and the vertical effective consolidation stress, σ'_{v0}.

In Figure 8.1(a) it can be seen that the stiffness index goes down with N only in one of the five cases, i.e., in test 7.1. In three tests it goes up (Test 4.6, Test 9.1 and Test 10.1) and in one it fluctuates around zero (Test 5.6). The cyclic pore water pressures in all 5 tests slightly increased but they are so small that their measurement may not be very accurate. Nevertheless, the results show that the phenomenon of increasing δ_N with N occurs at very small cyclic strains below 0.01% way more often than not, and that it happens when very small cyclic pore water pressures build up. It should be noted that the above trends do not show any correlation with the sequence of loading, i.e., whether the cyclic stage was or was not preceded with stages having larger or smaller, Υ_c. They also do not show any correlation with the effective confining stress.

For the cases when there was no reconsolidation between the stages, shown in Figure 8.1(b), very similar trends can be observed, i.e., that the stiffness index increases in three out of four cases. Furthermore, the above results are obtained on three different sands. Tests 4, 5 and 7 are conducted on Nevada Sand, Test 9 on Toyoura Sand and Test 10 on Red Coarse Sand.

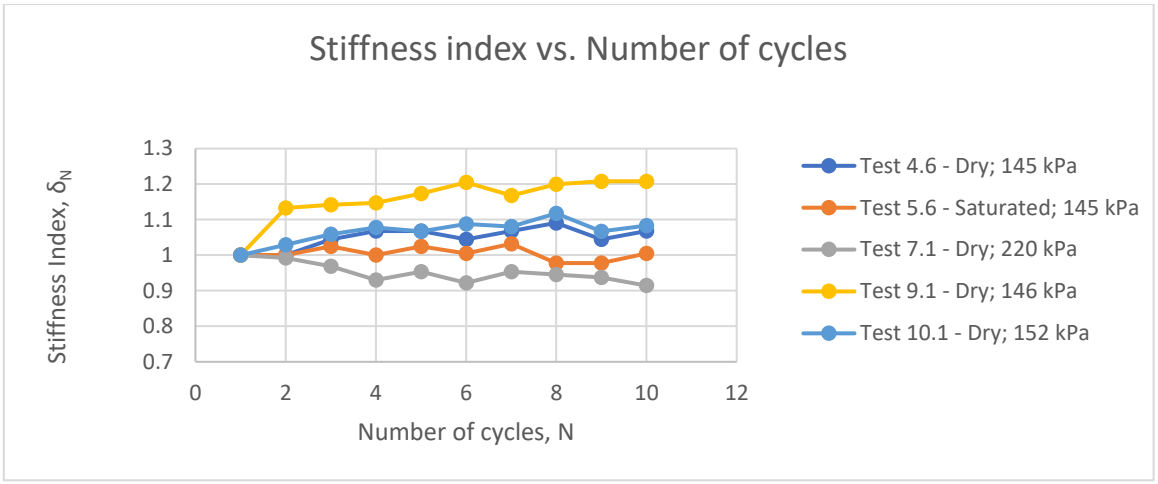

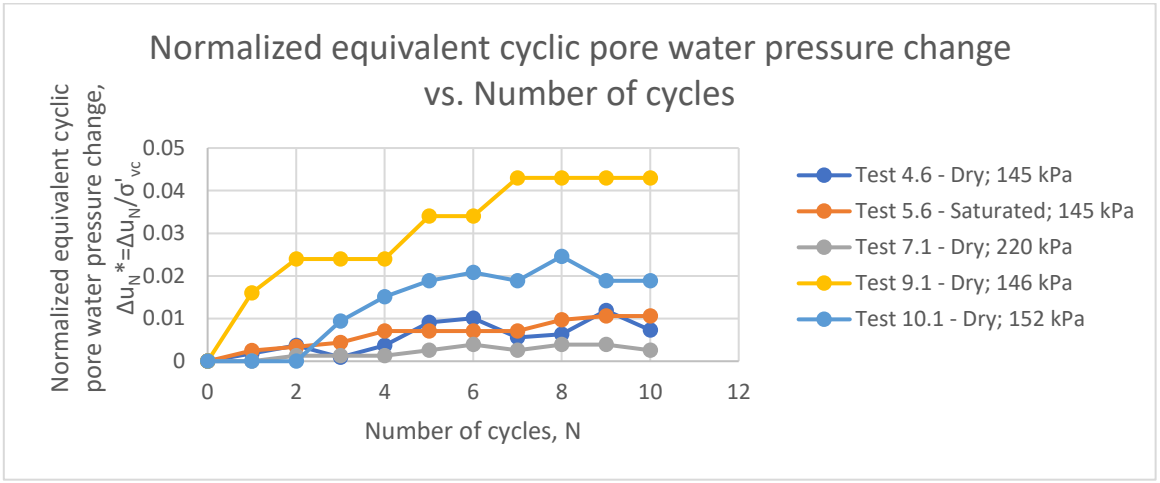

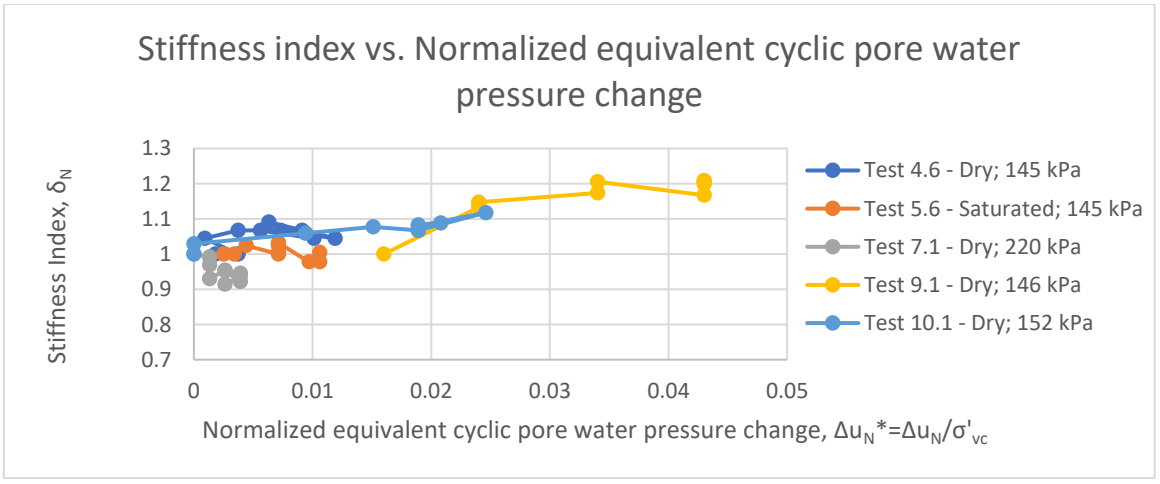

a) Specimen is reconsolidated between the cyclic stages

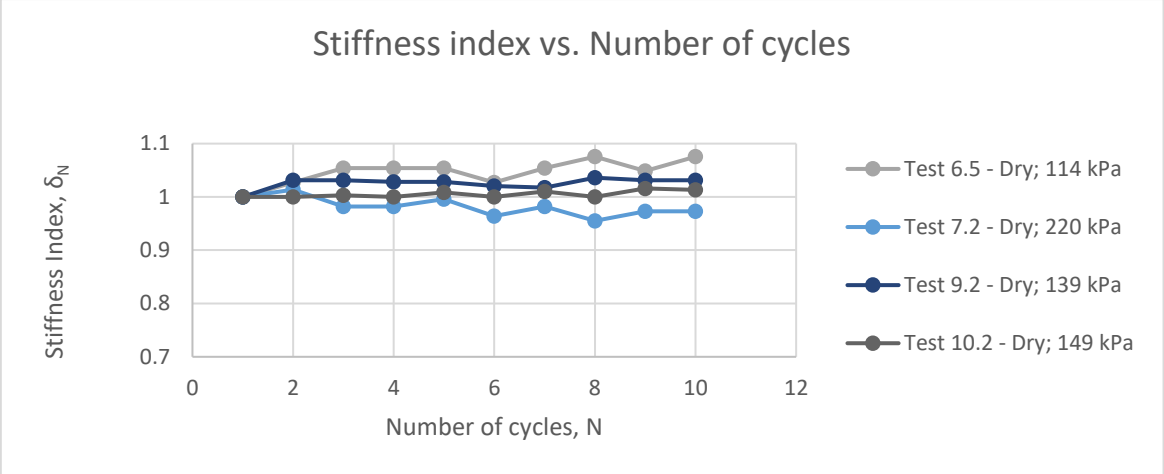

b) Specimen is not reconsolidated between the cyclic stages

Figure 8.1 Behavior of sands at Υ_c<0.01% - specimens in Tests 4, 5 and 7 are Nevada Sand, in Test 9 Toyoura Sand and in Test 10 Red Coarse Sand

Tests with Υ_c=0.01%

Figure 8.2(a) shows the stiffness index, δ_N, with the number of cycles, N, negligible normalized cyclic pore water pressure buildup, Δu_N*, with N, and the relationship between δ_N and Δu_N* for two cyclic tests (cyclic stages) when the specimens were consolidated before the cyclic shearing with Υ_c = 0.01%. The stiffness index, δ_N, with the number of cycles, N, for two cases when there was no reconsolidation between the stages is shown in Figure 8.2(b).

In Figure 8.2(a) it can be observed that in one case δ_N slightly increase with N and in the other it more or less does not change, i.e., stays around δ_N=1, while in both cases Δu_N* slightly increases with N. These trends are also evident in the Δu_N* versus δ_N relationships. It should be noted that these two stages were conducted at the same σ'_{v0} but one was on dry and the other on saturated sand. The results of the two tests are very similar, indicating that the dry specimen can be tested in the constant-volume equivalent-undrained NGI-DSS device to obtain the results corresponding to the saturated specimen. However, so obvious similarities are not

obtained between other stages of Tests 4 and 5 that were identical except that one test was conducted on dry and the other on saturated specimen.

For the cases when there was no reconsolidation between the stages, shown in Figure 8.2(b), in one case δ_N slightly increase with N and in the other it slightly decreases.

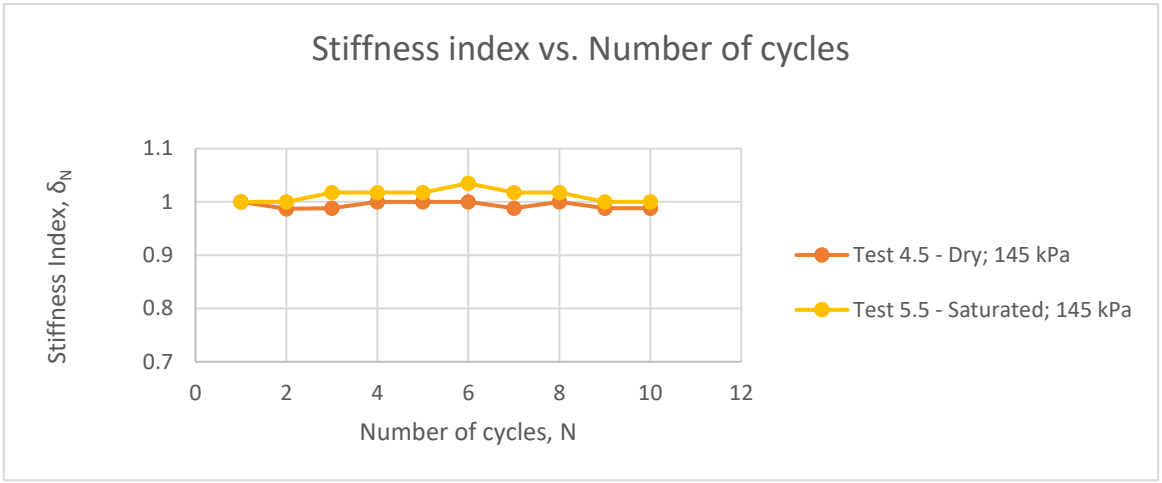

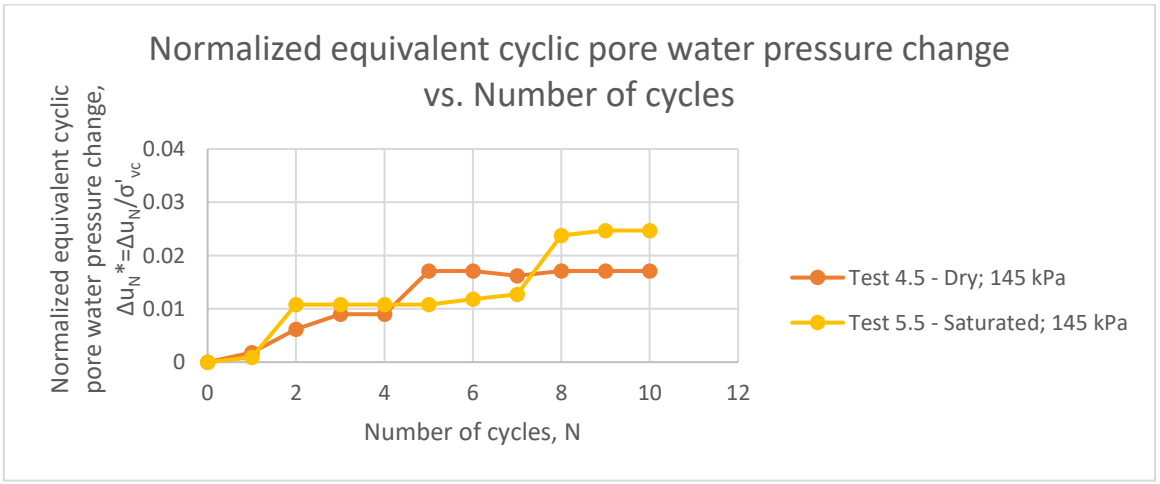

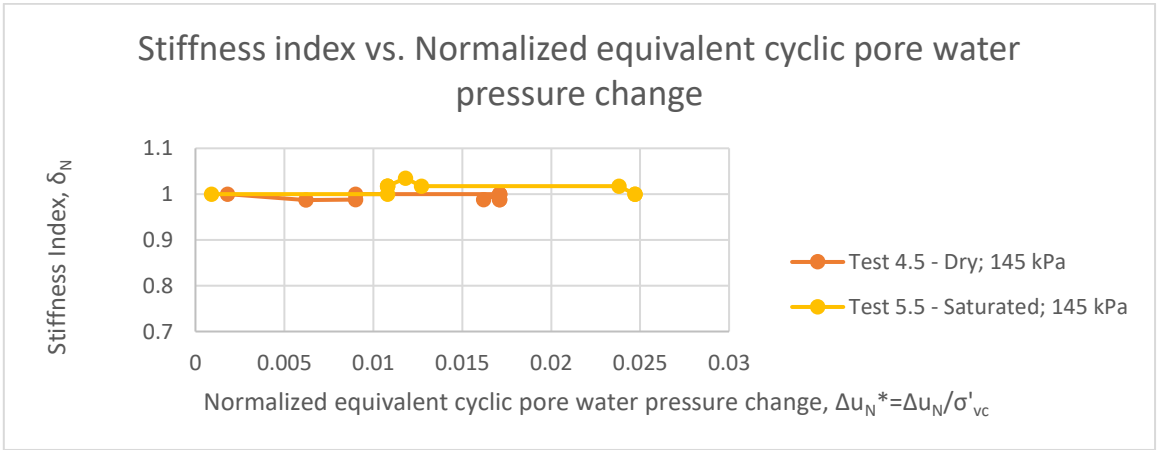

a) Specimen is reconsolidated between the cyclic stages

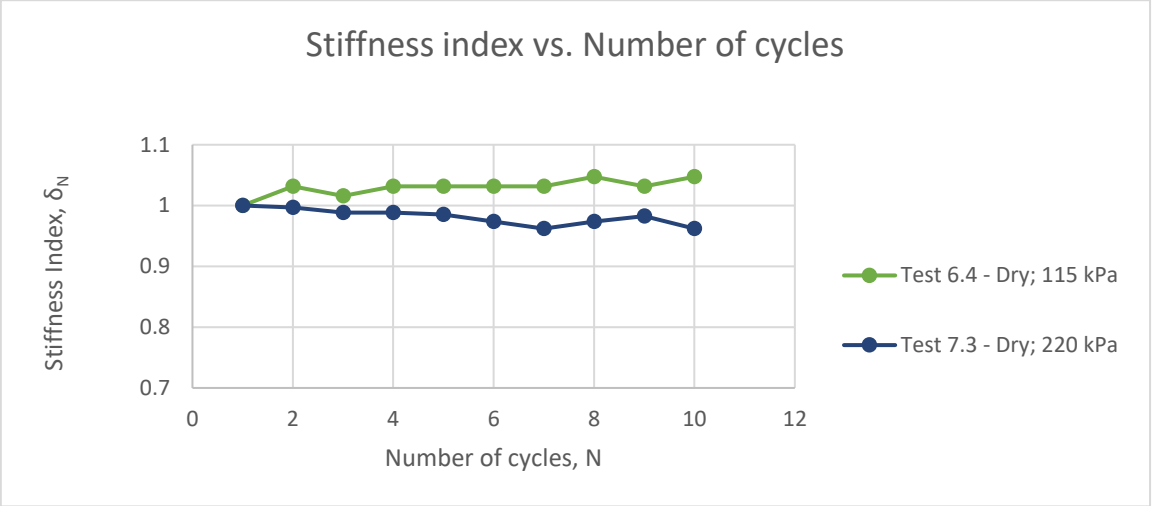

b) Specimen is not reconsolidated between the cyclic stages

Figure 8.2 Behavior of sands at Υ_c=0.01% - specimens in all Tests are Nevada Sand

Tests with Υ_c=0.016%

Figure 8.3 shows the stiffness index, δ_N, with the number of cycles, N, from two stages that have shear strain amplitude, Υ_c = 0.016% and similar σ'_{v0}. One stage was conducted on Toyoura Sand (Test 9.3) and the other on Red Coarse Sand (Test 10.3). Both stages are from the test that had no reconsolidation between the stages. In both stages δ_N first slightly increase with N, and then for Toyoura Sand it seems to level off while for Red Coarse Sand it decreases.

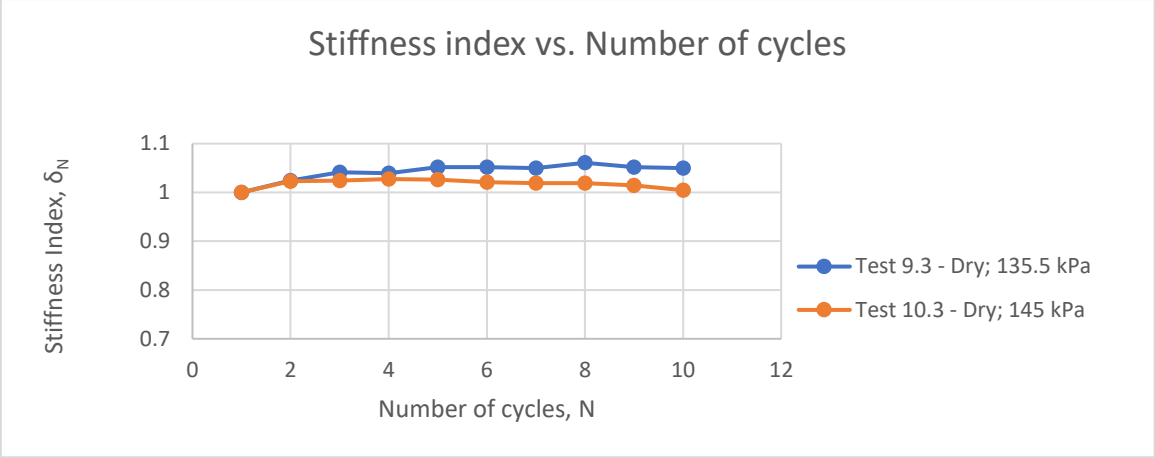

Figure 8.3 Behavior of sands at Υ_c=0.016% - specimen in Test 9 is Toyoura Sand and in Test 10 Red Coarse Sand - specimens are not reconsolidated between the cyclic stages

Tests with Υ_c=0.02%

Figure 8.4 shows the results from five tests (five stages) conducted at shear strain amplitude, Υ_c = 0.02%. All of them are conducted on Nevada Sand. The results for two cyclic stages that had reconsolidation between the stages are presented in Figure 8.4(a), while the results for three stages without reconsolidation are presented in Figure 8.4(b).

In Figure 8.4 (a) it can be observed that in both stages, δ_N initially slightly increase with N. In one case it then more or less levels off, while in the other it decreases. These trends are also evident in the Δu_N* versus δ_N relationships. It should be noted that these two stages were conducted at the same σ'_{v0} but one was on dry and the other on saturated sand. While the relationships δ_N versus N are quite similar, Δu_N* versus N relationships are not. In saturated specimen Δu_N* increases faster with N. However, such small measurement of equivalent cyclic pore water pressure may not be very accurate.

For the cases when there was no reconsolidation between the stages, shown in Figure 8.4(b), in all three cases δ_N slightly increase with N and then slightly decreases.

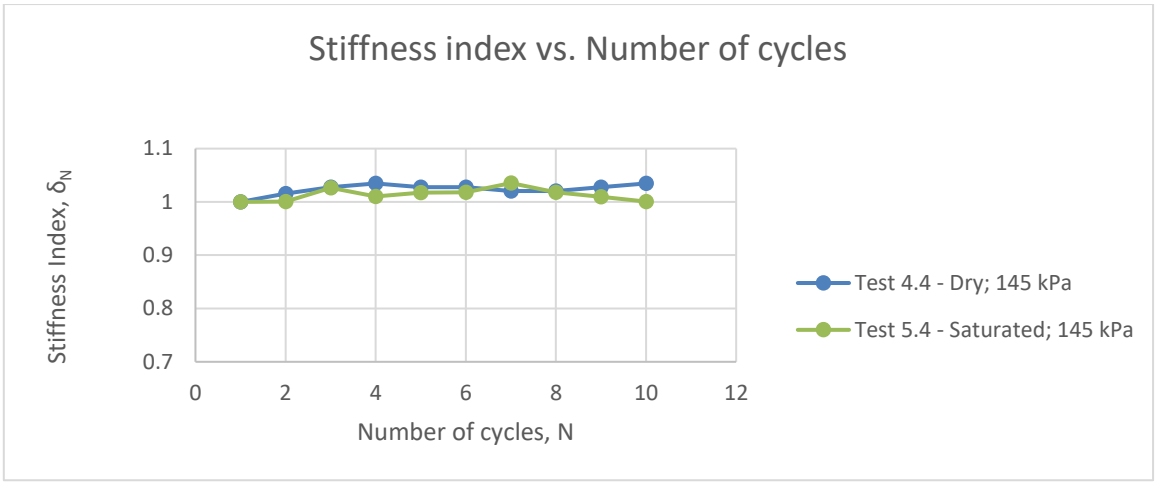

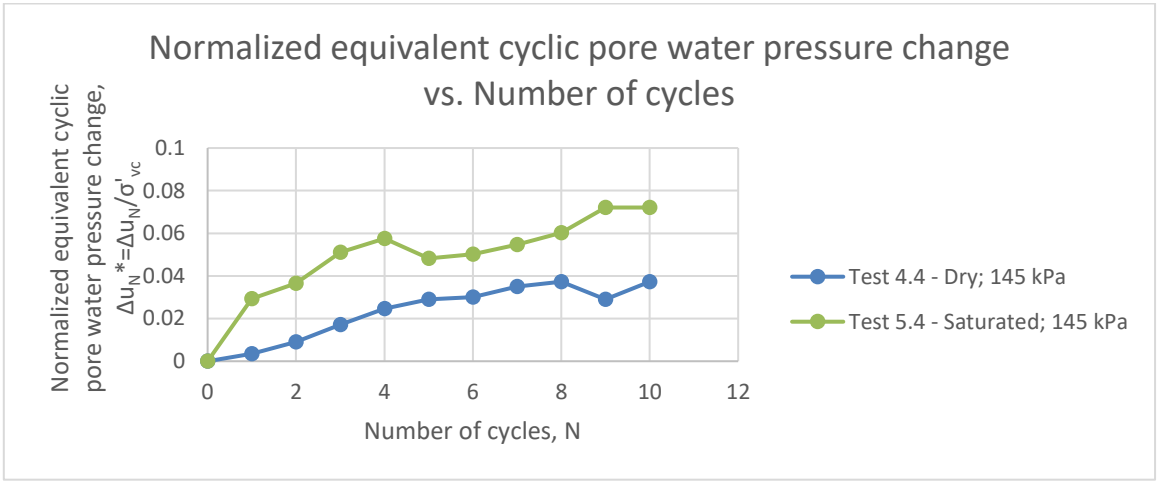

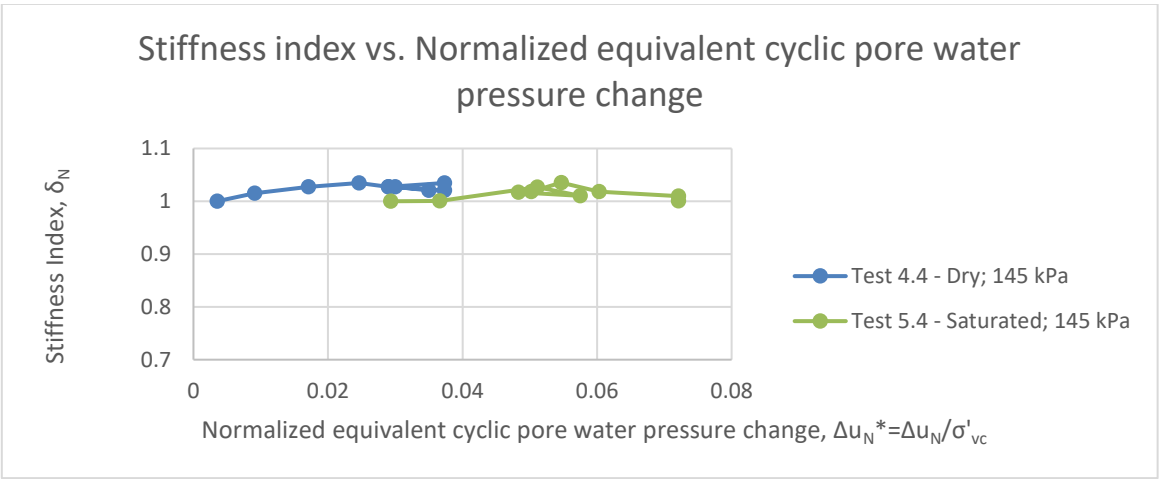

a) Specimen is reconsolidated between the cyclic stages

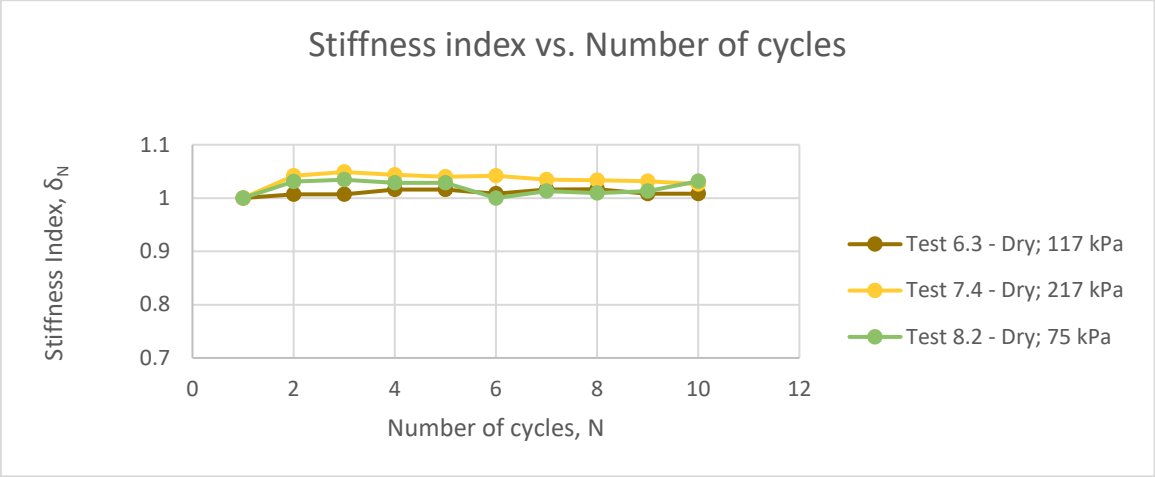

b) Specimen is not reconsolidated between the cyclic stages

Figure 8.4 Behavior of sands at Υ_c=0.02% - specimens in all Tests are Nevada Sand

Tests with Υ_c=0.03%

Figure 8.5 shows the stiffness index, δ_N, with the number of cycles, N, from three stages that have shear strain amplitude, Υ_c = 0.03%, different σ'_{v0}, and are conducted on three different soils. One stage was conducted on Nevada Sand (Test 8.3), the other on Toyoura Sand (Test 9.4) and the third on Red Coarse Sand (Test 10.4). All three stages are from the tests that had no reconsolidation between the stages. In all three cases δ_N first increased with N and then decreased. However, in Toyoura sand the increase was substantial, by 10%, while in the other two cases it was small, and in the case of Nevada Sand δ_N dropped slightly below 1.

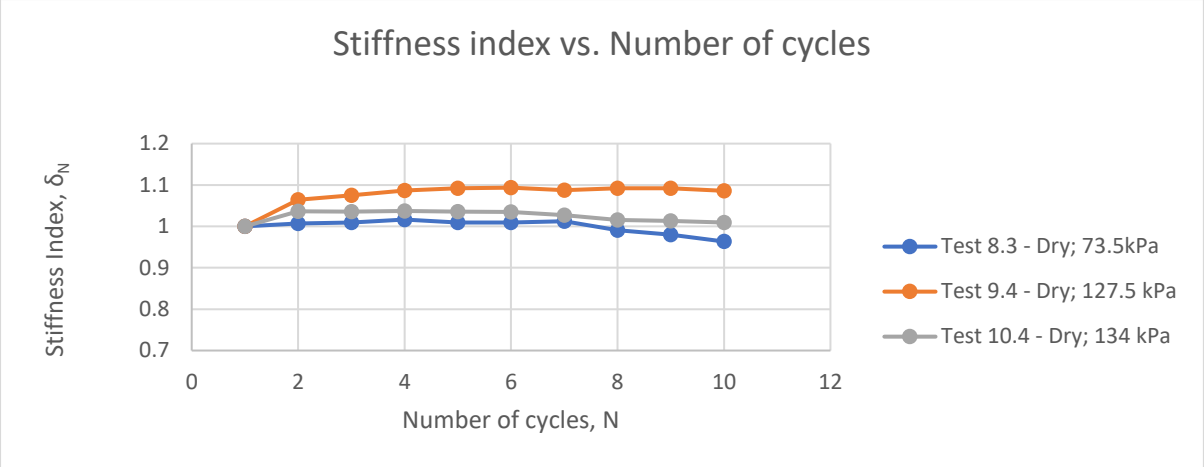

a) Specimen is not reconsolidated between the cyclic stages

Figure 8.5 Behavior of sands at Υ_c=0.03% - specimen in Tests 8 is Nevada Sand, in Test 9 Toyoura Sand and in Test 10 Red Coarse Sand

Tests with Υ_c=0.04% with many cycles

Figure 8.6 shows the stiffness index, δ_N, with the number of cycles, N, from two stages from Test 2 on Nevada sand with amplitude Υ_c = 0.04% that were conducted in sequence at different σ'_{v0} for many cycles. Between the stages the specimen was reconsolidated. The δ_N variation with N from both stages is quite similar, but due to the different σ'_{v0} the variation of Δu_N* with N is not. If the confining stress is larger it can be expected that the increase of Δu_N* with N in cyclic strain-controlled tests is slower (see Dobry at al, 1982). This is the trend in Figure 8.6. Consequently, due to the different rates of Δu_N* increase, the δ_N versus Δu_N* relationships are similar in shape but shifted along the Δu_N* axis.

These two test results confirm the behavior of saturated sands described earlier by Mortezaie Vucetic. They confirm that for Υ_c between the threshold cyclic strain Υ_{tp}≈0.01% and 0.10 to 0.15%, Δu_N continuously increases with N while modulus G_{SN} first increases for up to approximately 10% of G_{S1} and then gradually decreases, and that in this range of Υ_c the pore

water pressure Δu_N can reach up to 40% of the initial effective confining stress before G_{SN} drops below G_{S1}.

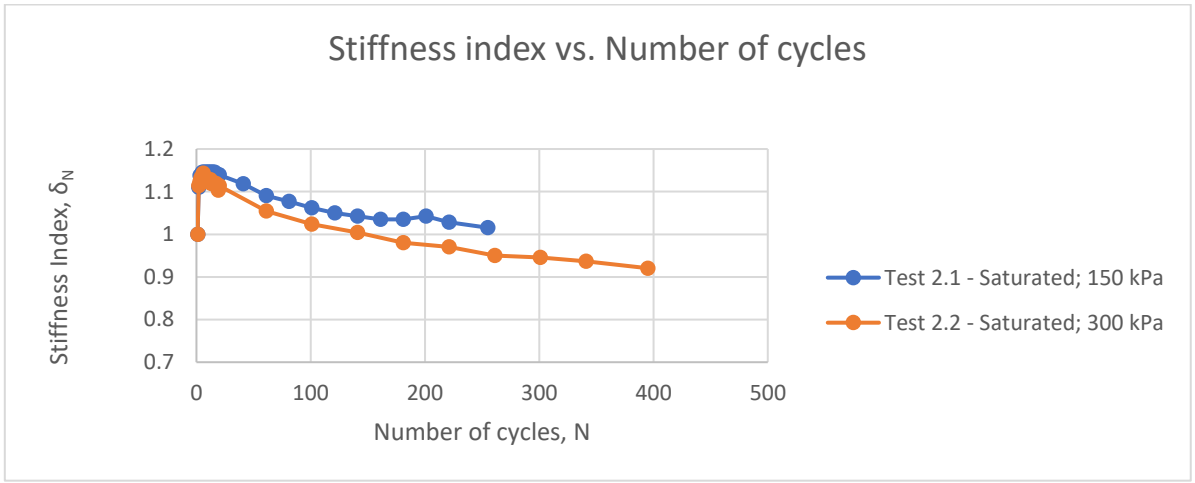

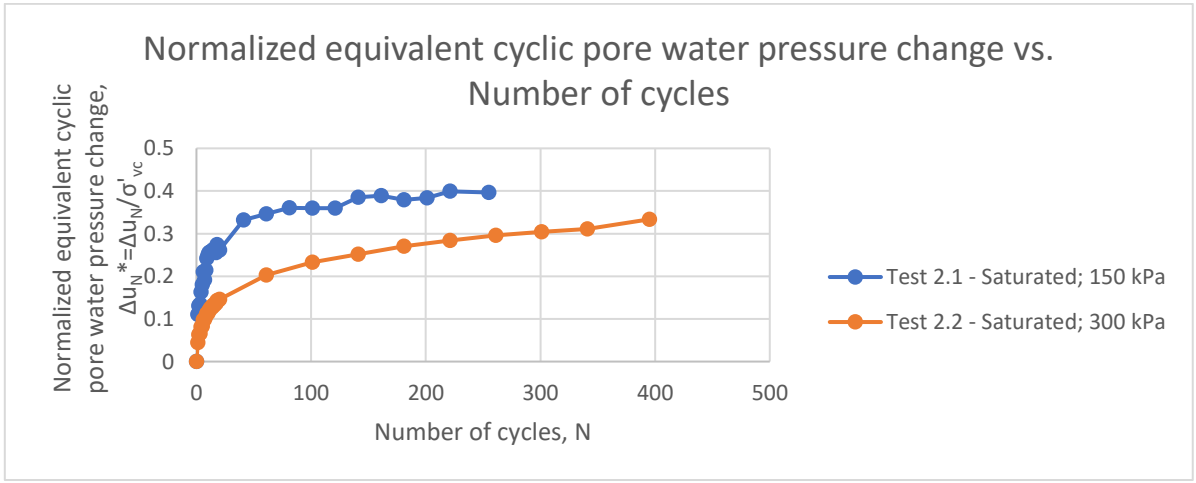

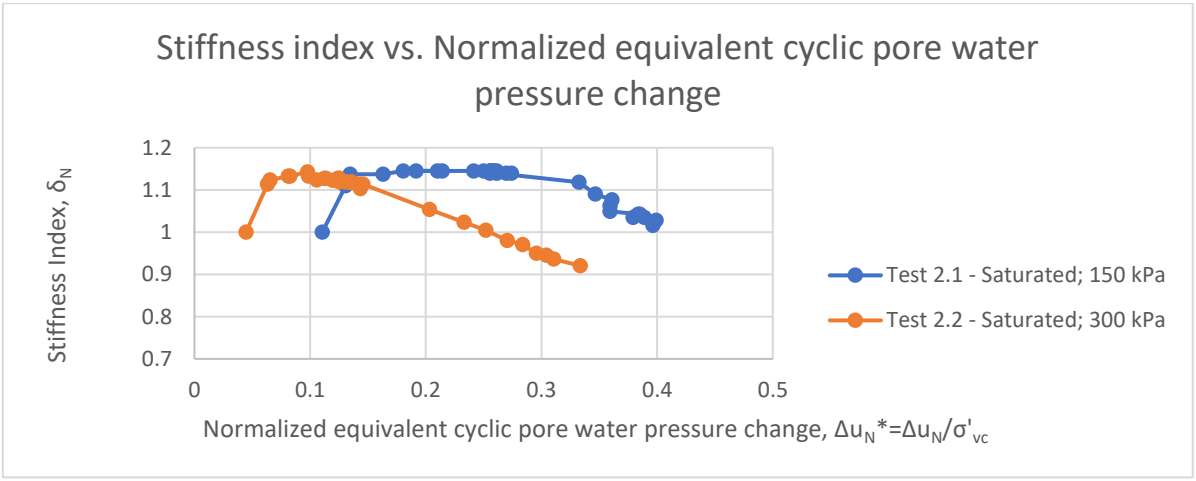

a) Specimen is reconsolidated between the cyclic stages

Figure 8.6 Behavior of sands at Υ_c=0.04% - specimens in all Tests are Nevada Sand

Tests with Υ_c=0.04% with 10 cycles

Figure 8.7(a) shows the results from six cyclic stages that were conducted at Υ_c = 0.04% in the tests that had reconsolidation between the stages. The results for a cyclic stage without reconsolidation are shown in Figure 8.7(b). All stages are conducted on Nevada Sand.

In Figure 8.7(a) it can be observed that in all five stages presented, δ_N initially increased with N. In three cases it then more or less leveled off, while in the other two cases it decreased. These trends are also evident in the Δu_N* versus δ_N relationships. It should be noted that in 4 out of 5 stages in Figure 8.7(a) σ'_{v0} was practically the same, ranging between 145 and 150 kPa, while in one stage it was 300 kPa. Also 3 out of 5 stages were conducted on saturated sand and two on dry sand. No particular effect of σ'_{v0} and saturation of specimen on δ_N versus N relationship can be recognized. The Δu_N* versus N relationships show that for the stages consolidated or reconsolidated to σ'_{v0} of 145 or 150 kPa the pressure Δu_N* increases with N at faster rate than for stage with σ'_{v0}=300 kPa. This is expected trend. Very similar rates of Δu_N* versus N for all four stages with σ'_{v0} =145 to 150 kPa, two on dry and two on saturated sand, confirm that a dry specimen can be tested in the constant-volume equivalent-undrained NGI-DSS device to obtain the results corresponding to saturated specimen.

For the case when there was no reconsolidation between the stages, shown in Figure 8.7 (b), δ_N first increases with N and then just slightly decreases, just like in the most of the stages with reconsolidation presented in Figure 8.7(a).

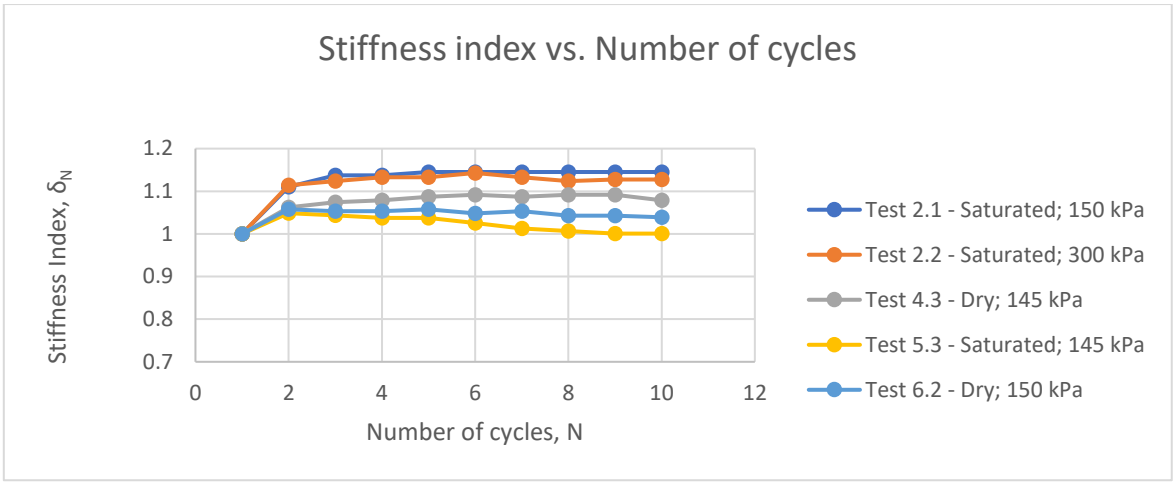

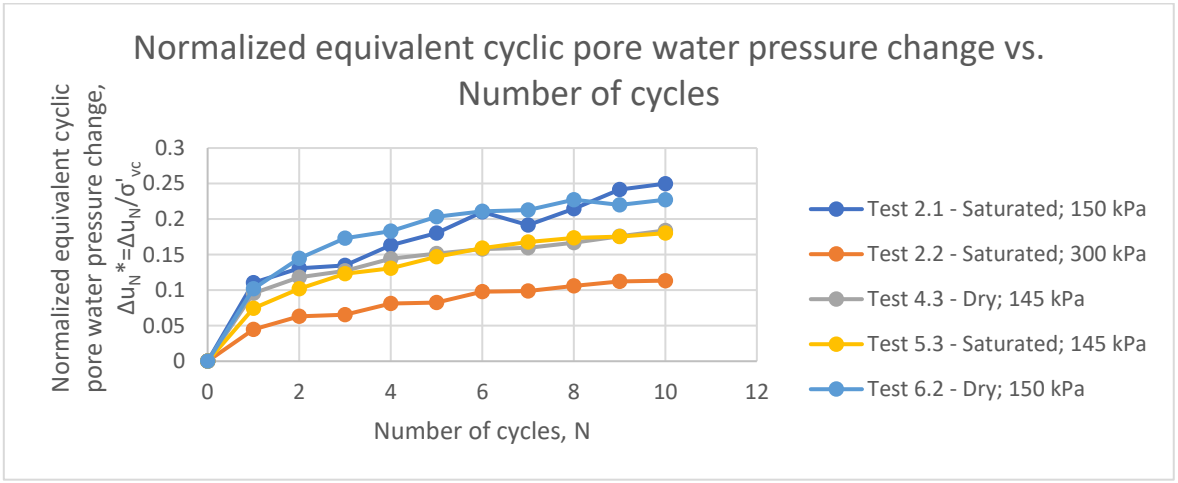

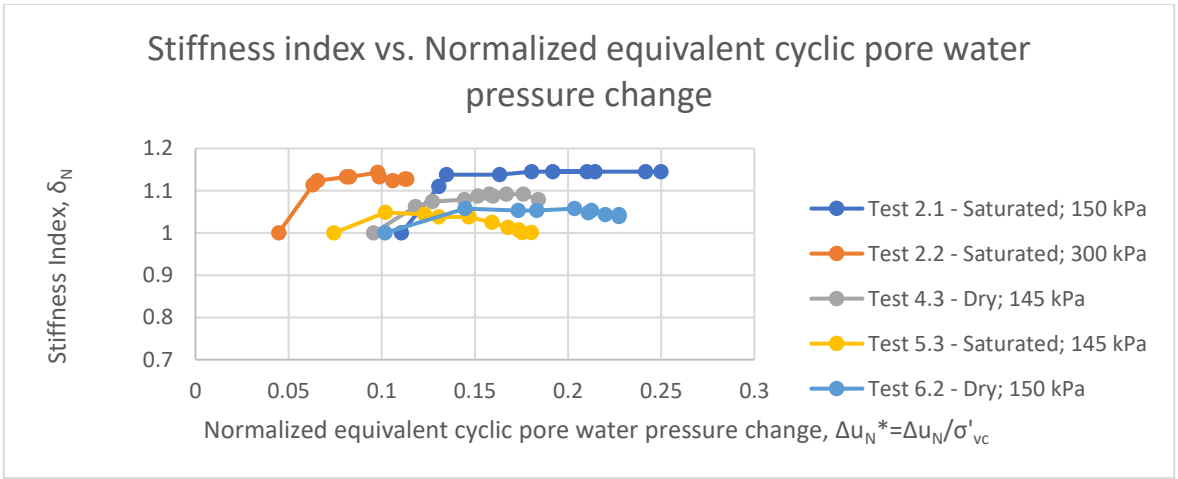

a) Specimen is reconsolidated between the cyclic stages

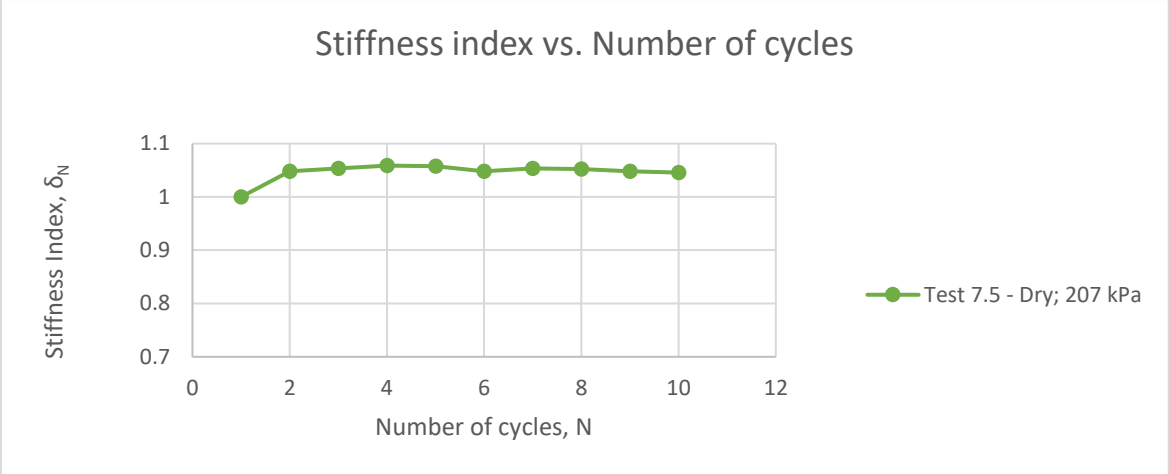

b) Specimen is not reconsolidated between the cyclic stages

Figure 8.7 Behavior of sands at Υ_c=0.04% - specimens in all Tests are Nevada Sand

Tests with Υ_c=0.06% with many cycles

Figure 8.8 shows the results from three stages from two tests on Nevada sand with amplitude Υ_c = 0.06% that were conducted at two different $\sigma'_{v0,}$ 150 and 300 kPa, for many cycles. Between the stages the specimen was reconsolidated. The variation of δ_N with N from two stages with σ'_{v0} =150 kPa is quite similar, same as the variation of Δu_N* with N in spite of the fact that one specimen was dry and the other saturated. For the stage with higher σ'_{v0}=300 kPa, δ_N versus N plots higher, while Δu_N* with N, as expected, plots lower. At σ'_{v0}=300 kPa the stiffness decreases slower with N than in tests with σ'_{v0}=150 apparently because of the slower increase of Δu_N*. The δ_N versus Δu_N* relationships reflect all the above trends.

Just like in the stages with Υ_c = 0.04% with many cycles (Figure 8.6), the test results from stages with Υ_c=0.06% confirm the behavior described earlier by Mortezaie Vucetic. They show clearly that for Υ_c between the threshold cyclic strain Υ_{tp}≈0.01% and 0.10 to 0.15%, Δu_N continuously increases with N while modulus G_{SN} first increases for up to approximately 10%

of G_{S1} and then gradually decreases, and that in this range of Υ_c the pore water pressure Δu_N can reach up to 40% of the initial effective confining stress before G_{SN} drops below G_{S1}.

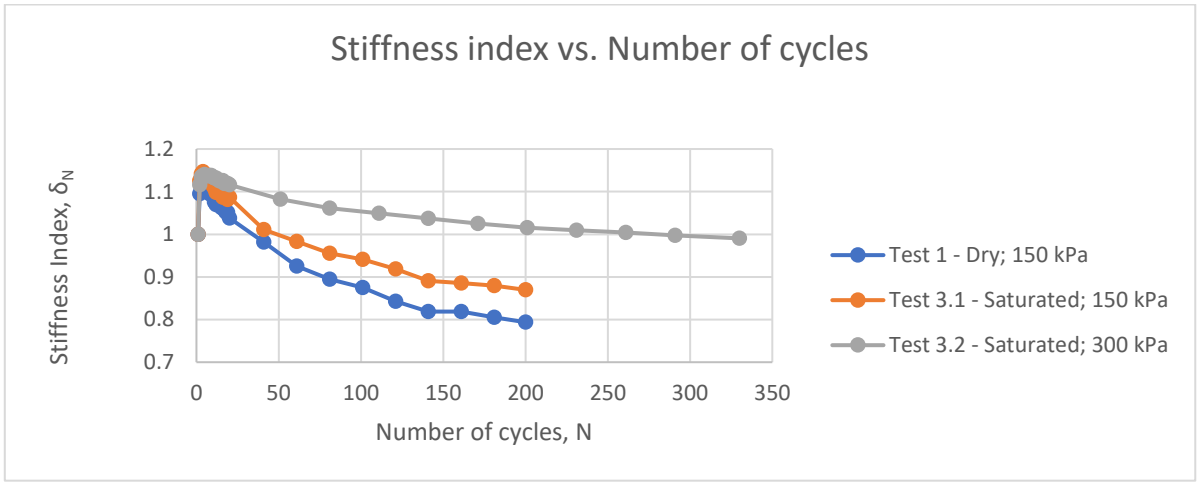

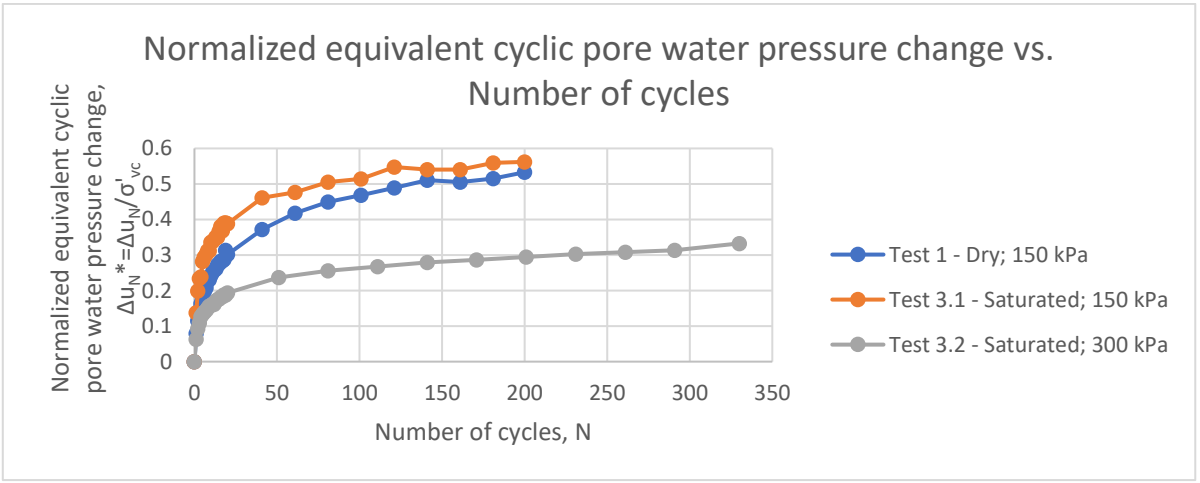

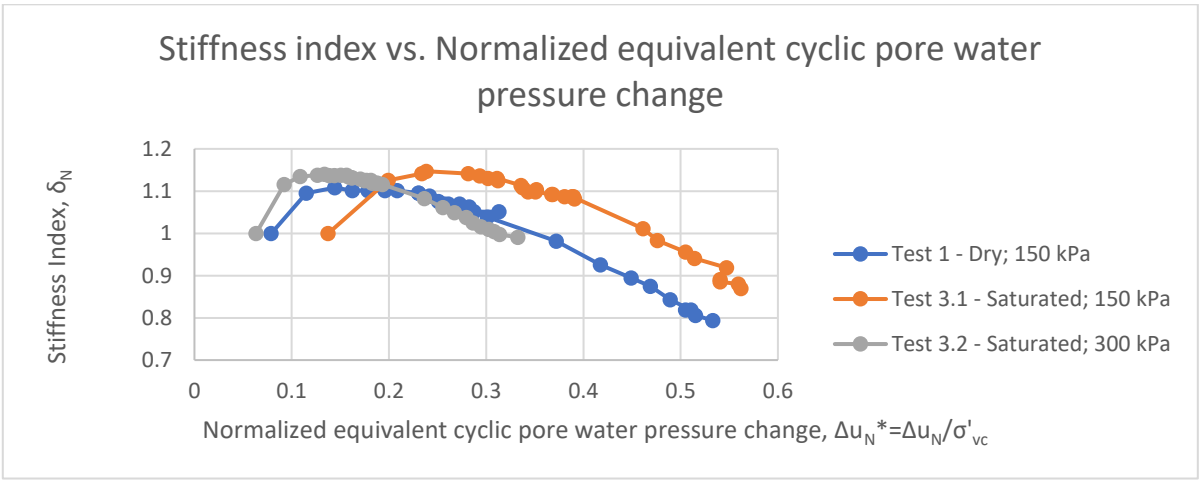

Figure 8.8 Behavior of sands at Υ_c=0.06% - specimens in all Tests are Nevada Sand

Tests with Υ_c=0.08%

Figure 8.9(a) shows the results from six stages conducted at shear strain amplitude Υ_c = 0.08% from the tests with reconsolidation between the stages. The stages are conducted on three different sands. The δ_N versus N relationships for three cyclic stages from the tests without reconsolidation are presented in Figure 8.9(b).

In Figure 8.9(a) it can be observed that in all six stages presented δ_N initially increases with N and then decreases. In some cases, the increase of δ_N is quite small while in others it is by 10%. Pressure Δu_N*, however, consistently increased at pretty much the same rate in all six stages. These trends are also evident in the Δu_N* versus δ_N relationships. It should be noted that in all stages σ'_{v0} is practically the same, either 145 or 150 kPa. In 4 out of 6 stages specimens were dry and in two they were saturated. It can be noticed that δ_N versus N relationships for dry sands plot somewhat higher than for saturated sand.

The results for three stages when there was no reconsolidation between the stages, shown in Figure 8.9(b), were obtained on three different sands. In two of them δ_N first slightly increases with N and then decreased, while in the third case of Test 10.5 it just decreased.

Except for the unexpected behavior in Test 10.5, all other results are in agreement with the trends obtained by Mortezaie and Vucetic, as well as those obtained above for great majority of tests.

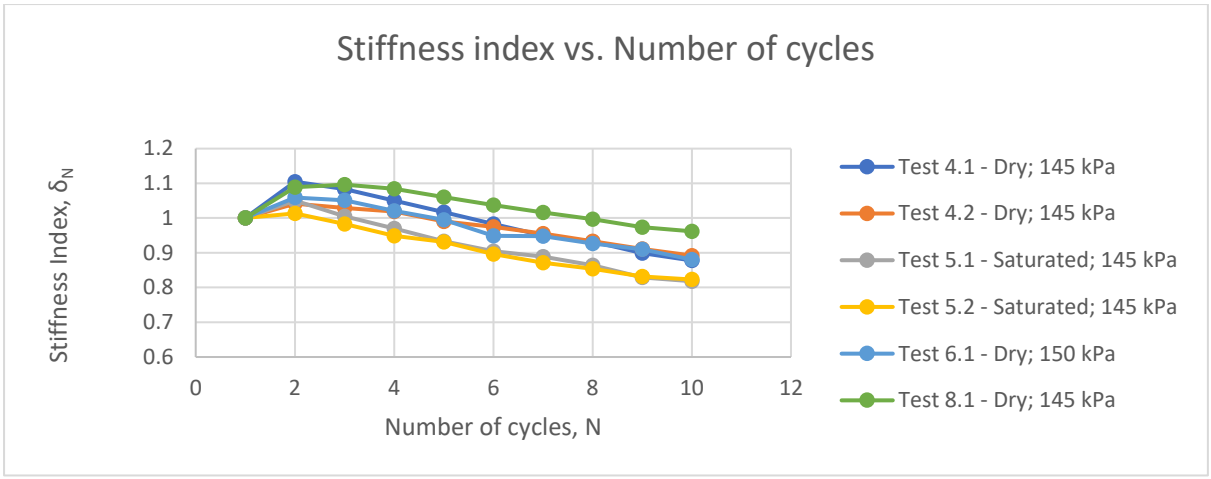

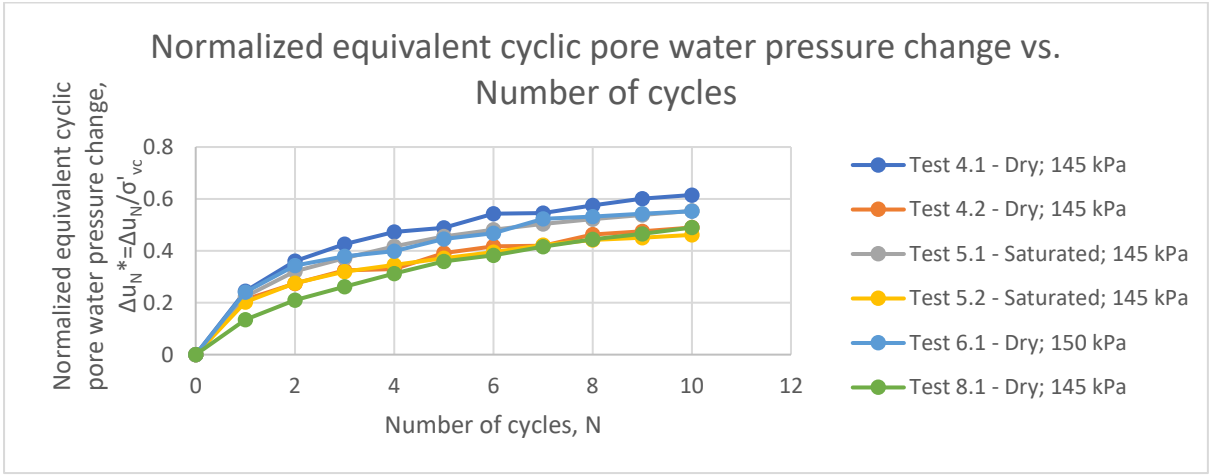

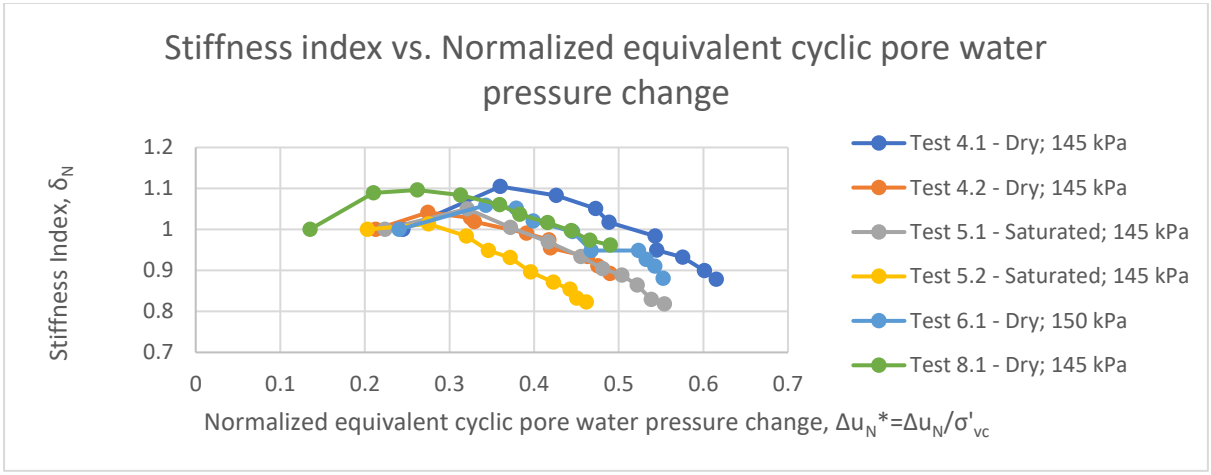

a) Specimen is reconsolidated between the cyclic stages

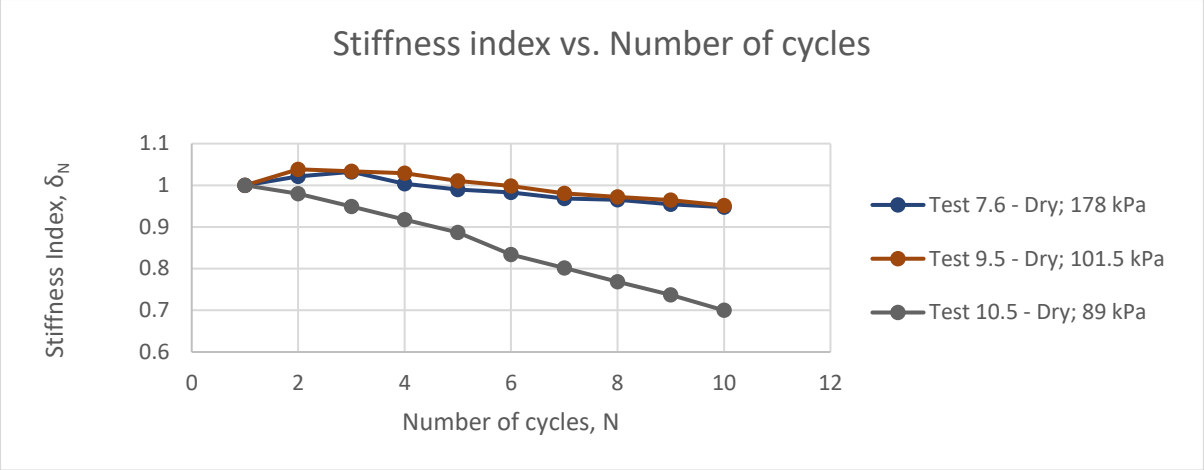

b) Specimen is not reconsolidated between the cyclic stages

Figure 8.9 Behavior of sands at Υ_c=0.08% - specimens in Tests 4, 5,6,7 and 8 are Nevada Sand, in Test 9 Toyoura Sand and in Test 10 Red Coarse Sand

Cyclic stress-controlled tests

For the analysis of the change of stiffness in the cyclic stress-controlled tests when the cyclic shear stress amplitude $\tau_{c1}= \tau_{cN} = \tau_c$ the stiffness index is defined as:

$$\delta_N = \frac{G_{SN}}{G_{S1}} = \frac{\tau_c/\gamma_{cN}}{\tau_c/\gamma_{c1}} = \frac{\gamma_{c1}}{\gamma_{cN}}$$

Mortezaie (2012) and Vucetic and Mortezaie (2015) have already concluded, based on just one test and the mechanism that is most likely responsible for the cyclic stiffening in the beginning of cyclic shearing at small cyclic strains, that the phenomena of cyclic stiffening while the cyclic pore water pressure increases must also occur in the cyclic stress-controlled tests on sands. They actually conducted Tests 11 and 12 but did not analyze them.

The results of Test 12 turned out as expected. During the cyclic shearing with constant cyclic shear stress, τ_c=0.1 σ'_{vc}, the strain first decreased and then increased, while the cyclic pore

water pressure gradually increased. The cyclic shear strains in the first 10 cycles were roughly between 0.06% and 0.04%. The cyclic behavior resulted in a relationship between the stiffness change and the cyclic pore water pressure buildup presented in Figure 8.10 that is typical of the strain-controlled test results.

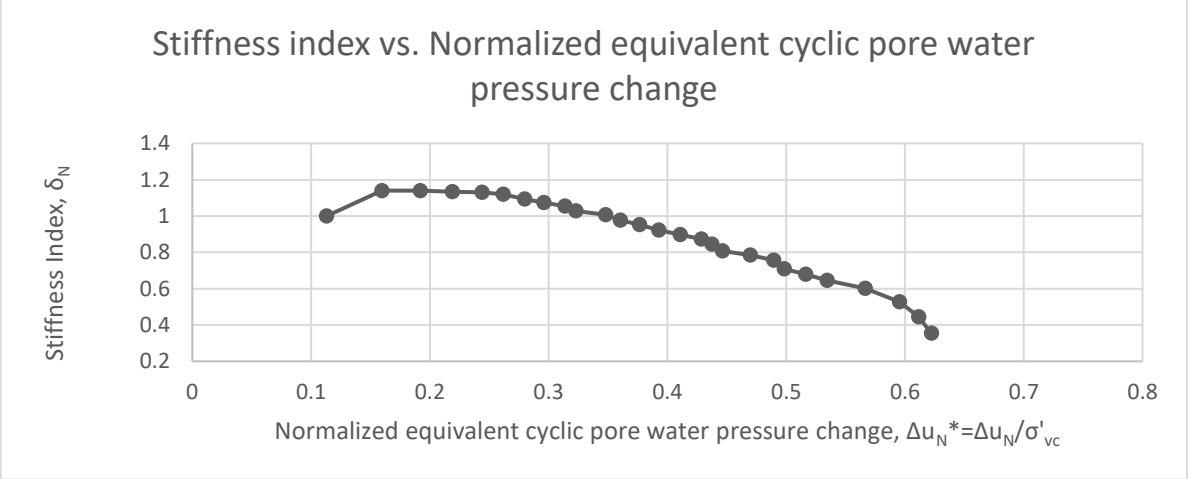

Figure 8.10 Behavior of Nevada sand in the cyclic stress-controlled Test 12 with $\tau_c=0.1\sigma'_{vc}$

[e=0.63; w=0%; σ'_{vc}=162 (kPa); OCR=1; $\tau_c=0.1\sigma'_{vc}$; f=0.01 Hz]

However, the test results of Test 11 conducted at constant $\tau_c=0.08\sigma'_{vc}$ are not as consistent with the strain-controlled test results with similar levels of Υ_c. The stiffness index increased in the first 4 cycles by staggering 40%, including the increase in the second cycle by 30%. The test results were reexamined and scrutinized but no explanation was found, except that the sand specimen was perhaps very nonuniform in terms of void ratio and density to start with and readjusted in the first few cycles. Although the trend of the relationship between the stiffness index and the cyclic pore water pressure is similar to the other tests with comparable conditions, the stiffness index values are clearly not. This test is apparently an outlier and it will not be considered in future analyses.

Conclusions

The cyclic strain-controlled test results analyzed above show that the phenomenon of the stiffness increase with the number of cycles occurs for different sands tested at small cyclic shear strain amplitudes up to approximately Υc=0.1% at various combinations of precycling, reconsolidation and no reconsolidation, saturation and confining stress. The shear modulus at cycle N, G_{SN}, may increase by 20% in comparison to the initial G_{S1} at N=1, although in most cases it does not increase by more than 10%. In only four cases (stages 7.1, 7.2, 7.3 and 4.5) out of 43 cases (43 cyclic stages) analyzed above had G_{SN} initially just slightly decreased in comparison to G_{S1} and those were all recorded at very small cyclic shear strains Υc=0.01% or smaller when testing and data interpretation are more delicate. Given enough cycles the stiffness that initially increased then decreased, as expected. The results also show that the initial stiffness increase occurs in spite of the increase of the cyclic pore water pressure, Δu_N, and associated decrease of the effective stress, and that Δu_N can reach up to 40% of the initial effective confining stress before G_{SN} drops below G_{S1}.

The phenomena described above also occurred in the cyclic stress-controlled tests, i.e., Tests 11 and 12, although in Test 12 the stiffness index increase was inexplicably large.

In conclusion, the above phenomena of cyclic behavior of saturated sands at small cyclic strains already identified and explained by Mortezaie (2012) and Vucetic and Mortezaie (2015) are confirmed for a number of different testing conditions. Consequently, these behavioral phenomena can be considered universal for sands.

9. Limitations of the effective stress principle as applied to cyclic loading

The aspect of the cyclic behavior of saturated sands in undrained conditions investigated in this thesis and before by Mortezaie and Vucetic are newly discovered and as such not adopted yet by the soil dynamics engineering practice. Because of their fundamental and universal nature these aspects are very important, in particular for the refinement of the analyses of the problems associated with the softening of sandy saturated deposits leading to liquefaction. They are not adopted and it will take some time to be adopted because they do not agree with the effective stress principle that is currently unconditionally used to evaluate the softening of sand due to the cyclic pore water pressure buildup. The general belief is that if the cyclic pore water pressure increases and the effective stress decreases accordingly, the saturated sand must soften, i.e., its stiffness must decrease. This concept is, as already explained in the Introduction, incorporated in various computer models for the evaluation of the seismic response of saturated sandy deposits, in particular the models for the evaluation of the liquefaction occurrence.

The results in this thesis and similar previous results show that in the case of the cyclic shearing of saturated sands in undrained conditions at cyclic shear strain amplitudes, γ_c, smaller than approximately 0.1 to 0.15% sand can increase in stiffness while the cyclic pore water pressure increase and then, after certain number of cycles, the stiffness starts to go down. The results show that by the time the soil stiffness comes down to the initial stiffness before the cyclic shearing started, the cyclic pore water pressure may reach up to 40% of the initial effective confining stress. This means that there is no softening of the sand even though the pore water pressure increased by 40% of its maximum possible value.

All of these indicate that the effective stress principle is not as useful for the analyses of the softening of the fully saturated sandy soils as it is currently believed. The effective stress

principle should be combined with the behavioral trends established by Mortezaie and Vucetic and confirmed in this thesis to improve the models for the evaluation of sand softening induced by cyclic loading, in particular the softening leading to liquefaction.

10. Analysis of the variation of the equivalent viscous damping ratio with the number of cycles

Mortezaie (2012) briefly tackled the relationship between the area of the loop and associated damping ratio and the change in stiffness of Nevada sand subjected to small cyclic shear strains. In this chapter, the variation of the equivalent viscous damping ratio, λ, with the number of cycles, N, and how it relates to stiffness index, δ_N, is analyzed further. The equivalent viscous damping ratio, λ, is plotted against N in Chapter 7 for 14 stages conducted on Nevada sand at σ'_{vc} between 145 and 150 kPa, OCR=1, f=0.01 Hz, water content, w, between zero and 18.63%, and Υ_c between 0.02 and 0.08%. The equivalent viscous damping ratio, λ, was not calculated for Υ_c smaller than 0.02% because at smaller Υ_c the results may not be reliable enough due to the false loads and their imperfect correction. Furthermore, λ was calculated from cycle 2 onwards, because the first cycle loop is not fully closed and therefore does not conform with the definition of λ in figure 6.1.

For convenience, the above 14 results on damping are repeated at the end of this chapter along with the variations of λ with log N. The λ versus log N graphs are added to examine if the relationships will be more or less linear like in some previous studies (e.g., Dobry and Vucetic, 1987; Hsu and Vucetic, 2002).

The results presented at the end of this chapter reveal that the general trend of λ with N is that it is always the largest in the first cycle considered, i.e., N=2, and that it is getting smaller with N at a lower and lower rate until it eventually almost stabilizes at around N=10. Such

trend yields in many cases almost linear relationship between λ and log N, or a trend of the rate of λ with log N very slowly dropping. In 13 out of 14 cases, from N=2 to N=10 λ dropped by 15 to 30%. This is a substantial drop that should not be ignored in certain soil dynamics analyses. In just one case λ dropped by only 6%.

The above trends have been observed in previous investigations of the cyclic-strain controlled behavior of sands and clays in the cyclic direct simple shear device (Vucetic et al., 1983; Dobry and Vucetic, 1987; Hsu and Vucetic, 2002). They indicate that smaller and smaller shear force is required to achieve the same shear distortion as the cycling with a constant Υ_c goes on. In other words, smaller and smaller energy input is required to describe the loop.

To investigate further these trends of λ and how they are related to the changes in soil stiffness and associated stiffness index, δ, one more cycle is added to the analysis. This is the cycle from ¼ of the first cycle to ¼ of the second cycle, i.e., from N=0.25 to N=1.25, such as shown in Fig. 10.1 for Test 5.1. This cycle is referred to as the cycle N=1.25, because λ is determined at the end of it. This is the earliest cycle that λ can be determined for, i.e., the earliest cycle to evaluate the energy required to describe the cycle at Υ_c. Results of only two representative tests, Test 5.1 conducted at Υ_c=0.08% and Test 4.3 conducted at Υ_c=0.02%, are analyzed below. For convenience only the damping obtained using standard method with just one triangle divided by the area of the loop is used in the analysis.

In Figure 10.2 four loops from Test 5.1, including the loop for cycle N=1.25, are presented for comparison. It can be seen clearly that the area of the loop, ΔW, is the largest in cycle N=1.25 and markedly larger than in cycle N=2, and that it decreases with N. In Table 10.1 the variations of ΔW, area of the associated triangle, W, damping ratio, λ, normalized cyclic shear stress, τ_c*, and stiffness index, δ, with N are tabulated for all 10 cycles, while the corresponding

graphs are presented in Figure 10.3. The same is done for Test 4.3 in Table 10.2 and Figure 10.4.

The data in the tables, and in particular the graphs in Figures 10.3 and 10.4, show that in the first few cycles the area of the loop, ΔW, dramatically decreases with N while the soil stiffness increases (Test 4.3) or increase and decreases (Test 5.1). This is counterintuitive, because if the stiffness is going up the average shear force is going up too, and the area of the loop, ΔW, that describes the specific energy associated with this larger force (energy per unit volume) in a given cycle over the constant path corresponding to constant shear strain, Υ_c, should go up too. But as δ goes up ΔW goes down. Apparently, because the energy per cycle is decreasing while the material is getting stiffer, there must be a strong mechanism for the loss of energy in the soil material. At the same time, as expected, the area of the triangle, W, changes in the same manner as the cyclic shear stress amplitude, τ_c, and the corresponding stiffness index, δ. It should be noted that no matter what the trend of W is, the changes of W with N are so small that the trend of λ follows the trend of ΔW and vice versa. In conclusion, since the damping decreases in all 14 tests, as well as in a number of cyclic strain-controlled undrained or constant-volume equivalent-undrained tests on other sands and clays conducted in the past, the energy required to execute a cyclic loop in a cyclic strain-controlled test at small to moderate Υ_c will always decrease with N. This also means that in order for ΔW to decrease with N soil must be getting less and less nonlinear with N. The fact that the nonlinearity decreases with N is evident in Figure 10.3.

In summary, the relationship between the variation of the equivalent viscous damping ratio, λ, and the change in soil stiffness described by stiffness index, δ, cannot be easily explained. This problem is out of the general scope of this thesis and is not tackled here further.

This interesting problem of cyclic soil behavior is of a fundamental nature and it should be studied in the future.

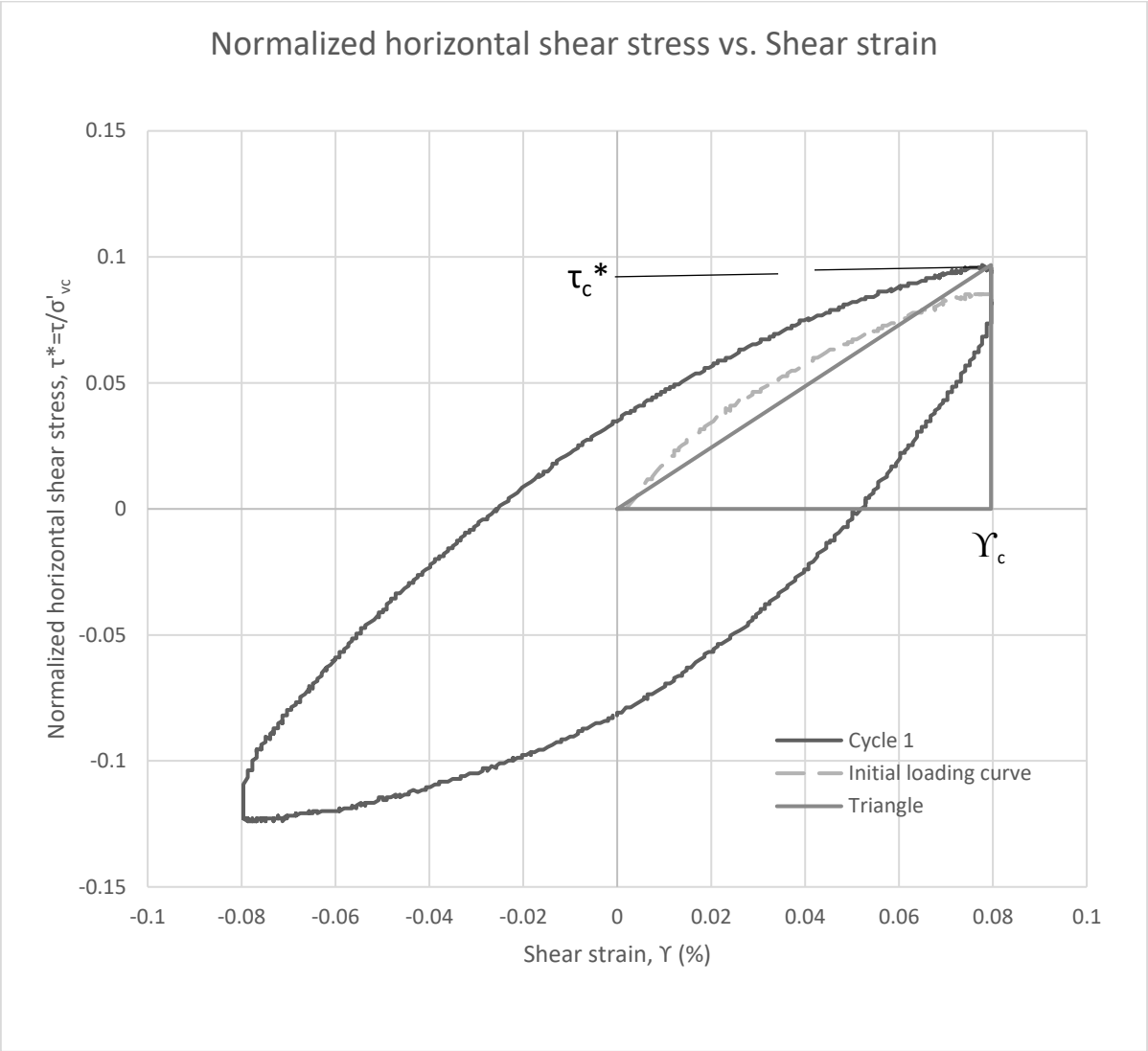

Figure 10.1 Loop at cycle N=1.25 in Test 5.1 with corresponding triangle ($0.5\ \tau_{c*} \cdot \gamma_c$)

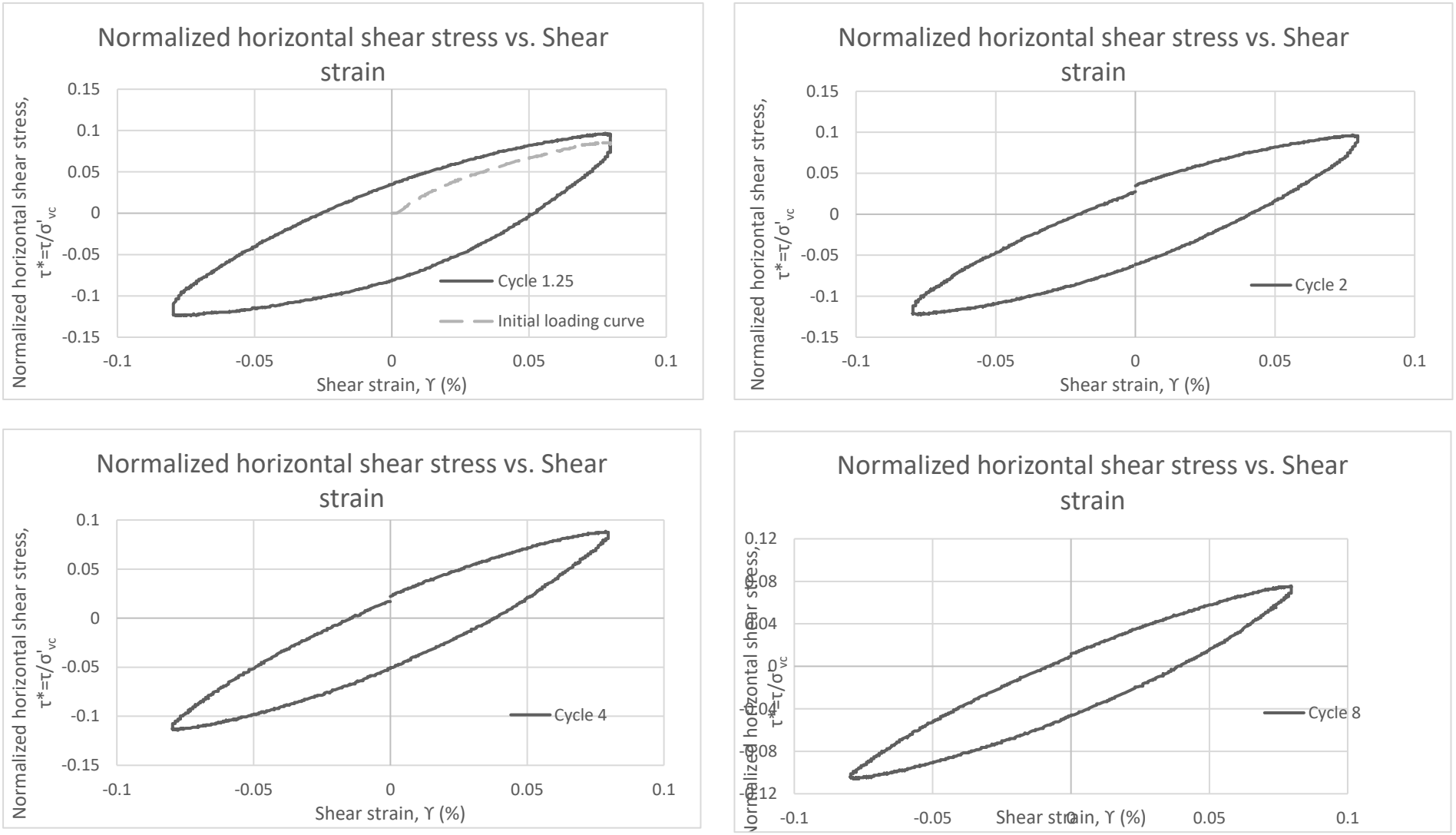

Figure 10.2 Stress-strain loops for four different cycles of Test 5.1
[Soil: Nevada Sand; e=0.774; w=18.63%, σ'_{vc}=145 (kPa); OCR=1; Υ_c=0.08%, f=0.01 Hz]

Table 10.1 Test 5.1 Damping and stiffness index data
[Soil: Nevada Sand; e=0.774; w=18.63%, σ'_{vc}=145 (kPa); OCR=1; Υ_c=0.08%, f=0.01 Hz]

Cycle number	Area of loop (Energy density)	Area of triangle (0.5 $\tau_c \cdot \gamma_c$)	Damping ratio	Normalized peak horizontal shear stress	Stiffness index according to column 5
1	2	3	4	5	6
N	ΔW	W	λ	τ_c*	δ
-	kPa	kPa	%	-	-
1				0.085	1
1.25	0.019	0.0038	27.9		
2	0.016	0.0038	22.3	0.096	1.05
3	0.013	0.0036	20.0	0.092	1.00
4	0.011	0.0035	18.6	0.088	0.96
5	0.0109	0.0033	17.8	0.085	0.93
6	0.0103	0.0032	17.5	0.081	0.90
7	0.0101	0.0030	17.9	0.077	0.88
8	0.0096	0.0029	17.8	0.074	0.86
9	0.0088	0.00288	16.8	0.072	0.82
10	0.0090	0.00280	17.7	0.070	0.81

Table 10.2 Test 4.3 Damping and stiffness index data
[Soil: Nevada Sand; e=0.802; w=0%, σ'_{vc}=145 (kPa); OCR=1; Υ_c=0.04%, f=0.01 Hz]

Cycle number	Area of loop (Energy density)	Area of triangle (0.5 $\tau_c \cdot \gamma_c$)	Damping ratio	Normalized peak horizontal shear stress	Stiffness index according to column 5
1	2	3	4	5	6
N	ΔW	W	λ	τ_c*	δ
-	kPa	kPa	%	-	-
1				0.098	1.00
1.25	0.0048	0.0022	12.1		
2	0.0035	0.0022	8.8	0.109	1.06
3	0.0031	0.00224	7.7	0.111	1.07
4	0.0029	0.00226	7.1	0.112	1.07
5	0.0027	0.0023	6.5	0.114	1.08
6	0.0026	0.0023	6.2	0.114	1.09
7	0.0025	0.00228	6	0.113	1.08
8	0.0024	0.0023	5.8	0.114	1.09
9	0.00238	0.0023	5.6	0.114	1.09
10	0.00232	0.00228	5.5	0.113	1.07

[Soil: Nevada Sand; e=0.774; w=18.63%, σ'_{vc}=145 (kPa); OCR=1; Υ_c=0.08%, f=0.01 Hz]

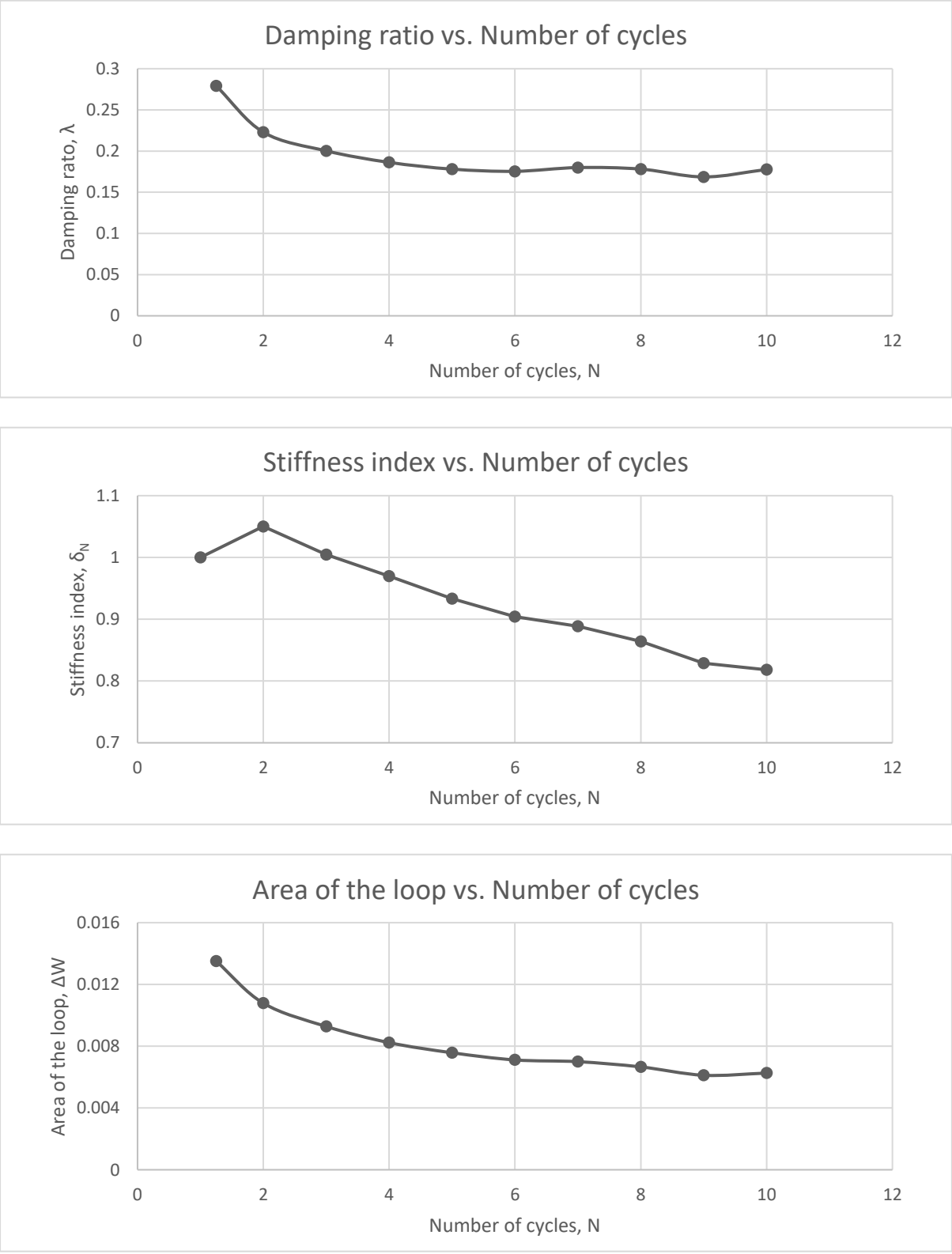

Figure 10.3 The variations of δ, ΔW and λ with N for Test 5.1

[Soil: Nevada Sand; e=0.802; w=0%, σ'_{vc}=145 (kPa); OCR=1; Υ_c=0.04%, f=0.01 Hz]

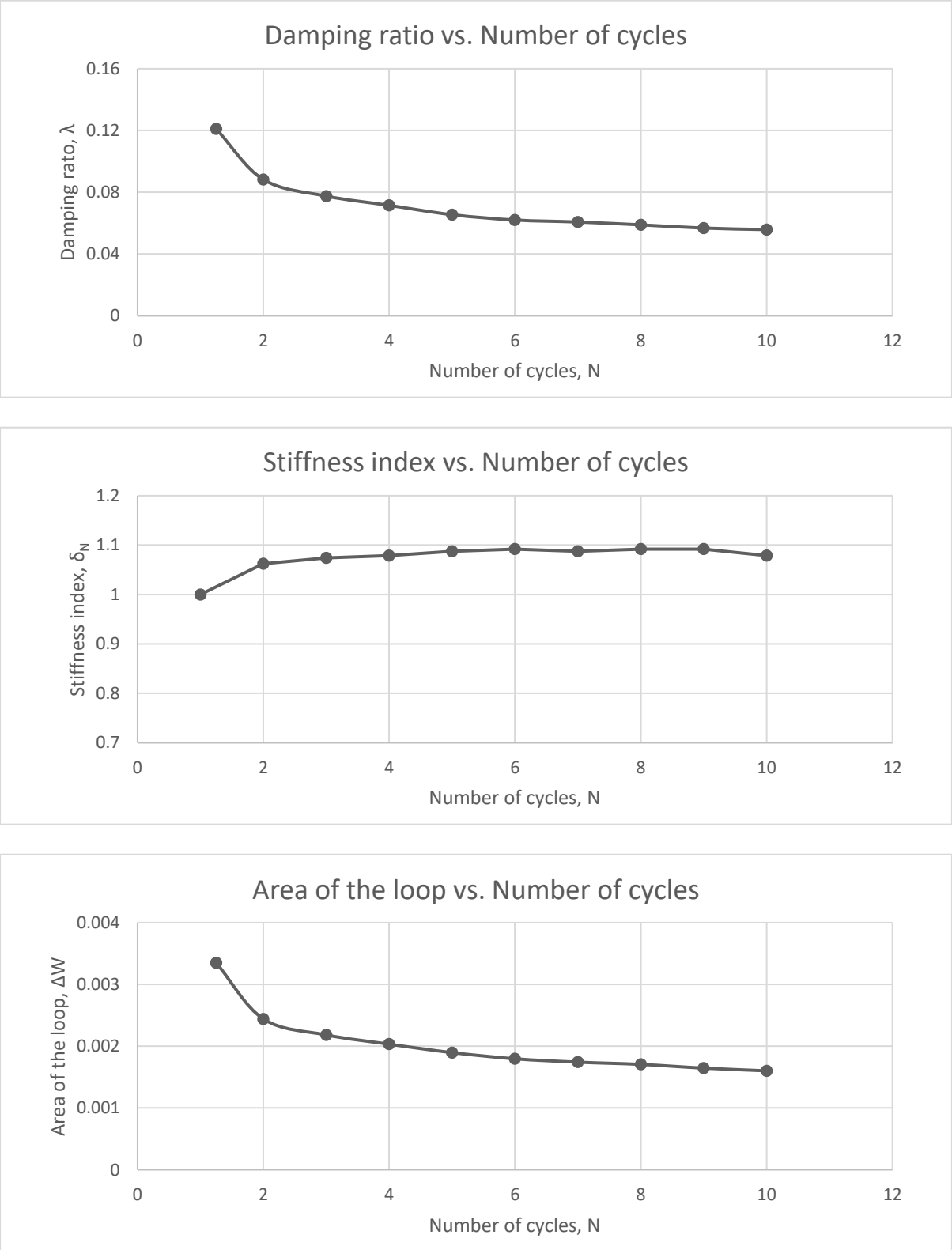

Figure 10.4 The variations of δ, ΔW and λ with N for Test 4.3

Results on damping extracted from Chapter 7. Test results

Test: 4.1; Soil: Nevada Sand; e=0.806; w=0%
σ'_{vc}=145 (kPa); OCR=1; Υ_c=0.08%, f=0.01 Hz

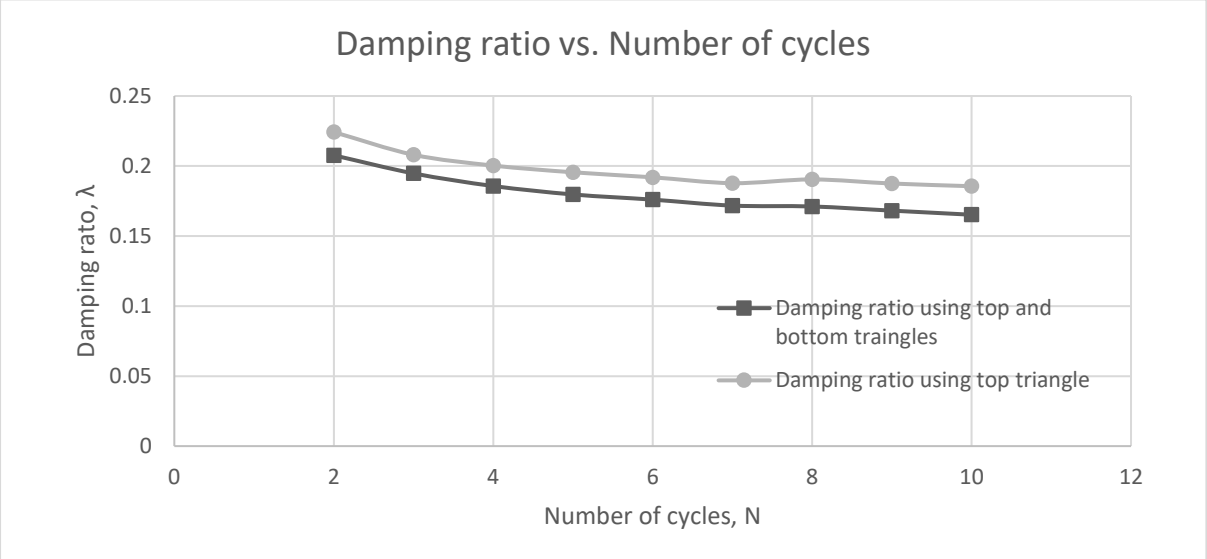

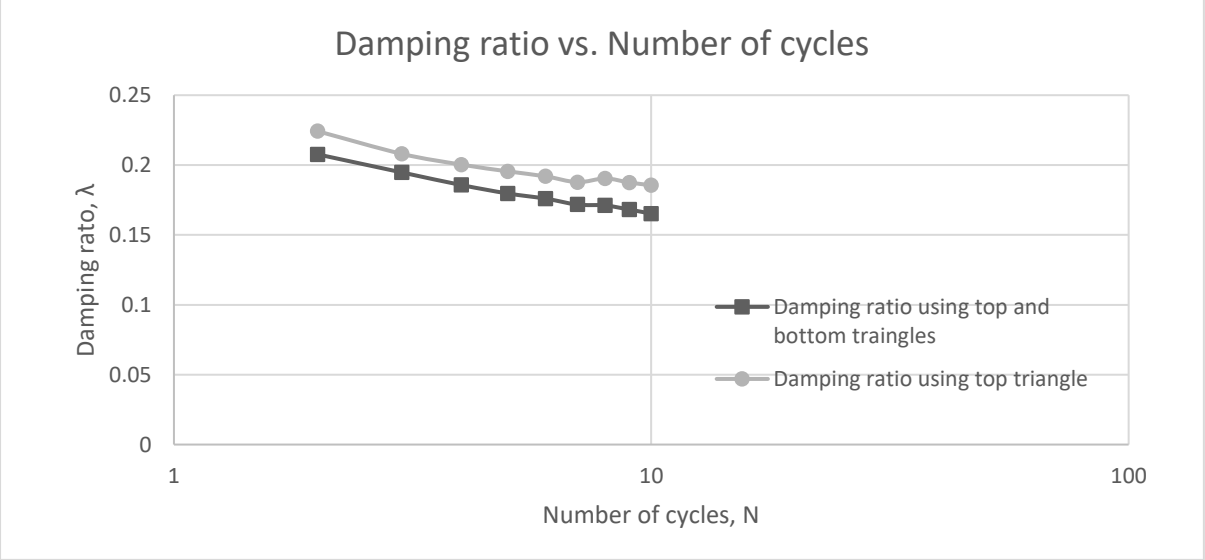

Test: 4.2; Soil: Nevada Sand; e=0.803; w=0%
σ'_{vc}=145 (kPa); OCR=1; Υ_c=0.08%, f=0.01 Hz

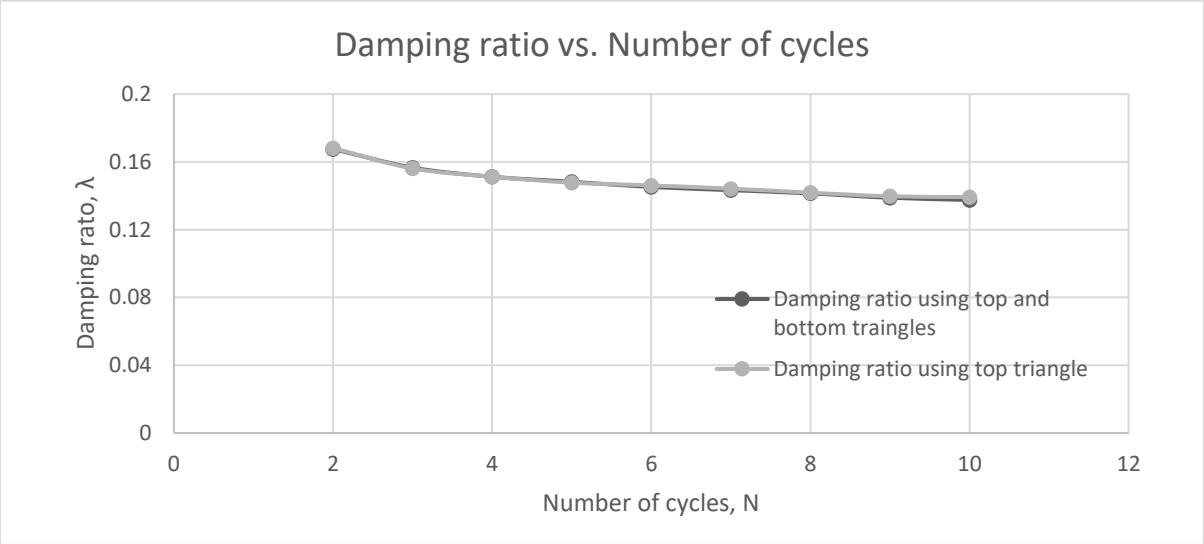

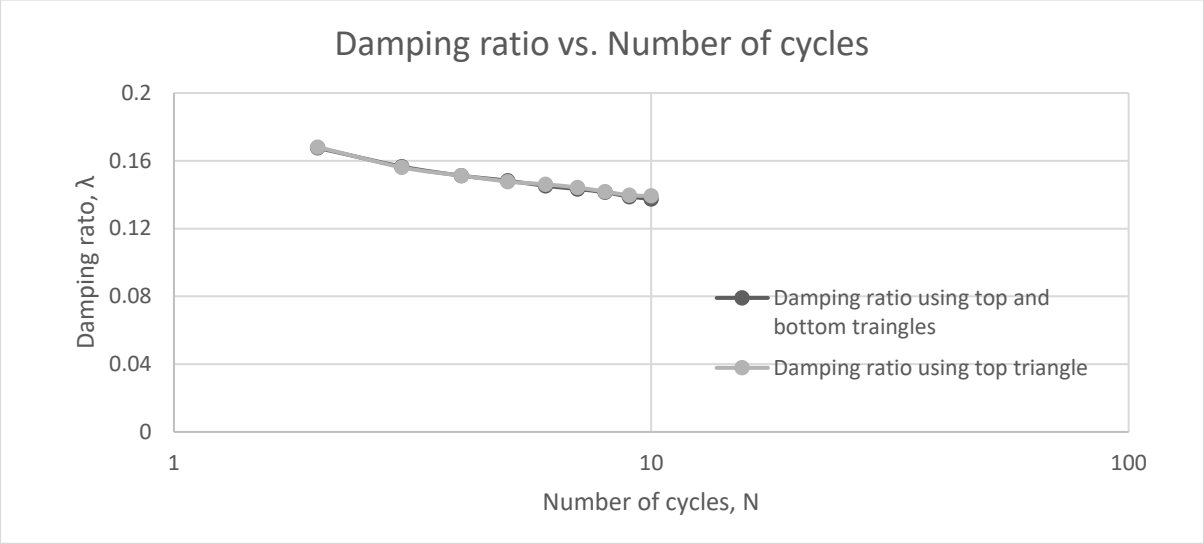

Test: 4.3; Soil: Nevada Sand; e=0.802; w=0%
σ'_{vc}=145 (kPa); OCR=1; Υ_c=0.04%, f=0.01 Hz

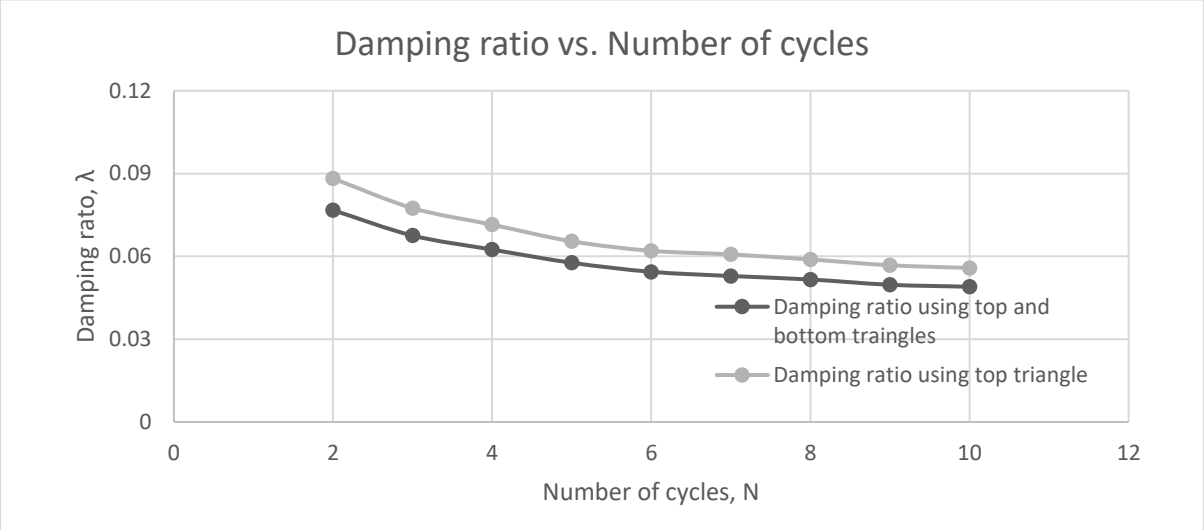

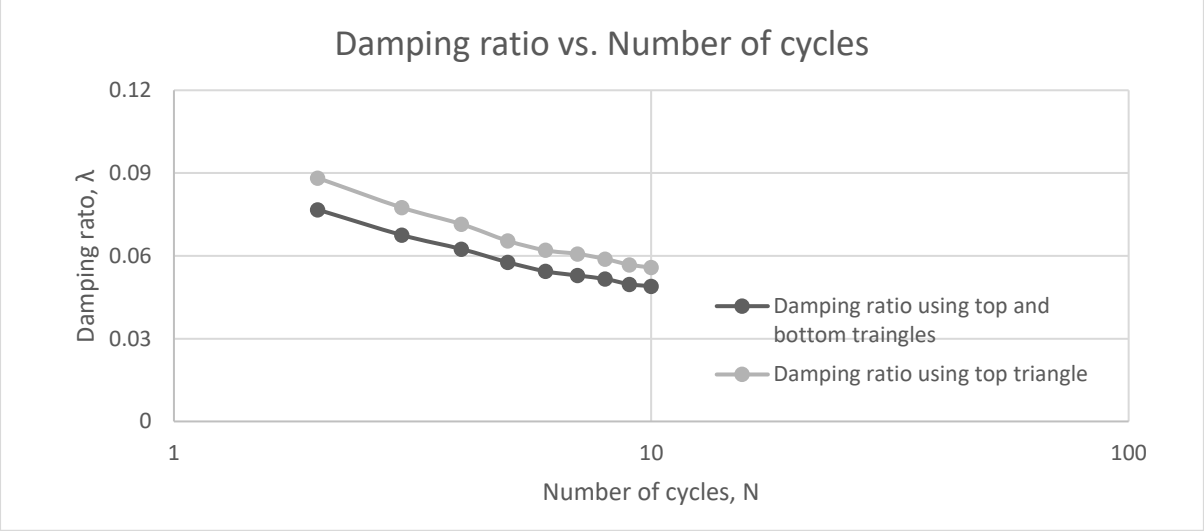

Test: 4.4; Soil: Nevada Sand; e=0.801; w=0%
σ'_{vc}=145 (kPa); OCR=1; Υ_c=0.02%, f=0.01 Hz

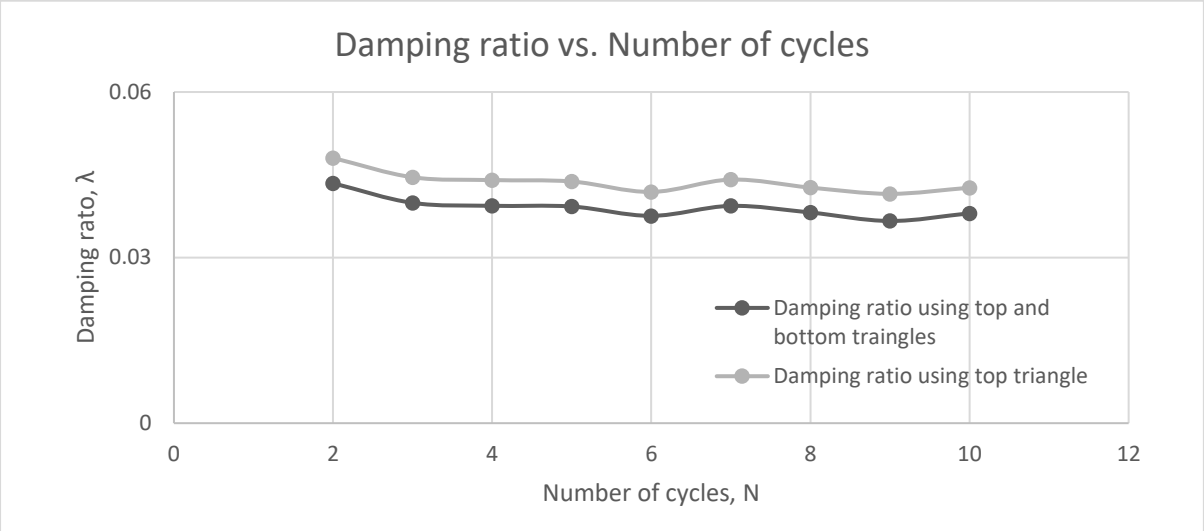

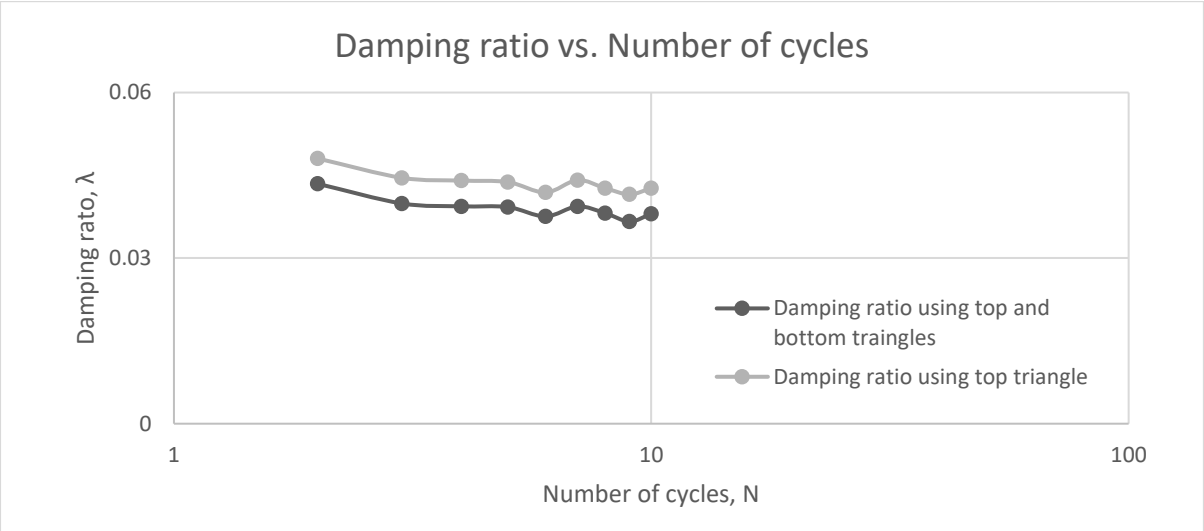

Test: 5.1; Soil: Nevada Sand; e=0.774; w=18.63%
σ'_{vc}=145 (kPa); OCR=1; Υ_c=0.08%, f=0.01 Hz

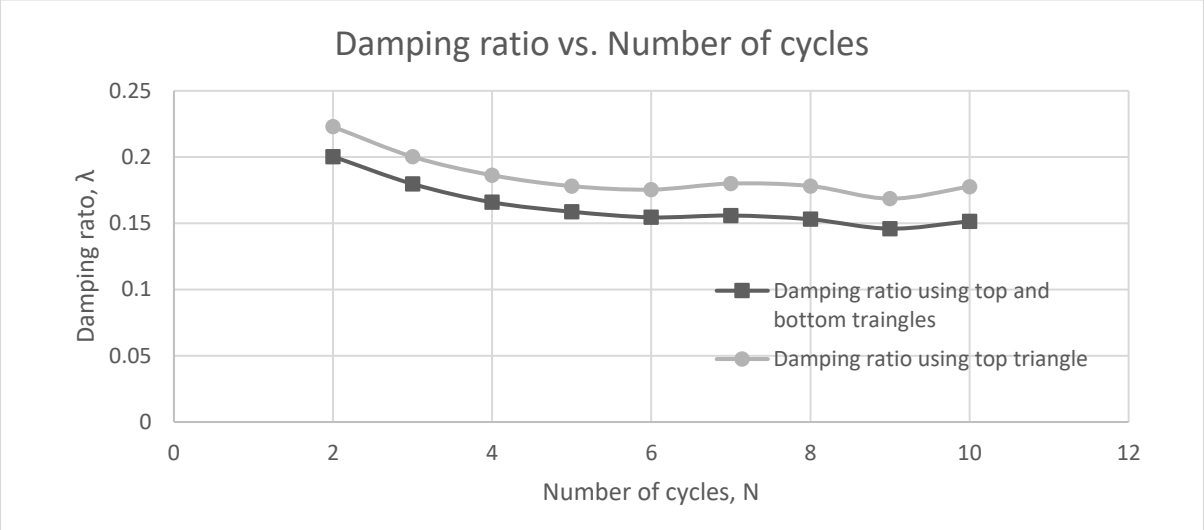

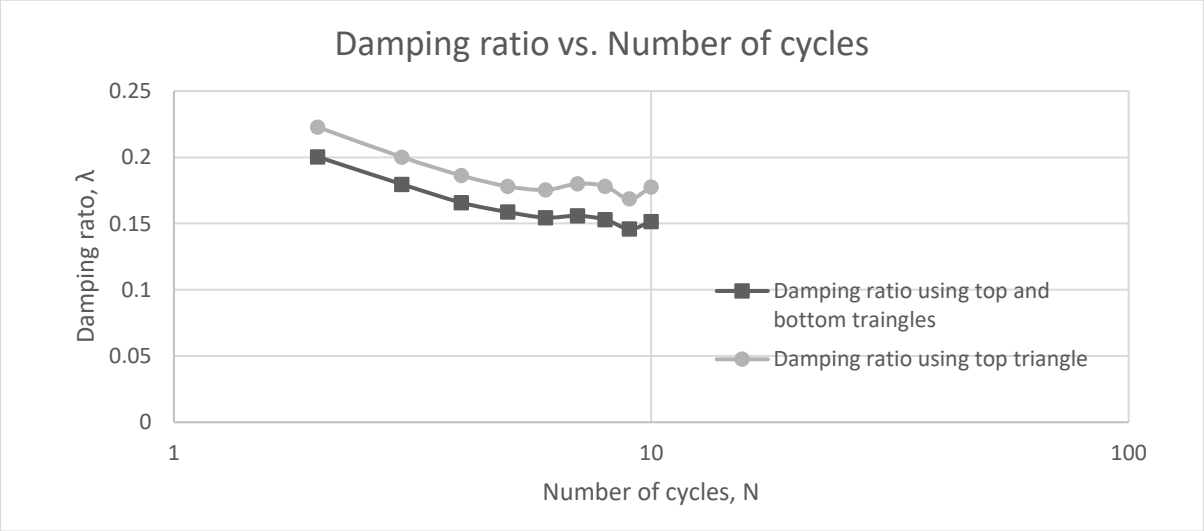

Test: 5.2; Soil: Nevada Sand; e=0.771; w=18.63%
σ'_{vc}=145 (kPa); OCR=1; Υ_c=0.08%, f=0.01 Hz

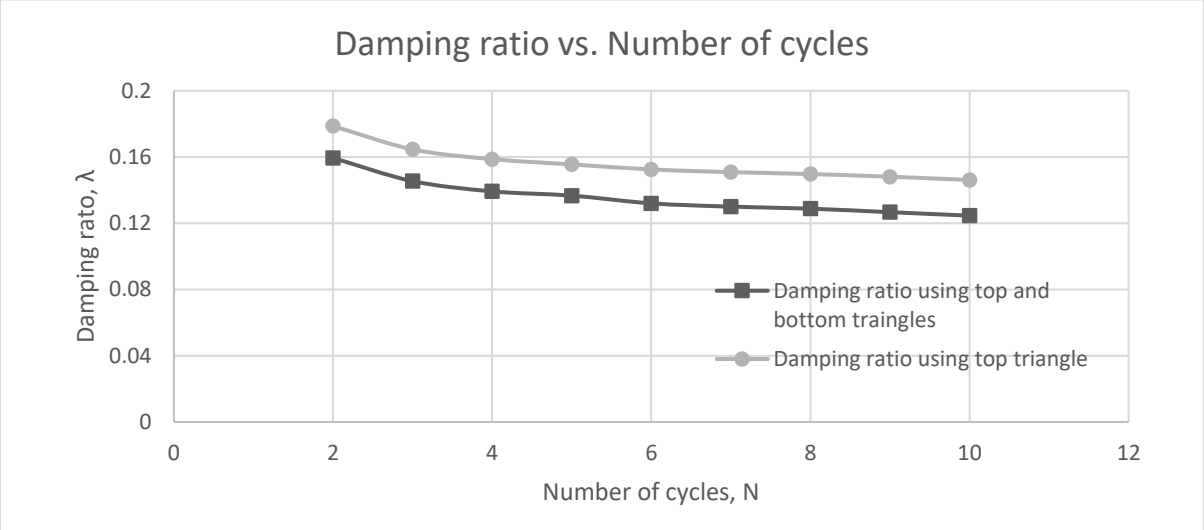

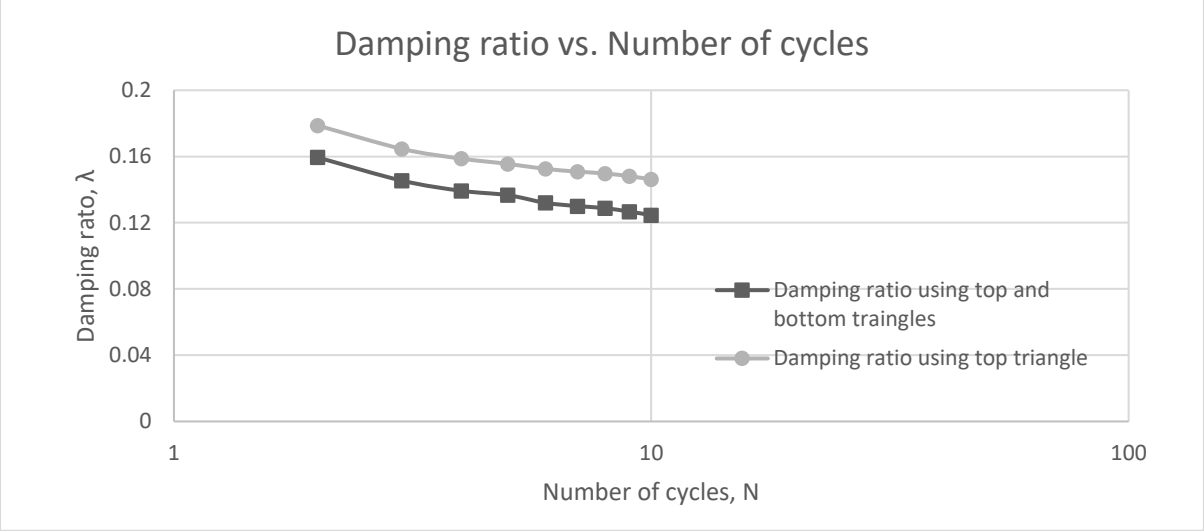

Test: 5.3; Soil: Nevada Sand; e=0.771; w=18.63%
σ'_{vc}=145 (kPa); OCR=1; Υ_c=0.04%, f=0.01 Hz

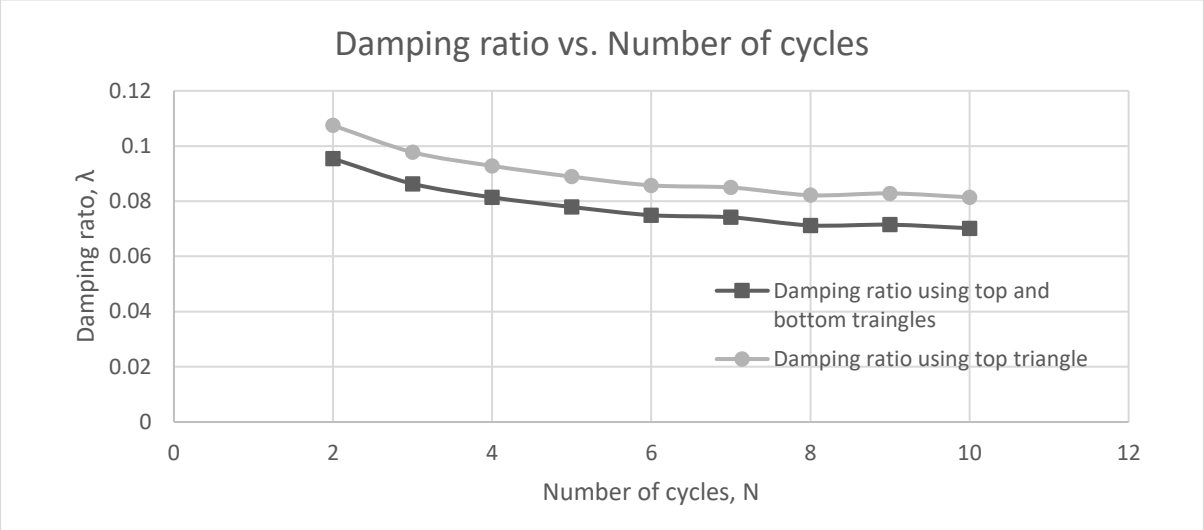

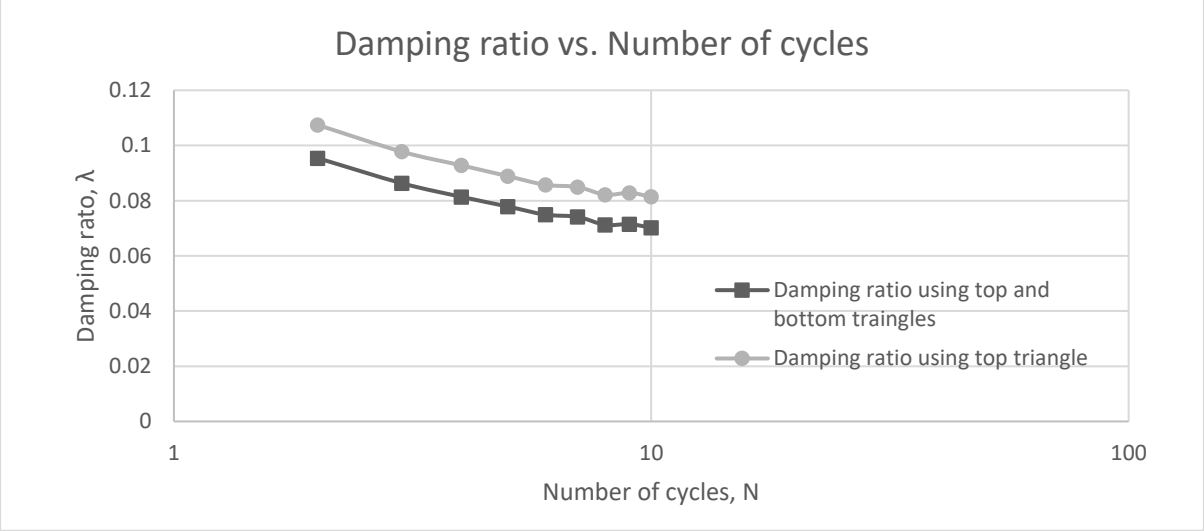

Test: 5.4; Soil: Nevada Sand; e=0.771; w=18.63%
σ'_{vc}=145 (kPa); OCR=1; Υ_c=0.02%, f=0.01 Hz

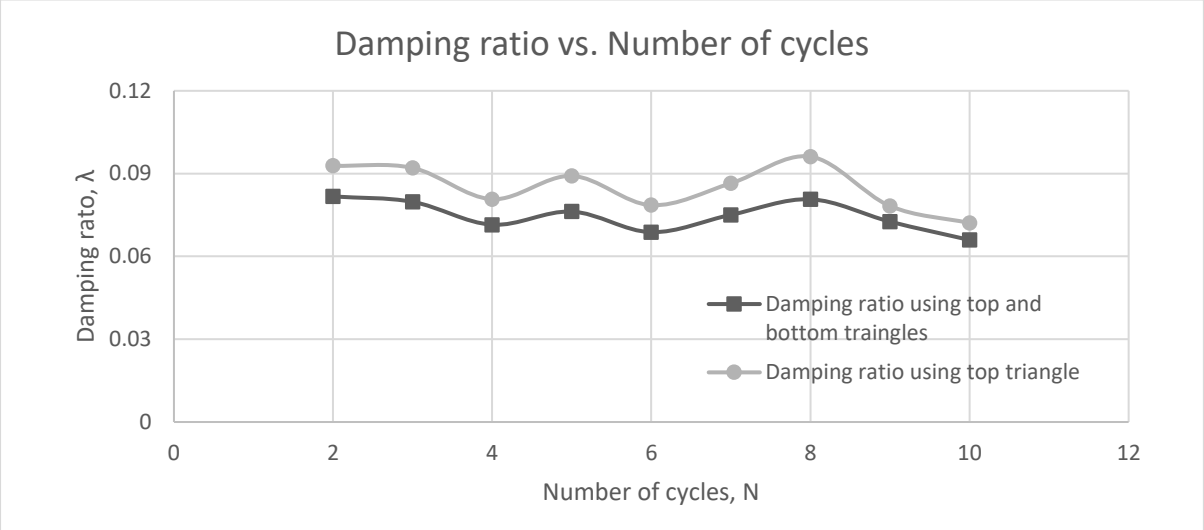

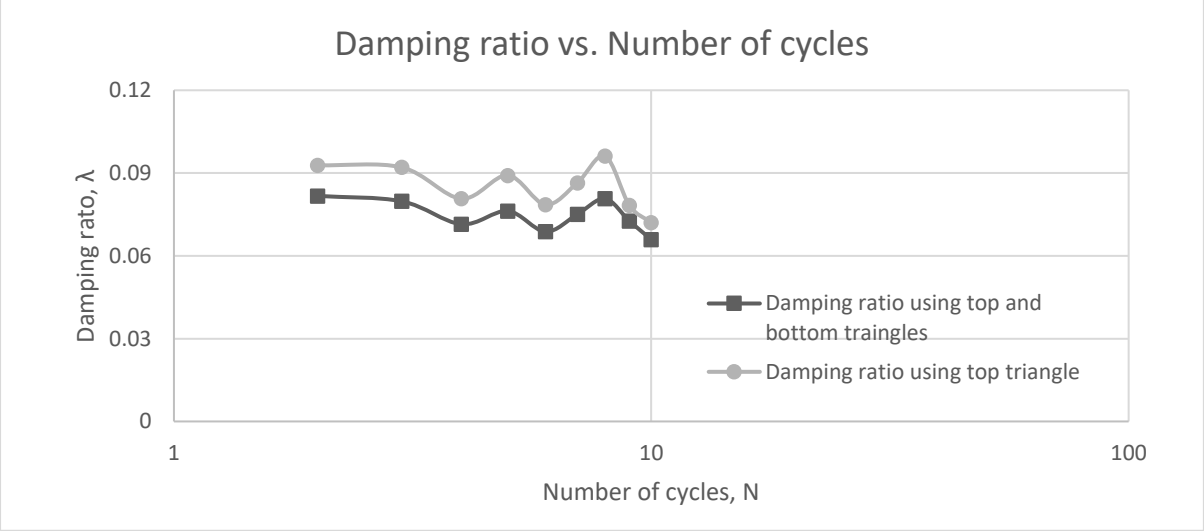

Test: 6.1; Soil: Nevada Sand; e=0.641; w=0%
σ'_{vc}=150 (kPa); OCR=1; Υ_c=0.08%, f=0.01 Hz

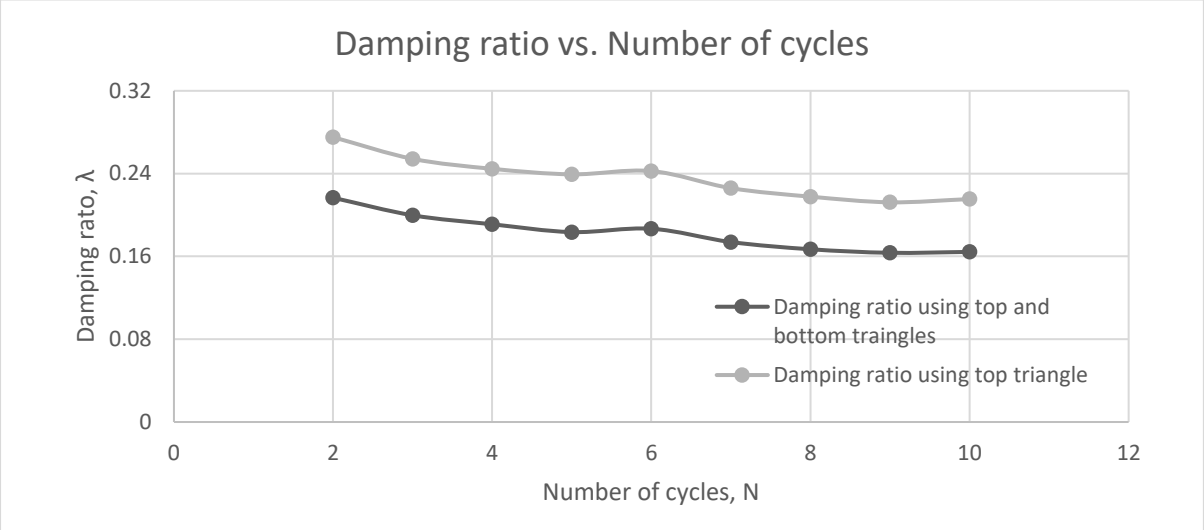

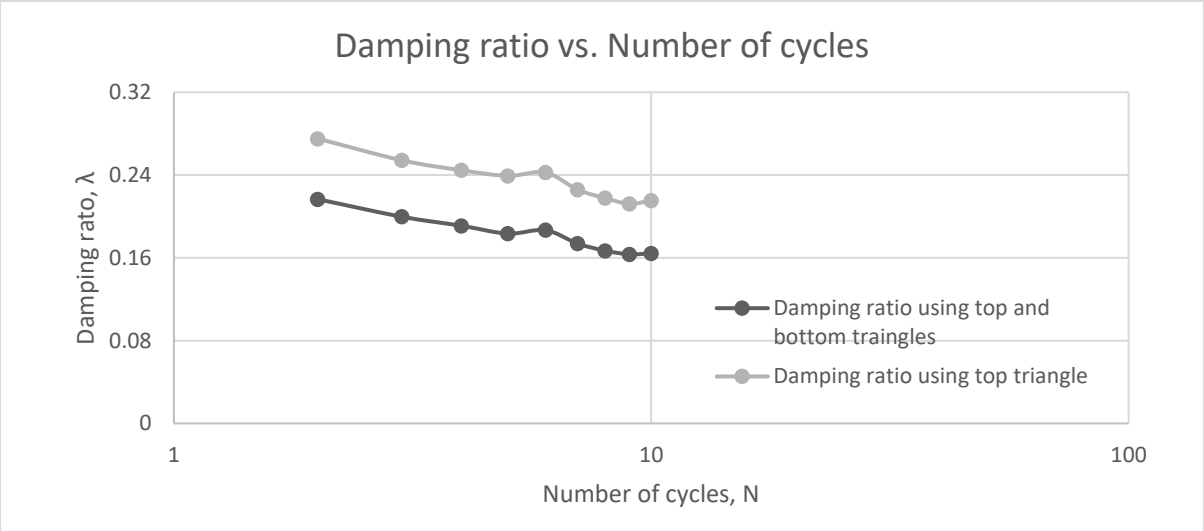

Test: 6.2; Soil: Nevada Sand; e=0.64; w=0%
σ'_{vc}=150 (kPa); OCR=1; f=0.01 Hz

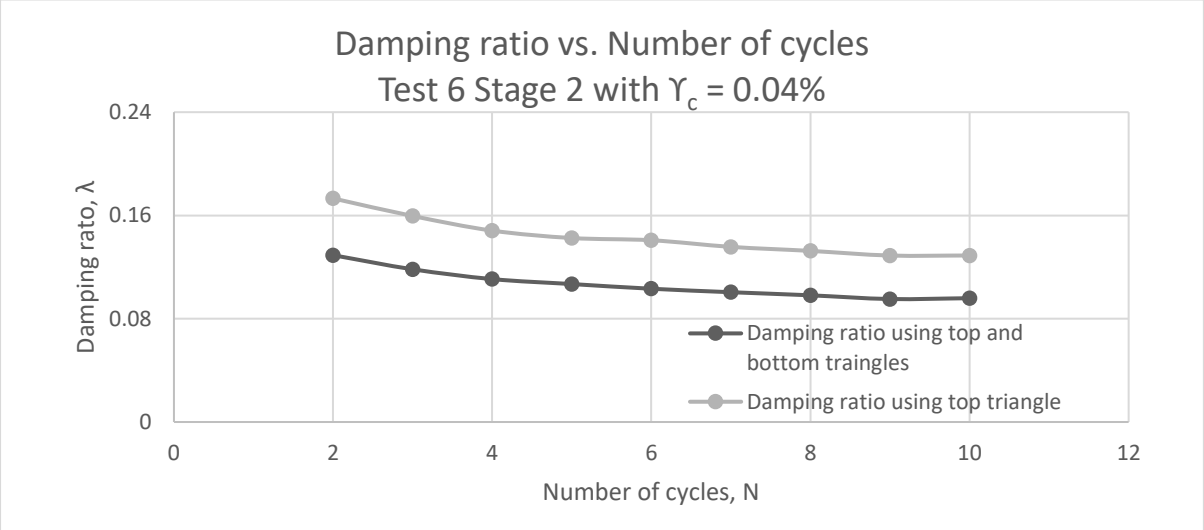

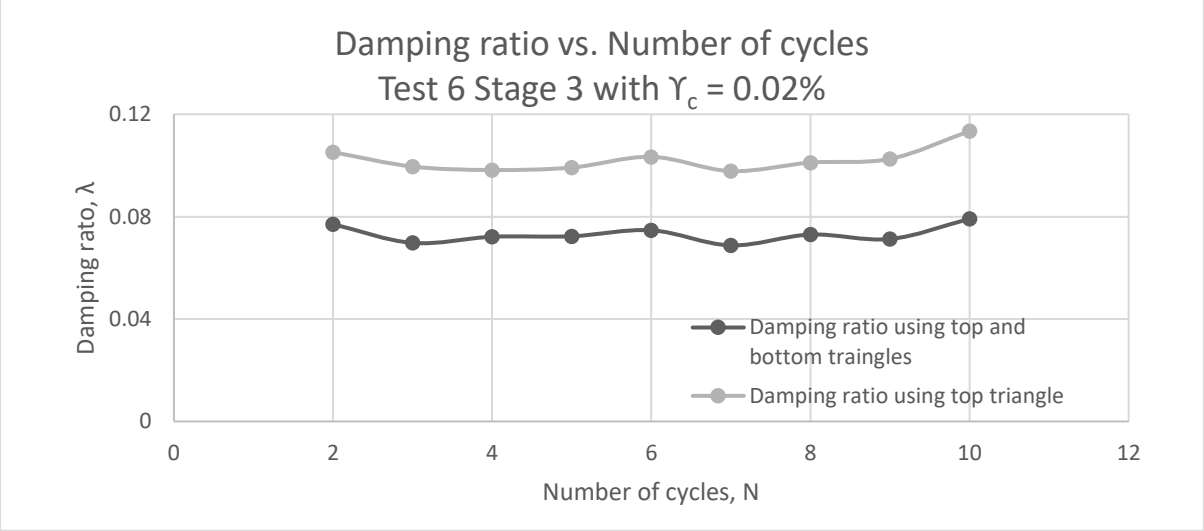

Test: 6.2; Soil: Nevada Sand; e=0.64; w=0%
σ'_{vc}=150 (kPa); OCR=1; f=0.01 Hz

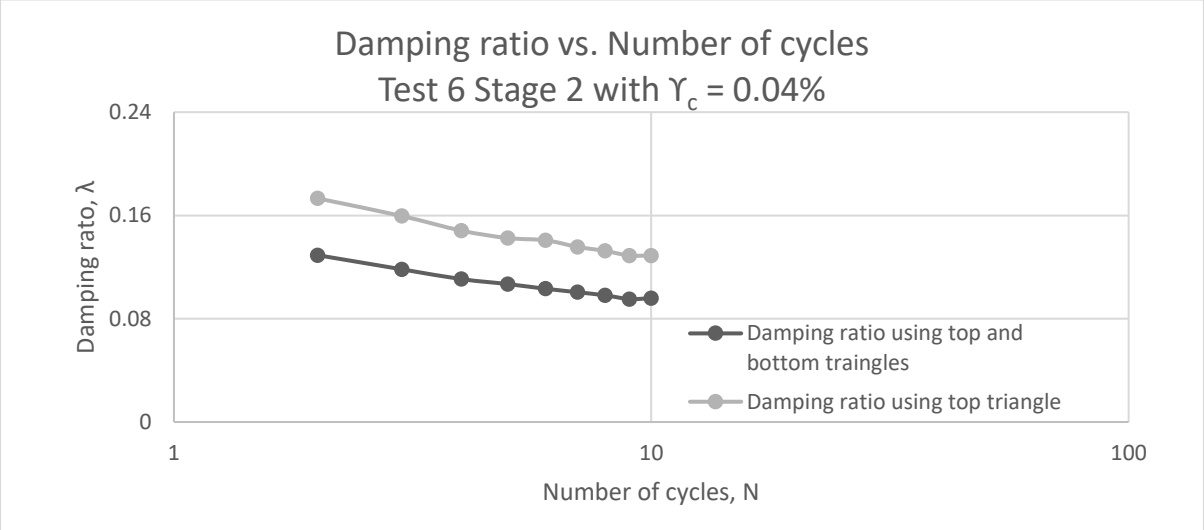

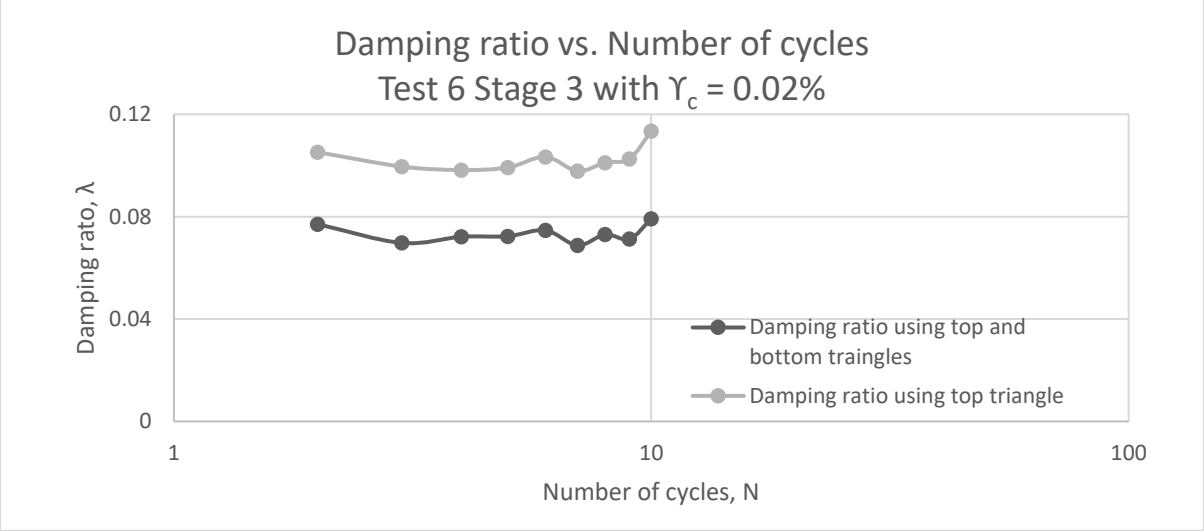

Test: 8; Soil: Nevada Sand; e=0.63; w=0%
σ'_{vc}=145 (kPa); OCR=1; f=0.01 Hz

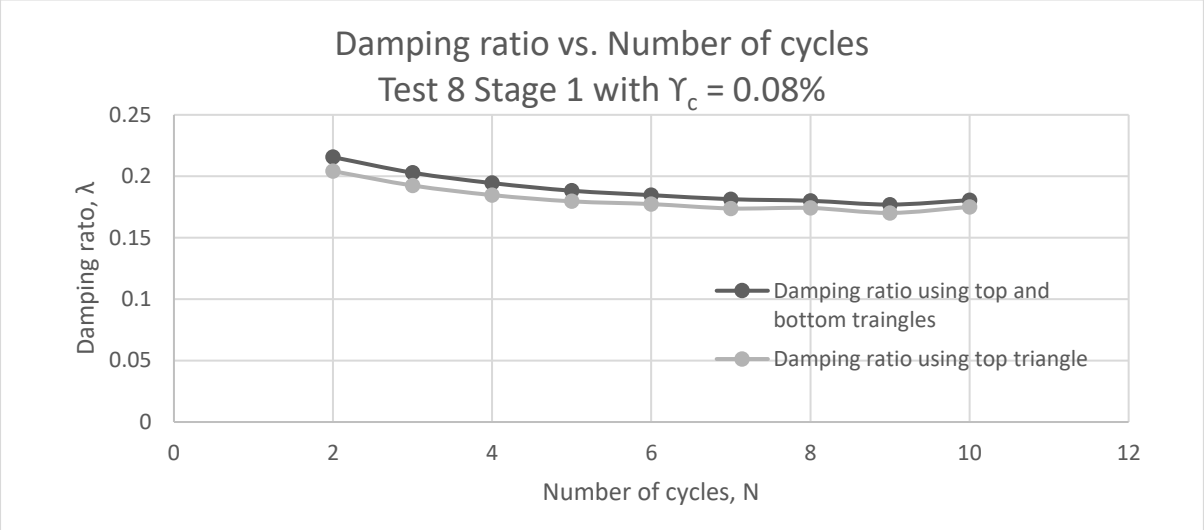

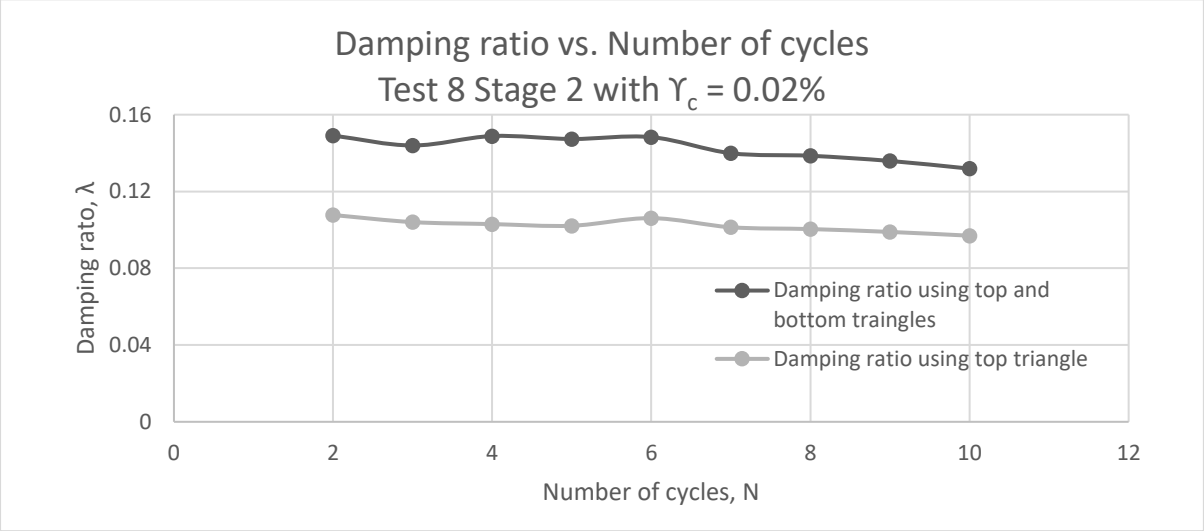

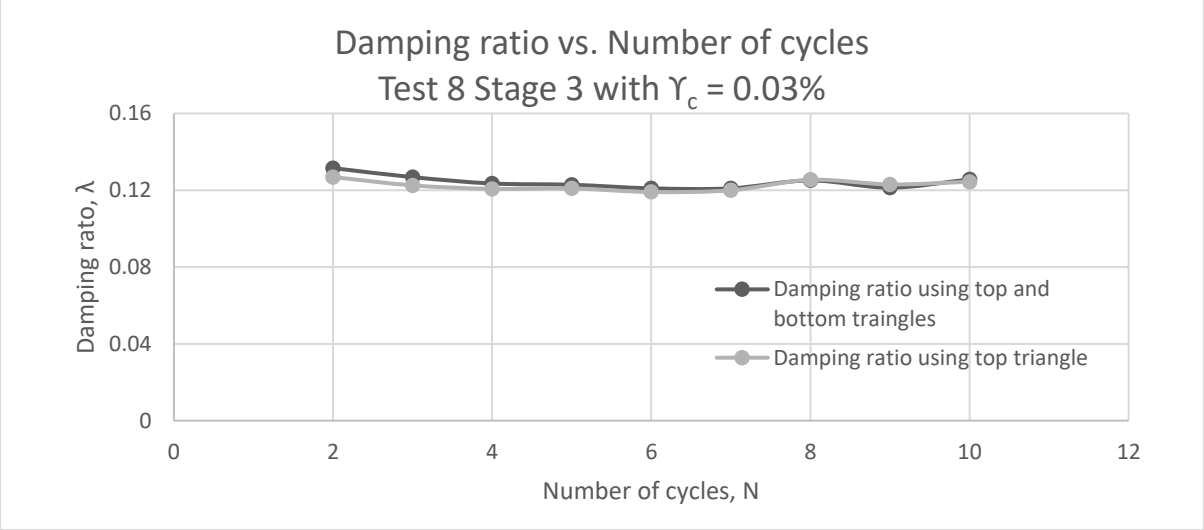

Test: 8; Soil: Nevada Sand; e=0.63; w=0%
σ'_{vc}=145 (kPa); OCR=1; f=0.01 Hz

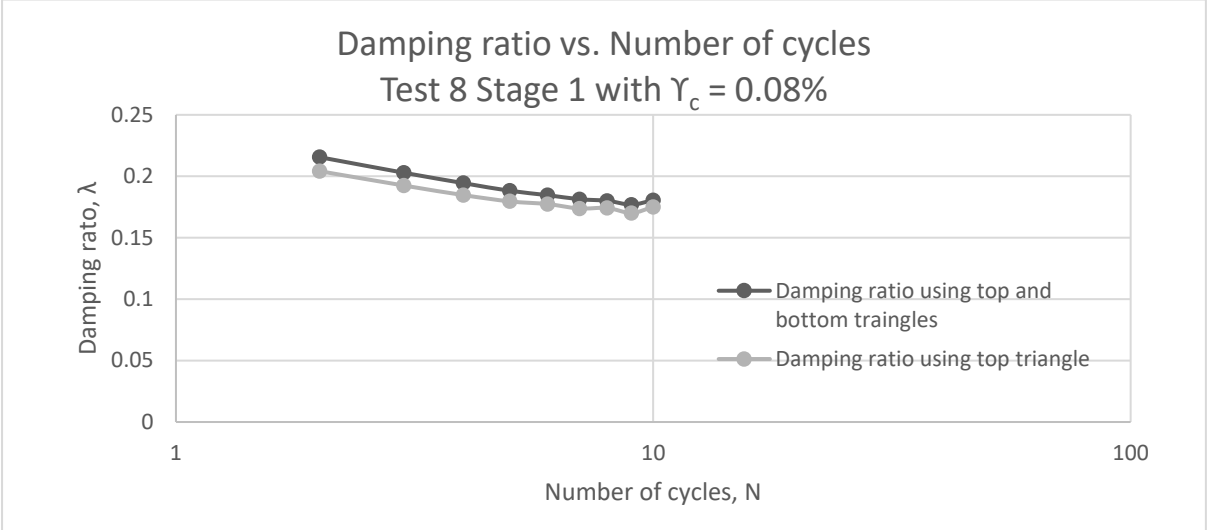

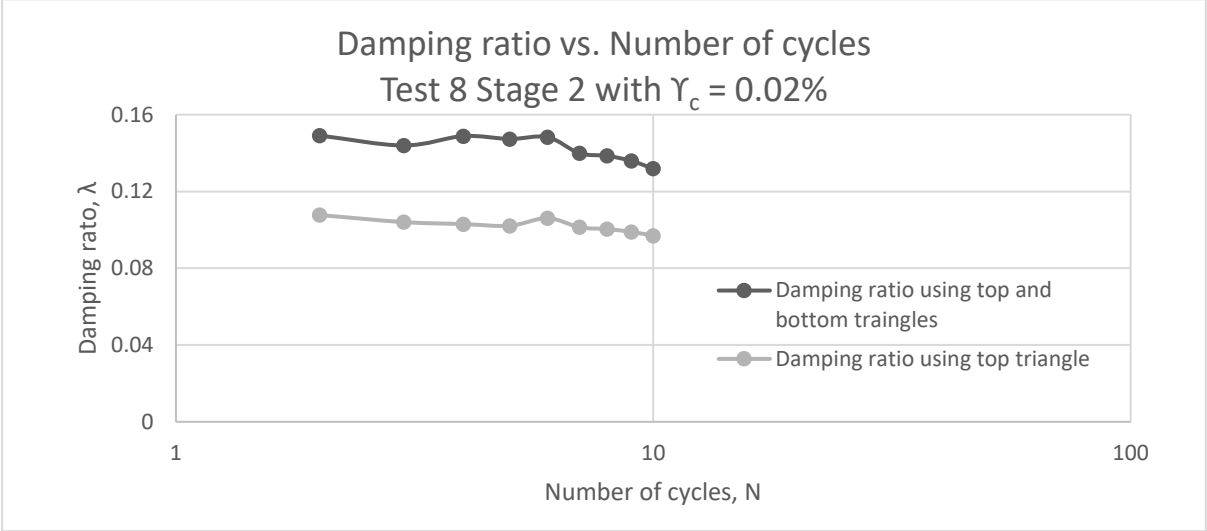

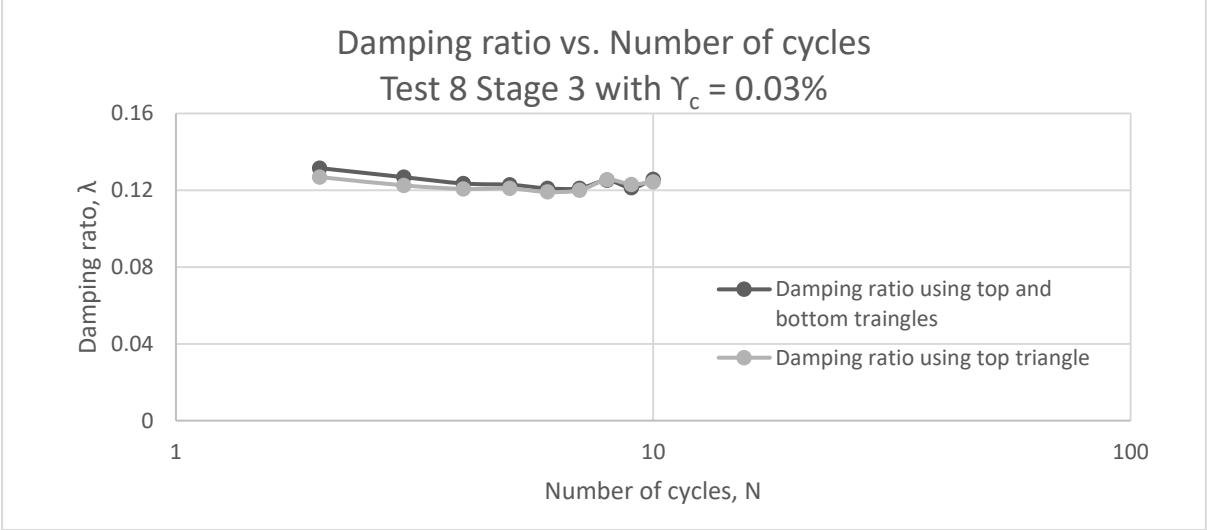

11. Summary and conclusions

Six constant-volume equivalent-undrained NGI direct simple shear cyclic tests on a sand called Nevada sand were conducted and analyzed and the results of six similar tests conducted earlier on Nevada sand and two other sands are analyzed. Ten tests were cyclic strain-controlled with constant cyclic shear strain amplitude, Υ_c, and two were cyclic stress-controlled with constant cyclic shear stress amplitude, τ_c. Some cyclic strain-controlled test had just one cyclic stage and some several stages with different Υ_c in each stage. The cyclic stress-controlled test were single stage tests. The amplitudes Υ_c applied in the tests were between 0.003% and 0.16%, so the conclusions from this investigation are applicable just for this rage of Υ_c.

The research is a second phase of the research on the cyclic behavior of fully saturated sands in undrained conditions focusing on the change of the soil's secant shear modulus, G_{SN}, with the number of cycles, N (change of soil stiffness), change of the associated stiffness index, $\delta_N=G_{SN}/G_{S1}$, buildup of cyclic pore water pressure, Δu_N, with N, and the relationship between δ_N and Δu_N. The variation of the specific energy, W, described by the area of the cyclic stress-strain loop and the associated equivalent damping ratio, λ, are also analyzed. The first phase of the research published in Mortezaie (2012), Mortezaie and Vucetic (2012) and Vucetic and Mortezaie (2015) provides the following conclusions on the relationships listed above:

"(i) at very small γ_c below the cyclic threshold shear strain γ_{tp} where there is no buildup of cyclic pore water pressure, Δu_N, with the number of cycles, N, the cyclic secant shear modulus, G_{SN}, initially increases with N for 10 to 20% of its initial value G_{S1} and then levels off or just slightly decreases,

(ii) at small γ_c between γ_{tp}≈0.01% and 0.10 to 0.15%, Δu_N continuously increases with N while modulus G_{SN} first increases for up to 10% of G_{S1} and then gradually decreases, and

(iii) at γ_c approximately larger than 0.15% relatively large Δu_N develops with N while modulus G_{SN} constantly and significantly decreases.

This means that at γ_c between γ_{tp} and 0.10 to 0.15% the sand stiffness initially increases with N in spite of the reduction of effective stresses caused by the cyclic pore water pressure buildup. In this range of γ_c the pore water pressure Δu_N can reach up to 40% of the initial effective confining stress before G_{SN} drops below G_{S1}."

"…… evidence shows that this kind of behavior is neither a consequence of laboratory procedure nor the specimen boundary conditions, nor the errors by experimentalists. In conclusion, the above undrained cyclic behavior is intrinsic to fully saturated sands, i.e., such a behavior is a common property of fully saturated sands cyclically sheared under different undrained loading conditions."

The test results analyzed in the first phase encompassed the following tests and conditions: single stage cyclic strain-controlled simple shear tests, a single cyclic stress-controlled simple shear test, multi-stage cyclic strain-controlled simple shear tests with Υ_c increasing in each subsequent stage, and multi-stage cyclic strain-controlled triaxial tests with Υ_c increasing in each subsequent stage. Because of the importance of the findings it was decided to run more tests and analyze some previous tests that cover more testing conditions. Accordingly, in the investigation described in this thesis the following additional conditions and tests are examined: various combinations of consecutive Υ_c in the cyclic strain-controlled tests with and without reconsolidation between the stages, including when Υ_c decreased stage after stage, cyclic strain controlled test with many cycles, cyclic stress-controlled tests with many cycles, same test at different confining pressures, same tests with saturated and unsaturated specimens tested under constant-volume equivalent-undrained conditions, and test on two more sands.

The above new tests and analyses of previous tests covering new conditions fully confirmed the findings and conclusions from the first phase. This means that the above aspects of the behavior of fully saturated sands are truly universal and must be taken into consideration in the analyses of soil dynamics problems, in particular the problems of cyclic shearing of sands leading to liquefaction. The only new finding is that in some cases δ_N may increase by 20% before it starts to decrease, not just 10% as suggested in the first phase.

The analysis of the areas of the loops representing the specific energy, W, and associated damping ratio, λ, confirmed previous observations that W and λ decrease with N, with the largest decrease in first few cycles and a gradual drop of the rate of decrease with N, such that λ versus log N relationship is often described by more or less a straight line.

12. References

Andersen, K.H., Pool, J.H., Brown, S.F. and Rosenbrand, W.F. (1980), "Cyclic and Static Laboratory Tests on Drammen Clays", *Journal of the Geotechnical Engineering Division*, ASCE, Vol. 106, No. GT5, pp. 499-529.

Arulanandan, K., Dobry, R., Elgamal, A-W., Ko, H.Y., Kutter, B.L., Prevost, J., Riemer, M.F., Schofield, A.N., Scott, R.F., Seed, R.B., Whitman, R.V., and Zeng, X. (1994). "Interlaboratory Studies to Evaluate the Repeatability of Dynamic Centrifuge Model Tests" *Dynamic Geotechnical Testing II, ASTM STP 1213*, R.J. Ebelhar, V.P. Drnevich, and B.L. Kutter, Eds., American Society for Testing and Materials, pp. 400-422,

Bjerrum, L., and Landva, A., (1966). "Direct Simple-Shear Test on a Norwegian Quick Clay,"Geotechnique, Vol. 16, No. 1, pp. 1-20.

Dobry, R. and Vucetic, M. (1987). "State-of-the-Art Report: Dynamic Properties and Response of Soft Clay Deposits." *Proceedings of the Intl. Symposium on Geotechnical Eng. of Soft Soils*, Mexico City, Vol. 2, pp. 51-87.

Doroudian, M. and Vucetic, M., (1995). "A Direct Simple Shear Device for Measuring Small-Strain Behavior," *ASTM Geotechnical Testing Journal,* Vol. 18. No. 1, pp. 69-85.

Hashash, Y.M.A., Musgrove, M.I., Harmon, J.A., Groholski, D.R., Phillips, C.A., and Park, D. (2016) "DEEPSOIL 6.1, User Manual". Urbana, IL, Board of Trustees of University of Illinois at Urbana-Champaign

Hsu, C-C., and Vucetic, M. (2002): "Dynamic and Cyclic Behavior of Soils Over a Wide Range of Shear Strains in NGI-type Simple Shear Testing Device", *UCLA Research Report* No.

ENG-02-228, Civil and Environmental Engineering Department, University of California, Los Angeles, January, CA, 267 p.

Ishihara, K. (1996). “Soil Behavior in Earthquake Geotechnics”, Clarendon Press, Oxford.

Kramer, S.L. (1996). ”Geotechnical Earthquake Engineering”, Prentice-Hall, Inc., Upper Saddle River, New Jersey.

Lee, M.K.W., and Finn, W.D.L. (1978). “DESRA-2, Dynamic effective stress response analysis of soil deposits with energy transmitting boundary including assessment of liquefaction potential”, Soil Mechanics Series No. 36, Department of Civil Engineering, University of British Columbia, Vancouver, Canada, 60 p.

“Liquefaction of Soils During Earthquakes.” National Research Council (NRC), Committee on Earthquake Engineering, Report No. CETS-EE-001 (1985) Washington, D.C., pp. 240.

Masing, G. (1926), “Eigenspannungen und Verfestigung beim Messing,” *Proceedings of Second International Congress of Applied Mechanics*, pp. 332-335.

Matasovic, N. and Vucetic, M., (1993). "Cyclic Characterization of Liquefiable Sands," *ASCE Journal of Geotechnical Engineering,* Vol. 119, No. 11, pp. 1805-1822.

Mortezaie, A.R. (2012) “Cyclic threshold strains in clays versus sands and the change of secant shear modulus and pore water pressure at small cyclic strains”, *Ph.D. Thesis,* Civil and Environmental Engineering Department, University of California, Los Angeles, May, 242 p.

Mortezaie, A. and Vucetic, M., “Small-strain Cyclic Testing with Standard NGI Simple Shear Device,” Geotechnical Testing Journal, Vol. 35, No. 6, 2012, pp. 1–14,

National Academies of Sciences, Engineering, and Medicine. 2016. *State of the Art and Practice in the Assessment of Earthquake-Induced Soil Liquefaction and Its Consequences*. Washington, DC: The National Academies Press. doi: 1017226/23474.

O'Reilly,M.P. and Brown, S.F, (1991),"Cyclic Loading of Soils: from Theory to Design", Blackie and Son Limited..

Towhata, I. (2008). "Geotechnical Earthquake Engineering", Springer-Verlag Berlin Heidelberg.

Vucetic, M., (1988). "Normalized Behavior of Offshore Clay Under Uniform Cyclic Loading," *Canadian Geotechnical Journal*, Vol. 25, No. 1, pp. 33-41.

Vucetic, M., (1990). "Normalized Behavior of Clay Under Irregular Cyclic Loading," *Canadian Geotechnical Journal*, Vol. 27, No. 1, pp. 29-46. 5.

Vucetic, M. and Dobry, R. (1986). "Pore Pressure Buildup and Liquefaction of Level Sandy Sites During Earthquakes," Report No. CE-86-03, Civil Engineering Department, Rensselaer Polytechnic Institute, Troy, New York, Prepared for USGS, 660 p.

Vucetic, M., Dobry, R., and Thomas, G.E., (1983). "Study of Venezuelan Marine Soils: Phase I, Static and Cyclic/Dynamic Tests and Characterization of Offshore Tuy-Cariaco Clays; Vol. I: Test Results and Interpretations", *Research Report No. CE-12-83-3*, Rensselaer Polytechnic Institute, Troy, New York, December, 27p.

Vucetic, M., Doroudian, M., and Matesic, L., (1999), "Results of geotechnical laboratory tests on soil samples from the UC San Diego Campus," Report for University of California's Campus - Laboratory Collaboration (CLC) Program Research Project: "Estimation of the Ground Motion Exposure from Large Earthquakes at Four UC

Campuses in Southern California," *UCLA Research Report* No. ENG-99-204, Civil and Environmental Engineering Department, University of California, Los Angeles, CA.

Vucetic, M and Mortezaie A. (2015). "Cyclic Secant Shear Modulus versus Pore Water Pressure in Sands at Small Cyclic Strains", *Soil Dynamics and Earthquake Engineering*, Vol. 70, March 2015, pp. 60-72.